Plasma Activation of Electrospun Scaffolds for Neural Tissue Engineering

Plasma-activatie van elektrogesponnen draagstructuren
voor regeneratie van zenuwweefsel

Rouba Ghobeira

Promotoren: prof. dr. R. Morent, dr. H. Declercq
Proefschrift ingediend tot het behalen van de graad van
Doctor in de ingenieurswetenschappen: toegepaste natuurkunde

UNIVERSITEIT
GENT

Vakgroep Toegepaste Fysica
Voorzitter: prof. dr. ir. C. Leys
Faculteit Ingenieurswetenschappen en Architectuur
Academiejaar 2018 - 2019

ISBN 978-94-6355-232-5
NUR 926
Wettelijk depot: D/2019/10.500/40

LEDEN VAN DE EXAMENCOMMISIE

Prof. dr. ir. F. De Turck (Voorzitter)
Vakgroep Informatietechnologie EA05
Faculteit Ingenieurswetenschappen en Architectuur
Universiteit Gent

Prof. dr. R. Morent (Promotor)
Vakgroep Toegepaste Fysica EA17
Faculteit Ingenieurswetenschappen en Architectuur
Universiteit Gent

Dr. H. Declercq (Promotor)
Vakgroep Structuur en Herstel van de Mens
Faculteit Geneeskunde en Gezondheidswetenschappen
Universiteit Gent

Prof. dr. ir. C. Leys
Vakgroep Toegepaste Fysica
Faculteit Ingenieurswetenschappen en Architectuur
Universiteit Gent

Prof. dr. J.-M. Pouvesle
Groupe de Recherches sur l'Energétique des Milieux Ionisés (GREMI)
UMR 7344, CNRS
Université d'Orleans

Prof. dr. A. Skirtach
Faculteit Bio-ingenieurswetenschappen
Vakgroep Biotechnologie
Universiteit Gent

Prof. dr. A. Van Tongel
Vakgroep Structuur en Herstel van de Mens
Faculteit Geneeskunde en Gezondheidswetenschappen
Universiteit Gent

Dr. R. Bitar
Vakgroep Toegepaste Fysica
Faculteit Ingenieurswetenschappen en Architectuur
Universiteit Gent

Universiteit Gent
Faculteit Ingenieurswetenschappen en Architectuur
Vakgroep Toegepaste Fysica EA17
Onderzoeksgroep Plasmatechnologie
Sint–Pietersnieuwstraat 41, B4–9000 Gent

The research leading to these results has received funding from the European Research Council under the European Union's Seventh Framework Program (FP/2007-2013): ERC Grant Agreement number 279022 (PLASMAPOR) and ERC Grant Agreement number 335929 (PLASMATS). The authors also acknowledge the support of the Special Research Fund (BOF 14/IOP/045) of Ghent University.

Summary

An alerting high incidence of peripheral nerve injuries (PNI) reaching over one million cases worldwide is still lingering over the centuries. This is due to the fact that peripheral nerves are not protected like the brain and the spinal cord by a bone tissue and a nerve-blood barrier, making them susceptible to physical, chemical, thermal and/or ischemic damages at any anatomic site. Luckily, unlike the central nervous system having a very limited to no ability of regeneration, the peripheral nervous system is marked by its regenerative machinery initiating nerve repair up to a certain extent. However, the complex pathophysiology involved in PNI makes the spontaneous regeneration not always successful. Therefore, interventions to achieve an effective repair are in most cases unavoidable. Direct nerve repair is the most efficient therapeutic approach but is limited to extremely short nerve gaps where a tensionless suturing can still be performed. In the frequent cases involving bigger nerve gaps, the interposition of a supportive structure is necessary to span the injured site. The use of autologous nerve graft is currently considered the gold standard and has stayed so all along the previous 50 years. However, the autograft is associated with some weighty drawbacks such as donor site morbidity, use of sensory-only nerve, size and fascicular pattern mismatching, extra surgical step, possible neuroma formation and a success rate of only 50%. In the last few decades, the advancements in the multidisciplinary tissue engineering (TE) field have led to the development of nerve guidance conduits (NGCs) as alternative. Just as most scaffolds used in different TE applications, NGCs typically consist of a physical scaffolding made up of natural or synthetic polymeric material possibly amalgamated with biomolecular components and/or support cells. Nerve gaps of maximum 4.0 cm in humans and 1.5 cm in rats have been successfully bridged. However, nerve regeneration becomes very limited or completely absent in bigger gaps and functional repair remains deficient across all gap sizes. Therefore, several inventive strategies focused on adding neurotrophic factors, Schwann cells (SCs), stem cells, intraluminal fillers, wall guidance structure or changing the whole conduit design were implemented. Moreover, combinatorial strategies merging the advantages of previous NGCs and adopting additional levels of complexities are investigated. However, all approaches are still failing in outperforming the regeneration levels of autograft or even in attaining similar outcomes especially in critical nerve gaps. Therefore, the main goal of this thesis is to tackle large nerve gaps by designing a novel NGC possessing the ideal topographical, mechanical, chemical and cellular cues triggering a robust regenerative capacity.

From a topographical point of view, one elemental factor that can guaranty the implant success is the mimicry of the fibrillary architecture of the extracellular matrix (ECM) that is known to govern most of the cellular activities in the body. Different physical, chemical and electrostatic techniques have already been developed for the recreation of ECM fibers. Of those available, electrospinning is by far the most widely used due to its simplicity, versatility and affordability. Moreover, its capacity to align the fibers and adapt their diameter down to the nanometer size renders it a powerful technique as it can recapitulate the *in vivo* tissue-specific properties in terms of orderliness and scale. In fact, the fiber diameter plays a decisive role in modulating cellular adhesion, gene expression, proliferation and differentiation. Moreover, fiber alignment provides directional cues triggering cell elongation, directed migration and regeneration enhancement of ordered tissues such as nerves. In this sense, NGCs made up of random and aligned electrospun fibers of different diameters have shown moderate successes in nerve regeneration over the other topographical designs. In this dissertation, the right electrospinning parameters leading to the finest fiber diameter and alignment are vigilantly picked to optimize the previous generation of electrospun NGCs.

From a mechanical point of view, the base material should be meticulously selected to match the strength and elasticity of the innate environment and support cell growth. Biodegradable aliphatic polyesters constitute the most eminent polymer group for NGC fabrication owing to their proper mechanical properties, biocompatibility and FDA approval for clinical suitability as nerve conduits. A remarkable supremacy of polycaprolactone (PCL) is observed in the literature dealing with electrospun NGCs. PCL fibers are non-toxic as they do not lead to the formation of high concentrations of organic acid degradation products, which minimizes the risk inflammatory responses. *In vivo* performances of PCL NGCs showed good results in bridging nerve gaps of 1 cm by exhibiting large number of myelinated axons. Recently, the copolymer poly(ethylene oxide terephthalate)-poly(buylene terephthalate) (PEOT-PBT) commercially known as Polyactive® (PA) was shown to support the regeneration in longer gaps because of its *in vivo* slower degradation rate coinciding with the longer regeneration time. Another advantage of PA over the conventional polymers is the possibility to tune more adequately its mechanical properties by tackling the composition of the two polymers. Therefore, both PCL and PA are used in this thesis dissertation.

From a biochemical point of view, adding free neurotrophic factors to NGCs is not enough to support cellular activities. A critical limitation of most NGCs is their deprivation of immobilized proteins because of

their hydrophobic base material surface lacking protein-binding functional groups. In fact, topographical and biochemical cues are concurrently recognized by cells at the cell-scaffold interface that plays a primordial role in the initiation of vital cellular processes such as adhesion and proliferation. However, given the narrow dimensions of the porous conduits, reaching and modifying the inner wall surface without altering the nanofibers delicate structure remain challenging tasks. To solve this issue, this thesis focuses on the application of non-thermal plasmas as a route to bio-activate NGC surface. Plasma treatments are nowadays gaining a great interest in TE over other traditional surface modification techniques. It is a solvent-free method that can be highly controlled to incorporate specific functional groups (plasma activation) or deposit thin polymer coatings (plasma polymerization) on biomaterials thus creating adequate surfaces for subsequent protein immobilization. Moreover, it is a gas-based technique that can reach and treat the overall surface of complex and porous scaffolds, hence NGCs. Despite the considerable improvements offered by plasma-functionalized scaffolds in several TE applications, plasma treatment was never, to the best of our knowledge, applied to NGCs. Yet, tailoring their surface properties using fine-tuned plasma parameters is believed to play a pivotal role in the enhancement of glial and neural cell activities thus activating nerve regeneration across critical nerve gaps. In the body, the directional guidance of neurites that ensures a successful nerve regeneration is mediated by spatial concentration gradients of biomolecules. Inspired by the theory "Nature knows the best", plasma treatments creating a chemistry gradient along the conduit surface are also performed in this thesis. Gradient plasma treatments were previously applied only on 2D sheets using complex redesigned plasma reactors. For instance, automated stepper motors moving the samples during the treatment, complex gas flow systems, reshaped electrodes and shielding covers were employed for this purpose. Relatively simple dielectric barrier discharge (DBD) and plasma jet (PJ) reactors are used in this thesis to plasma-treat the more complex 3D NGCs in a gradient way.

From a cellular point of view, NGCs cultured with SCs prior to *in vivo* implantation were shown to considerably enhance nerve regeneration compared to their acellular counterparts. If autograft is the gold standard for PNI repair, adding autologous SCs to NGCs is similarly judged as the present gold standard for cellular-based approaches. In addition to their active secretion of growth factors, SCs express cell adhesion molecules, build their own basal lamina and intensely assist, at a later stage, in the remyelination of growing nerve fibers. However, SC cultures are difficult and time-consuming and SC extraction from demands the sacrifice of a nerve tissue. As alternative stem cells are

cultured on the NGCs, of which the frequently used adipose derived stem cells (ADSCs). In fact, ADSCs are abundant and easily accessible by a simple liposuction, proliferate rapidly in culture, have a low cost and can differentiate into glial and neural cell lineages. Both, undifferentiated and differentiated ADSCs were shown to enhance the functional recovery when injected in NGCs. Therefore, ADSCs and SCs are cell types studied in this thesis.

An evolutionary methodological strategy is adopted in this dissertation gradually paving the way towards the generation of an ideal NCG:

In a first step, the effects of different sterilization methods on the physico-chemical and bioresponsive properties of plasma-treated PCL are studied. In fact, the material sterility is a prerequisite for the use of NGCs *in vitro* and *in vivo*. This crucial step is often neglected as tissue engineers are mainly focusing on implementing complex scaffold topographies and advanced biofunctionalization. However, given the high sensitivity of biodegradable polymers, the harsh sterilization methods normally used are associated with big risks of compromising the physical and chemical properties of the scaffolds, thereby altering the cell-material interactions. Therefore, the sterilization should be considered early in the scaffold designing process especially when it comes to fine structures subjected to a previous surface modification. This prevents from the risk of damaging the NGCs at advanced stages after the whole optimization processes of biofabrication and plasma treatment. The first experimental chapter is thus dedicated to sterilize PCL films pre-subjected to a plasma treatment using a medium pressure DBD. The second experimental chapter further advances in complexity and transfer from 2D films to 3D electrospun fibers. In this way, an examination of different polymeric topographies is completed to check if the nanofibrous scaffolds are more or equally prone to sterilization-induced damages compared to films. Results show that air and argon plasmas significantly increase the films and fibers wettability due to the incorporation of oxygen-containing functionalities onto PCL surface. Besides surface modification, the plasma potential to sterilize PCL is studied in function of appropriate treatment times, but sterility is not achieved so far. Therefore, plasma-modified samples are subjected to UV, H_2O_2 plasma (HP) and ethylene oxide (EtO) sterilizations. EtO decreases the wettability of plasma-treated films and fibers and changes the morphology of plasma-treated fibers mainly due to reactions between EtO molecules and the grafted functional groups. Moreover, HP modifies the surface morphology of PCL films and provokes a total loss of the fibrillary architecture of fibers because of the complex thermo-oxidative reactions occurring during the process. UV does not affect the physico-chemical properties

of all samples which shows a significantly higher adhesion and proliferation of ADSCs compared to EtO and HP sterilized samples. Overall, it can be concluded that plasma-treated NGCs and other TE scaffolds should be sterilized by UV to maintain their beneficial surface properties induced by non-thermal plasma.

After the selection of a suitable sterilization, the second step of this dissertation focuses more on PCL electrospinning process itself. Several highly toxic solvent systems providing a good PCL solubility-spinability are recurrently applied in the overwhelming majority of studies. One of the current major focuses revolves around the challenging generation of aligned fibers that are very desirable in numerous TE applications of which peripheral nerve TE. Moreover, the critical influence of fiber size on cellular performance has led to the use of different solvent systems for the production of specific nano- or micro-sized PCL fibers while neglecting the solvents toxicity. Therefore, the goal of the third experimental chapter is to use the unconventional and non-toxic solvent system acetic acid/formic acid, recently defined as the system producing ultra-thin PCL fibers, in a trial to outspread the size range and to tackle fiber alignment. After profound analysis of the effect of varying collector motion and collector design on fiber alignment, a novel collector producing highly aligned PCL fibers based on synchronic mechanical and electrical effects is designed. In a subsequent step, the fiber diameter is manipulated by analyzing 3 influential parameters: polymer concentration, tip-to-collector distance and the frequently overlooked parameter humidity. The parameters fine-tuning study has resulted in very broad PCL fiber diameter ranges of 94 to 1548 nm and 114 to 1408 nm for random and aligned fibers respectively. The generated fibers are then used in the fourth experimental chapter to investigate the synergistic influence of PCL fiber size, orientation and plasma-modified surface chemistry on ADSC behavior. Despite the incorporation of approximately the same oxygen amount on all samples post-plasma treatment, the hydrophilicity significantly differ between the different fiber sizes and orientations. This highlights the outstanding influence of the fibrous mesh topography on the liquid-solid interface. Extended plasma exposure starts damaging the fibers with a growing risk of drastic alterations on thicker and random fibers compared to thinner and aligned fibers. The diverse responses to plasma stem from the distinct molecular chain arrangement and crystallinity of different fiber diameters and orientations. Plasma treatment strikingly enhances the cell metabolic activity, adhesion, proliferation and cytoplasmic remodeling on all samples. ADSCs adhere multi-directionally on random fibers with a gradual change from a more circular to a more elongated shape on increasing diameters. In contrast, ADSCs overextend in a bipolar and aligned

fashion on aligned fibers with a tendency to attach on fewer fibers with increasing fiber diameter. A mimicry of the natural bands of Büngner structure guiding axon extension during nerve regeneration is thus gradually observed, making from the aligned plasma-treated fibers promising candidates in the design of NGCs.

Coming to the last experimental chapter of this dissertation, NGCs are electrospun using fine-tuned process parameters engendering an innovative bi-layered architecture. An inner wall composed of aligned fiber bundles with random fibers in between is obtained, thus guiding neurite extension and SC elongation while still allowing nutrient supply through the random fiber pores. In contrast, randomly deposited nanofibers entirely compose the outer wall thus further supplying nutrients and consolidating the whole NGC structure. Medium pressure argon DBD treatment homogeneously increased the inner surface oxygen content from 17 % to 28 % thus highlighting the plasma ability to penetrate through the porous wall. Atmospheric pressure argon PJ treatment created a gradient chemistry throughout the inner wall with an oxygen content gradually increasing from 21% to 30%. A significantly enhanced SC adhesion is observed on plasma-treated NGCs compared to untreated NGCs. A uniform cell distribution is perceived along the homogeneously plasma-treated NGCs. However, cell gradients towards increased surface oxygen contents are interestingly detected on the NGCs subjected to a gradient plasma treatment. With time, the cell gradient becomes steeper and more prominent owing to the better cell proliferation on the oxygen-rich end and to a directed cell migration along the NGCs. A gradual change from a more circular shape to a more elongated SC shape is visualized along the oxygen gradient thus forming SC columns mimicking the natural bands of Büngner structure. Finally, when PC12 cells are cultured on SC pre-seeded scaffolds, neurite outgrowth is only seen on plasma-treated NGCs: DBD treated NGCs display relatively short neurites extending in multiple directions, while PJ treated NGCs show gradually longer neurites mainly directed towards higher oxygen contents.

Overall, it can be concluded that the joint use of the electrospinning technique and the non-thermal plasma technology in the engineering of NGCs has a great potential in enhancing peripheral nerve regeneration. Particularly, plasma-induced chemistry gradient along the inner NGC wall offers high promises in bridging critical nerve defects and ensuring a complete functional recovery. A future translation from *in vitro* to *in vivo* will hopefully constitute a big step towards the clinical use of plasma-treated NGCs.

Samenvatting

Een onrustwekkend hoog aantal perifere zenuwletsels (PZL), meer dan één miljoen wereldwijd, blijven onveranderd voorkomen. Een van de voornaamste redenen hiervoor is dat perifere zenuwen niet in dezelfde mate beschermd zijn in vergelijking met het brein en de ruggengraat, waar een zenuw-bloedbarrière aanwezig is. Dit maakt hen kwetsbaar voor fysische, chemische, thermische en/of ischemische schade aan gelijk welke anatomische site. Gelukkig, in tegenstelling tot het centraal zenuwstelsel, wat een zeer beperkte regeneratiecapaciteit heeft, is het perifere zenuwstelsel gekenmerkt door een sterk regeneratief complex, hetgeen zenuwherstel initieert tot op zekere hoogte. Niettemin, door de complexe pathofysiologie betreffende PZL, is spontane regeneratie niet altijd succesvol. Hierdoor is een chirurgische interventie vaak niet te vermijden. Direct zenuwherstel is de meest efficiënte therapeutische methode, maar is gelimiteerd tot extreem korte zenuwonderbrekingen waarbij spanningsvrij naaien nog steeds kan uitgevoerd worden. In het vaak voorkomend geval van grotere zenuwonderbrekingen is het noodzakelijk om te werken met een support die de onderbreking overbrugt. De autologe graft is op dit moment nog steeds de gouden standaard en dit reeds voor de laatste 50 jaar. Niettegenstaande is de autologe graft gekenmerkt door een aantal zware nadelen zoals donor site morbiditeit, het beperkt gebruik van gevoelszenuwen, grootte en fasciculaire patroonmismatch, extra chirurgische ingrepen, mogelijke vorming van neuroma's en een kans op succes van slechts 50%.

In de laatste tientallen jaren heeft de vooruitgang binnen de discipline "tissue engineering" (TE) geleid tot de ontwikkeling van artificiële zenuwbaangeleiders (ZG's) als mogelijk alternatief. Net zoals de meeste scaffolds ontwikkeld voor verschillende TE toepassingen, zijn ZG's opgebouwd uit een natuurlijk of synthetisch polymeer, mogelijks in combinatie met biomoleculaire componenten en/of ondersteunende cellen. Zenuwonderbrekingen van maximaal 4.0 cm (mens) en 1.5 cm (rat) zijn succesvol overbrugd. Niettemin is gebleken dat de zenuwregeneratie sterk gelimiteerd is of zelfs ontbrekende voor langere onderbrekingen en blijkt dat het functioneel herstel lakende is voor alle defectgroottes. Daarom heeft men verschillende inventieve strategieën toegepast die gefocust zijn op het toevoegen van neurotrofische factoren, Schwanncellen, stamcellen, intraluminaire vullers, wandgidsstructuren of paste men het volledige design van de scaffold aan. Op dit moment worden de voordelen van de verschillende reeds bestaande ZG's gecombineerd en worden toenemende graden van complexiteit onderzocht. Desondanks slagen deze ZG's er niet in om het beter te doen dan de autograft of zelfs een vergelijkbaar resultaat neer

te zetten. Daarom is het doel van deze dissertatie om grotere zenuwonderbrekingen te overbruggen m.b.v. het ontwerp van nieuwe ZG's die de ideale topografische, mechanische, chemische en cellulaire eigenschappen bezitten om een robuuste regeneratie te ondersteunen.

Vanuit topografisch punt is het nabootsen van de fibrilstructuur van de extracellulaire matrix (ECM) een cruciale factor om tot een succesvol implantaat te komen aangezien de ECM gekend staat om de meeste cellulaire activiteiten van het lichaam mee te controleren. Verschillende fysische, chemische en elektrostatische technieken zijn reeds toegepast geweest om de ECM vezels te gaan nabootsen. Binnen de selectie van mogelijke technieken is gebleken dat electrospinnen veruit de meest populaire techniek is, dankzij zijn eenvoud, kostprijs en veelzijdigheid. Daarboven maakt zijn capaciteit om vezels gealigneerd te gaan spinnen en dit met diameters in de nm range het tot een heel krachtige techniek, aangezien het de *in-vivo* weefselspecifieke eigenschappen zoals order en schaal kan nabootsen. Het is namelijk gebleken dat de vezeldiameter een bepalende rol speelt in het regelen van celadhesie, genexpressie, proliferatie en differentiatie. Daarnaast voorzien de vezels ook directionele cues, triggeren ze celelongatie, staan ze in voor geleide migratie en stimuleren ze de regeneratie van geordende weefsels zoals zenuwen. Dit in acht nemende is gebleken dat ZG's bestaande uit random en gealigneerde electrogesponnen weefsels beperkt succesvol gebleken zijn in vergelijking met andere topografische ontwerpen. In deze dissertatie werd er daarom sterk gefocust op het verkrijgen van die electrospinning parameters die leidden tot de fijnste vezeldiameter en uitstekend aligneren om zo de vorige generaties ZG's verder te optimaliseren.

Vanuit mechanisch standpunt is de selectie van het juiste materiaal uitermate kritisch om tot een goede match te komen van sterkte en elasticiteit met zijn directe omgeving zodat celgroei optimaal ondersteund kan worden. Biodegradeerbare alifatische polyesters blijken een van de meest veelbelovende polymeerklasses te zijn dankzij hun uitstekende mechanische eigenschappen, goede biocompatibiliteit, en FDA toestemming om gebruikt te worden voor zenuwregeneratie in een klinische setting. Polycaprolacton (PCL) blijkt uitermate populair te zijn in de literatuur wanneer het aankomt op electrosgesponnen ZG's. PCL nanovezels zijn niet-toxisch, aangezien ze niet leiden tot de vorming van hoge concentraties van organische zuren, wat het risico op inflammatoire respons minimaliseert. Het *in-vivo* testen van PCL ZG's toonde aan dat ze in staat zijn om zenuwonderbrekingen van 1 cm succesvol te overbruggen door de aanwezigheid van grote aantallen myeline axons. Recentelijk is er aangetoond geweest dat het

copolymeer poly(ethylene oxide terephthalate)-poly(buylene terephthalate) (PEOT-PBT), commercieel gekend als Polyactive® (PA), in staat was de regeneratie van langere onderbrekingen te overbruggen dankzij de tragere degradatie, hetgeen overeenkomt met de langere regeneratietijden. Een ander voordeel van PA in vergelijking met conventionele polymeren is de mogelijkheid tot het aanpassen van de samenstelling van het copolymeer om zo tot een betere match te komen van de mechanische eigenschappen. Op basis van bovenstaande vaststellingen werd er daarom geopteerd om met zowel PCL als PA te werken binnen dit proefschrift.

Vanuit biochemisch standpunt is gebleken dat het toevoegen van vrije neurotrofische factoren aan de ZG's niet voldoende was om de celactiviteit te ondersteunen. Een kritische limiterende factor bij de meeste ZG's blijkt het gebrek aan proteïnebinding te zijn, mede door het hydrofobe karakter van het scaffoldmateriaal. Verder is er gebleken dat de topografische en biochemische cues concurrentieel herkend worden door de cellen en dat de cel-ZG interface een belangrijke rol speelt in de initiatie van cellulaire processen zoals adhesie en proliferatie. Niettegenstaande blijkt dat de kleine dimensies van de poreuze ZG's mee verantwoordelijk zijn voor de moeilijkheidsgraad waarmee de binnenwanden van de ZG's kunnen gemodificeerd worden zonder dat de nanovezelstructuur aangetast wordt. Om dit probleem aan te pakken, focust dit proefschrift zich op het gebruik van niet thermische plasma's om het oppervlak van de ZG's te bioactiveren. Op dit moment genieten plasma behandelingen veel belangstelling binnen TE in vergelijking met andere modificatietechnologieën. Het is een solvent-vrije methode die toelaat om verschillende functionele groepen (plasma activatie) in te bouwen of dunne films (plasma polymerisatie) af te zetten op biomaterialen, waarbij oppervlakken gevormd worden die uitermate geschikt zijn voor proteïne-immobilisatie. Verder is het ook een gasgebaseerde techniek die toelaat om complexe poreuze structuren efficiënt te gaan behandelen. Ondanks de sterke vooruitgang die er gemaakt is dankzij plasma gefunctionaliseerde scaffolds binnen verschillende TE toepassingen is plasma, voor zover wij weten, nog nooit toegepast geweest op ZG's. Niettemin speelt het aanpassen van de oppervlakeigenschappen een essentiële rol in het verbeteren van gliale en neurale celactiviteit, wat zou moeten leiden tot het activeren van zenuwregeneratie voor kritische zenuwonderbrekingen. Het directioneel geleiden van neurieten in het lichaam die succesvolle zenuwregeneratie verzekert wordt gemedieerd door spatiale concentratiegradiënten opgemaakt uit biomolecules. Geïnspireerd door de theorie "de natuur weet het best", worden er binnen deze dissertatie ook plasmabehandelingen ingezet om een chemische gradiënt te introduceren doorheen de ZG. Plasma-

gebaseerde gradiënten werden voorheen enkel toegepast op 2D-oppervlakken, gebruik makende van plasmareactoren met een complex design. Voorbeelden hiervan zijn stapmotoren die de samples bewegen gedurende de behandeling, complexe gasflow systemen, aangepaste electroden en maskers. Wij opteerden voor het gebruik van relatief simpele DBD en plasmajet reactoren die ons ook toelieten gradiënten te introduceren in de complexe geometrie kenmerkend voor een ZG.

Vanuit een celbiologisch standpunt is gebleken dat ZG's pre-gecultiveerd met Schwanncellen voor implantatie ertoe leiden dat zenuwregeneratie veel efficiënter plaatsvindt in vergelijking met niet-cellulaire scaffolds. Wanneer je autografts beschouwt als de gouden standaard voor perifeer zenuwherstel, worden ZG's verrijkt met Schwanncellen gezien als de celgebaseerde gouden standaard. Naast de secretie van groeifactoren door de Schwanncellen, scheiden deze ook adhesiemoleculen af, bouwen ze hun eigen basale lamina en, in een latere fase, zijn ze intens betrokken bij de remyelinatie van de groeiende zenuwvezels. Desondanks zijn Schwanncelculturen moeilijk en tijdsrovend en vereist de extractie van deze cellen het opofferen van zenuwweefsel. Een beter alternatief is het gebruik van stamcellen gecultiveerd op ZG's. Hiervoor kan gebruik gemaakt worden van vetstamcellen die veelvuldig beschikbaar zijn uit het vet dat gerecupereerd wordt van liposucties. Deze sneldelende cellen zijn goedkoop en kunnen gedifferentieerd worden in gliale en neurale cellijnen. Zowel voor niet-gedifferentieerde als gedifferentieerde vetstamcellen is er vastgesteld geweest dat deze het functioneel herstel van zenuwen stimuleren wanneer geïnjecteerd in ZG's. Daarom is er binnen deze thesis gewerkt geweest met vetstamcellen en Schwanncellen.

Een methodologische aanpak met voortschrijdend inzicht is toegepast in deze thesis die gradueel geleid heeft tot het fabriceren van de ideale ZG:

In een eerste stap werden de effecten van verschillende sterilisatiemethodes op de fysisch-chemische eigenschappen en bioresponsiviteit van plasma-geactiveerde PCL films bestudeerd, aangezien steriliteit een vereiste is voor *in-vitro* en *in-vivo* gebruik. Dit is een cruciale stap die vaak genegeerd wordt door TE ingenieurs, daar zij voornamelijk focussen op scaffoldoptimalisaties. Niettemin is de schade die harde sterilisatiemethodes kunnen aanrichten aan de fragiele polymeerstructuren niet te onderschatten, aangezien dit de chemische, mechanische en celinteractie eigenschappen van het materiaal significant kunnen veranderen. Om deze reden is het essentieel om sterilisatie vroeg in het onderzoek mee te nemen, zeker

voor oppervlakgemodificeerde scaffolds. Het eerste experimentele hoofdstuk is daarom toegespitst op het steriliseren van PCL films die eerder met een DBD geactiveerd geweest zijn. Het tweede experimentele hoofdstuk legt zich hier verder op toe en onderzoekt de meer complexe situatie waarbij er overgegaan wordt naar 3D electrogesponnen nanovezels. Hierbij werd er gekeken wat de impact was van de verschillende sterilisatiemethodes op de topografie van de nanovezels en of er mogelijk schade werd aangebracht. Resultaten tonen aan dat hoewel argon en luchtplasma in staat zijn om efficient polaire groepen te introduceren op de scaffolds zonder deze te beschadigen, de technologie niet in staat is om de scaffolds te steriliseren zonder verdere hulp. Daarom zijn de verschillende samples blootgesteld geweest aan UV, waterstofperoxide plasma (HP) en ethyleen oxide (EtO) sterilisaties. EtO verhoogde de watercontacthoek van de samples en had een negatieve impact op de vezelmorfologie en dit voornamelijk door interacties tussen de EtO molecules en de gegrafte groepen. HP sterilisatie veranderde ook de morfologie van de PCL films en leidde tot het verlies van de vezelstructuur door thermo-oxidatieve reacties die plaatsvonden tijdens de sterilisatie. UV behandelingen hadden geen impact op de fysisch-chemische eigenschappen van de samples, hetgeen leidde tot een significant hogere celadhesie en proliferatie van vetstamcellen in vergelijking met de andere sterilisatietechnieken. Algemeen kan er geconcludeerd worden dan plasma behandelde ZG's het best gesteriliseerd worden met UV indien men de positieve effecten van de behandeling wil behouden.

Na de selectie van de optimale sterilisatie, is het tweede deel van deze dissertatie toegespitst op het PCL electrospinnen. Op basis van de literatuur was het duidelijk dat het verkrijgen van goede nanovezels makkelijjk is wanneer er gebruik gemaakt wordt van toxische solventen. Dit vormt echter een probleem voor TE toepassingen aangezien het niet ongewoon is dat solventresten gevangen blijven in de nanoporiën van de vezelstructuur, iets wat vaak genegeerd wordt in de zoektocht naar nieuwe solventsystemen voor het spinnen van (gealigneerde) nanovezels met specifieke diameters. Daarom is het derde experimentele hoofdstuk toegespitst op het onderzoeken van het minder conventionele solventsysteem azijnzuur/mierenzuur als een niet-toxisch alternatief voor het verkrijgen van ultradunne PCL vezels met een range van diameters en variërende alignering. Na een diepgaande analyse van verschillende types collectoren, inclusief bewegingssnelheid werd er geopteerd om een nieuwe collector te ontwerpen die sterk gealigneerde vezels kon produceren dankzij een synchroon samenwerken van mechanische en elektrische effecten. In een volgende stap werd de vezeldiameter gevarieerd met behulp van 3 parameters: 1) de polymeerconcentratie; 2) de naald-collectorafstand en

3) de vochtigheidsgraad. Het afstellen van deze parameters resulteerde in vezeldiameters tussen de 94 en 1548 nm en 114 tot 1408 nm voor respectievelijk willekeurige en gealigneerde vezelstructuren. De gegenereerde vezels werden vervolgens in een vierde experimentele hoofdstuk gebruikt om de synergetische effecten van vezelgrootte, oriëntatie en oppervlaktechemie op de interactie met vetstamcellen te bestuderen. Ondanks het inbouwen van dezelfde hoeveelheid aan polaire groepen voor alle samples, bleek de graad van hydrofiel zijn sterk af te hangen van vezelgrootte en oriëntatie. Deze resultaten benadrukten nogmaals de grote invloed van de vezeltopografie op de bevochtigingsgraad. Langdurige blootstelling aan plasma resulteerde in schade aan de vezels met een toenemend risico op veranderingen van de bulkeigenschappen. De sterk verschillende respons op plasma vindt zijn origine in hoe de moleculaire ketens zich oriënteren en de graad van kristalliniteit. De resultaten toonden aan dat de plasmabehandelingen verantwoordelijk waren voor een verbeterde celmetabolische activiteit, een verbeterde adhesie en proliferatie alsook een stimulatie van de cytoplastische hervorming van alle samples. Cellen hechtten zich multidirectioneel op de random georiënteerde vezels met een graduele transitie naar een meer uitgerekte vorm met toenemende vezeldiameters. Erwerd vastgesteld bij de vetstamcellen dat deze zich overstrekten in een bepaalde richting en dat op gealigneerde vezels ze zich minder goed hechtten wanneer de vezeldiameter toenam. Het nabootsen van de Bügnerbanden werd waargenomen wanneer de mate van alignering toenam wat deze vezels excellente kandidaten maakte voor zenuwregeneratietoepassingen.

Het laatste experimentele hoofdstuk spitste zich toe op het fabriceren van ZG's met geoptimaliseerde spinparameters wat leidde tot een duaal-gelaagde structuur. De binnenwand was samengesteld uit gealigneerde vezelbundels die neuriet uitgroei en Schwanncel uitrekking moet stimuleren. De buitenwand bestond uit random afgezette nanovezels die voor een verbeterde ingroei moesten zorgen in de directe omgeving. 2 verschillende plasmamodificatiestrategieën werden afgetoetst: De eerste, een medium druk parallele plaat DBD reactor werd gebruikt om de binnenwanden van de ZG homogeen te behandelen, wat leidde tot een toename van de elementaire zuurstof met 11%. De tweede, een atmosferische PJ, werd gebruikt om een gradient te introduceren doorheen de ZG wat resulteerde in een graduele toename in elementaire zuurstof van 21% tot 30%. Voor de plasmabehandelde ZG's werd er een significante toename vastgesteld in Schwannceladhesie in vergelijking met onbehandelde ZG's. Voor de gradient scaffolds werd vastgesteld dat dit leidde tot een celgradiënt. Voor langere celincubatietijden werd de celgradiënt meer uitgesproken dankzij een betere celproliferatie aan de zuurstofrijke kant en dankzij

een gestuurde celmigratie doorheen de ZG. Een graduele verandering van meer geronde cellen naar uitgestrekte cellen werd vastgesteld, wat sterk leek op het gedrag vastgesteld bij een Bügnerstructuurstructuur. In het laatste gedeelte van deze thesis werd er aandacht besteed aan het uitzaaien van PC12 cellen op ZG's waar reeds Schwanncellen op uitgezaaid waren. Hierbij werd vastgesteld dat enkel voor de plasmabehandelde stalen er sprake was van neurietuitgroei: Voor de DBD behandelde ZG's werden er relatief korte neurieten vastgesteld die zich uitspreidden in alle richtingen. Voor de PJ behandelde ZG's werden er gradueel langere neurieten geobserveerd die zich voornamelijk oriënteerden in de richting van de zuurstofrijke kant van de ZG.

In het algemeen kan er vastgesteld worden dat het gecombineerd gebruik van electrospinnen met niet-thermische plasmatechnologie voor ZG-fabricatie uitstekend potentieel toont voor het verbeteren van perifere zenuwregeneratie. Voornamelijk de plasma-geïnduceerde gradiënt lijkt veelbelovend voor het overbruggen van langere zenuwonderbrekingen, garanderend een compleet functioneel herstel. In de toekomst, de translatie van *in-vitro* naar *in-vivo* is de volgende horde die moet genomen worden om tot het klinisch gebruik van plasma behandelde ZG's te komem

Acknowledgements

Four years ago, I packed my bag, left my country and started the journey within RUPT group. It was a wonderful and unforgettable adventure that led to the present PhD dissertation. Next to the efforts of my hands and gray matter, a lot of helping hands, firing brains but also caring and supportive hearts were involved in crossing the obstacles along the way and reaching the destination. I hope to be able to express, through my next words, at least a part of my unlimited gratitude.

In the first place, I am extremely grateful to Prof. Rino Morent for giving me, as a biologist, the great opportunity to pursue a PhD in Engineering Physics. He and Prof. Nathalie De Geyter provided me with the keys to success, progression and high-quality maintenance of my research through their special guidance, worthwhile advices and refined experimental ideas. Additionally, an exceptional "thank you" goes to them for offering me the chance to present my research in several international conferences around the world.

I would like to express my sincere appreciation to my successive co-promotors Prof. Ria Cornelissen and Dr. Heidi Declercq for their useful instructions, help and precious biological feedback. A special gratitude goes to Dr. Charlot Philips for all the cell work she performed all over the last 4 years. Her distinctive skills were indispensable for the successful realization of the present research. It was a great pleasure and comfort working with her.

A profound thankfulness goes to Prof. Christophe Leys, head of the Department of Applied Physics where my PhD took place. I was honored by his acceptance together with Prof. Jean-Michel Pouvesle, Prof. Andre Skirtach, Prof. Alexander Van Tongel and Dr. Rim Bitar to be members of my PhD examination board. I am grateful for the time they spent in reading my thesis.

The secret of a happy workspace is being surrounded by awesome people like my colleagues. I wish to sincerely thank them one by one for their daily support and specialized help based on their different fields of expertise, which made this interdisciplinary study more fruitful. Chance made us colleagues but all the good times we spent in and outside the lab and the nice memories we shared made us friends.

I would like to specifically recognize the efforts of the technical staff Joris Peelman and Tim Poelman who were always ready to help by immediately solving all technical problems and ensuring a faster continuation of the experiments.

One of the most appealing period during my PhD was my 5-month research stay in MERLN Institute of Maastricht University. From the very first day, everyone made me feel very welcomed and was there to help me with anything I needed. I would like to express a deep gratitude to Prof. Lorenzo Moroni who gave me access to all facilities of the different labs and fueled my research with his unique expertise, useful instructions and inspiring discussions. A big "thank you" goes to Dr. Paul Wieringa for the rigorous training he offered me, his day-to-day guidance and his carefulness to maintain a very high research level. The numerous skills I acquired led to the results presented in Chapter XI of this PhD dissertation.

Countless thanks go to my dear fiends Rim Bitar, Gaelle Aziz and Elie Merhej. I will always recall with a big smile all the fantastic memories we shared and tell the funny stories we went through. You turned every difficult moment of living abroad into a nice adventure full of laughter. You provided me with non-stop support and relief every time I needed them.

To the endless source of love, encouragement, reassurance, motivation and support, my father Raymond, my mother May, my brother Elie, my uncles and my beloved cousins, a "thank you" from the deepest recesses of my heart. Your presence by my side in every single step of the way was the direct reason of my perseverance and constituted the crucial pillars on which my dissertation stands. I am very blessed to have you in my life and I dedicate these pages to you in particular.

Albert Einstein was totally right by saying: "The more I study science, the more I believe in God". I wish to thank God for giving me the strength to achieve my goals and for surrounding me with people believing in my capacities.

List of Acronyms and Abbreviations

A

AC: Acetic Acid
Aam: Allylamine
Aac: Acrylic Acid
ADSC: Adipose Derived Stem Cell
AEO: 2-(2-Aminoethoxy)ethanol
ALP: Alkaline Phosphatase
APPJ: Atmospheric Pressure Plasma Jet
ARXPS: Angle Resolved X-ray Photoelectron Spectroscopy

B

BAEC: Bovine Aorta Endothelial Cell
BMDSC: Bone marrow Derived Mesenchymal Stem Cell
BSMC: Bovine Smooth Muscles Cell

C

CMNB: 5-Carboxymethoxy-2-nitrobenzyl
CSS: Cholesteryl Succinyl Silane

D

DBD: Dielectric Barrier Discharge
DCM: Dichloromethane
DG: Diethylene Glycol dimethyl ether
DMF: Dimethylformamide
DRG: Dorsal Root Ganglia
DTA: Diethylnetriamine

E

ECs: Endothelial Cells
ECM: Extracellular Matrix

EDC/NHS: 1-ethyl-3-(3-dimethylaminopropyl) carbodiimide/N-hydroxysuccinimide
EtO: Ethylene Oxide

F

FA: Formic Acid
FBS: Fetal Bovine Serum
FCS: Foetal Calf Serum
FGF 4: Fibroblast Growth Factor 4
FITC: Fluorescein Isothiocyanate
FTIR: Fourrier transform infrared spectroscopy
FTT: fast Fourier Transform

G

GAG: Glycosaminoglycan

H

HA: Hydroxyapatite
HCAEC: Human Coronary Artery Endothelial Cell
HFP: 1,1,1,3,3,3-Hexafluoro-2-Propanol
HMDS: Hexamethyldisilazane
HP: H_2O_2 Plasma ‘
HS: Heparan Sulfate
HSP: Heat Shock Protein
HUVEC: Human Umbilical Vein Endothelial Cell

I

IgG: Immunoglobulin G

M

Me.PEG-PLA: Poly (D,L-Lactic Acid)-Poly(Ethylene Gycol)-Monometyl ether diblock copolymer
MSC: Mesenchymal Stem Cell

MTS: 3-(4,5-dimethylthiazol-2-yl)-5-(3-carboxymethoxyphenyl)-2-(4 sulfophenyl)-2H-tetrazolium
MTT: 3-(4,5-dimethylthiazol-2-yl)-2,5-diphenyltetrazolium bromide
MW: Microwave MW

N

NGC: Nerve Guidance Conduit
NSC: Nerve Stem Cell

O

OC: Octodiene

P

PA: Polyactive®
PBS: Phosphate Buffered Saline
PC 12: Pheochromocytoma
PCL: Polycaprolactone
PCLA: Poly(ε-caprolactone)-block-poly(L-lactic acid-*co*-ε-caprolactone)
PDLLA: Poly(D,L-lactic Acid)
PDMS: Polydimethylsiloxane
PE: Polyethylene
PEG: Poly(Ethylene Glycol)
PEO: Polyethylene Oxide
PGA:Polyglycolic Acid
PGS: Poly (Glycerol-co-Sebacic acid) PLA: Polylactic Acid
PLCL: Polylactide-Caprolactone
PLGA: Poly(lactic-co-glycolic acid)
PLLA: Poly (L-lactide)
PLLA-CL: Poly(L-Lactide-co-ε-Caprolactone)
PEOT-PBT: Poly(Ethylene Oxide Terephthalate)-Poly(Buylene Terephthalate)
PG: Polyethylene Glycol
PGS: Poly (Glycerol-co-Sebacic acid)
PJ: Plasma Jet
PMMA: poly(methyl methacrylate)
PNI: Peripheral Nerve Injury

PSC: Pluripotent Stem Cell
PU: Polyurethane

Q

Q-dot: Quantum Dots
qRT-PCR: Quantitative Reverse Transcription–Polymerase Chain Reaction

R

RF: Radiofrequency
RH: Relative Humidity
ROS: Reactive Oxygen Species
RS: Rotational Speed

S

SAM: Self-Assembled Monolayers
SAV: Streptavidin
SC: Schwann Cell
SEM: Scanning Electron Microscopy
SEP: Soluble Eggshell membrane Proteins

T

TCD: Tip-to-Collector Distance
TE: Tissue Engineering
TFBA: trifluoromethyl benzaldehyde
THF: Tetrahydrofuran

U

UV: Ultraviolet

W

WCA: Water Contact Angle

X

X-ray Photoelectron Spectroscopy

List of publications

A.1 International journal publications

(1) **Ghobeira, R.**, Philips, C., Declercq, H., Cools, P., De Geyter, N., Cornelissen, R. & Morent, R.
Effects of different sterilization methods on the physico-chemical and bioresponsive properties of plasma-treated polycaprolactone films
Biomedical Materials, *12* (1): 015017 (2017).
IF 2017: 2.897; Q2

(2) **Ghobeira, R.**, Philips, C., De Naeyer, V., Declercq, H., Cools, P., De Geyter, N., Cornelissen R. & Morent, R.
Comparative study of the surface properties and cytocompatibility of plasma-treated PCL nanofibers subjected to different sterilization methods
Journal of Biomedical Nanotechnology, 13(6): 699-716 (2017).
IF 2017: 5.068; Q1

(3) De Jaeghere, P., De Vlieghere, E., Van Hoorick, J., Van Vlierberghe, S., Wagemans, G., Pieters, L., Melsens, E., Praet, M., Van Dorpe, J., Van Hoorebeke, L., **Ghobeira, R.**, De Geyter, N., Bracke, M., Vanhove, C., Neyt, S., Berx, G., De Geest, B., Dubruel, P., Declercq, H., Ceelen, W. & De Wever, O.
Heterocellular 3D scaffolds as biomimetic to recapitulate the tumor microenvironment of peritoneal metastases in vitro and in vivo
Biomaterials, 158(2018): 95-105 (2017).
IF 2017: 8.806; Q1

(4) Cools, P., Mota, C., Lorenzo-Moldero, L., **Ghobeira, R.**, De Geyter, N., Moroni, L. & Morent, R.
Acrylic acid plasma coated 3D printed scaffolds for improved cartilage regeneration
Scientific Reports, 8:3830 (2018).
IF 2017: 4.122; Q1

(5) Cools, P., Declercq, H., **Ghobeira, R.**, Morent, R. & De Geyter, N.
Acrylic acid plasma coatings for enhanced cell migration in PCL 3D additive manufactured scaffolds
Surface and Coatings Technology, 350(2018): 925-935 (2018)
IF 2017: 2.906; Q1

(6) **Ghobeira, R.**, Asadian, M., Vercruysse, C., Declercq, H., De Geyter, N. & Morent, R.
Wide-ranging fiber diameter scale of random and highly aligned PCL fibers electrospun using controlled working parameters
Polymer, 157(2018): 19-31 (2018).
IF 2017: 3.483; Q1

(7) **Ghobeira, R.**, Philips, C., Liefooghe, L., Verdonck, M., Asadian, M., Cools, P., Declercq, H., De Vos, W., De Geyter, N. & Morent, R.
Synergetic effect of electrospun PCL fiber size, orientation and plasma-modified surface chemistry on stem cell behavior
Applied Surface Science, 485(2019): 204-221 (2019).
IF 2017: 4.439; Q1

(8) Bar, C., **Ghobeira, R.**, Nabbout Azzi, R., Ville, D., Riquet, A., Tourraine, R., Chemaly, N. & Nabbout, R.
Perception of transition and follow-up from pediatric to adult health care of patients with Tuberous Sclerosis Complex with childhood epilepsies.
Epilepsy and Behavior, 96(2019): 23-27 (2019).
IF 2017: 2.6; Q2

B.2 Book chapters

(1) Cools, P., **Ghobeira, R.**, Van Vrekhem, S., De Geyter, N. & Morent, R.
Non-thermal plasma technology for the improvement of scaffolds for tissue engineering and regenerative medicine: a review
Book title: Plasma science and technology: progress in physical states and chemical reactions
Pag: 173-212
Ed: Tetsu Mieno
Publ: Intech, Rijeka, Croatia (2016).

(2) **Ghobeira, R.**, De Geyter, N. & Morent, R.
Plasma surface functionalization of biodegradable electrospun scaffolds for tissue engineering applications
Book title: Biodegradable polymers: recent developments and new perspectives
Pag: 191-236
Ed: Geraldine Rohman
Publ: IAPC, Zagreb, Croatia (2017).

(3) Aziz, G., **Ghobeira, R**., Morent, R. & De Geyter, N.
Plasma polymerization for tissue engineering purposes
Book title: Polymerization
Pag: 69-93
Ed: Nevin Çankaya
Publ: Intech, Rijeka, Croatia (2018)

C.4 Active conference participations

(1) Annual Meeting of the Belgian Society for Microscopy-When Materials Meet Biology, Mons University, Belgium. (2015)
"Poster presentation"

(2) 10th Asian-European International Conference on Plasma Surface Engineering, Jeju Island, Korea. (2015)
"Oral presentation"

(3) 2nd International Workshop on Plasma and micro structures, Ghent University, Belgium. (2015)
"Poster presentation"

(4) 20th International Vacuum Congress, Busan, Korea. (2016)
"Poster presentation"

(5) 44th International Conference on Plasma Science, Atlantic City, USA. (2017)
"Oral presentation"

(6) Nanomaterials in Biomedical Sciences, F-tales Workshop, Ghent, Belgium. (2017)
"Oral and poster presentations"

(7) 5th Nano Today Conference, Hawaii, USA. (2017)
“Poster presentation”

(8) Cold Plasma Sources and Applications Conference, Ypres, Belgium (2018)
"Poster presentation"

Doctoral training program

Courses

(1) Plasma Technology and Fusion Technology

(2) Surface Analysis

(3) Doctoral Course on Mathematical Techniques for Engineering Science

Seminars

(1) Introduction Day for new PhD students 2015

(2) Advanced Academic English: Conference Skills - Effective Slide Design

(3) Effective professional networking

(4) Grant writing workshop (Grant wining day)

TABLE OF CONTENTS

Chapter I: Introduction

I.1. Peripheral nerve injury

Peripheral nerve injury (PNI) is, up to the minute, a substantial clinical problem mainly affecting young individuals leaving them with potentially devastating life-lasting consequences [1-4]. The incidence of PNI is extensively high with some alerting numbers. For instance, PNI affects millions of people worldwide with over 100 000 peripheral nerve surgeries performed annually in the United States and Europe alone [1, 3]. Approximations from retrospective studies reveal that over one million and around 360 000 patients in the United States, suffer yearly from serious impairments associated with lower limb trauma and upper paralytic syndromes respectively [5, 6]. Moreover, it is estimated that over 300 000 PNI cases occur annually in Europe [6, 7]. This is due to the common exposition of the peripheral nerves to physical, chemical, thermal and/or ischemic damages mostly caused by traumatic accidents or degenerative disorders [2, 6]. In fact, peripheral nerves are not protected like the brain and the spinal cord by the spine bone, skull and brain-blood barrier, making them vulnerable to damage at any anatomic site. The severity of the injury and the specific sensory, motor or autonomic nerves it affects govern the functional outcome [8]. Luckily, unlike the central nervous system having a very limited to no capacity of intrinsic regeneration, the peripheral nervous system is marked by its regenerative machinery initiating nerve repair up to a certain extent [7]. However, the complex pathophysiological processes involved in PNI make the spontaneous regeneration not always sufficient to ensure functional recovery. Therefore, interventions to achieve an effective repair are in most cases unavoidable [6, 9]. Nowadays, many treated patients continue to present long-term incomplete recovery characterized by partial or complete loss of motor function, impaired sensation, failure of autonomic function and intractable neuropathic pain [3, 6]. The choice of the "best" therapeutic procedure to be followed depends on the degree of nerve injury. For a better understanding of the different injury degrees, the anatomy of a nerve should be first identified. Peripheral nerves consist of bundles of nerve fibers forming fascicles surrounded by blood vessels. Each fiber is enveloped, with its supporting Schwann cells (SCs), by a loose connective tissue called endoneurium. The fibers in a fascicle are maintained by collagen fibrils and ensheathed by a dense connective

tissue, the perineurium. The whole nerve is enclosed by an irregular and dense connective tissue known as epineurium (Fig.I.1) [2, 10].

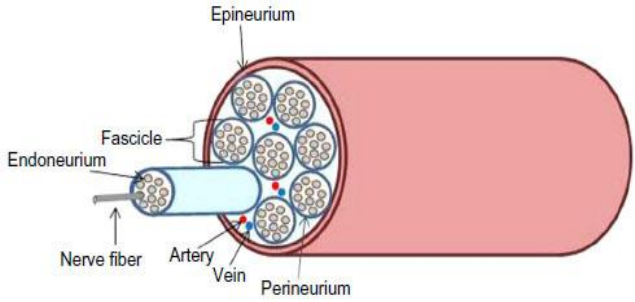

Fig. I.1. *Anatomy of a peripheral nerve [2].*

In 1943, Seddon was the first to describe 3 categories of nerve injuries based on the damage severity of the connective tissue and the axons: neurapraxia, axonotmesis and neurotmesis. Few years later, Sunderland added 2 intermediate categories and classified the injuries as first to fifth degree injuries. In the first-degree injury, corresponding to neurapraxia, the axons and connective tissue remain intact but a focal demyelination occurs threatening the impulse transmissions. Such injuries are restored within a few months without the need of a treatment. In the second-degree injury, corresponding to axonotmesis, SCs and the endoneurium are not damaged but axons are severed. The intact endoneurial tube helps the regeneration without surgical interventions. In the third-degree injury, the endoneurium is potentially disrupted leading to fibrosis and considerably delayed functional recovery. The fourth-degree injury is distinguished by disrupted axons, endoneurium and perineurium with an intact epineurium. A greater degree of degeneration takes place in comparison to lower-degree injuries. In this case, a surgical intervention removing the scar tissue and repairing the nerve may be required to accomplish a successful regeneration. The fifth-degree injury, corresponding to neurotmesis, is marked by a complete transection of the nerve trunk followed by scar formation, neuroma and degeneration at the distal and proximal ends making the surgical repair inevitable (Fig.I.2) [4, 11, 12].

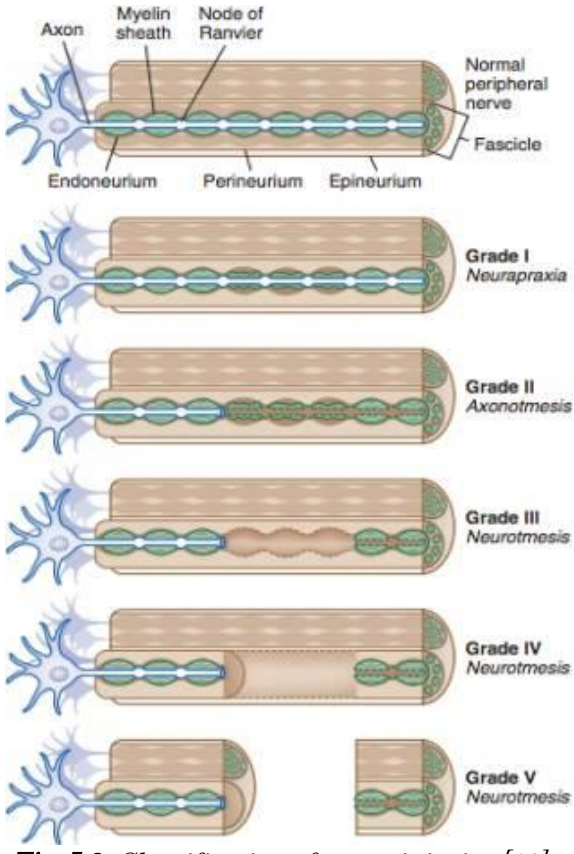

Fig. I.2. *Classification of nerve injuries [12].*

I.2. Traditional therapeutic approaches

Given the harsh impact of PNI on the patient and the society at large, clinical interventions started to be performed early in the 17th century when Ferrara first documented a suture technique for the repair of a severed nerve (1608) [13]. In 1864, Mitchell et al. inspected PNI during the Civil war and advocated suturing for a torn nerve and amputation in critical injuries [14]. In the first and the second world wars, nerve repair was extensively promoted and many surgical procedures were put into use. Despite the great efforts, poor functional recovery and amputation in case of severe injury continued to be observed [15, 16]. Therefore, a plethora of researchers started elucidating the pathophysiological processes in PNI in order to improve the therapeutic procedures. In the last 3 decades, a steep rise in the PNI literature was

thus observed, classifying the surgical procedures into two main categories: manipulative peripheral nerve operations and bridging operations (Fig. I.3) [7].

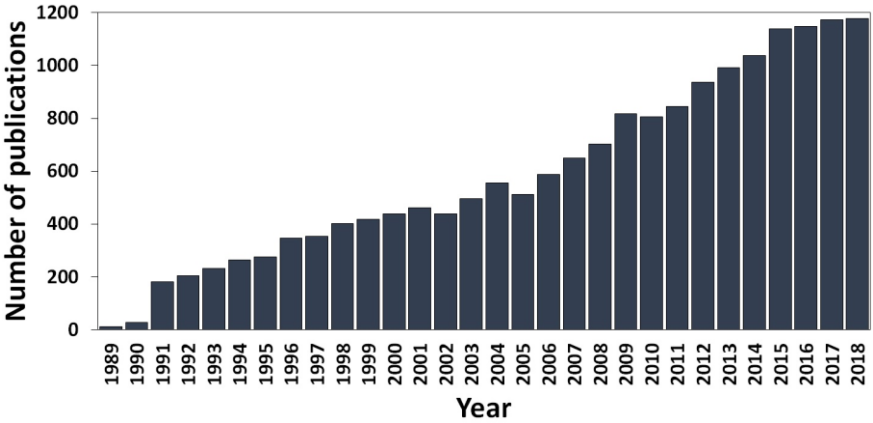

Fig. I.3. *Number of publications implicating peripheral nerve injuries during the last 3 decades (Source: Web of Science®, topic keyword used during the search: "peripheral nerve injuries").*

I.2.1. Manipulative nerve operations

The manipulative nerve techniques include the direct repair and the nerve transfer. These operations are only performed in case of clean-cut transection without tissue loss for a possible tension-free approximation. The direct nerve repair also known as neurorrhaphy refers to the suturing of the proximal and distal nerve parts via end-to-end coaptations in a way ensuring a lining up of the internal nerve fascicles and blood vessels. Nerve transfer, so-called neurotization, corresponds to the relocation of nerves or nerve branches with less important functions to reestablish the more crucial function of the severed nerve. Overall, the end-to-end suturing is by far the preferred method for surgical peripheral nerve interventions. However, it is only limited to very short nerve gaps as the fascicular coaptation can lead to unwanted tension over the suturing line, thus hindering nerve regeneration [1, 3, 7].

I.2.2. Bridging operations

In the frequent cases involving bigger nerve gaps and precluded from manipulative nerve operations, the interposition of a supportive structure as a bridge between the distal and proximal nerve ends is necessary to span the injured site. The most widely used bridging strategy is the autologous nerve graft that is currently considered the gold standard and has stayed so all along the previous 50 years [1, 2]. Functionally less vital nerves, such as superficial cutaneous nerves, sural nerves or medial and lateral antebrachii nerves, are normally selected as donor sites and self-donated as autografts [7, 17]. These grafts provide viable SCs, appropriate neurotrophic factors and the natural structural guidance essential for axonal extension from the proximal to the distal nerve end [3, 18, 19]. Despite being the gold standard compared to other treatments, the autografting stays unfortunately limited by a number of weighty drawbacks confining the success rate to only 50% of the treated patients. First, given the inaccessibility of motor nerves, only sensory nerves are used as grafts which constitutes one of the main reasons behind the poor functional recovery rates in the repair of pure motor nerve injuries. Some studies have indeed shown that motor and sensory neurons display different modalities of SCs that can limit the regenerative capacity if placed in the wrong microenvironment [1, 20]. Moreover, the very restricted sources of donor nerves lead to morphometric differences with the injured nerve such as mismatches in axonal and fascicular size, pattern, alignment and distribution. In addition to this, the harvested nerve graft undergoes a degeneration thus merely providing a mechanical guidance for the regenerating axons. Secondary to these limitations, sacrificing a functional nerve causes a sensory loss at the donor site as well as scarring, neuroma formation and pain. An extra surgical step caused by painful neuromas is possibly required on top of the two surgical procedures primarily performed at the donor and repair sites. Fibrosis from suturing and damage from tissue handling are in most of the cases unavoidable at the repair site. Lastly, autografts are constrained to a nerve gap length of approximately 5 cm and over this distance, the use of allografts can be an alternative [4, 18, 21-23]. Nerve allograft is another bridge operation that is readily available with limitless supply of neural tissue and without donor-site morbidity consequences. However, next to the high cost of allografts, an extensive systemic immunosuppression is required up to 18 months post graft implantation resulting in opportunistic infections and

potential tumor formation [2, 3, 17]. The limitations associated with these grafting techniques have led researchers to consider and explore inventive tissue engineering alternatives in order to address the challenging peripheral nerve repair.

I.3. Nerve tissue engineering: guidance conduits

The warning drawbacks of autografts resulted, after extensive investigations, in the development of nerve guidance conduits (NGCs) as substitutes for nerve repair [21, 22]. Tubular nerve grafts were originally proposed as early as 1879, with a first application involving the use of a hollow bone tube as NGC. The experiment failed because of scar formation [24]. Afterwards, different forms of biological and artificial nerve conduits have been developed but all showed very poor outcome in comparison to nerve autografts [16, 22]. In the last few decades, tissue engineering (TE), an expanding multidisciplinary field, has advanced at a considerable rate. This modern discipline has offered great opportunities and has facilitated the work of neurobiologists and surgeons who have been cooperating to develop effective tissue engineered NGCs. Just as most scaffolds used in different TE applications, NGCs typically consist of a physical scaffolding made up of natural or synthetic polymeric material possibly amalgamated with growth factors, biomolecular components or support cells [7]. Several advantages are associated with the use of such manufactured nerve grafts that serve to: 1) guide axonal sprouting from the proximal nerve stump to the distal end and help SCs to form bands of Büngner; 2) maintain appropriate mechanical and physical support for the re-growing nerves; 3) afford a channel for the accumulation of neurotropic and neurotrophic factors secreted by the injured nerve stump; 4) provide a conduit wall for the bi-directional exchange of nutrient supply and waste products; 5) hamper the infiltration of myofibroblasts that obviate nerve regeneration; 6) reduce scarring and neuroma formation 7) prevent collateral sprouting; 8) protect the regenerating nerve against compression by the neighboring tissues and 9) allow the neovascularization to take place [2, 3, 7, 25]. Given these benefits, the clinical use of hollow NGCs has been currently approved as alternative to autograft repair. The clinically translated NGCs are mainly fabricated from collagen extracted from animals or synthetic polymers such as polycaprolactone (PCL), polyglycolic acid (PGA), polylactide-caprolactone (PLCL) and different combinations of PGA and PLCL [1,

17]. Despite attaining some success in nerve regeneration, these hollow conduits are still failing to meet the regenerative capacity of autograft and are therefore showing very poor functional recovery. Early trials to improve NGCs involved some variations in the base material and the conduit design. Unnoticeable enhancements in functional recovery followed, pointing out that crucial elements still need to be fulfilled in the use of hollow NGCs alone [3, 26, 27].

I.3.1. Peripheral nerve regeneration inside a hollow nerve conduit

Understanding the regenerative sequence taking place within a NGC is essential to further improve peripheral nerve scaffolds. Five main phases underline the process:

1) The fluid phase: an inflow of plasma exudate emerging from both the distal and the proximal nerve ends and containing extracellular matrix (ECM) precursor biomolecules and neurotrophic factors accumulates within the conduit.
2) The matrix phase: the secreted ECM precursors form a cell-free fibrin cable between the 2 nerve stumps, serving as a bridge for the next regeneration stage
3) The cellular phase: SCs, fibroblasts and endothelial cells migrate from both nerve stumps along the fibrin cable turning it into a cellular cable. Afterwards, SCs proliferate and elongate forming an aligned glial cable so-called bands of Bùngner. This tissue provides tropic and trophic supports for the following phases.
4) The axonal phase: re-growing axonal sprouts, driven by their growth cone are guided by the biological cable to reach the distal target. It is worth mentioning that the fibrin cable, having a limited degradation time, disintegrates after fulfilling its role in cellular guidance and migration.
5) The myelination phase: SCs switch from proliferative phenotype to a more mature "myelinating" phenotype. The new nature of SCs leads to the formation of myelin sheath around the large regenerating axons, thus initiating some functional recovery of the nerve fibers (Fig. I.4) [1, 17, 28].

This regenerative succession was shown to occur in hollow NGCs used to bridge nerve gaps of maximum 4.0 cm in humans and 1.5 cm in rats (sciatic nerve model). The regeneration becomes very limited or completely absent in bigger gaps and functional repair remains deficient across all nerve gap dimensions [29-32].

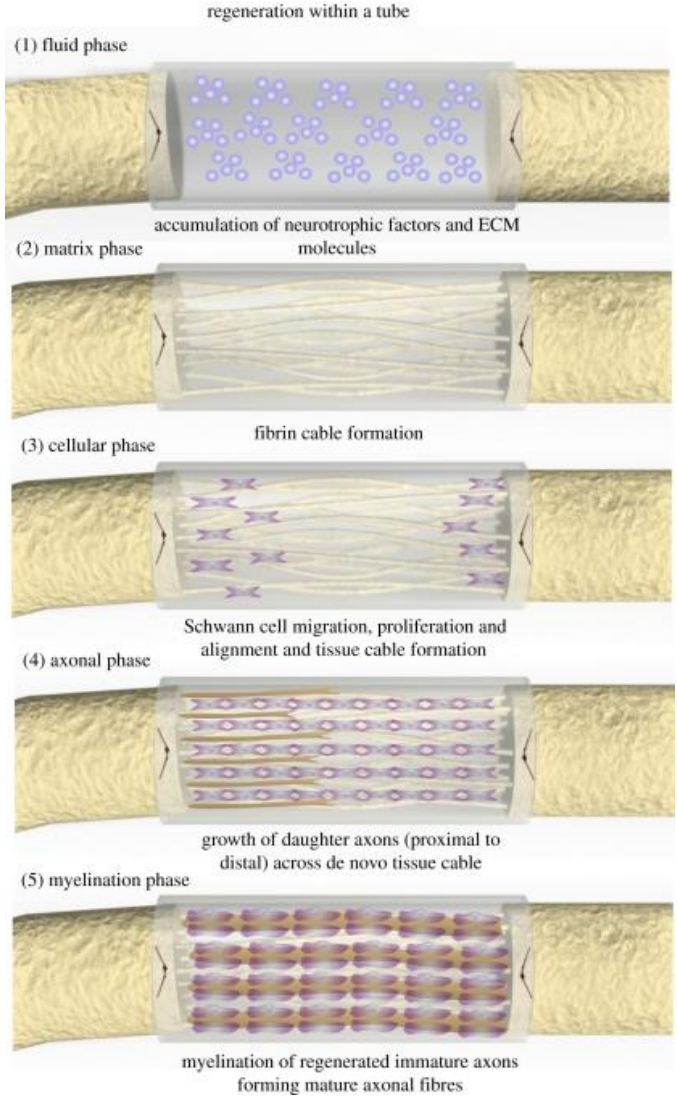

Fig. I.4. *Peripheral nerve regenerative phases occurring inside a hollow NGC [1].*

I.3.2. Innovative approaches for improved nerve regeneration

The mediocre levels of regeneration within the conventional hollow NGCs, particularly across large nerve gaps, can be attributed to the deficient accumulation of ECM precursors during the fluid phase. This undersupply can lead to an inadequate formation of the fibrin cable, indispensable for cell migration and subsequent bands of Bùngner development. In attempts to mimic and replace the topographical guidance offered by this ECM cable, several inventive strategies focused on adding structural cues or changing the whole conduit design were implemented [1, 27]. Nevertheless, the perfected regeneration that may be induced by refining the structural features is not enough to improve the functional recovery in both short and critical nerve gaps. In addition to the poor ECM formation that might occur in early stages, a variety of other challenging factors can affect the process such as: insufficient SCs numbers, limited neurotrophic support with decreased effects at the distal nerve end and inadequate SC proliferation and migration. Molecular and/or cellular cues should therefore be complemented to the structural cues for the creation of a more bioconductive microenvironment ensuring a robust functional recovery [7, 30, 33]. In what follows, the innovative structural, molecular and cellular strategies that are currently used to improve NGCs will be listed (Fig. I.5).

I.3.2.1. Structural cues

- Intra-luminal guidance fillers: Intra-luminal filaments, sponges, gels and microfibers have been added to the NGCs to replace the unformed or partially formed fibrin cable or act as extra anchor for its development [3, 6, 27, 32]. Examples of such fillers include bundles of collagen fibers, poly (L-lactide) (PLLA) microfilaments, poly(lactic-co-glycolic acid) (PLGA), fibers, collagen sponges and fibrous keratin hydrogels [6, 34-38]. Few studies showed that gaps of 2 cm were well bridged but functional reestablishment stayed trivial [1, 39]. Nevertheless, some researchers highlighted an important challenging consideration: the "packing density" or "void fraction". At low densities, the fillers settle at the conduit bottom, while at high densities, the regeneration is inhibited. This inhibition was observed in many studies using for instance PLLA microfilaments, dense collagen sponges and juxtaposed fibers [36, 40, 41]. Another limitation in the use of the

current intraluminal structures is their slow degradation rate. These fillers are only beneficial at early stages of regeneration after which they start to hamper nerve growth and create axon and SC-depleted areas [29, 36, 42]. Therefore a short degradation time is required but leads to another issue related to the increase in toxicity levels [1, 43].

- Conduit wall guidance structures: In order to enhance NGC porosity and/or cell guided migration, physical guidance features ranging from micrometer scale to a more biomimetic nanometer scale are considered in the design of the luminal wall. These alterations involve the inclusion of longitudinal micro-grooves or channels on the inner wall or the creation of a wall completely composed of aligned or randomly-oriented electrospun micro or nanofibers [1, 22, 27]. Promoted guidance effect and alignment of the re-growing neurons were detected after introducing these wall characteristics. For instance, micro-channeled poly(D,L-lactic acid) (PDLLA) and collagen-chitosan conduits showed an enhanced nerve regeneration across nerve gaps of 1.5 cm in comparison to their non-grooved counterparts [44, 45]. These microstructures have approximately similar sizes as axon diameters or cells but are incapable of supporting the sub-cellular pathways controlled by the ECM. Therefore, electrospun conduits offering several advantages over continuous and grooved wall strategies were introduced: 1) NCGs become porous safeguarding for an efficient nutrient supply; 2) electrospun scaffolds are highly flexible and thus well adapted to be used within histological bio-environments; 3) micro and nanofibers are characterized by their elevated surface-to-volume ratio creating more area for cell adhesion and 4) fibers can be easily aligned which results in an improved SC elongation, migration and proliferation promoting guided axonal regeneration [1, 6, 22, 46, 47]. Moreover, the issue of uneven fiber dispersion seen in case of low-density intra-luminal fillers is avoided when using wall guidance [36, 47]. Likewise, the potential regeneration inhibition occurring in response to overlapping and high-density fillers is also eliminated [29, 36, 41]. *In vivo* tests using PCL/collagen, PCL, caprolactone/ethyl ethylene phosphate (PCLEEP), silk fibroin poly(L-lactic acid-co-ε-caprolactone (P(LLA-CL) and poly(ethylene oxide terephthalate)/poly(butylene terephthalate) (PEOT/PBT) fibrous conduits showed enhanced functional nerve regeneration in nerve gaps of 8mm, 14 mm, 15 mm, 10 mm and 15 mm respectively [19, 21, 47-49]. Despite accomplishing some functional recovery, electrospun NGCs are still failing in attaining the autograft outcome and bridging longer gaps.

➢ Variations in the overall conduit design: In an attempt to mimic the micro-architecture of a native nerve and improve nerve regeneration, multi-channel conduits were designed [1, 50, 51]. Nonetheless, PLGA and collagen multi-channel NGCs did not show any significant differences compared to single channel NGCs in terms of nerve regeneration. The only visible advantage of such multi-channel conduits was the decrease in axonal misdirection and dispersion compared to the control conduits [50-52]. However, an important limitation of this design is the possible occlusion of the channels after polymer swelling thus blocking the axon regrowth [52].

I.3.2.1. Molecular and cellular cues

➢ Neurotrophic factors: Since nerve regeneration is not only modulated by complex interactions between the fibrous ECM and cells but also by neurotrophic factors, such factors were added to NGCs [7]. Growth biomolecules are expected to improve functional regeneration by reinforcing axonal growth, supporting SC performances and enhancing neuroprotection via receptor-mediated initiation of specific signaling pathways [1, 53]. The factors commonly used in nerve TE mainly belong to 3 different families: 1) the neurotrophins including nerve growth factor (NGF), neurotrophin 3 (NT3) and brain-derived neurotrophic factor (BDNF); 2) the glial cell line-derived neurotrophic factor family ligands (GFLs) including glial-derived neurotrophic factor (GDNF) and 3) the neuropoeitic cytokines including ciliary neurotrophic factor (CNTF) [54, 55]. Several studies incorporating these factors to NGCs have shown that NGF, GDNF and NT3 increase the number of myelinated axons, CNTF enhances axonal growth of sensory and motor neurons and BDNF accelerates nerve regeneration and reduces neuropathic pain [43, 56-59]. However, other studies have detected conflicting results leaving a question mark around the use of neurotrophic factors within NGCs [7, 60]. The reasons behind the inconsistent outcomes might be due to leakage from NGCs, inactivation of the molecules, inadequate delivery method and insufficient concentrations [1, 61]. Another more undesirable limitation associated with the use of growth factors in NGCs is the unpremeditated activation of several signaling pathways leading to adverse biological influences such as the abnormal sprouting linked to the use of NGF [1, 55].

➢ Schwann cells: As already mentioned in the nerve regeneration sequence occurring within a NGC, SC migration and proliferation taking place in the cellular phase are indispensable for a successful repair. At this stage, SCs starts secreting neurotrophic factors such as NGF, BDNF, CNTF and GDNF and their number increases up to 4-17

times compared to the number seen in a healthy nerve [1, 62]. Nonetheless, when the nerve gap reaches a critical length, SC migration, alignment and proliferation decline and SC numbers become insufficient to create a conductive environment [7, 33, 62]. Therefore, cellular-based therapies start to be considered in the treatment of critical nerve gaps. If autograft is the gold standard for PNI repair, adding autologous SCs to NGCs is similarly judged as the present gold standard for cellular-based approaches [63-66]. In addition to their active secretion of growth factors, SCs express cell adhesion molecules, build their own basal lamina and intensely assist, at a later stage, in the remyelination of growing nerve fibers [63, 66]. These advantages led some researchers to implant SCs in NGCs since they would induce a conductive microenvironment across long nerve gaps. A doubled regeneration rate was observed in SC-seeded silicon conduits compared to the control hollow conduits [67]. Fibrin-SC conduits also showed enhanced regeneration within a 10 mm nerve gap compared to the acellular conduits [66]. Early nerve regeneration was improved when polyhydroxybuturate (PHB) conduits were seeded with SCs, but late stage functional regeneration still needs to be explored [64]. Despite the positive results associated with the use of autologous SCs, a number of drawbacks needs to be pondered: cultures are difficult and time-consuming and the SC extraction from the host is potentially painful and demands the sacrifice of a nerve tissue. The use of allogenic SCs as alternative requires an immune suppression similar to that executed in case of allografts [1].

- Stem cells: In order to obviate the drawbacks of autologous and allogenic SCs, stem cells are used as an alternative cellular-based strategy. Numerous stem cell sources were considered in nerve regeneration such as embryonic stem cells, neural stem cells and human induced pluripotent stem cells. The majority of studies were focused on adipose derived stem cells (ADSCs) or bone marrow derived mesenchymal stem cells (BDMSCs) [1, 38, 68]. In opposition to other stem cells, ADSCs are abundant and easily accessible by a simple liposuction and BDMSCs are effortlessly derived by aspiration from the bone marrow of the patient. These cell types are particularly ideal for transplantation due to several reasons: 1) easy extraction; 2) rapid proliferation in culture; 3) low cost; 4) absence of ethical and political issues and 4) multilineage differentiation capacities in particular the differentiation into glial and neural cell lineages [1, 66, 69-71]. In an interesting study carried out by Oliveira et al., undifferentiated BDMSCs were suspended in a PCL NGC that was implanted in a mouse median nerve model. An enhanced angiogenesis and an upsurge in the number of myelinated axons were detected [72]. Comparably, in a study

conducted by Ding et al., a combination of undifferentiated BDMSCs and PLGA intraluminal fillers were added to a chitosan conduit and showed an increased functional recovery in a canine nerve model in comparison to the control group [38]. An enhanced functional recovery and an increase in the thickness of a rat sciatic nerve were also observed when Santiago et al. engineered a PCL NGC suspended with undifferentiated ADSCs [68]. The enhanced regeneration could be due to the multipotent nature of these stem cells and their capability to secrete several neurotrophic factors. However, the detailed mechanisms underlying nerve repair remain largely unknown because of the variability of such undifferentiated stem cells [1, 72]. Therefore, trials to differentiate ADSCs and BDMSCs into more neural and glial cell lineages via combinations of neurotrophic factors were conducted prior to their addition into NGCs. Both cell types displayed a great ability to be differentiated, in a controlled manner, into SC-like cells, having a positive influence on neurite growth [65, 66, 73]. In the case of ADSCs, the enhancement of neurite outgrowth may be accredited to their elevated secretion of NGF and BDNF [74]. In a study conducted by Di Summa et al., differentiated ADSCs and BDMSCs were injected into the lumen of fibrin glue NGCs and showed an increased regeneration length and SC migration in a rat sciatic nerve model [66]. In a succeeding study, ADSCs exhibited a significant increase in functional recovery and a nerve morphometry approaching the one of the autograft in late stages of regeneration [75]. ADSCs may thus be proven, in the near future, as a robust and valid alternative to the gold standard autologous SC use.

- Genetically modified cells: The genetic modification of SCs was carried out *ex vivo* and less frequently *in vivo* in order to produce more neurotrophic factors [1, 7]. For instance, Li et al. transfected allogenic SCs using a retrovirus encoding for GDNF overexpression. The modified SCs were filled in silicon NGCs and transplanted in a rat sciatic nerve model. A significant enhancement in nerve regeneration and myelination were observed compared to the conduits filled with unmodified SCs [76]. However, it was also found that the overexpression of GDNF via lentiviral vector leads to the trapping of the re-growing axons and the failure of adequate target innervation in the repair of injured rat sciatic nerve [77]. Further *in vivo* studies for the use of genetically modified cells are required in order to assess their possible benefits in functional nerve regeneration.

Despite all the above-mentioned innovative structural, molecular and cellular-based approaches implemented to NGCs and aiming at improving peripheral nerve regeneration, functional outcomes are still

not satisfactory. Current optimizations and combinatorial strategies merging the advantages of previous NCGs and adopting additional levels of topographical, biomolecular and cellular complexities are failing in outperforming the regeneration levels of autograft or even in attaining similar results especially in critical nerve gaps.

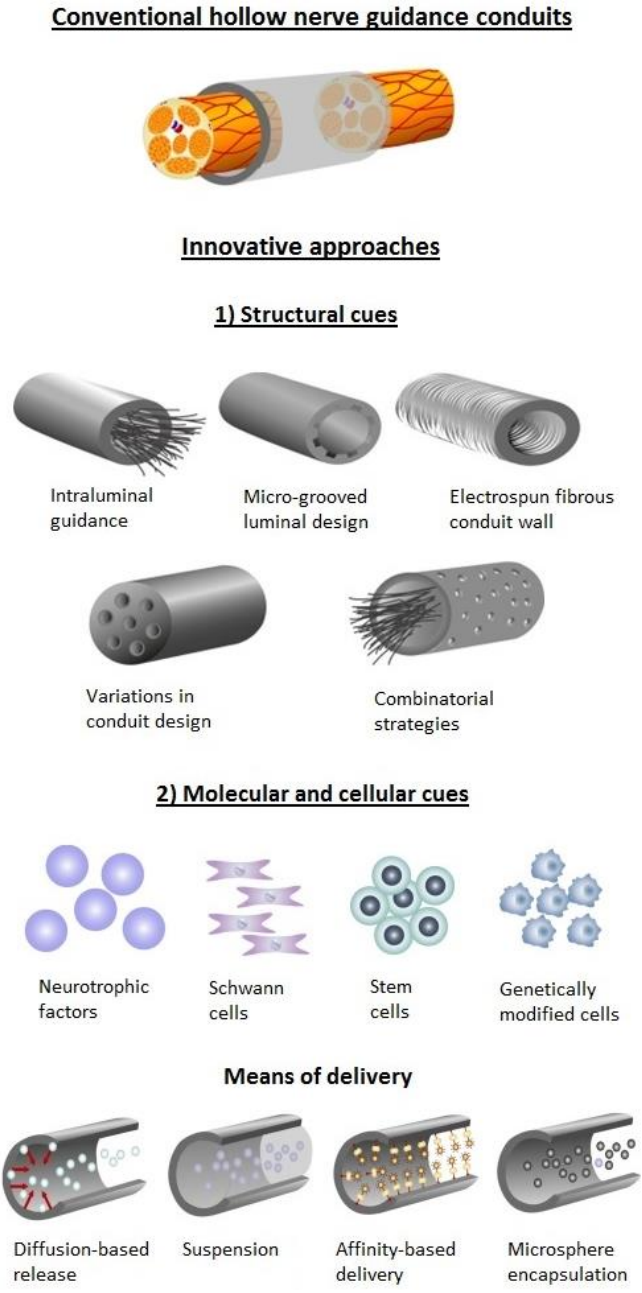

Fig. I.5. *Summarized scheme of the structural repair techniques as well as the molecular and cellular-based therapies (with their delivery strategies) used for improving conventional hollow NGCs. Adapted from [1].*

I.4. Objectives of this thesis

Acknowledging the above state-of-the-art, it becomes evident that the design of NGCs is still missing the best combination of aspects: 1) directing regeneration levels equivalent or superior to the autograft; 2) extending the regeneration beyond the current maximal nerve gap; 3) accomplishing a functional recovery approaching that of a healthy nerve and 4) acting as top-quality replacement compared to other TE approaches. Therefore, the main goal of this thesis is to tackle large nerve gaps by designing a novel NGC possessing the physical, chemical and cellular properties that recapitulate the topographical organization of the neural ECM, the mechanical performance of the neighboring tissues and the biological cues triggering a potent regenerative and cell supportive capacity.

- From a topographical point of view: Aligned and randomly-oriented nanofibers are used to fabricate the NGCs as moderate successes of nanofibrous conduits were observed over the other investigated structural cues. Next to their cell guidance contact, nanofibers are preferred over other structures for their mimicry of the neural ECM fibrillary arrangement governing a wide range of primordial cellular activities. In this dissertation, an optimized conduit configuration is targeted making use of the electrospinning as biofabrication technique. In addition to its simplicity, a major advantage of electrospinning is its ability to adapt the fiber diameter down to the nanometer scale and to adjust the fiber alignment and mesh porosity by tailoring the process parameters. Neurite outgrowth and SC migration and maturation were shown to be critically influenced by the fiber diameter and highly boosted by aligning the fibers [78-80]. Moreover, the porosity of the conduits is a primordial aspect as the size of the pores should be carefully selected to allow a sufficient nutrient supply while hindering the invasion of inflammatory cells. Therefore, the right parameters in the fabrication process are vigilantly picked for an ideal conduit combining the finest fiber diameter, alignment and pore size as a first step paving the way for the repair of critical nerve gaps.

- From a mechanical point of view: As the base material is one of the main criteria determining the implant success, it has been well researched and the biodegradable polymer PCL has first been selected. A plethora of studies has used biodegradable poly(α-hydroxy ester) based polymers for NGC production owing to their mechanical stability, biocompatibility and FDA approval for clinical suitability as nerve conduits [81, 82]. Particularly, PCL is the most considered polymer in

literature dealing with electrospun NGCs. PCL possesses superior viscoelastic and rheological properties rendering its electrospinning tailorable and relatively easy [83]. Moreover, the degradation rate of PCL fibers was shown to be the slowest among common electrospun biodegradable polyesters on account of the 5 $-CH_2$ moieties in its replicating units. Consequently, PCL fibers do not generate degraded acidic compounds thus abating the risk of inflammatory responses [84, 85] . *In vivo* performances of PCL NGCs showed promising results in enhancing nerve regeneration by bridging nerve gaps of 10 mm and over, exhibiting large number of myelinated fibers and favoring angiogenesis [25, 68, 72, 86, 87].

In a recent study, the copolymer poly(ethylene oxide terephthalate)-poly(buylene terephthalate) (PEOT-PBT) commercially known as Polyactive® (PA) has been used to fabricate NGCs. In addition to its biocompatibility, history of safe clinical use in humans and its easy processability with electrospinning, the first advantage of PA over the conventional polymers is the possibility to choose the appropriate mechanical properties by tackling the composition of the two polymers. PEOT-PBT 300 55/45 was shown to offer the proper elasticity, toughness and strength for a NGC. *In vivo* implantation of PA conduit was spotted to support the regeneration in long gaps because of its slower degradation rate. It is well known that electrospun scaffolds degrade faster than macroscale scaffolds of the same material because of the higher area-to-volume ratio and the enhanced porosity. The fast degradation time of the conduits is a limiting factor since it does not coincide with the slow regeneration time in long gaps and it leads to a local accumulation of the degradation products causing inflammatory responses. Despite their relatively thin wall and the high degree of porosity, PA conduits did not collapse and remained intact four months after implantation thus continuing to afford a sufficient nutrient influx while supporting a directed ingrowth. A progressive degradation over time was then observed thus balancing between the maturation of the regenerated nerve and the prevention of its compression. A significantly higher success of PA conduits was detected for critical nerve gaps compared to the standard silicone conduits, but sensory and motor functional recovery did not reach yet the outcomes obtained with autograft [21]. In this sense, in the last stage of this PhD dissertation, PCL is replaced by PA to fabricate NCGs since it is believed that this copolymer, together with an optimized NGC design and an extra surface modification step can considerably enhance axonal regeneration to attain and most likely overtake the performance of autografts.

- From a biochemical point of view: As already mentioned, the direct and indirect administration of growth factors together with the scaffold implantation or via genetic modification of the cells are giving very conflicting results in terms of nerve regeneration. Despite their added benefits, free factors are not enough to support cellular activities. A major weakness of most NGCs is their deprivation of immobilized proteins because of their inappropriate base material surface lacking protein-binding functional groups. Nerve tissue engineers were focused on designing complex topographies while mostly overlooking the biofunctionalization step. In fact, topographical and biochemical cues are complementary recognized by cells at the cell-scaffold interface that plays a key role in the initiation of vital cellular processes such as adhesion [88]. Moreover, combining immobilized cell adhesion molecules and growth factors on one backbone was shown to further improve cell bioactivity and signaling [89]. However, given the narrow dimensions of the porous conduits, reaching and modifying the inner wall surface without altering the nanofibers delicate structure remain challenging tasks. In most cases, the properties of the central part of a porous material are determined by its production process. Therefore, a lot of efforts are aimed at optimizing these production processes by varying the operating parameters to achieve the desired characteristics for the porous material. Unfortunately, most production techniques show limited flexibility in changing their operating parameters. This is the reason why tailoring the central part of porous materials after their production would greatly enhance the possible applications and potential. To tackle this need, this thesis will focus on the application of non-thermal plasmas as a route to change NGCs surface. Plasma treatment is nowadays gaining a substantial interest in TE over other traditional surface modification techniques. It is a solvent-free method that can be highly controlled to incorporate specific functional groups or deposit thin polymer coatings on biomaterials thus creating adequate surfaces for subsequent protein immobilization. Moreover, it is a gas-based technique that can reach and treat the overall surface of complex and porous scaffolds, hence NGCs [90-92]. Despite the significant improvements offered by plasma-functionalized scaffolds in several TE applications, plasma treatment was never, to the best of our knowledge, applied to NGCs. Yet, tailoring their surface properties using fine-tuned plasma parameters is believed to play a pivotal role in the enhancement of glial and neural cell activities thus activating the peripheral nerve regenerative machinery. In this thesis, in addition to homogenous inner wall plasma treatment, a surface chemistry gradient with gradually increasing oxygen content is implemented along the conduit length using novel plasma modification techniques. This chemical gradient is anticipated to boost nerve regeneration across

critical gaps by reinforcing SC elongation and favoring a guided chemotaxis. Moreover, neural cell fate is expected to be significantly improved as chemotaxis mediates nerve generation and guidance during nervous system development. Based on this fact, we hypothesize that such plasma-induced surface gradient will favor axon sprouting with fast and long extensions towards higher surface oxygen content.

- From a cellular point of view: The previously stated benefits of ADSCs and their positive effects in a broad number of experimental PNI studies, made them the cell type of choice in this PhD dissertation [8, 93]. A meta-analysis conducted by Hundepool et al. investigated most of the studies that added stem cells as luminal fillers when bridging peripheral nerve defects. Forest plots of 3 key measurements (electrophysiology, muscle mass ratio and walking track analysis) revealed the positive influence of stem cells, mainly ADSCs, on nerve regeneration [94]. However, since the definitive mechanisms of action underlying the use of undifferentiated ADSCs are still uncertain because of their multipotency, SCs are used in a later stage of this PhD thesis. In this way, the delicate and time-consuming differentiation of ADSCs into SC-like cells is avoided and plasma-treated PA NGCs are tested effectively as SCs constitute the gold standard cellular-based strategy for peripheral nerve repair. In order to examine the efficacy of these NGCs, pheochromocytoma (PC12) cells are co-cultured with SCs and neurite growth and direction are analyzed. PC12 cells have been largely considered in neurobiological studies as they differentiate into nerve cells in the presence of neural growth factors [95].

I.5. Structure and research strategy of this thesis

A well-defined evolutionary step-by-step approach is adopted in this dissertation with all the pre-phases involving 2D samples, electrospinning, plasma treatment, sterilization until the final phase implicating the 3D construction of NGCs. In all the phases, profound studies investigating the physico-chemical and bioresponsive properties of the prepared materials are performed to optimize and pave the way towards the generation of an ideal NCG. In the end, a series of small steps equals big gains.

This PhD thesis is divided in 4 main parts and conceived in the following way:

- Part 1: Literature overview

Chapter II provides the description and the requirements of TE in general but that are also in line with nerve TE in particular. The chapter will also briefly depicts the ECM architecture and composition in addition to the mechanisms underlying the cell/ECM communications to understand the basis on which the researchers were centered to fabricate tissue-engineered scaffolds. A short review will then be given on the natural and synthetic biodegradable polymers that are commonly used to develop electrospun scaffolds of which nerve conduits. Thereafter, the theory behind the electrospinning technique will be explained, accompanied with a concise overview on the effects of changing the working parameters on the nanofibers properties.

Chapter III gives a brief overview on the traditional surface modification methods used for electrospun nanofibers. A general description of different plasma surface functionalization approaches including activation, polymerization and grafting of bioactive molecules on electrospun polymers will follow. The subsequent section will provide an extensive overview on how recent achievements of plasma-functionalized nanofibers have improved the performance of different types of polymeric biodegradable nanofibers in several TE fields. This chapter keeps the reader up-to-date on the different plasma treatments that are performed on electrospun scaffolds and can therefore serve as a reference to successfully treat electrospun NGCs.

As surface modification in a gradient way is anticipated to further enhance nerve regeneration through cell elongation, chemotaxis and haptotaxis effects, Chapter IV will introduce the new and growing research interest that is being shifted from homogeneous plasma treatments towards the development of plasma gradient surfaces. First, the effects of adding neurotrophic gradients into NGCs, done in a few studies via techniques not involving plasma, will be described. Then, an overview on the complex plasma reactors that were extensively redesigned to treat surfaces in a gradient way and a broad literature review on gradient plasma activation and polymerization of surfaces will be presented. This chapter illustrates the positive effects of graded surfaces on the behaviour of different cell types that can be extrapolated to nerve and glial cells for an improved nerve regeneration. Since plasma gradient treatments are relatively new in the TE field, they are still mainly focused on 2D scaffolds. In the following experimental part, a new approach involving a simple plasma jet (PJ) design will be used for the first time in the plasma treatment

literature to create activation gradients on the inner wall of 3D electrospun NGCs.

Once an efficient surface modification is accomplished, a crucial and final prerequisite for the use of NGC *in vitro* and *in vivo* is required: the material sterility [96, 97]. Therefore, Chapter V will reveal all the sterilization techniques that have been used for biodegradable polymers in TE applications ranging from the traditional heat, chemical and irradiation methods to the unconventional plasma sterilization. Besides toxic residues and the incomplete inactivation of microorganisms, alterations in scaffold physical and biochemical properties post-sterilization can rise problems related to the material efficacy and safety. Therefore, the mechanisms underlying each sterilization technique will be summarized and a detailed review on the advantages, residue effects, influence on polymer properties and particular drawbacks of each method will be provided.

- Part 2: Materials and Methods

Chapter VI is dedicated to the materials, methods and experimental setups used in this thesis. The biofabrication methods, plasma treatments, surface characterization techniques, sterilization methods and *in vitro* cell tests will be described with their different operating parameters.

- Part 3: Experimental results

The focus on the optimization of the topography and surface properties of biomaterials has led researchers to often neglect a crucial step that is mandatory for clinical translation: the sterilization process. This sterilization step, performed at the last stage before *in vivo* implantation, can compromise the plasma-treated NGC design and physical properties as well as the optimized surface properties, thereby altering the cell-material interactions. Therefore, the strategy in this thesis is to first find the best sterilization method not altering the polymer structure and plasma-induced surface properties. This prevents from the risk of damaging the NGCs at advanced stages after fabrication, plasma treatments and optimizations. Hence, chapter VII will study the effects of 3 different sterilization methods on the physico-chemical and bioresponsive properties of plasma-treated PCL films: ethylene oxide (EtO), H_2O_2 plasma (HP) and ultraviolet sterilizations.

Chapter VIII will further advance in complexity and transfer from 2D films to 3D electrospun fibers. Plasma-treated PCL nanofibers will thus be subjected to the same sterilization methods and a similar comparative study will be conducted. In this way, an examination of different polymeric topographies will be completed to check if the delicate structure of nanofibers is more or equally prone to sterilization-induced damages compared to films.

After selecting the best sterilization method, Chapter IX will focus more on the electrospinning process itself. Despite the reported simplicity of the electrospinning theory, the process is extremely complicated when it comes to its stability, reproducibility and fiber properties. This is due to the complex interactions between numerous process and substrate-related parameters besides the frequently neglected environmental parameters such as temperature and especially humidity that can influence the fiber production to a high extent [98-100]. Since fiber properties play a decisive role in modulating the phenotype, proliferation, differentiation and guidance of glial and neural cells, the ideal fiber diameter and orientation should be selected to produce NGCs [101, 102]. Therefore, in this chapter, a wide-ranging fiber diameter scale of random and highly aligned PCL fibers will be electropun using the unconventional non-toxic solvent system acetic acid/formic acid. The most influential working parameters will be profoundly studied and varied to attain this goal. Finally, the physico-chemical properties of the obtained fibers will be investigated and comparisons will be made between different fiber orientations and diameters.

In Chapter X, random and highly aligned PCL fibers with 3 different diameters will be selected from the previous study and subjected to a plasma-treatment. The synergistic influence of PCL fiber size, orientation and plasma-modified surface chemistry will then be investigated on ADSC behavior.

Chapter XI will constitute the last part of the experimental section in which electrospun PA NGCs will be biofabricated. These NGCs will be subjected to different plasma treatments using different plasma reactors in order to reach the inner wall and treat it homogeneously or in a gradient way. The optimized plasma-treated NGCs will then form the subject of an *in vitro* analysis involving primary SCs. The novel implant structure, surface topographies and plasma-modified chemistries will thus be biologically tested by performing several biological assays. A proof of concept will be conducted by co-culturing

PC12 cells on the SC-seeded NGCs to study their effect on neurite growth and hence nerve regeneration.

- Part 4: Conclusion

Chapter XII gives a general conclusion on the conducted work and an outlook on future perspectives and considerations.

Chapter II. Tissue Engineering: Electrospun Scaffolds

The literature study presented in Chapter II was partly published in a B2 book chapter:

Ghobeira, R., De Geyter, N. & Morent, R.
Plasma surface functionalization of biodegradable electrospun scaffolds for tissue engineering applications
Book title: Biodegradable polymers: recent developments and new perspectives
Pag: 191-236
Ed: Geraldine Rohman
Publ: IAPC, Zagreb, Croatia (2017).

II.1. Introduction

Tissue engineering (TE) represents a rapidly evolving research area overcoming the limitations of conventional transplantation methods and holding promises to revolutionize the quality of life of patients suffering failure or loss of organs and tissues [103]. The concept of engineering human tissues was first coined in 1987 by Dr. Fung at the National Foundation Science (NSF) workshop [104]. During the same workshop of the subsequent year, the term "tissue engineering" was described as the application of the methods and principles of life sciences and engineering to understand the relationships between the structure and the function in pathological and novel tissues and the development of substitutes for the restoration, maintenance and improvement of tissue functions [105]. However, it was until 1993, when Langer and Vacanti wrote their world-shattering paper about TE and its possibilities, that the scientific community began its investigations [106]. The collective effort of biologists, engineers, chemists, material scientists and clinicians has led to phenomenal advances in the regeneration of almost all tissue types. Four TE approaches are being adopted to achieve this goal: 1) the transplantation or injection of isolated cells that can be manipulated via gene therapy to help tissue regeneration, 2) the use of a biomaterial membrane as scaffold to promote the regeneration, 3) the use of scaffolds combined with bioactive factors and 4) the use of scaffolds in combination with cells with or without biological molecules [107]. Scaffold-based approaches (Fig. II.1) are nowadays gaining a huge popularity due to the potential of novel technologies to provide the scaffolds with adequate chemical, physical and biological cues ensuring a harmonized interaction between the cells and the material. The requirements that must be fulfilled by the scaffolds are the following:

-Biodegradability which is often a fundamental prerequisite eliminating the need of a surgical intervention to remove the implant. Therefore, natural and synthetic biodegradable polymers have gained a widespread interest in the TE field since they are chosen to be the basic materials for the fabrication of most of the scaffolds. The selection of appropriate polymers is important in every specific application since their degradation rate should coincide with the tissue regeneration rate to support but also provide room for tissue formation and neovascularization [108, 109].

-Non-toxicity of the material and its degradation products that should not provoke any genotoxicity or immunogenicity [110].

-Possession of mechanical properties matching those of the neighbouring tissues and making the selection of suitable polymers more challenging [111].

-Mimicry of the ECM which is a primordial factor for effective cell-material interactions. In the body, a wide range of vital cellular activities such as adhesion, proliferation, migration, gene expression and differentiation, is governed by the ECM/cells interactions [109]. The fibrillary nanostructure of the ECM was thought to be the only factor modulating some of the cellular activities. However, many studies have shown that the ECM components provide biochemical cues necessary for cell signalling and tissue morphogenesis [112]. Therefore, the more closely the scaffold mimics the ECM physical arrangement and biochemical properties, the more successful is the tissue regeneration process. Researchers were able to develop several techniques in order to recreate the ECM architecture. Among them electrospinning is the most broadly used since it creates nanofibers in a very practical and affordable way [113] . Biochemical cues can be afforded by tailoring the surface chemistry of the electrospun mats to promote the adsorption of proteins and subsequent cell-signalling pathways. To this end, different surface modification techniques have been performed such as ion-beam, X-ray, gamma radiation, wet chemical treatment and plasma-based techniques [114]. Specific bioactive molecules can be grafted onto the surface after modifying its chemistry or can be blended with the polymer solution prior to the electrospinning [115]. Plasma surface engineering of electrospun materials has known an abrupt rise during the past decade due to its potential to selectively modify the surface chemistry with a precise control of all the process parameters to avoid the damage of the delicate nanofibrous structure [116, 117]. In the next chapter, surface modification of electrospun nanofibers will be discussed in detail, particularly highlighting the different plasma treatments.

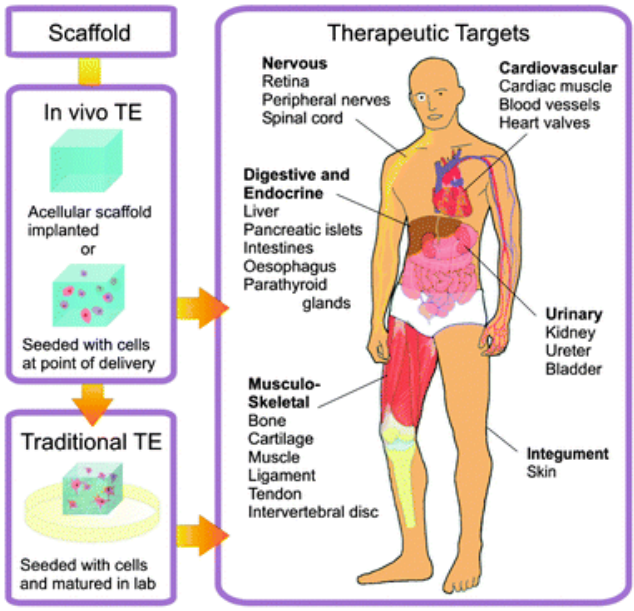

Fig. II.1. *Traditional and in vivo TE approaches. (Traditional TE: in vitro maturation of the cells cultured on the scaffold before being implanted into the patient; In vivo TE: Direct implantation of the scaffold into the patient with or without cells) [118].*

II.2. Extracellular matrix

The ECM represents the non-cellular constituent of all tissues and organs affording a three-dimensional (3D) scaffolding for the cells, modulating cell-cell communication and providing biochemical and physical cues governing a wide range of cellular activities [107]. Many studies have shown its primordial importance in tissue morphogenesis and regeneration which is also clearly illustrated by the numerous diseases arising from genetic defects of its constituents. It is composed of a very complex crosslinked network of fibrillary proteins and glycosaminoglycans (GAGs) generally attached to the ECM proteins to form proteoglycans in which small bioactive molecules such as growth factors are trapped. The fibrous proteins are mainly collagen, laminin, elastin and fibronectin (Fig. II.2). The classification of the ECM components into structural and functional categories is impossible since most of the studied molecules have synchronic roles [112, 119].

Concerning the structural role, many *in vitro* studies have shown that the cells are extremely sensitive to the fibrous 3D architecture offered by the ECM. The considerable difference in the behavior of cells cultured on 2D or 3D scaffolds revealed that 2D biomaterials cannot ensure a successful tissue regeneration when implanted in the body [107]. An important role of the ECM is triggering of cellular motility and migration that are critical aspects in tissue regeneration. The cells contain a polymeric network of microtubules, actin and intermediate filaments structurally organized to generate pushing and pulling forces able to move the cells. The interaction between this network and the ECM fibrous network causes a spontaneous succession of depolymerization and polymerization of the cytoskeletal fibers leading to a coordinated cellular motility [108]. The functional role of the ECM, provided by the nonstop cross-talk between cells and biochemical cues of the ECM effectors, can be supported by the highly cell and tissue specific ECM composition that is diverse throughout the body. The binding of specific growth factors to specific ECM components leads to an increase in the stability of the growth factors thus creating an adequate microenvironment regulating cell proliferation and differentiation [107]. Moreover, cellular receptors can recognize specific ECM sites thus mediating the adhesion of the cells to ECM. The main group of cellular receptors is the integrin transmembrane proteins consisting of one α and one ß subunits. Up until now, around 18 α subunits and 8 ß subunits are identified and 24 diverse heterodimers are recognized, each binding to specific ligands within the peptide sequences forming the ECM proteins such as collagen, fibronectin and laminin known as the "ECM glue" [120]. Integrin attachment to ECM ligands provoke a cascade of processes. The actin proteins inside the cell form microfilaments bundles also called stress fibers triggering the formation of focal adhesion which links the actin cytoskeleton to ECM molecules. The focal adhesion structures will initiate several signal transduction pathways in the cells changing their gene expression thus modulating a wide range of cell activities [107, 121]. The importance of the biological components in the integrin-mediated cell adhesion and the growth factor attachment has led the tissue engineers to consider the use of natural components in the fabrication of scaffolds.

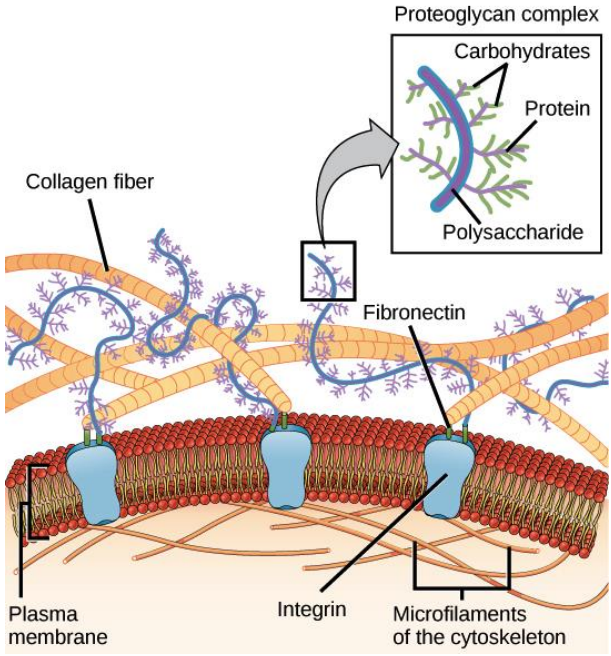

Fig. II.2. *Schematic representation of the ECM structure in contact with a cellular membrane (open source) [122].*

II.3. Natural ECM-derived components used in TE applications

The main ECM components used in the development of biomaterials are: collagen, laminin, fibronectin, elastin, keratin, hyaluronic acid, chitosan and GAGs. In what follows, a brief description will be given on the natural components that are mostly used in the fabrication of electrospun scaffolds or in the biofunctionalization of electrospun fibers.

II.3.1. Collagen

Collagen is the major polymeric component of the ECM. It is constituted of polypeptide chains displaying triamino acid sequences of glycine-A-B where A and B are mostly hydroxyproline or proline but can be any of a series of amino acids. These polypeptides are organized into a micro-fibrillary triple helices that arrange together following different architectures to form collagen fibers. More than 28 different collagen types have been identified up to date from which types I, II, III and IV are the most studied with an excessive use of collagen type I in TE

applications [110]. Collagen generally binds to glycoproteins, growth factors and structural proteins such as laminin and elastin to afford specific tissue characteristics and it was shown that each of the collagen types play a role in the constructive remodeling of tissues [123]. The use of collagen in TE applications is mainly due to its biocompatibility, great ability to enhance cell adhesion and proliferation, mechanical properties and enzymatic degradation by metalloproteinases and collagenases [124, 125]. Many authors have electrospun collagen nanofibers for their use in wound dressings, blood vessel, cartilage, tendon and other TE applications. Collagen is a thrombogenic component since it activates the conversion of fibrogen into fibrin known by its capacity to capture activated platelets to generate a clot [110]. Electrospun collagen fibers were rarely used to fabricate NGCs, however several FDA-approved non-fibrous NGCs were created with collagen type I as base material such as: NeuraGen®, Neuroflex™, NeuroMatrix™, NeuraWrap™ and NeuroMend™ [2, 17]. The commercial collagen type I is generally obtained from bovine dermis, human placenta or rat tail. Although extensively researched, many drawbacks are associated with use of collagen in biomedical applications. In addition to the high cost of purification and high risk of disease transmission, collagen possesses some antigens in its central helix that were shown to cause immunological responses *in vivo* [110, 126].

II.3.2. Gelatin

Gelatin is a derivative of collagen obtained by a physico-chemical degradation and denaturation of its triple-helix structure. The production process highly affects the gelatin properties. It is composed of 19 amino acids and is organized in single-stranded structure. It possesses comparable hemostatic characteristics to collagen and is degraded enzymatically by collagenases [126]. A major advantage of gelatin is its possession of a great non-antigenicity, thus it is less immunogenic than its precursor. Gelatin-based scaffolds were commonly used in TE applications due to their good biocompatibility and their ability to promote cell adhesion, proliferation, differentiation and migration [127]. However, unlike other polymers, gelatin is a polyelectrolyte polymer possessing quite a number of anionic and cationic groups associated with a strong ability of hydrogen bonding. As a consequence, a 3D macromolecular network can be formed, tremendously decreasing the mobility of gelatin chains thus making the development of fibers a challenge [128]. Despite the poor electrospinnability of gelatin, some authors succeeded to electrospun gelatin fibers but the solvents used to obtain relatively good fibers were

rather toxic such as trifluoroethanol and hexafluoropropanol [129]. Therefore, gelatin has been broadly coated on electrospun nanofibers made up of other polymers. Some studies have blended gelatin with other synthetic polymers to electrospin fibrous meshes and test them as potential scaffolds for peripheral nerve regeneration. For instance, Mobarakeh et al. and Perez et al. have shown that PCL/gelatin nanofibers are very effective in supporting neurite outgrowth when seeded with nerve stem cells (C 17.2 cells) and PC12 [130, 131]. Moreover, Gupta et al. have illustrated the positive effect of PCL/gelatin nanofibers on SC proliferation thus confirming their suitability as biomaterials for neural TE [78]. Gelatin has been also successfully mixed and electrospun with PLA promoting neural cell differentiation into motor neuron lineages and enhancing neurite outgrowth [132].

II.3.3. Laminin

Laminin is a complex protein found in the ECM particularly within the basal lamina and that can independently self-assemble into networks or associate with other ECM components such as collagen IV. Three polypeptide chains (α, ß and γ) intersected into the form of a cross-like structure are found to compose this protein. There are several variants of this heterotrimeric protein that depend on the particular composition of each polypeptide chain [123]. Laminin has been reported to be among the first and most critical ECM components to play a role in enhancing and supporting adhesion, growth, differentiation and migration of several cell types in particular neuronal cells. It contains the amino acid sequence isoleucine-lysine-valine-alanine-valine that enhances and controls neurite outgrowth. Therefore laminin was extensively used in neural TE [133, 134]. Neal et al. demonstrated that electrospun laminin fibers promoted a higher degree of cell attachment and neurite extension from ADSCs than laminin films [135]. However, the electrospinning of laminin have been mainly hindered by the instability of the resulting fibers, but coating or conjugating electrospun fiber surface with laminin has been extensively performed and showed promising results in tissue regeneration [136].

At first, tissue engineers considered natural polymers as promising materials for the fabrication of scaffolds because of their attractive bioactivity. However, many studies rapidly revealed that most of the natural materials are associated with several drawbacks:
- Weak mechanical stability [137]
- Difficulty of obtaining large amounts of materials and high processing cost [138]

- Restricted designing possibilities without alteration of the biological properties [139]
- Weak resistance of enzymatic degradation; uncontrolled degradation rate since enzymatic activity differs between hosts [140]
- Intense immunogenic reactions [141]
- Risk of disease transmission from allogenic or xenogenic materials [142]

Therefore, synthetic biodegradable polymers overcoming all these limitations were developed and were extensively used as basic materials for the fabrication of scaffolds. The major downside of synthetic biomaterials is their hydrophobicity and the lack of biochemical recognition sites necessary for different cellular processes. Nowadays several advances in surface TE come to solve this issue.

II.4. Synthetic biodegradable polymers used in TE applications

Since an ideal polymer does not exist because of the wide-ranging TE applications, researchers have developed numerous synthetic polymers. A library of materials was used to synthetize polymers and then to engineer scaffolds that match to the best the specifications of a particular application. Among the synthetized biodegradable polymers, the aliphatic polyester family is nowadays the most appealing group meeting various medical and physical requirements for safe clinical applications. The biocompatibility and biological inertia of polyesters were confirmed after their use in several biomedical applications [110, 143]. Moreover, their synthesis via condensation polymerization or ring-opening is relatively easy which increases their commercial availability. Although numerous polyesters are nowadays available, their hydrolytically steady ester bond limits their degradability and makes only the ones with relatively short aliphatic chains appropriate for tissue-engineered scaffolds [110, 144]. PGA, polylactic acid (PLA), PLGA, PCL, polybutylene succinate (PBS) and polyhydroxyalkanoate (PHA) are the ones that are currently adopted in the majority of biomedical applications [139, 145]. In addition to their versatility regarding chemical and physical properties, a custom-tailored degradation rate can be obtained. Therefore, a plethora of papers have focused on the fabrication of nanofibers using these synthetic polymers, but PCL is by far the most extensively considered in the wide literature of electrospinning, followed by PLGA, PLA and PGA (Fig. II.3). Therefore, in what follows, we will be restricted to a brief overview on these aliphatic polyesters.

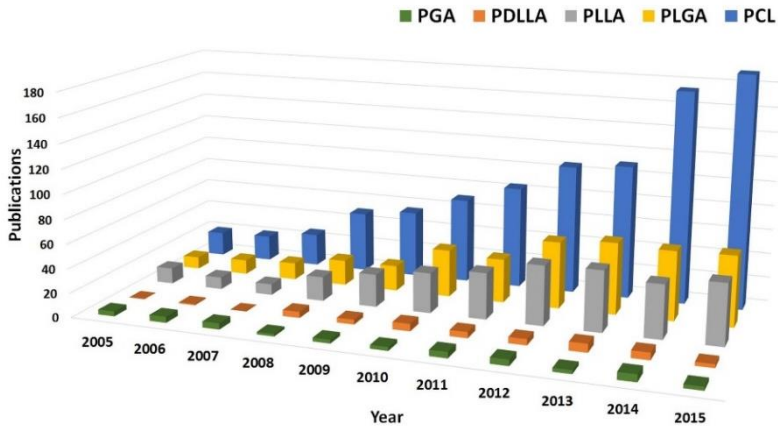

Fig. II.3. *Publications using electrospun biodegradable polyesters during the last decade (Source: Web of Science®, topic keywords used during the search: "PGA electrospinning", "PDLLA electrospinning", "PLLA electrospinning", "PLGA electrospinning" and "PCL electrospinning").*

II.4.1. Polyglycolic acid (PGA)

Polyglycolic acid also known as polyglycolide is one of the first biodegradable polymers ever explored in biomedical applications. PGA is characterized by an elevated melting temperature exceeding 200 °C, a high crystallinity (44-55%) and an excellent tensile strength (12.5 GPa) [146]. These characteristics, together with PGA's great biodegradability, have attracted the medical community to use it in the fabrication of resorbable sutures that were commercialized under the name of DEXON® and have been extensively used since 1970. With the rise of TE applications, the physico-chemical properties of PGA accompanied with its acceptable bioresponsive properties such as good cellular viability, have also appealed tissue engineers to fabricate PGA scaffolds for tissue regeneration [110, 141]. When implanted in the body, PGA degrades into the non-toxic glycolic acid that can be excreted via the urinary system or via the respiratory system after being converted into CO_2 and H_2O [146]. PGA scaffolds were therefore fabricated and were used in several TE applications such as bone, tendon, cartilage, intestinal, and neural regeneration [110]. Nevertheless, several studies have rapidly demonstrated that the use of PGA in TE involves several drawbacks. First, the rapid degradation of PGA leads to a reduced mechanical strength of the scaffold within 1 to 2 months with a total loss of its mass within 6 to 12 months [147]. Therefore, this degradation rate does not coincide with the regeneration rate of most of the tissues. In particular, when it comes to nanofibers, the degradation is even faster compared to macroscale scaffolds. The

higher area-to-volume ratio and enhanced porosity facilitate the penetration of water into the highly crystalline PGA nanomatrix which increases its degradation rate [140]. Dong et al. showed that PGA nanofibers degraded only within 20 days and barely supported the growth of porcine smooth muscle cells in the first few days [148]. This is one of the reasons explaining why the electrospinning of PGA is less considered compared to the other polyesters. Moreover, the fast degradation of PGA causes a rapid production of glycolic acid leading to its local accumulation at high levels which is associated, despite its aforementioned non-toxicity, with undesired strong inflammatory responses [149, 150]. Furthermore, PGA exhibits a limited solubility in the most common solvents, it is rather soluble in toxic highly fluorinated solvents such as hexafluoro-2-propanol, which also reduces the electrospinning of PGA fibers [145].
Recognizing the above, PGA-based NGCs are in most cases not fabricated using the electrospinning technique and are limited to treat very short nerve gaps given their instable nature [151, 152]. Recent TE applications have coupled PGA with other biodegradable polymers in the development of electrospun scaffolds.

II.4.2. Polylactic acid (PLA)

Lactic acid is a natural metabolic by-product generated in the muscles by anaerobic glycolysis and can be degraded into CO_2 and H_2O which are further eliminated from the body via the respiratory system. It is a chiral molecule that constitutes the monomer building unit of PLA or polylactide. It can be produced by converting a starch having a vegetable origin or a sugar via a petrochemical process or a bacterial fermentation [146, 153]. Because of its chirality, PLA can be synthetized in four different forms: poly(D-lactic acid) (PDLA), PLLA, poly(D,L-lactic acid) (PDLLA) and meso-poly(lactic acid). PLLA and PDLLA have been widely studied and have shown promises in the biomedical and TE fields [110]. PLLA has a relatively high melting temperature of around 175 °C and a tensile strength of 4.8 GPa [154]. The extra methyl group in PLA renders it more stable and more hydrophobic than PGA. Therefore, it exhibits a slow degradation compared to PGA. When hydrolyzed, PLLA loses its strength within approximately 6 months, but preserves its mass for long periods of time and it can take up to several years to totally degrade [145]. After commercializing an internal bone pin made up of PGA under the name of Biofix® in 1984, the base material was converted to PLLA starting from 1996 since it demonstrated a much better stability at long-term. PLLA has also been used in the fabrication of surgical sutures [110]. Moreover, it attracted a strong interest for the use in tissue

regeneration because of its proper mechanical characteristics and degradation rate matching the properties and the healing time of a number of tissues. Furthermore, tissue engineers can take advantage of its piezoelectric characteristics (d_{25} =10 pC/N) by stimulating the tissue via an electro-mechanical transduction thus activating the scaffolds not to just serve as passive structural support for cells [155, 156]. Nerve, bone, blood vessel, tendon, cartilage, liver and other TE fields have experienced a successful use of PLLA scaffolds [110]. Particularly, in the past decade electrospun PLLA scaffolds are being increasingly utilized. This is partially due to the fact that PLLA is soluble in the majority of organic solvents such as chlorinated solvents, tetrahydrofuran (THF), dioxane and acetonitrile; and by choosing appropriate solvent systems, a very good quality of PLLA fibers can be obtained [157, 158]. Several electrospun PLA NGCs and sheets have been generated to check their effectiveness in nerve TE [22]. For instance, PLLA fibers have been detected to be compatible for the growth of motor and sensory neurons even in serum –free conditions [159]. In an *in vivo* study using electrospun PLLA NGCs, an enhanced functional recovery has only been observed when the conduits were filled with PLGA intra-luminal nanofibers [6].
The amorphous nature of PDLLA is due to the arbitrary positioning of its 2 isomeric monomers. This results in a significantly reduced mechanical strength (1.9 GPa) compared to PLLA [146]. PDLLA further loses its strength when hydrolyzed after 1 to 2 months and its mass within almost a year. Therefore, PDLLA has been used in drug delivery systems or in the rare TE applications requiring low strength scaffolds [147]. As a consequence, PDLLA nanofibers were rarely electrospun for TE purposes, unless the polymer is blended with other biodegradable polymers [160-162].

II.4.3. Poly(lactic-co-glycolic acid) (PLGA)

The slow degradation time of PLLA is a limiting factor in some TE applications that involve relatively fast-regenerating tissues. Therefore, tissue engineers randomly copolymerize PLLA or PDLLA and PGA to obtain PLGA also known as poly(lactic-co-glycolide), thus combining the properties of the two polymers. The high commercial availability of PLGA, together with its easy processability in almost all sizes and shapes makes it one of the most investigated synthetic polymer in TE but also in other biomedical applications such as drug delivery systems and sutures [141, 147]. Depending on the intended TE application, the copolymer composition should be delicately selected, since PLGA degradation is strongly influenced by the lactic acid/ glycolic acid ratio. A composition of lactic acid between 25 and 75

% leads to the formation of PLGA having an amorphous nature that is much more hydrolytically unstable than the homopolymers. For instance, a 50/50 PLGA degrades within 1 to 2 months, a 75/25 PLGA degrades within 4 to 5 months and a 85/15 PLGA degrades within 5 to 6 months [154]. PLGA has demonstrated great cell-responsive properties (adhesion and proliferation) in different TE fields such as bone, nerve, cartilage, tendon, liver and skin. For these applications, PLGA scaffolds were developed making use of various techniques such as porogen leaching, gas foaming, microsphere sintering and electrospinning [110, 163]. In particular, fibrous PLGA scaffolds with controlled diameter and porosity are reported to be easily produced by electrospinning [164]. Several solvents can be used for the electrospinning process since PLGA is soluble in a broad range of common solvents including tetrahydofuran, chlorinated solvents, acetone and ethyl acetate [165]. In opposition to PGA, PLGA (50/50) nanofibers (550 nm) have shown a slower degradation compared to PLGA films (0.5 mm) because of the reduced bulk autocatalysis effect resulting from the accumulation of the degraded acidic products [166]. The porosity of the nanofibrous matrices is the leading cause of this reduction in the autocatalysis effect [167, 168]. Electrospun PLGA fibers have been frequently considered for nerve TE applications as sheets, wall of NGCs or intraluminal fillers [2, 22]. For instance, Bini et al. have shown that 5 out of 11 PLGA nanofiber-based NGCs were capable of supporting nerve regeneration across a 10 mm gap upon histomorphometric and immunohistochemical analysis, however functional recovery was not studied [169]. Lee et al. have detected that polypyrrole-coated PLGA electrospun fibers favored the growth and differentiation of hippocampal neurons and PC 12 cells [170]. Koh et al. have filled PLLA NCGs with aligned PLGA nanofibrous intrafillers and found that such constructs can efficiently promote peripheral nerve regeneration, as proven by histological and functional recovery assessments [6].

II.4.4. Polycaprolactone (PCL)

In 1930, PCL was synthetized by the Carothers group to be one of the first developed synthetic polymers. It is obtained via a ring-opening polymerization of the relatively cheap monomer building block ε-caprolactone by using cationic and anionic catalysts [83]. It is a semi-crystalline polymer having a crystallinity that tends to decrease with increasing the molecular weight and a melting temperature between 55 and 60 °C [110, 171]. In the 1970s and 1980s, PCL has attracted some attention together with other synthetic biodegradable polyesters for its use in biomedical applications, especially in the developing of drug-

delivery devices. However it was rapidly overwhelmed by the polyglycolides and the polylactides because of its very prolonged degradation time that can reach up to 3-4 years. Two decades later, a massive resurgence of PCL has coincided with the rise of the TE field due to its several advantages over other biodegradable polymers [83]. Despite its relatively low tensile strength (23 MPa), PCL possesses great rheological and viscoelastic properties such as a very high elongation at break (4700%), which makes the development of a broad range of PCL scaffolds having various sizes and shapes relatively very easy [110]. Therefore, numerous techniques were involved in the manufacturing of PCL scaffolds such as: porogen leaching, phase-separation methods, liquid-liquid phase separation, supercritical fluid methods, solid-free form fabrication, stereolithography, 3D printing, fused deposition modeling and electrospinning [83]. In particular, PCL electrospinning has known a steep continuous rise starting from 2003. PCL is soluble in wide-ranging solvents such as THF, dimetylformamide, acetic acid, formic acid, methylene chloride, pyridine, dichloroethane, methylene chloride, chloroform and other chlorinated solvents [172]. Previous studies have revealed that PCL fibers are absolutely non-toxic since they do not generate acidic degradation products, which is an issue to be considered sometimes in the degradation of PLGA and PLA because of possible inflammatory responses [173, 174]. PCL has been blended or co-polymerized with other polymers in order to increase the degradation rate. Nevertheless, PCL nanofibers, like PGA, have been reported to degrade faster than PCL macroscale scaffolds [140]. Interestingly, PCL fibers and other scaffolds were revealed as effective candidates in bone, nerve, cartilage, tendon, ligament, skin, blood vessel and other tissue regeneration processes [83, 171, 175]. Numerous nerve tissue engineers have considered electrospun PCL fibers alone or blended with other natural or synthetic polymers to fabricate NGCs and have obtained very promising results in bridging nerve gaps of various lengths [22, 46, 176-181]. Therefore, the use of electrospun PCL fibers in nerve TE continues to expand and to be considered in very recent studies. For instance, Farzamfar et al. fabricated electrospun PCL/gelatin NGCs loaded with unrestricted somatic stem cells. After 14 weeks of *in vivo* implantation in rat sciatic nerve model, results of histopathological examinations and functional recovery analyses showed a nerve regeneration in 10 mm nerve defect close to the autograft model [182]. Pan et al. have electrospun PCL NGCs and coated them with pyrrole to study the biocompatibility of SCs. The constructs were very conducive to SC adhesion and proliferation thus showing a good potential in nerve repair [183].

II.5. Electrospinning

After a great deal of efforts, several chemical, physical, electrostatic and thermal techniques were developed to fabricate scaffolds mimicking the fibrillary structure of the ECM, such as template synthesis, liquid-liquid phase separation, vapor-phase polymerization, self-assembly and electrospinning [184-187]. This last technique, also called electrostatic spinning has been first introduced in the 1930s, but it was until the end of the 20th century that it received a great surge of interest within the scientific community, after Reneker et al. discovered the possibility of generating electrospun fibers from various polymers [188, 189]. The massively increasing literature on electrospinning has paved the path towards great achievements in the TE field. It is preferred over the other techniques due to its versatility, simplicity and low cost. Moreover, an attractive strength of electrospinning is its capacity to easily adjust the fiber diameter down to the nanometer scale thus not only recapitulating the structure of the ECM but also its size. Electrospun nanofibers display a higher surface-to-volume ratio compared to microfibers, thus providing much more binding sites for proteins which leads to a good cellular adhesion that is essential for other cellular activities [109, 140, 190, 191]. Binulal et al. showed that human mesenchymal stem cells (MSCs) adhere, spread and proliferate more efficiently and rapidly on PCL nanofibers compared to PCL microfibers. Furthermore, a successful differentiation of HMSCs into osteoblastic lineage and subsequent mineralization were observed on PCL nanofibers [192]. Wang et al. cultured human embryonic stem cells on fibers made up of Tussah silk fibroin and having diameters of 400 and 800 nm and showed increased cellular viability on the 400 nm fibers [193]. In a study conducted by Yang et al., the rate of neural stem cells differentiation was shown higher on PLLA nanofibers than on microfibers [194]. Another key feature of electrospinning is its capacity to tailor the nanofiber mesh porosity providing a large number of intra/inter connected pores allowing the cellular migration and the essential supply of nutrients for the cells [191, 195]. Electrospinning can be also employed to design the nanofibers into specific arrays or 3D hierarchical architectures (e.g. hollow tubes, stacked arrays). Moreoever, several fiber morphologies can be obtained such as porous, ribbon, beaded and core-shell fibers [196].

II.5.1. Concept and mechanism of electrospinning

A combination of the two concepts namely electro-spraying and spinning is involved in the electrospinning process. The basic set-up is mainly composed of five major parts: a syringe containing the polymer solution, a syringe pump, a power supply, a metallic tip or needle and

a metallic collector that can have various morphologies (e.g. plate, cylinder). A schematic representation of the set-up is shown in Fig. II.4. The flow rate of the solution is regulated by the pump in order to carry the solution via tubes or capillaries from the syringe to the metallic tip. When a droplet of the solution comes out of the tip, a high electric field is applied between the tip and the collector which both serve as electrodes. This causes an instability within the solution resulting from the induction of electric charges on the droplet, thus forcing the ions of the solution to aggregate at the surface of the droplet. Simultaneously, the spherical droplet deforms adopting a conical shape named "Taylor cone" and undergoes two main types of electrostatic forces: a reciprocal repulsion of the surface charges and a Coulombic force expended by the external electric field generated between the tip and the collector. When increasing the voltage above a critical threshold, the electrostatic forces oppose and overcome the surface tension of the polymer solution and a charged jet is erupted from the Taylor cone and accelerated towards the metallic collector. During the travelling of the jet through the air between the tip and the collector, it experiences spreading and elongation processes accompanied with the evaporation of the solvent. Therefore, thin solid polymeric fibers are deposited on the collector in the form of non-woven mat [139, 140, 196].

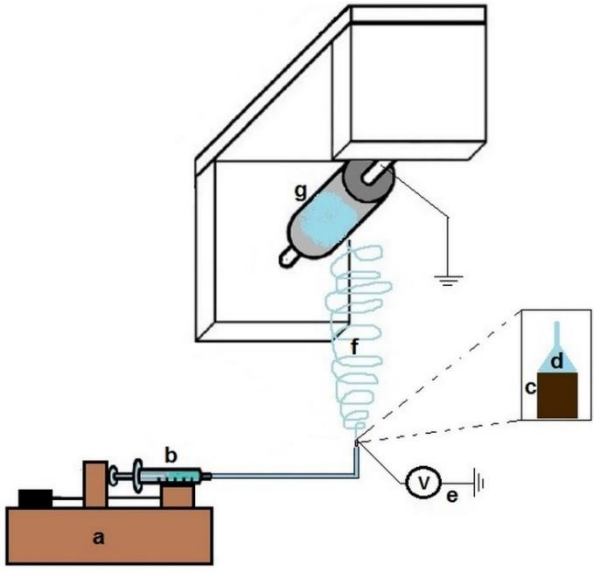

Fig. II.4. *Schematic representation of the electrospinning set-up (a: syringe pump, b: syringe containing the polymer solution, c: metallic tip, d: Taylor cone, e: high voltage power supply, f: polymer jet, g: collector).*

II.5.2. Electrospinning parameters

Despite the theoretic simplicity of the electrospinning process, some challenges are to be faced in order to obtain a good quality of fibers. The spinnability as well as the fiber diameter, morphology, uniformity and alignment are mainly influenced by 2 types of parameters: substrate-related parameters and process-related parameters. The fiber defects such as the formation of beads, junctions and pores are controlled by optimizing these parameters. Recently, environmental factors such as temperature and relative humidity (RH) were shown to have considerable effects on the fiber size and morphology. Complete reviews and book chapters have discussed in detail the influence of the electrospinning parameters on the fibers [191, 197]. In what follows, the most important parameters will be cited and very briefly discussed.

II.5.2.1. Substrate-related parameters

The main substrate-related parameters include the polymer concentration, molecular weight, viscosity and surface tension. The polymer concentration and molar mass affect the solution viscosity, widely known to have an influence on the uniaxial stretching of the electrically charged jet [109, 140]. For example, a low concentration or molar mass result in a low viscosity limiting the erupted jet from withstanding the electrical forces. Therefore, the polymer chains are broken up into fragments and beads are generated. Increasing the concentration or the molar mass gives rise to more entanglements among the polymer chains thus forming a mixture of fibers and beads. A further increase in the polymer concentration finally results in optimized solution viscosities and subsequent formation of smooth beadless fibers [197]. Increasing the concentration is reported in many studies to generate uniform fibers with larger diameters (Fig.II.5) [189, 198, 199]. However, when the concentration exceeds a critical value, a very high viscosity is obtained thus hindering the flow of the polymer solution that frequently dries and obstructs the tip [140].
The literature concerning the influence of the solution surface tension on the fiber size and morphology is controversial [197]. While some authors have reported that reducing the surface tension is beneficial and results in bead-free fibers, others showed that it is not always the case. It is clear that it mainly depends on the polymer and the system of solvents used [140, 197].

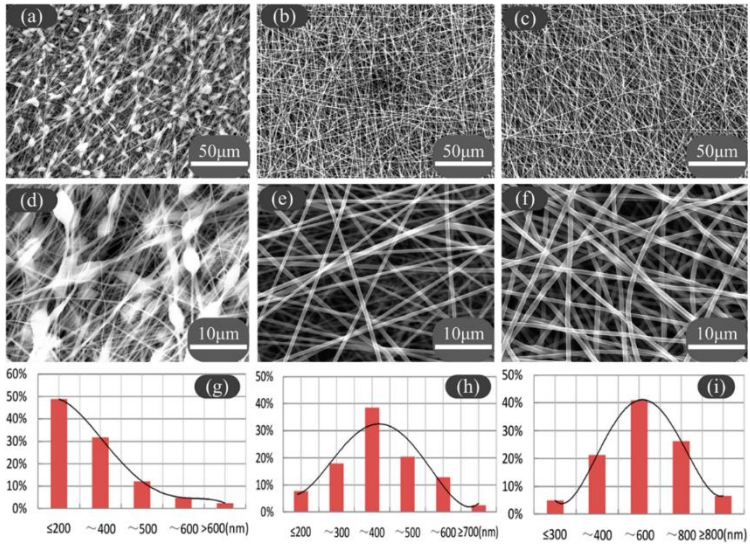

Fig. II.5. *PLGA nanofibers electrospun from solution (PLGA-Tetrahydrofuran/Dimethylformamide 3/1) having a concentration of 0.2 g/mL (a,d,g), 0.3 g/mL (b,c,h) and 0.4 g/mL (c,f,i) [198].*

II.5.2.2. Process-related parameters

The most important process-related parameters are the applied electric field, the polymer flow rate and the distance between the tip and the collector. A crucial step in the electrospinning process is optimizing the applied voltage in order to obtain a continuously steady Taylor cone over time with the same amount of polymer ejected towards the collector per time unit [172]. Some studies have reported that increasing the applied voltage reduces the fiber diameter because it can increase the electrostatic repulsion forces on the jet leading to an additional stretching of the polymer solution [140, 197]. For instance, Katti et al. found that an increase in the applied voltage from 0.375 to 1.000 kV/cm significantly reduced the diameter of PLGA fibers, but above this voltage the fiber diameter was no more considerably changed [200]. In contrast, other studies have demonstrated that higher voltages gave rise to larger fiber diameters. In addition to those observations, many groups stated that a high voltage is accompanied with a great probability of bead formation [109, 197]. Therefore there is an optimal range of applied voltage for each particular polymer-solvent system.

Most of the studies agreed that low feeding rates of the polymer solution within the syringe are preferable over high flow rates. On one hand,

when the flow rate is low, the polymer solution will have time to polarize. On the other hand, high flow rates lead to the formation of bead fibers with large diameters largely owing to the insufficient solvent evaporation before the jet reaches the collector [109, 197, 201]. The solvent evaporation also depends on the distance between the tip and the collector. This distance affects as well the whipping processes, thus it should be optimized in order to generate uniform and smooth nanofibers. Defective fibers with large diameters are generally observed when this distance is small, whereas as the distance increases, the fiber diameter normally decreases [109, 191].
The deposition of the fibers on the collector can be affected by the collector's shape. A number of metallic collectors has been developed in order to generate aligned fibers. Three different types of forces are involved in order to obtain aligned fibers: a rotating mandrel exerts mechanical forces, parallel permanent magnets exert magnetic forces and parallel electrodes exert electrostatic forces. In many TE applications, in addition to the fibrillary structure of the scaffold, the anisotropy in the topography was demonstrated to have a positive effect on the mechanical properties and the cellular behavior [187, 202].

II.6. Influence of electrospun fiber size and orientation on cellular behavior

As already mentioned, considerable improvements in biomaterial cytocompatibility was noticed when cells were grown on fibrous structures compared to 2D flat surfaces [203]. However, a fibrous morphology is not enough to achieve the near-perfect complex biomimicry. Very specific topographical features seem to be highly characteristic of a particular end application [204]. In fact, the ECM has a heterogeneous hierarchical nature since it is comprised of bioactive proteins structured to form randomly oriented or aligned fibers having dimensions ranging from a few nanometers to a few micrometers [203, 205]. Some authors have researched the topography size on cellular behavior and have stated that a microtopography affects the cytoskeletal structure and therefore cell morphology while a nanotopography is more involved in subcellular sensing pathways, gene expression, proliferation and differentiation [206, 207]. In contrast, other studies have concluded that a nanostructured topography influences cellular morphology, adhesion and migration [203, 208]. This discrepancy in literature suggests that the optimal topographical size is strongly dependent on the cell type and its distinctive sensing organelles. Chen et al. seeded fibroblasts on PCL fibers having diameters between 480 and 1051 nm and noticed that cell adhesion and

growth kinetics decreased when increasing the fiber diameter [209]. On the other hand, Badami et al. showed that the density of osteoblastic cells tend to increase when increasing the fiber diameter from 0.14 to 2.1 μm [210]. In an interesting study conducted by Jiang et al., NGCs made up of electrospun PCL nanofibers or microfibers were implanted in a rat sciatic nerve gap model of 15 mm for an in vivo assessment of the fiber size influence on nerve regeneration. Three months post-implantation, nanofibrous conduits gave rise to a significantly higher number of myelinated axons and denser myelin sheaths compared to microfibrous conduits. Moreover, a considerable increase in the number of regenerated dorsal root sensory neurons were found in the nanofibrous conduits. Functional recovery in electrospun conduits remained however inferior compared to the autograft group [179]. Cells were also shown to sense small size differences within the nanometer scale and to accordingly form diverse focal contact complexes depending on the frequency of available anchor points and their membrane receptors [211]. For instance, He et al. found that the viability and proliferation of neural stem cell was better on PLA fibers of 350 nm compared to 550 nm [79]. Pelipenko et.al compared the performance of keratinocytes and fibroblasts on nanofibers with 5 different diameters. Keratinocytes exerted the best proliferation on 305 nm-tick fibers while fibroblasts reached the same effect on 667 nm-thick fibers [205]. Nevertheless, the formation of focal sites is not only influenced by fiber sizes but also by their random or aligned deposition, hence the presence of anisotropic ECM alignment in some native tissues such as the heart myocardium and the inner wall of blood vessels [79, 206]. Fiber alignment provides directional cues playing a crucial role in cell shape, directed migration and regeneration enhancement of ordered tissues such as nerves and ligaments [79, 203, 211]. Uniaxially oriented fibers were shown to have a noticeable influence on nerve cell guidance. A few cell types cultured on aligned electrospun fibers were shown to elongate and align along the axis of the fibers such as SCs emulating the natural Band of Bunger structure and neurons extending directed axons for an enhanced nerve regeneration [78-80]

Chapter III. Surface Functionalization of Electrospun Polymers: Plasma Treatment

The literature study presented in Chapter II was published in a B2 book chapter:

Ghobeira, R.., De Geyter, N. & Morent, R.
Plasma surface functionalization of biodegradable electrospun scaffolds for tissue engineering applications
Book title: Biodegradable polymers: recent developments and new perspectives
Pag: 191-236
Ed: Geraldine Rohman
Publ: IAPC, Zagreb, Croatia (2017).

III.1. Different functionalization approaches of electrospun biodegradable polymers

Once the mimicry of the ECM structure addressed by creating nanofibers, a biofunctionalization needs to be tackled since cells do not only recognize topographical cues but also biochemical cues that significantly affect their behavior. Surfaces play a pivotal role in TE since the majority of biological processes are initiated at the interface between cells and material [88, 212]. Therefore modifying the surface chemical properties of electrospun nanofibers can strongly and positively impact the cellular behavior. The choice of an appropriate surface modification not compromising the delicate structure of nanofibers is a challenging step. Ion-beam, X-ray, ozone oxidation and gamma radiation are able to introduce reactive chemical functionalities on polymer surfaces, however they often alter the mechanical stability and degrade the polymer, thus rapidly damaging nanofibers [118, 190, 213-215]. A traditional method used to incorporate and enhance the density of functional groups on biomaterial surfaces is wet chemical treatment. For example, the incorporation of COOH can arise when applying a surface hydrolysis with NaOH solution. NH_2 groups are added to the surface by aminolysis in which a chemical reaction involves the splitting of a molecule into 2 parts when reacting with a molecule of NH_3 [216-218]. Despite the enhanced surface wettability obtained after the incorporation of such groups, many drawbacks associated with wet chemical treatments set some question marks concerning their utilization. First, such treatments are very harsh leading in some cases to a decrease in the mechanical performance and an increase in the rate of degradation thus it can particularly destroy fine structures such as nanofibers [219]. Secondly, many studies have shown that these surface modifications can cause irregular and unwanted etching strongly modifying the surface thus they are not appropriate for nanosized fibers [220, 221]. Furthermore, these techniques are not eco-friendly since they demand large amounts of liquids and produce hazardous chemical waste [147]. To avoid these surface modifications, some researchers have blended natural polymers and other bioactive molecules with the synthetic polymer solution prior to the electrospinning thus specifically functionalizing the nanofibers for particular TE applications. Collagen, laminin, gelatin, elastin and chitosan have extensively been blended with synthetic polymers to produce nanofibers serving as scaffolds for nerve, blood vessels, skin and bone regeneration together with other TE applications [130, 222-226]. Carbon phosphates, serving as bone grafting replacements to fill bone empty spaces and damaged areas, have been blended with polymer solutions to fabricate nanofibers having potentials in

osteoconductivity, osteoinductivity and osteointegration [227-229]. Short peptide sequences of specific ECM proteins constituting bioactive ligands for particular cellular receptors have been added to electrospinning solutions [230]. Table III.1 shows some of the blending solutions that have been prepared so far to fabricate nanofibers used in different TE applications. Although this method showed enhanced cell-material interactions, several disadvantages cannot be ignored. Embedding bioactive molecules inside the nanofibers can cause the masking of their bioactivity [227]. The harsh conditions of the electrospinning might modify the bioactive sequences of the some peptide-based functionalities and proteins [231]. Moreover, because of the limited solubility of natural polymers in water, highly acidic and toxic solvents such as trifluoroacetic acid and 1,1,1,3,3,3-hexafluoro-2-propanol (HFP) are being used for electrospinning. In addition to their undesired toxicity, these solvents can compromise the biological activity of the added molecules [232]. For example, Zeugolis et al. revealed that the beneficial properties of collagen are lost when it is dissolved in 2,2,2-trifluoroethanol or HFP and electrospun. These solvents caused a collagen denaturation thus altering the specific biological sites recognized by the cellular receptors [233]. Yang et al. also showed that collagen type I electrospun fibers were denaturated when using HFP [234]. Furthermore, the presence of natural bioactive materials inside the nanofibers can weaken the electrospun fibrous network. An important downside of adding bioactive materials in the electrospinning solution, is the difficulty of controlling the process parameters to obtain good nanofibers [127].

As an alternative to the abovementioned functionalization methods, plasma-based surface modification is gaining a great interest in the TE field. It is a simple, versatile and suitable method to incorporate functional groups on polymer surfaces without the use of solvents. A highly controlled treatment can be performed by adjusting all the process parameters to specifically modify polymer surfaces while avoiding the damaging of the scaffolds [117, 235, 236]. Therefore plasma is very adequate to treat delicate structures such as nanofibers. Moreover, the action of plasma treatments is limited in depth to few nanometers below the surface thus not affecting the bulk properties of the base material that conserves its mechanical stability [145, 190, 237]. Plasma treatment has the potential to homogenously modify the surface of complex shaped biomaterials which makes it even more attractive for the functionalization of nanofibers [238, 239]. In addition to its capacity to incorporate functional groups onto polymer surfaces, plasma treatment is also performed to deposit polymer coatings. These can be followed by the immobilization of proteins or other bioactive molecules on the scaffolds [240-244]. Plasma biofunctionalization can

overcome the downsides of blending biomolecules with the polymer solution prior to the electrospinning as well as the limitations of the direct coating of such molecules on the nanofibers. In the latter, a stable deposition is difficult to attain and biomolecules can aggregate in the interfiber spaces masking the pores of the electrospun matrix which hinders cellular in-growth and migration [227]. Furthermore, the concentration of proteins on the scaffold surface was demonstrated to be an important factor in regulating cellular activities. Shi et al. detected a correlation between the concentration of fibronectin and the adhesion of NIH 3T3 cells on nanofibers [245]. By plasma-treating the nanofibers, the density of the covalently immobilized biomolecules can be optimized since a highly specific surface chemistry can be obtained. Fig. III.1 gives a schematic illustration summarizing the surface modification techniques of nanofibers. Acknowledging these numerous advantages, the following section will give a more general description of different plasma surface functionalization approaches, accompanied with an overview on how these approaches have improved the performance of different types of polymeric biodegradable nanofibers in several TE fields.

Table III.1. *Synthetic polymer/biomolecule solutions used for the electrospinning of nanofibers used in various TE applications.*

Synthetic polymer	**Bioactive agent**	**Solvent**	**Potential application**	**Ref.**
PCL	Collagen type I	HFP	Nerve TE	[246]
P(LLA-CL)	Fibrinogen	HFP/Dulbecco's modified eagle medium (DMEM)	Skin TE	[247]
PCL	Gelatin Collagen/elastin	HFP	Cardiovascular TE	[248]
PLA	Gelatin	2,2,2-trifluoroethanol	Bone TE	[226]
P(LLA-CL)	Collagen type I	HFP	Vascular TE	[222]
PLGA	Silk fibroin/Collagen	HFP	Nerve TE	[249]
P(LLA-CL)	Collagen	HFP	Skin TE	[232]
PLLA	Hydroxyapatite (HA)	1,4-dioxane and dichloromethane	Bone TE	[229]
PCL	Chitosan	Trifluoroacetic acid/	Nerve TE	[224]

		Dichloromethane /HFP		
PLLA	Granulocytes colony-stimulating factor	Dichloromethane	Cardiac TE	[250]
PLLA	HA HA/Collagen	HFP	Bone TE	[251]
PCL	Laminin	HFP	Nerve TE	[225]
P(LLA-CL)	Gelatin HA/Gelatin	HFP	Bone TE	[228]

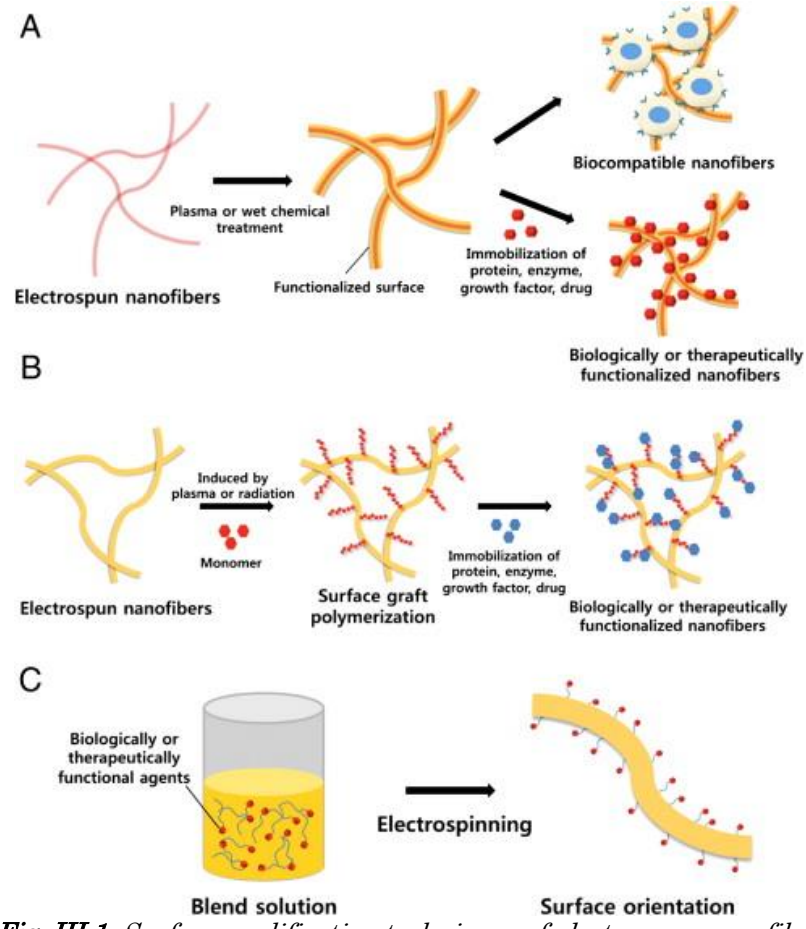

Fig. III.1. *Surface modification techniques of electrospun nanofibers. (A: Plasma activation or wet chemical treatments, B: Plasma or radiation surface graft polymerization, C: Co-electrospinning) [252].*

III.2. Plasma-assisted surface functionalization of nanofibers

Plasma was designated as the fourth state of matter by Langmuir in 1928 as its properties differ from gases, liquids and solids and a transfer to the plasma state can be obtained by supplying energy to a gas [253]. Plasma is a partially ionized but quasi-neutral gaseous mixture of ions, radicals, free electrons, UV photons and neutral particles such as atoms and molecules [254]. Plasmas are generally classified into 2 categories: equilibrium and non-equilibrium plasmas. Heavy electrons, ions, neutrals and excited species have the same temperature when plasma is in equilibrium. This category is referred to as thermal or hot plasma since the particles have a temperature of 4000 K or more, thus it cannot be employed to treat heat-sensitive biodegradable polymers. In contrast in a non-equilibrium plasma, a thermal inequilibrium is obtained between the heavy particles and the electrons when only the electrons are accelerated by applying for example an electrical field. This gives rise to of a cold or non-thermal plasma which is used to modify the surface of polymers for TE applications [145, 255, 256]. Several reactors have been built to generate plasma such as corona, radiofrequency (RF) and microwave (MW) discharge reactors. The description of these reactors falls outside the scope of this dissertation but is discussed in some book chapters and review papers [255, 257]. Initially, the scientific community was focusing on low-pressure systems as they display excellent plasma stability giving positive results in term of cellular adhesion, growth and proliferation. An interest in atmospheric pressure systems is progressively growing due to several advantages such as cost efficiency since no vacuum equipment is required and reduced process time. Since the feasibility of electrospinning biodegradable polymers was only demonstrated in the 1990s, researchers were busy in exploring the process and it was until 2004 that plasma treatment of nanofibers began to be studied [140]. Nowadays, the majority of studies involving a plasma surface modification of electrospun nanofibers is therefore still limited to low-pressure treatments mainly involving 3 different approaches: plasma activation, polymerization and grafting.

III.2.1. Plasma activation

When exposing a polymer to a plasma discharge, the reactive species will induce several plasma-surface reactions enhancing the polymer surface energy. Depending on the choice of the working gas, different functional groups will be added directly or indirectly on the surface. For example, a plasma generated in air, O_2, N_2 or NH_3 will incorporate

oxygen and/or nitrogen-containing functionalities during the plasma exposure and can create free radicals that could serve after the treatment for the grafting or cross-linking of oxygen groups on surfaces exposed to air. Argon and helium plasma discharges trigger the generation of surface radicals leading to the incorporation oxygen-containing functionalities after the treatment in the same way. In fact, post-plasma treatment oxidation will take place via secondary reaction pathways between oxygen molecules of the surrounding air and the plasma-generated radicals. [147, 258, 259]. The presence of these polar groups on the polymer surfaces were found to increase the polymer wettability which promotes focal adhesion formation, cellular spreading, growth and several metabolic processes [159]. Changing the plasma process parameters such as treatment time and power can be associated with a change in the hydrophilicity degree of the polymer surface. This degree was shown to be one of the major parameters influencing cellular activities. Webb et al. found that the optimal water contact angle (WCA) for a good adhesion is between 20 and 40 ° [260]. However, another study revealed that a high level of cell attachment and proliferation is obtained for a WCA of 55 ° [261]. This discrepancy in literature suggests that every cellular type has a particular optimal wettability on a specific type of polymer. Moreover the nature of the grafted groups can have an influence on different cellular behaviors. For example, surface carboxyl and hydroxyl groups were speculated to improve cellular attachment [262]. NH_2 groups resulting from NH_3 plasma treatment were proven to be more effective in enhancing cellular growth than oxygen containing groups induced by air and O_2 plasma treatments [263, 264]. The type and amount of functional groups incorporated on nanofibers can be more or less custom-tailored by adjusting the plasma conditions. However, because of the highly porous structure of nanofibers, the surface wettability is more difficult to control. Untreated nanofibers display a higher hydrophobicity compared to films made up of the same biodegradable polymer because the pores of the nanofibers increase air entrapment. Moreover, during the electrospinning, chemical groups having lower binding energies can be enriched on the nanofiber surface [265]. After plasma treatment, the incorporation of polar groups on nanofibers causes a sudden increase in the surface wettability since polar liquids will then rapidly penetrate in the porous mats [266]. Many authors experienced an abrupt transfer from superhydrophobic to superhydrophilic nanofibers having a WCA of 0 °after plasma treatment [114, 267, 268]. It is worth mentioning that the plasma activation effect is not permanent over time, a partial hydrophobic recovery occurs by the reorientation of the incorporated groups towards the material bulk and by post-plasma reactions between the modified surfaces and some atmospheric minorities [269,

270]. Interestingly, our research group has recently discovered that this hydrophobic recovery is less pronounced for PCL nanofibers compared to PCL films. Moreover, no surface modifications of plasma-treated PLLA nanofibers were detected by Dolci et al. at different ageing times after the treatment (Fig. III.2) [266]. This is presumably due to the fact that the electrospun network is not very exposed to the ambient air since each nanofiber is protected by the neighboring nanofibers.

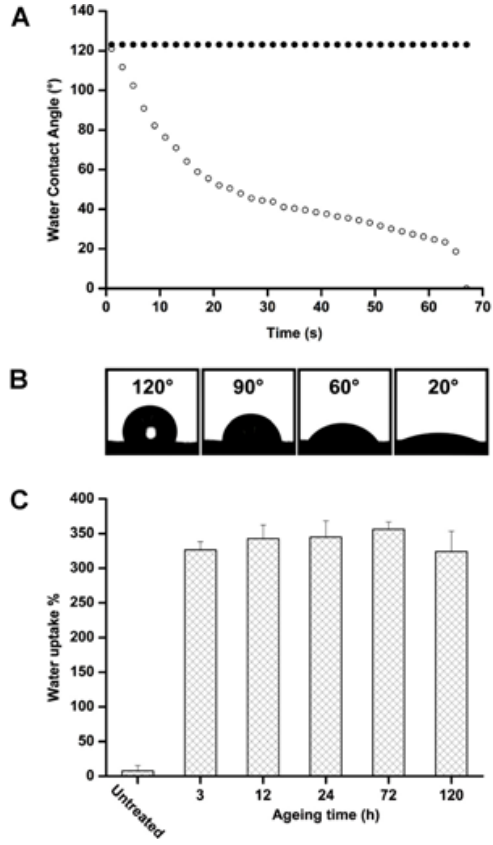

Fig. III.2. *A: Water contact angle behavior of electrospun PLLA fibers soon afterair atmospheric plasma treatment (black circles: untreated, White circles: plasma-treated). B: Evolution of the water drop profile. C: Percentage of the water uptake at different ageing times after the treatment [266].*

III.2.2. Plasma-activated nanofibers in TE applications

III.2.2.1. PCL fibers

As PCL is the most widely electrospun biodegradable polymer, it is the material of choice in the majority of studies involving a plasma surface modification of electrospun fibers. To the best of our knowledge, Fujihara et al. (2004) were one of the first groups to modify electrospun nanofibers making use of plasma technology [267]. Membranes for guided bone regeneration were fabricated by electrospinning a first layer of PCL nanofibers followed by a composite layer of $CaCO_3$/PCL nanofibers on the surface. The PCL nanofibrous membrane having a high tensile strength served as a mechanical support layer. The second layer was spun after dissolving $CaCO_3$ nanoparticles in the PCL solution to serve as a functional layer since $CaCO_3$ is known to be a good bone filling material enhancing the osteoconductivity. The fabricated membrane was then subjected to an RF plasma treatment operating in air at low pressure. The treatment remarkably modified the nanofiber wettability as the WCA decreased from 139 ° to 0 °. MTS (3-(4,5-dimethylthiazol-2-yl)-5-(3-carboxymethoxyphenyl)-2-(4-sulfophenyl)-2H-tetrazolium) assay and scanning electron microscope (SEM) study revealed good attachment and proliferation of osteoblasts on the treated surfaces thus highlighting the potential of using such membranes in enhancing bone regeneration. No cell tests were performed on untreated nanofibers thus making from the efficiency of plasma treatment a questionable issue [267]. Several studies followed to confirm the plasma efficiency in the development of PCL nanofibers offering promises in bone TE applications. Four years after the research conducted by Fujihara et al. [267], Venugopal et al. spun PCL and PCL/HA nanofibers and also subjected them to an RF air plasma treatment at low pressure. A complete adsorption of water drops was also observed on PCL and PCL/HA nanofiber meshes that were having WCA of around 131 ° and 125 ° respectively before the treatment. The proliferation of human fetal osteoblasts on plasma-treated scaffolds was significantly higher than on the untreated fibers as shown by MTS assay. Alizarin red staining was performed to detect and quantify calcium mineralization and showed a limited mineralization on PCL fibers compared to PCL/HA fibers with the highest staining intensity on plasma-treated PCL/HA fibers. Therefore the synchronic effect of HA and plasma treatment was shown to be a promising tool for bone regeneration [271]. Proper surface analysis not only limited to WCA measurements but giving precise qualitative and quantitative ideas about the surface chemistry was found essential to deeply understand the mechanisms by which plasma treatment of nanofibers enhances bone regeneration. Therefore, researchers began to chemically

characterize PCL surfaces making use of X-ray photoelectron spectroscopy (XPS) and Fourrier transform infrared spectroscopy (FTIR). Yan et al. published two papers on PCL nanofibers exposed to low-pressure RF plasma to study the behavior of mouse osteoblast cells (MC3T3-E1) when cultured on such scaffolds. In the first paper random and aligned fibers were subjected to $NH_3 + O_2$ plasma whereas in the second paper only random fibers were subjected to plasma generated in 3 different working gas atmospheres: $N_2 + H_2$, $NH_3 + O_2$ and $Ar + O_2$. In all cases, the WCA decreased from around 135 ° to 0 °. Since water rapidly penetrates in the treated nanofibrous matrix, the change of the surface hydrophilicity in function of the plasma treatment time could not be monitored. Therefore, glycerol which is a very viscous polar liquid was used and showed a gradual decrease in the CA with the increase of the plasma exposure times. As a result of the increased wettability, the mechanical properties of the nanofibers such as tensile strength and Young modulus slightly changed after plasma treatment. XPS measurements showed an increase in the surface oxygen that was incorporated in form of C-O and C=O groups after the treatment. Moreover an incorporation of N-containing functionalities was detected after $N_2 + H_2$ and $NH_3 + O_2$ plasma treatments. An amine titration test demonstrated that amine groups were only present on the $N_2 + H_2$ plasma-treated fibers. These incorporated functional groups enhanced cellular adhesion, proliferation and growth as showed by MTT (3-(4,5-dimethylthiazol-2-yl)-2,5-diphenyltetrazolium bromide) assay and SEM study. When cultured on the aligned fibers, MC3T3-E1 cells followed the fiber orientation by growing and spreading parallel to the fibers [114, 262]. In 2014, Sankar et al. electrospun nano-, micro- and multiscale PCL fibrous scaffolds, subjected them to argon and nitrogen plasma treatment under vacuum and studied their osteoconductivity. A gradual decrease in the WCA was observed when increasing the treatment power with a significant WCA reduction for the nanofiber-containing mats. XPS and FTIR measurements confirmed the surface functionalization of the fibers. Argon plasma treatment incorporated OH, C=O and C-O groups on the fiber surface while nitrogen incorporated OH and NH groups. An enhanced adhesion, spreading, and proliferation of human MSCs was detected on plasma-treated fibers with a remarkable adhesion improvement on nanofibers. The differentiation of hMSCs towards osteogenic lineage was evaluated by quantifying the alkaline phosphatase (ALP) activity. An enhanced differentiation was identified on plasma-treated fibers and was further confirmed by the mineralization (alizarin red staining) of the treated scaffolds, revealing the maturation of the differentiated osteoblasts [272]. In a recent study conducted by Jeon et al. plasma technology was used to generate nanosized patterned on electrospun PCL microfibers

and to subsequently study the behavior of osteoblast-like-cells (MG63) [273]. A modified plasma reactor containing porous (100 nm and 800 nm) templates and operating in oxygen at low-pressure was fabricated for this purpose. No chemical surface analysis was performed since the goal of that novel plasma technique is mainly to physically alter the surface. SEM analysis showed that increasing the plasma exposure time or power is accompanied with the formation on nanopatterns on the fibers probably due to a plasma etching. As a result a slightly lower Young's modulus was detected. Nanopatterned fibers considerably enhanced cellular attachment and proliferation compared to untreated and conventionally plasma-treated fibers, thus making from this new plasma treatment a promising tool for bone and various TE applications [273]. In addition to the bone TE field, plasma-treated PCL fibers were also employed in several other applications such as nerve, cardiac, vascular, skin, hair and ocular TE. Low pressure RF systems were mainly employed to generate plasma in these applications. Sharma et al. were one of the rare groups to use atmospheric pressure plasma to enhance the bioactivity of PCL fibers used to reconstruct ocular surface. Similar surface analysis techniques and cell tests were performed in most of the studies. De Valence et al. went into more advanced *in vivo* tests by implanting plasma-activated electropun PCL scaffolds as a vascular graft (Fig. III.3). The corresponding studies are summarized in Table III.2.

Table III.2. *Overview of literature on plasma activation on PCL electrospun fibers not discussed in the text.*

Author (Year)	**Reactor and gas**	**Physico-chemical properties**	**Cell type**	**Bioresponsive properties**
Prabhakaran et al. [138] (2008)	RF low pressure air	-Enhanced wettability -Incorporation of O-containing groups -Decreased tensile strength -Unmodified elongation at break	Schwann cells (RT4-D6P2T)	-Better attachment and proliferation -Expression of bipolar elongations
Martins et al. [88] (2009)	RF low pressure O_2 or Ar	-Enhanced wettability	-Mouse fibroblasts (L929)	Better viability,

		-Incorporation of C-O, C=O and O-C-O groups	-Human primary osteosarcoma cells (Saos-2) -Mouse chondrocyte teratocarcinoma cells (ATDC5)	adhesion and proliferation
Jahani et al. [274] (2012)	RF low pressure O_2	-Enhanced wettability -Reduced mechanical strength	Mesenchymal stem cells	Better proliferation
De Valence et al. [275] (2013)	RF low pressure O_2	-Enhanced wettability -Unchanged mechanical strength and elasticity	Primary porcine smooth muscle cells	-Elongated cell morphology -*In vivo* implantation: Better cellularization and more dense and extended cellular infiltrate in the scaffold
Abbasi et al. [276] (2014)	RF low pressure O_2	-Enhanced wettability -Decreased mechanical strength and elongation at break	Mouse embryonic stem cells	Better proliferation
Sharma et al. [277] (2014)	Atmospheric pressure He/O_2	-Enhanced wettability -Unchanged mechanical strength -Enhanced transparency	-Human corneal epithelial cells -Limbal epithelial cells	-Better cell adhesion and proliferation -Cell morphology showing abundant microvilli -Retained cell phenotype showed by gene expression
Pappa et al. [278]	40 kHz low	-Enhanced wettability	Mouse fibroblasts L929	Enhanced viability,

(2015)	pressure O_2	-Incorporation of C-O and C=O groups -Modified roughness -Unchanged mechanical properties		adhesion and proliferation
Recek et al. [279] (2016)	RF low pressure O_2 or NH_3 or SO_2	-Incorporation of: C-O, C=O, O=C-O, C-S (SO2 plasma), C-N and O=C-N (NH_3 plasma) groups	Human umbilical endothelial cells	-Enhanced adhesion and proliferation (O_2 and NH_3 plasmas) -Elongated cell morphology
Yari et al. [186] (2016)	Low pressure O_2	_	Rat nestin-positive hair follicle stem cells	Good adhesion and proliferation

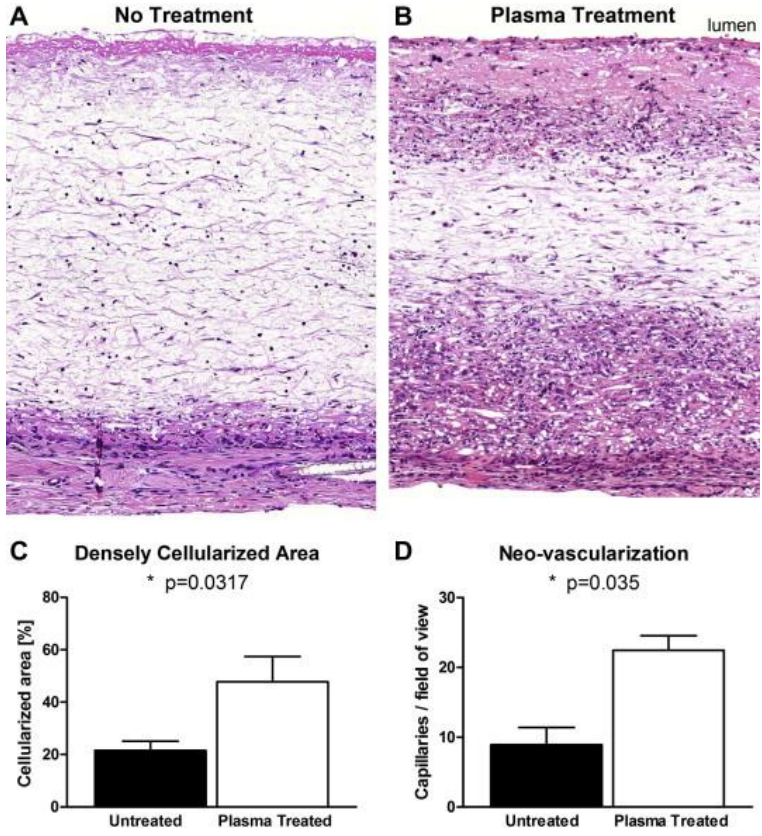

Fig. III.3. *Vascular implantation of untreated and plasma-treated electrospun PCL grafts. Improvement of the cellular invasion in the plasma-treated graft wall (A) compared to the untreated graft (B). Significant improvement of the densely cellularized area (C) and the number of capillaries (D) in the graft wall after plasma treatment [275].*

Two very recent studies integrating novel biomimetic scaffolds with atmospheric plasma activation showed interesting results in stimulating tissue regeneration. Zhu et al. developed a PCL electrospun mat on which PLGA microspheres containing TGF-β1 and bovine serum albumin were distributed to induce chondrogenesis. The scaffolds were then subjected to an atmospheric He plasma that decreased their WCA by 61% leading to an enhanced proliferation of

primary MSCs (Fig. III.4). An improved cell infiltration capacity on the treated scaffolds was detected by immunofluorescence microscopy. Moreover, after maintaining the seeded scaffolds in a chondrogenic media, significantly enhanced GAG production and collagen synthesis were detected on the plasma-treated samples compared to the untreated samples thus revealing the differentiation of MSCs into a chondrogenic lineage [117]. Another biomimetic electrospun scaffold involving the layer-by-layer approach was fabricated by Surucu et al. for L929 fibroblast cultivation. Three layers were successively electrospun on top of each other: PCL/Chitosan/ PCL. A plasma treatment was applied by using a dielectric barrier discharge (DBD) operating in Ar + N_2 or Ar +O_2 at atmospheric pressure. Ar + N_2 plasma was unable to significantly enhance the wettability of the fibers, thus Ar + O_2 atmosphere was used for subsequent experiments. A combination of O-group incorporation and nanoroughness change resulted in an improved cellular performance in terms of adhesion, viability and proliferation [280].

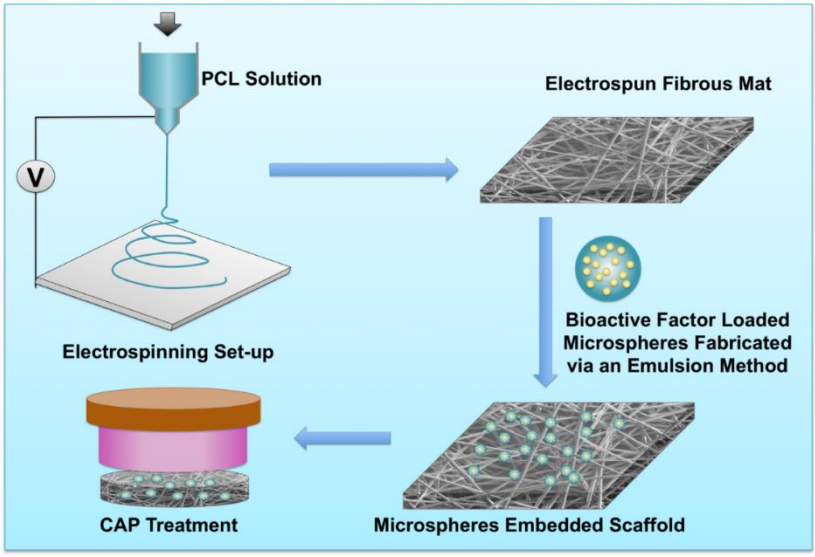

Fig. III.4. *Schematic illustration of embedding PLGA microspheres on PCL electrospun fibers and cold atmospheric plasma (CAP) modification for cartilage TE [117].*

III.2.2.2. PLLA fibers

After PCL, the second most plasma-activated electrospun scaffolds for TE applications are PLLA nanofibers. One of the first attempts conducted by Corey et al. and aiming to improve the behavior of neurons cultured on plasma-treated PLLA fibers was unsuccessful. Air plasma treatment worsened the survival of primary motor neurons when seeded at low densities on PLLA fibers despite that it decreased the mat's WCA from 63 ° to 32 °. Since this undesirable effect was not observed on untreated scaffolds, one can conclude that plasma treatment negatively altered the fiber chemistry and/or morphology which reduced cellular viability. Therefore, plasma process parameters should be selected more carefully based on a detailed chemical and physical surface analysis characterizing what changes are occurring and to what extent, which was absent in this study [159]. The subsequent studies involving a plasma activation of PLLA fibers presented very promising results in enhancing tissue regeneration. Low pressure RF systems were used to create plasma discharges in different working gas atmospheres: O_2, Ar and Ar-NH_3/H_2. The hydrophobic PLLA fibers having WCA values above 115 °were switched to superhydrophilic fibers with WCA values depending on the working conditions (used gas, treatment time and power). XPS measurements revealed an incorporation of O-containing groups (C-O, C=O and O-C=O) for all plasma treatments with an additional incorporation of N-containing groups on the fibers treated by Ar-NH_3/H_2 plasma. In this last case, trifluoromethyl benzaldehyde (TFBA) derivatization particularly demonstrated the incorporation of NH_2 groups. As a result of these surface modifications, Liu et al. detected an improved adhesion of porcine MSCs on O_2 plasma-treated fibers while Correia et al. showed a good metabolic activity of MC3T3-E1 cells when cultured on Ar or O_2 plasma-treated fibers [281, 282]. Cheng et al. demonstrated that argon plasma treatment is very efficient in improving the proliferation of bovine aorta endothelial cells (BAECs) and bovine smooth muscles cells (BSMCs) while Ar-NH_3/H_2 plasma treatment is more efficient in enhancing their spreading on PLLA fibers. The visualization of the scaffold cross sections by fluorescent microscopy after DAPI staining revealed that both plasma treatments are efficient in improving BAEC infiltration into the scaffolds. *In vivo* subcutaneous implantation of PLLA scaffolds under rat skin also enhanced the cellular infiltration when plasma-treated [283]. Atmospheric pressure plasma was also employed to activate PLLA fibers and similar surface analysis techniques and cell tests were conducted. Liu et al. increased the amino group content and thus enhanced the wettability of PLLA fibers by placing them in a plasma cleaner and treating them for different

plasma exposure times. In addition to cell proliferation tests, showing a greater performance of bone marrow stem cells on plasma-treated fibers, quantitative reverse transcription–polymerase chain reaction (qRT-PCR) analysis was performed to assess the expression of osteogenic-specific genes. The treated nanofibers promoted high levels of osteogenic gene expression accompanied with an excessive ALP activity thus revealing the differentiation of the cells towards an osteogenic lineage. Therefore plasma-treated PLLA nanofibers are promising candidates for bone regeneration [284]. Dolci et al. plasma-treated PLLA nanofibers using a linear corona discharge system operating in air at atmospheric pressure. A significantly greater wettability is attained (WCA: 120 ° to 20 °) correlating with the detected incorporation of COOH groups. In order to assess the amount of COOH incorporated on the fibers, a chemical derivatization and conjugation with fluorescein isothiocyanate (FITC) is performed followed by a measurement of the fluorescence intensity. When cultured on plasma-treated fibers, mouse embryonic fibroblasts exhibited a dendritic-like and more elongated morphology compared to cells grown on untreated fibers [266].

III.2.2.3. PLGA fibers

Despite the excessive use of electrospun PLGA nanofibers in a wide range of TE applications, the modification of their surface by plasma treatment is still overlooked in literature. Park et al. are one of the rare groups, if not the only one, that considered studying the plasma activation of PLGA fibers. They published 3 papers in which a Miniplasma-station® operating in O_2 and NH_3 at low pressure was used to activate PLGA nanofibers. The first paper was restricted to a physico-chemical surface analysis. A loss of the nanofibrous structure was observed after an exposure to O_2 plasma for 180 s. However the fibers retained their morphology and dimension when exposed to NH_3 plasma. An enhanced wettability was detected by the decrease of the WCA from 139 ° to 112 ° and 47 ° after O_2 and NH_3 plasma treatment respectively. The WCA results correlate with the XPS measurements that revealed a slight increase in the O/C ratio after O_2 plasma exposure and a significant increase in the N/C ratio after NH_3 plasma treatment [285]. In the second paper, in addition to a more detailed surface analysis, the authors investigated the degradation of the fibers *in vitro* as well as their bioresponsive properties using mouse NIH 3T3 fibroblasts. When incubated in phosphate buffered saline solution for 2 weeks, plasma-treated fibers showed a much faster degradation than untreated fibers. A well-controlled degradation rate is critical in TE and should be therefore reconsidered after plasma treatment. An enhanced

cell adhesion and proliferation were detected after the surface activation especially on the NH_3 plasma-treated samples [239]. Based on the obtained results, in the third study, the fibers were only treated with NH_3 plasma and the expression of Bcl-2 and heat shock protein (HSP) in the cultured fibroblasts was assessed by RT-PCR as a function of N-density and wettability. It is well known that HSP genes are expressed when cells are subjected to various types of stress while Bcl-2 expression is reduced when a stress apoptotic pathway occurs. A prominent expression of HSP was detected on untreated and plasma-treated fibers having the lowest WCA with almost no expression of Bcl-2 genes. Inversed gene expression levels was perceived on fibers having a WCA around 51 °. Therefore, a moderate hydrophilicity is favorable for the cells as it suppressed the cellular stress which was in accordance with an enhanced cell viability as shown by a dead/live staining assay [286].

III.2.3. Plasma polymerization and grafting

A thin polymeric film-forming approach involving a plasma exposure refers to as plasma polymerization and is chemically different from the conventional wet-chemical polymerization. The former can be defined as a radical polymerization in which propagating reactions between monomers and a polymeric substrate are initiated by radical species at the polymer surface while the latter is known as an ionic polymerization involving chemical reactions generated by ionic species [287]. During plasma polymerization, liquid or gaseous monomers are exposed to the reactive plasma and are therefore converted into reactive components that recombine to the substrate initiation sites also induced by the plasma exposure. As a consequence, an amorphous highly branched and cross-linked nm-thick polymer film is deposited on the substrate. Plasma polymers are generally characterized by a high stability and density, a great adhesion to a variety of substrates, a chemical inertia, a mechanical toughness and a pinhole-free structure [145, 147]. All these characteristics are extensively influenced by a set of parameters used during the plasma process [137]. Although extensively used in TE applications, this solvent-free deposition technique is mainly limited to non-electrospun scaffolds since optimizing all the plasma parameters in order to simultaneously obtain a stable coating while preserving the delicate structure of nanofibers remains a major challenge. Few authors succeeded to attain this goal and highlighted the importance of this promising technique in enhancing the performance of specific cell types when cultured on nanofibers [190, 288, 289].

Plasma grafting is a two-phase technique of which the first phase requires a plasma exposure while the second phase involving a direct contact with a (macro)monomer occurs post-plasma irradiation. The plasma treatment introduces, as described above, reactive groups on the polymer surface serving afterwards as initiation sites for direct radical vinyl polymerization or for covalent immobilization of biomolecules which involves a wet-chemical step. The resulting coating is characterized by a high stability and functional specificity [137, 147, 258]. The synchronic effect of electrospinning and plasma grafting was recently associated with several advances in the TE field. This was illustrated by the significant enhancement of several cellular activities when plasma grafts biomolecules such as ECM components and growth factors on nanofibers [115, 187]. Both plasma grafting and plasma polymerization techniques are considered superior to the plasma activation in terms of ageing effect.

III.2.4. Plasma polymerization and grafting applied on nanofibers in TE applications

III.2.4.1. PCL fibers

In addition to the simple plasma activation, plasma grafting of bioactive molecules on electrospun PCL fibers was studied and showed great achievements in different TE fields. Vascular TE was one of the first fields in which plasma grafting applied on PCL fibers was investigated. Electrospun biodegradable polymers were being used to fabricate tubes that can be implanted in the body as vascular substitutes. Seeding endothelial cells (ECs) onto the tubes can help to prevent intimal hyperplasia after implantation since these cells release factors that control fibrinolysis and thrombogenesis [290, 291]. However ECs are often detached from the graft surface when exposed to blood circulation. Grafting ECM proteins on the material surface was shown to favor the cell attachment. Therefore, in 2005, Ma et al. subjected PCL nanofibers to an RF air plasma in order to introduce COOH groups onto their surface for subsequent grafting of gelatin. Toluidine blue O, a dye that can specifically combine with carboxyl groups, was used and showed that increasing the plasma exposure time and the electrospun mat thickness is associated with an increase in the COOH density. Water- soluble carboiimide was employed to activate COOH groups which served as binding sites for gelatin. Human coronary artery endothelial cells (HCAECs) kept a rounded morphology when cultured on untreated fibers, while they became totally spread

with the formation of pseudopods on gelatin-grafted fibers. Moreover, MTS assay showed an enhanced proliferation on the treated fibers and immunostaining assay revealed that the proliferating cells retained their phenotype as they expressed 3 characteristics markers: vascular cell adhesion molecule 1, intercellular adhesion molecule 1 and platelet-endothelial cell adhesion molecule 1. Therefore gelatin plasma-grafted PCL fibers are promising candidates in blood vessel TE [243]. In the same year, this research group thought of testing of efficiency of collagen coating in the endothelialization of electrospun nanofibers. In order to control the degradation rate of the nanofibers, PCL was replaced by the copolymer P(LLA-CL). After subjecting the fibers to an almost similar plasma treatment, the fibers were immersed in a collagen solution then dried. XPS and BCA protein assay confirmed the immobilization of a good amount of collagen on the fibers and rhodamine staining showed an excellent distribution throughout the scaffold. Similar cell tests were performed and showed more or less the same positive results which also highlights the potential of collagen plasma-grafted fibers to serve as vascular grafts [292]. In 2014, Guex et al. conducted 2 studies in which PCL fibers were coated with a CHO-type layer rich with ester bonds using an RF plasma process ($C_2H_4/CO_2/Ar$). In the first study, vascular endothelial growth factors (VEGF) were immobilized on the plasma-coated fibers to study the behavior of primary and immortalized human umbilical vein endothelial cells (HUVECs). EDC/NHS (1-ethyl-3-(3-dimethylaminopropyl) carbodiimide/N-hydroxysuccinimide) based coupling chemistry was adopted to convert the incorporated COOH groups into amine reactive ester groups used to covalently couple VEGF by creating amide bonds. An additional linker molecule was added to this functionalization route in order to diminish the steric hindrance during protein immobilization. The biological integrity of VEGF was maintained after the grafting as shown by immunohistochemistry assay using anti-VEGF antibodies. The functionalized fibers induced a higher number of primary and immortalized cells, 9 days after culturing, compared to untreated fibers. Thus, these growth factor-loaded nanofibers can also provide successful scaffolds for vascular TE [242]. In the second study, the CHO-coated PCL fibers were used to repair damaged myocardium. Bone-marrow-derived MSCs were seeded on the scaffolds that were subsequently implanted into a rat model of chronic myocardial infraction. Echocardiograms and histological evaluation of the implanted scaffolds revealed a steadied cardiac function associated with a diminished dilatation in case of the plasma-coated scaffolds. Moreover, a significant decrease in the ejection fraction and the fractional shortening was observed 4 weeks after implantation in the group implanted with the plasma-coated scaffolds

compared to the control group [235]. These results demonstrate that optimized PCL electrospinning associated with plasma grafting and polymerization can allow translational research in the cardiovascular field.

Bone TE also experienced some advances when adopting plasma grafting and polymerization to functionalize PCL fibers serving as bone grafts. For instance, Yang et al. subjected PCL fibers to an RF plasma treatment using a plasma cleaner operating in argon at low pressure. Then the plasma-treated fibers were immersed in a simulated body fluid (SBF) for immobilization of CaP. After 2h of immersion, a coating composed of nanoapatite and dicalcium phosphate apatite was found to cover the fibers with the preservation of the porous structure. A continuous immersion in SBF for a week transformed the coating into pure calcium with nanocrystallinity closely comparable to the biological apatite. The obtained scaffold is expected to serve as a successful cell carrier promoting bone regeneration [293]. Recently, Ko et al. investigated the plasma deposition of acid rich coating on PCL nanofibers and the performance of pre-osteoblasts MC3T3-E1 when seeded on such fibers. An argon low pressure RF plasma was applied followed by a plasma polymerization phase using acrylic acid as precursor. XPS measurements showed an increase in the O/C ratio from 0.30 to 0.34, accompanied with an enhanced wettability. MTT assay revealed an improved cell proliferation on the plasma-coated fibers with a greater alkaline phosphatase activity suggesting a successful differentiation towards osteoblastic lineage [288].

In addition to the cardiovascular and bone TE, the potential of plasma-coated PCL fibers in improving nerve regeneration was also explored. Zander et al. published 2 papers in which neurite outgrowth on PCL fibers was studied. In the first paper, collagen and laminin were used to functionalize the fibers by physical adsorption or covalent attachment chemistries. Prior to the covalent attachment, fibers were subjected to air RF plasma treatment at low pressure to introduce carboxylic groups onto the fiber surface. EDC/NHS based coupling chemistry was then adopted to graft collagen and laminin on the fibers. Concerning the physical adsorption, the fibers were directly incubated in laminin and collagen solutions. After seeding PC12 neuron-like cells on the fibers, neurite outgrowth was visualized by confocal microscopy after actin staining. Cells grown on the modified fibers exhibited significantly longer neurites than the cells cultured on untreated fibers. Among the protein-modified scaffolds, shorter neurites are observed on the collagen plasma-coated fibers. This is suggestive of an altered collagen conformation after covalent attachment or low protein content on the fibers. The bioavailability of the laminin-coated fibers was tested by an immunofluorescence assay using anti-laminin antibodies and no

difference was observed between the physically adsorbed and the covalently attached laminin. The covalent chemistry did not alter the laminin conformation or reduce its activity which makes from the plasma-coating of laminin a suitable method for enhancing nerve regeneration [133]. Therefore, in their second paper, the authors plasma-coated PCL fibers with laminin and studied the effect of the incorporated protein amount on the neurite outgrowth. The protein concentration was assessed by several methods (XPS, UV spectroscopy and fluorescence-based assays) and longer neurites were observed on fibers containing higher concentrations of laminin [294].

Some authors studied the bioresponsive properties of plasma-coated PCL fibers and demonstrated their efficiency in tissue regeneration without being limited to a TE field in particular. Jia et al. immobilized soluble eggshell membrane proteins (SEP) on PCL fibers by treating them with low pressure RF argon plasma and immersing them in SEP solution. They expected a great potential of these fibers in TE applications since the eggshell membrane is to some extend very similar to the ECM. It contains several proteins such as collagen type I, V and X that play an important role in the development of the embryo and the mineralization of the eggshell. Human dermal fibroblasts were seeded on the SEP-coated fibers. MTT assay, SEM and confocal microscopy revealed a significant improvement in cellular attachment, spreading and proliferation which confirmed the hypothesis of the authors (Fig. III.5) [295]. Safaeijavan et al. studied the behavior of fibroblasts on gelatin plasma-coated PCL fibers. The fibers were subjected to an oxygen plasma treatment using a low frequency (40 kHz) plasma generator operating at low pressure then a covalent immobilization of gelatin was performed by carbodiimide wet chemistry. MTT assay showed an enhanced cellular viability and proliferation on the treated fibers [296]. Very recently, Cohn et al. adopted a new strategy to functionalize electrospun PCL fibers. First, an air plasma treatment at low pressure was applied then the plasma-treated fibers were immersed in a solution containing cholesteryl succinyl silane (CSS). CSS vesicles were therefore immobilized on the fibers then ruptured and fused into a lipid bilayer. CSS immobilization on the plasma-treated fibers was confirmed by a fluorescent probe for lipid bilayers and by Raman spectroscopy. Then anti-CD20 were immobilized on the CSS to biologically functionalize the fibers with a high cell specificity. After seeding Granta-22 B lymphoma cells, anti-CD20 functionalized fibers were shown to capture the cells 2.4 times more than the untreated fibers. Important TE applications may thus be improved by this lipid-mediated protein functionalization of nanofibers [231].

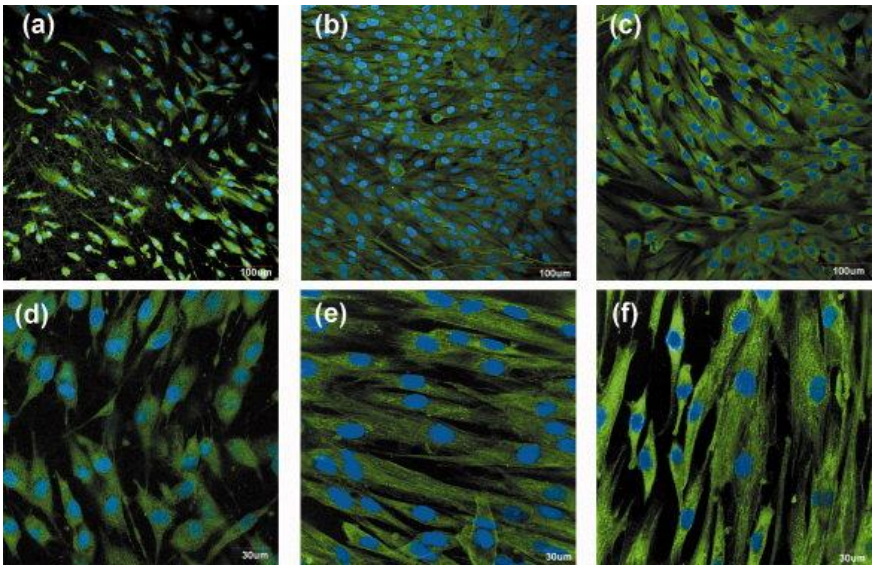

Fig. III.5. *Morphology of cytoskeleton and nuclei of fibroblasts cultured on (a, d) untreated PCL nanofibers, (b, e) SEP plasma-modified PCL nanofibers, and (c, f) glass coverslips after 3 days. F-actin microfilaments are visualized by phalloidin-FITC (green). Cell nuclei are visualized by Hoechst 33258 (blue). The fibers are visualized by auto-fluorescence [295].*

III.2.4.2. PLLA fibers

Several plasma polymerization and grafting strategies were also applied on electrospun PLLA nanofibrous scaffolds in order to be effectively used in bone, blood vessel, liver, cartilage, nerve and other TE applications. Park et al were one of the first groups to investigate plasma polymerization of acrylic acid on nanofibers. In 2 papers, published in 2006 and 2007, they subjected PLLA fibers to a simultaneous low pressure oxygen plasma treatment and in situ acrylic acid polymerization for 30s using an RF glow discharge device. In the first paper PLLA films were also tested while in the second study PGA and PLGA fibers were explored. In all cases, no significant morphological or mechanical (tensile strength and elongation-at-break) difference was perceived after the treatment. A decreased WCA associated with an incorporation of O-containing functionalities such as COOH were detected on the fibers by performing ESCA measurements and toluidine blue O assay. MTT assay showed an

enhanced proliferation of NIH 3T3 fibroblasts when cultured on the acrylic acid-grafted scaffolds for 6 days [190, 289].
In 2008, Koh et al. conducted a comparative study about neuron viability and outgrowth on PLLA fibers functionalized with laminin by means of three different methods. In the first 2 methods, the fibers were subjected to an RF plasma treatment using a plasma cleaner operating in air. Afterwards, a covalent binding of laminin was performed on some of the plasma-treated fibers based on the EDC/NHS coupling chemistry, while a physical adsorption of laminin was done on the other plasma-treated fibers by simply immersing them in a laminin solution. In the third method, laminin was blended with the PLLA solution prior to the electrospinning. MTS assay showed that laminin-PLLA nanofibers supported better neuron-like PC12 cell viability compared to untreated fibers. Moreover, laminin was able to promote axonal extensions as revealed by immunohistochemistry assay with extensive neurite outgrowth particularly on the blended laminin-PLLA fibers containing more laminin. This suggests that the high voltage of the electrospinning and the solvent HFP did not adversely affect the laminin bioactivity. Therefore, plasma functionalization was in this case less efficient than the blending method in enhancing nerve regeneration [134]. Recently, unsatisfying neurite outgrowth results were also obtained by Schaub et al. when applying a plasma grafting of different molecules on electrospun PLLA fibers. An RF oxygen plasma treatment was carried out on the PLLA fibers that were subsequently modified by EDC/NHS to covalently bind diethylnetriamine (DTA) for amine functionalization, 2-(2-aminoethoxy)ethanol (AEO) for alcohol functionalization or GRGDS sequences as bioactive ligands interacting with integrins. Unexpectedly, the untreated fibers exhibited the best neurite outgrowth after culturing chick dorsal root ganglia (DRG). The longest neurites were detected on untreated fibers followed by fibers containing GRGDS. Shorter neurites were observed on plasma-treated fibers and on fibers functionalized with DTA and significantly short neurites were detected on fibers grafted with AEO. These results suggest that neurite extension needs a very specific surface functionalization using adequate bioactive ligands rather than a randomly increased hydrophilicity [297]. When it comes to bone, liver, cartilage and blood vessel TE, several studies have recently shown that combining PLLA electrospinning with plasma surface grafting of biomolecules was rather very promising. These studies and their general results will be summarized in table III.3.

Table III.3. *Overview of literature on plasma grafting on electrospun PLLA fibers not discussed within the text.*

Author (Year)	**Reactor and gas**	**Precursor**	**Cell type**	**Effect (Potential application)**
Paletta et al. [298] (2010)	RF low pressure O_2	Cyclic RGD grafted (EDC/NHS coupling chemistry)	Human mesenchymal stem cells	-No enhanced proliferation and cell density because of limited RGD densities -Differentiation towards osteoblastic lineage (Bone TE)
Seyedjafari et al. [227] (2010)	MW low pressure O_2	Nanohydroxyapatite grafted	Unrestricted somatic stem cells	-Enhanced attachment, spreading and proliferation -Efficient differentiation towards osteogenic lineage: High ALP activity, biomineralization and expression of bone-related genes -*In vivo* subcutaneous implantation: ossification and formation of trabeculi (Bone TE)
Chen et al. [127] (2011)	DC pulsed system low pressure O_2	Cationized gelatin grafted (EDC coupling chemistry)	Rabbit articular chondrocytes	-Enhanced viability, proliferation and differentiation : improved collagen and glycosaminoglycan secretion and expression of chondrocyte markers -*In vivo* subcutaneous implantation: Formation of ectopic cartilaginous tissue (Cartilage TE)
Ghaedi et al. [299] (2012)	MW low pressure O_2	Collagen grafted (EDC/NHS coupling chemistry)	Human bone-marrow derived mesenchymal stem cells	Efficient differentiation into hepatocyte lineage: high expression of liver-specific markers such as α-fetoprotein, albumin and cytokeratins 8

				(Liver TE)
Seo et al. [300] (2013)	DC atmospheric pressure He	Fibronectin adsorption	_	Deep penetration of the fibronectin in the nanofibrous matrix (TE)
Cheng et al. [116] (2014)	RF low pressure Ar-NH_3/H_2	Heparin grafted (EDC/NHS coupling chemistry)	Bovine aorta endothelial cells	Enhanced cellular infiltration through the nanofibrous scaffold (Blood vessel TE)

III.2.4.3. PLGA fibers

Plasma polymerization and grafting strategies were rarely applied on electrospun PLGA scaffolds despite the promising results obtained when plasma functionalizing PLLA and PCL fibers. In 2010, Park et al. indirectly used plasma to graft PLGA fibers on polyurethane (PU) films. This was done by electrospinning PLGA fibers on PU films previously subjected to an atmospheric pressure MW plasma treatment operating in argon. The whole PU/PLGA scaffolds were then again plasma-treated to crosslink the PLGA fibers. After culturing human umbilical vein endothelial on the scaffold, MTT assay revealed a better adhesion and proliferation on PU/PLGA compared to PU scaffolds thus highlighting the importance of the grafted fibers. Moreover, a significantly enhanced adhesion was particularly detected on the plasma-treated PU/PLGA scaffolds thus highlighting the importance of the plasma. Therefore, such scaffolds can be considered, after in-depth studies, for their use as vascular grafts [301]. In 2012, Meade et al. plasma-functionalized PLGA fibers to afford biological and topographical cues to regulate pluripotent stem cells (PSCs) fate. Therefore, in a first step allylamine was plasma-polymerized on the fiber by using a low pressure RF plasma generator. Then the fibers were incubated in heparan sulfate (HS) solutions. The allylamine coating was found to immmobilize HS on the fibers with a retained ligand binding capacity. HS is a GAG that modulates the activity of wide-ranging growth factors and cytokines thus particularly controlling various signaling pathways directing PSCs behavior. HS-deficient mouse embryonic stem cells seeded on the treated fibers were successfully differentiated into neuronal lineage when adding the fibroblast growth factor 4 (FGF4) suggesting that the growth factor is activated by the immobilized HS on the fibers [302].

III.3. Conclusion

In this chapter, a quite extensive overview has been given on the literature involving a joint use of electrospinning and non-thermal plasma surface modification technologies for TE applications. In the past decade, electrospinning of synthetic biodegradable nanofibers has experienced a steep continuous rise due to their structural resemblance to the ECM. In parallel, plasma surface engineering techniques were been widely investigated to functionalize these nanofibers thus also mimicking the biological role of the ECM. Plasma activation, polymerization and grafting of bioactive molecules applied on electrospun scaffolds have shown great improvement in supporting various cell types that attached, proliferated, migrated and differentiated more efficiently compared to the untreated scaffolds. These results revealed that plasma is a powerful tool in enhancing bone, nerve, blood vessel, liver, cartilage and other tissue regeneration and should be therefore adopted by every tissue engineer. In the next few years, more attention should be given concerning the effects of the surface modification on the molecular processes induced in different cell types such as gene expression analysis. This will give more insights on how to specifically optimize the plasma process parameters for each cell type or tissue to be regenerated. Moreover, a translation from *in vitro* tests to *in vivo* tests should be more considered to pave the ways for the use of patient-customized electrospun scaffolds in humans suffering from tissue loss or failure.

Chapter IV. Plasma gradients

IV.1. Introduction

After accomplishing significant advancements in homogeneous biofunctionalization of surfaces, a growing research interest is being shifted towards the development of gradient surfaces presenting graded wettability, chemistry, biomolecule density and nanoparticle distribution [303]. This interest stems from the fact that many essential and poorly understood biological activities are driven by such gradients. For instance, chemotaxis mediate a number of physiological processes such as leukocyte recruitment to the infection site, guidance of neuronal and glial cells during nervous system development or regeneration and cancer metastasis. Moreover well-ordered gradient distribution of specific functional groups, ECM components, signaling biomolecules and even topographical cues induce particular cell type proliferation, migration and differentiation [304-306]. Besides their biological importance, gradients are also powerful for high throughput screening in several applications such as biomaterial development, TE and sensors, in the sense that a single sample designed with a gradient surface is used to procure multiple data points. This reduces dramatically the number of samples and cells, eliminates inaccuracies triggered by sample reproducibility and speeds up the analysis [240, 303, 307].

IV.2. Effect of growth factor gradients in NGCs on nerve regeneration

During the embryonic nervous system development, the growing axons are driven by chemotactic and haptotactic signals to reach their target. The guidance of growth cones is mediated by several growth factors distributed in a spatial concentration gradient [308-310]. At the tip of the developing nerve, the growth cone senses these growth factor gradients and changes its shape to promote a well-defined directional extension towards higher concentrations. This directional guidance is a key factor ensuring successful nerve regeneration and efficient functional recovery [311-313]. Many studies have homogeneously incorporated neuro-stimulatory molecules into NGCs and have shown enhanced regeneration across short nerve gaps [43, 56-59]. However, mimicking the natural *in vivo* conditions for axonal guidance by introducing molecular gradients into NGCs was very rarely considered. Up to date, this strategy was observed, to the best of our knowledge, in only 3 studies attempting to optimize the conventional NGCs, bridge critical nerve gaps and attain the functional outcome of autografts. In 2008, Dodla et al. engineered polysulfone NGCs in which agarose

hydrogel containing immobilized laminin and NGF-loaded microtubules was injected in a way creating a gradient of laminin and NGF across the conduit length. To do so, 4 agarose solutions with gradually decreasing concentrations of laminin and NGF-loaded microtubules were filled into the conduit one after the other to occupy each 25 % of the scaffold volume. Before every injection, the previously infused agarose solution was allowed to become a gel by cooling it at 4 °C for 10 min (Fig. IV.1). The NGCs were then implanted in a 20 mm rat sciatic nerve injury model. Four months post-implantation, growing axons were only detected in gradient NGCs but not across NGCs filled with uniformly distributed laminin and NGF. Moreover, the number of myelinated axons and the axonal diameter distribution were similar between the gradient NGC and the nerve graft groups. In terms of functional recovery, the gradient NGCs gave significantly better results than the uniform NGCs as assessed by the relative gastrocnemius muscle weight [314].

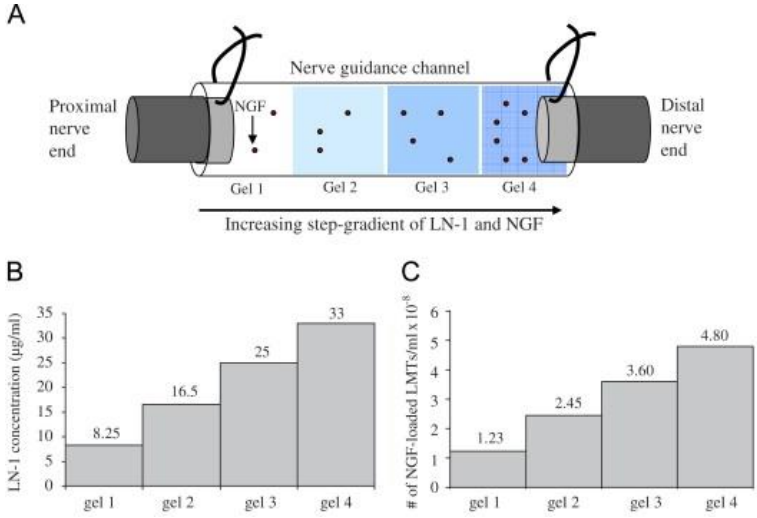

Fig. IV.1. *Polysulfone NGCs with step-gradient anisotropic distribution of laminin and NGF. A: Schematic representation of the NGC connected to the severed nerve stumps; B: Concentration of laminin in the 4 different gels; C: Concentration of NGF-loaded microtubules in the 4 different gels. Laminin gradient is immobilized while NGF will form a gradient after diffusion [314].*

In 2007, Tang et al., also inspired by the theory "Nature knows the best", implemented NGF gradients on poly(ε-caprolactone)-block-poly(L-lactic acid-*co*-ε-caprolactone) (PCLA) membranes and in PCLA NGCs. The gradients were created by differential exposure to a solution of NGF/silk fibroin across the length of the membranes and NGCs. The

gradient efficacy was investigated by a quantitative comparison of DRG neurite outgrowth on gradient versus homogeneous NGF-immobilized membranes. The neurite length of DRG was shown to gradually increase along the NGF gradient towards higher concentrations. Moreover, the neurites in the middle of the gradients were significantly longer than those on the uniformly treated membranes, despite the approximated NGF average concentration on both membranes. A high frequency of neurites oriented towards the gradient direction was found in gradient compared to uniform membranes where neurite orientation was completely random. In addition to that, the overall turning neurite ratio (=1: all neurites turning to the gradients; =0: no turning) was 0.48 for the gradient samples and close to 0 for the uniform samples (Fig IV.2). The NGCs were then implanted in rat nerve sciatic model of 14 mm gap length. Twelve weeks post-implantation, satisfying and superior nerve regeneration results illustrated by morphological and functional enhancements were observed in case of the gradient NGF-immobilized NGCs compared to the uniform NGCs. Compound muscle action potentials, sciatic function index, overall number of myelinated nerve fibers and myelin sheath thickness were comparable between the gradient NGCs and autografts. This positive outcome highlighted the major role of implementing growth factor gradients into NGCs in promoting nerve regeneration [315].

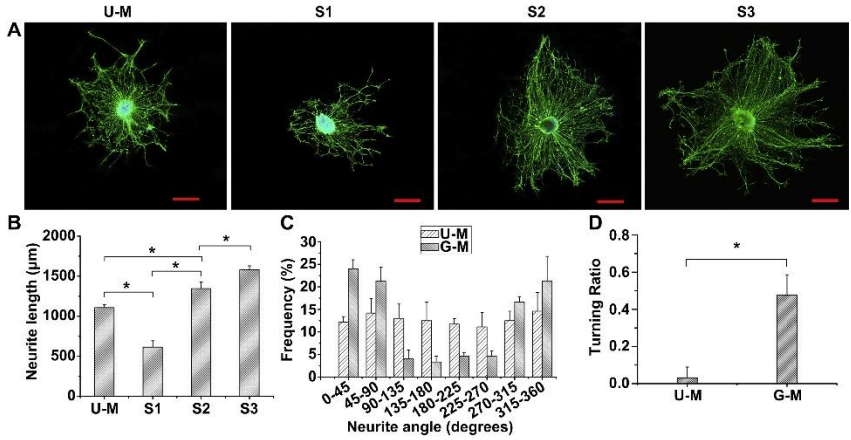

Fig. IV.2. *DRG neurite outgrowth on uniform (U-M) and gradient (G-M) NGF-immobilized PCLA membranes. A: Confocal fluorescence images of DRGs staining with anti-neurofilament 200 (green); B: Neurite angles measured between the neurite tip and the gradient direction; C: Turning ratio values [315].*

In 2016, Yeh et al. adopted higher levels of complexity in fabricating NGCs by synergistically adjoining 3 stimulating factors: 1) Physical

cue: generation of poly (glycerol-co-sebacic acid) (PGS) micro-patterned surface by a laser ablation system for a directional guidance of axonal growth; 2) Chemical cue: creation of NGF gradient by immobilization of NGF in gelatin membrane making use of a commercialized gradient maker for a continuous attraction of axon outgrowth form the proximal to the distal nerve stump and 3) Cellular cue: seeding SCs to support axon growth and myelination (Fig. IV.3). After co-culturing with nerve stem cells (NSCs), results showed that the average neurite area/field and neurite length/field increased with the increase in NGF concentration. Moreover, the expression of Map 2 and ßIII tubulin genes by differentiated NSCs was significantly higher on the zone containing the highest NGF concentration compared to the one with the lowest concentration. A directional extension of the differentiated NSCs was visualized in the micro-channels. These results revealed that combining physical cues, chemical gradient and cells in one integrated system greatly improves peripheral nerve regeneration [316]. Therefore, in this PhD thesis, multifunctional NGCs combining electropun fibers as physical cue, SCs as cellular cue and chemistry gradient surface as chemical cue will be engineered. In fact, surface gradients are more efficient than soluble diffusible and transient gradients as biochemical cues are recognized by cells mainly at the cell-scaffold interface. Moreover, surface bounded form of gradients allows the biomolecules or growth factors to be retained at stable concentration gradients and prevents their proteolytic degradation. Given the numerous benefits and satisfying results of homogenously plasma-treated surface in various TE applications, innovative gradient plasma treatments will be considered for the first time in the surface functionalization of NGCs. In what follows, an extensive overview of the different gradient plasma activation and polymerization treatments applied so far on various surfaces will be given as a picture-perfect reference of plasma-induced gradients.

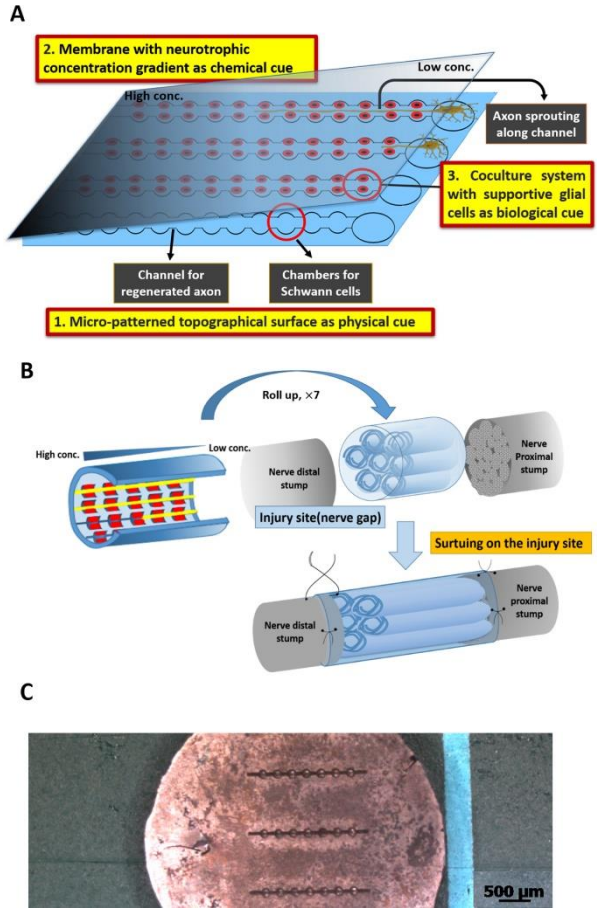

Fig. IV.3. *A: Design concept of a multifunctional membrane with micro-patterned channels, neurotrophic gradients and SC inoculation; B: Rollup of several membranes for the creation of an implantable NGC sutured at the nerve injury site; C: Top view of the micro-patterned membrane [316].*

IV.3. Gradient plasma activation

Different approaches are commonly adopted to create surface gradients such as self-assembled monolayers (SAMs), grafting on hydrogels and Boyden chambers and filters. Several limitations are associated with these traditional methods including the substrate dependency (e.g. gold-coated surface is required for SAMs), the short term gradient "shelf-life", the restricted chemistries that can be obtained and the long

experimental timing [317-319]. As an alternative, applying high energy source plasmas that are associated with many advantages such as the absence of solvent, the specificity and the substrate independency, has shown great successes in the generation of gradient surfaces. In 1989, Pitt el al. were one of the first groups if not the first, to generate wettability gradients on polyethylene, polystyrene, polydimethylsiloxane, and polytetrafluoroethylene by An RF plasma activation operating in oxygen, ammonia and sulfur dioxide atmospheres. A special gradient apparatus consisting of an aluminum box with a translating cover and two aluminum plates serving as electrodes, was designed for this purpose. During the treatment, the cover is retracted with a constant velocity automatically controlled by a microprocessor driving the stepping motor. This movement linearly increases the plasma exposure time over the sample length. As a result, WCA decreased along the length of the sample thus ensuring the presence of a wettability gradient. Moreover, a wide range of wettability gradients is obtained by varying the gas, the radio frequency power, the cover retraction velocity and the plasma exposure time. This investigation highlighted the high flexibility of the plasma treatment to generate gradients with defined length and magnitude and pointed out, by using several substrates, that the process is substrate independent [320, 321]. Therefore, a steep rise in literature focusing on the generation of gradients by plasma activation followed. In 1991, Lee et al. introduced a new custom-made corona discharge reactor for the generation of wettability gradients on low density polyethylene (PE) sheets. The apparatus is composed of 2 key components responsible for the gradient surface creation: a knife-type aluminum electrode and a moving sample holder made up of silicone rubber-covered iron. The electrode is connected to an RF generator with a power increasing gradually through an automatic operation of a motorized drive (Fig.IV.4). During the treatment, the sample holder translates at a constant speed of 1cm/s and the sample (5 cm x 5 cm) is simultaneously exposed to an air corona discharge ignited form the knife-type electrode with increasing power. In order to characterize the plasma-induced gradients, WCA, FTIR in attenuated total reflectance mode, electron spectroscopy and SEM measurements were performed all along the sample length. The WCA gradually decreased from 96° to 43° because of the increase in oxygen-containing functionalities of which ether, aldehyde and ester groups along the treated sheets. This is accompanied by a mild roughening of the surfaces towards the zones that were more exposed to plasma [322].

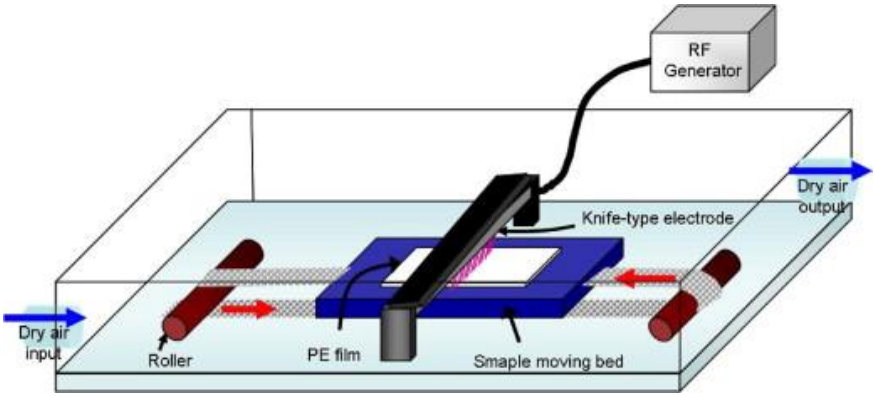

Fig. IV.4. *Schematic representation of the corona discharge setup used for activation of PE surfaces in a gradient way [323].*

Five subsequent studies were performed by the same research group to investigate the interactions between the successfully generated PE gradient surfaces and several biological species. The first study, performed in 1997, aimed at exploring the adhesion of serum proteins and the behavior of fibroblast, ovary and endothelial cells on the treated PE sheets. The cells adhered and proliferated more on the zones with moderate hydrophilicity compared to the zones of extreme hydrophilicity or hydrophobicity. The best cell performance was detected at a WCA of 55°, regardless of the used cell type. These results closely correlated with the protein adsorption that was maximal on a moderate hydrophilicity [261]. The goal of the second study, dating back to 2003, was to examine neurite formation on PE surfaces with graded wettability. Therefore, PC12 were seeded on the samples and their behavior was studied. Similar to the other cell types, PC12 underwent the best adhesion and differentiation on moderately hydrophilic positions with the formation of more and longer neurites at a WCA position of 55° [324]. In the third (2004) and fourth (2006) studies, the gradient PE sheets were treated with polyeththyleneimine and then biotin. Afterwards, 5-Carboxymethoxy-2-nitrobenzyl (CMNB) caged fluorescein-conjugated streptavidin (SAV) or quantum dots (Q-dot) SAV were adsorbed on the biotinylated gradient surfaces. In this way, linking the concentration or intensity of bioactive molecules adsorbed on the surface to the chemical gradient would allow gradient surfaces to become a practical and useful method for several biomedical applications such as diagnostic examination of biomolecular interactions. In fact, CMNB-caged fluorescein-conjugated SAV becomes fluorescent upon photoirradiation as an external stimulus, while Q-dot SAV emanates intense light in the region between near-infrared to ultraviolet at ambient temperature. Fluorescence images taken all

along the gradient PE surfaces revealed a gradual increase of the fluorescent intensity towards the more hydrophilic zones [325, 326] (Fig. IV.5). In the fifth study, conducted in 2008, the behavior of bone marrow stem cells on gradient PE surfaces was explored. Results indicated that the cells adhered and proliferated better on highly hydrophilic zones compared to hydrophobic zones. Moreover, cells were more spread and flattened on hydrophilic zones versus hydrophobic surfaces where a rounded cell morphology was dominant [323].

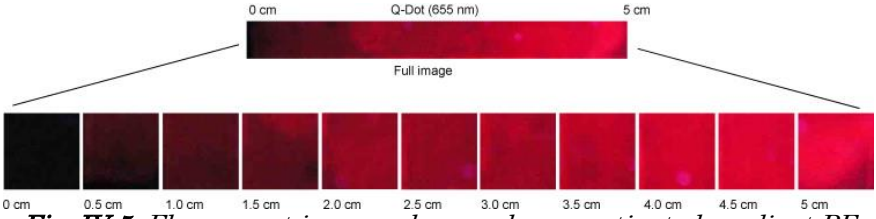

Fig. IV.5. *Fluorescent images along a plasma activated gradient PE surface with adsorbed Q-dot SAV [326].*

The complex design of the corona discharge apparatus involving knife-edge electrode and motorized movable sample bed, has led researchers to conceive simpler and technically more practical reactors for a gradient plasma activation. A new glow discharge setup, not implicating moving elements in the discharge chamber, was therefore introduced by Spijker et al. in 1999 to treat PE surfaces. It consists of a cylindrical chamber containing 2 electrodes separated by 4 cm and an aluminum cover placed in between with an adjustable height (0.5-1.7 cm). PE samples were positioned halfway under the cover and an argon discharge was applied followed by an air ventilation of the chamber. Electron spectroscopy demonstrated that oxygen containing functionalities were incorporated onto the surface in gradually increased amounts across a length of 4.5 cm but were the same (C-O, C=O and COO bonds) on the whole sample. This led to a wettability gradient highlighted by a decrease in WCA from 100° to 40°. The steepest surface gradient was attained when the cover was placed at its minimal height. The adsorption of immunoglobulin G (IgG), fibrinogen and albumin on the treated surfaces proportionally followed the wettability gradient meaning that the more the surface is hydrophilic the more it binds proteins [327]. In a subsequent study, PE sheets were subjected to the same gradient plasma activation and the thrombogenic response of blood towards such sheets with varied wettability was tested. To do so, PE samples were incubated in anticoagulated human blood. An enhanced platelet adhesion and clotting activation was detected on the hydrophilic end compared to the hydrophobic end.

Inversely, the platelets were more activated on hydrophobic zones as deduced from their morphology and the exposure of GPIIb-IIIa receptor involved in the binding of several adhesive blood proteins [328].

IV.4. Gradient plasma polymerization

The different plasma activation methods that were described are mainly limited to the production of wettability gradients with a relatively restricted control over specific chemical group incorporation. Other concerns include the ageing effect of the treated surfaces due to the reorientation of the incorporated groups away from the surface and the roughening of the surface due to the plasma etching effect [320, 329]. Consequently, the interest was shifted towards the generation of polymer gradients via plasma polymerization to be able to control more precisely the functional group nature and densities, the gradient stability and the gradient shape. Nevertheless, it was until 2003 that the first method enabling the deposition of controllable horizontal plasma chemical gradients was described by Whittle et al. [329] and was subsequently adopted as it is or with some amendments by several other groups [319, 330]. In their study, Whittle et al. created hydrocarbon/carboxyl and amine/carboxyl functionality gradients on glass substrates over a distance of 11 mm. Instead of using the traditional cylindrical plasma reactor, a RF glow discharge T-shaped reactor presenting a drawer as sample holder was used [329]. As a first step, an amine coating was deposited on the whole glass substrate by performing a plasma polymerization using allylamine (Aam) monomers as precursors and a continuous power of 10 W while the drawer was fully extended. An underlayer presenting a good adhesion was thus formed for the subsequent gradient deposition. In the second step, the power was decreased to 5 W and a plasma polymerization was performed while the drawer was slowly closed at a constant velocity of 1 mm/min along with a controlled change in the plasma composition. This was performed by introducing acrylic acid (Aac) as the second monomer while decreasing instantaneously the flow rate of Aam by 4 cm^3 stp / min. For the deposition of hydrocarbon/ carboxyl gradients, the same procedure was followed but with the use of octa-1,7-diene instead of Aam precursors. The obtained plasma polymerized surfaces were characterized by XPS and chemical derivatization of acid functionalities using trifluoroethanol. A gradual increase in the concentration of acid functionalities was observed in the case of hydrocarbon/ carboxyl gradients and an increase of acid and amine functionalities was attained in opposite directions in the case of the amine/carboxyl gradients. These findings demonstrated the power of

this first-hand methodology to successfully generate plasma polymer gradients that can subsequently allow the grafting of a broad range of biochemical entities in a spatially structured manner [329]. Surface engineers waited around 3 years after the study of Whittle to begin their investigations regarding the grafting of biomolecules and the cell-biomaterial interactions when a plasma polymer gradient is implicated. Moreover, several other methods generating plasma polymer gradients were described with a distinctive focus on amine and carboxylic acid being the most 2 extensively considered functionalities in the subsequent literature of gradient plasma polymerization. In what follows, an overview on the achievements of these carboxylic acid and amine plasma gradients in several TE and biomedical applications will be given.

IV.4.1. Surface plasma polymer gradient of carboxylic acid functionalities

In 2006, Parry et al.[319] performed a plasma copolymerization of Aac and octadiene (OD) based on the mechanism described by Whittle et al. [329] but with a modification of the setup in a way allowing the production of 20 similar gradients at a time. Up to 20 substrates could thus be placed in the redesigned RF plasma reactor and moved under a slot by an automated stepper motor in 250 µm paces at a rate of 750 µm/min. Simultaneously, a controlled composition of the monomer mixture is sent to the chamber via two computer-regulated valves. A thorough characterization of the surface gradient was executed by angle resolved x-ray photoelectron spectroscopy (ARXPS) that showed in great details how acid functionalities changed on different positions of the gradient and highlighted the presence of vertical changes especially when it comes to the plasma polymer thickness. An assay investigating the passive adsorption of IgG as a function of the acid surface density was supplemented to the study to be, to the best of our knowledge, the first reported biological assay done on plasma polymer gradients. ARXPS measurements showed that IgG was by far more absorbed on the OD gradient end and that IgG amount decreased gradually as the concentration of Aac increased thus creating an IgG gradient [319]. In 2009, Walker et al. [331] also deposited a gradient of OD/Aac on coverslips using the plasma deposition/masking method of Whittle et al. but this time with a renovated protocol permitting the generation of submillimeter-scale gradients instead of millimeter scale length. In the updated method, OD was constantly fed to the reactor as the slot moves across the substrate surface, then it was brusquely turned off and Aac was sent to the reactor in 3a pulse of a certain duration. The scale length and density of the carboxylic groups were thus tailored by varying the pulse width of Aac. The obtained gradient

surface was used to immobilize the intercellular signaling molecule delta-like-1 Dll 1, a factor enhancing stem cells self-renewal and preventing cell differentiation which is an issue to be considered when developing cell therapy technologies. Since tiny changes in surface properties can considerably affect the stem cell behavior either by enhancing the commitment path towards their differentiation to particular cell types or by maintaining and stabilizing the stem cell pluripotent phenotype, concentration-based factor and chemical group gradients are highly expedient to study stem cells. Instead of directly grafting Dll 1 factor on the generated gradient, a mouse monoclonal antimyc-tag (9E10) antibody is covalently coupled, then Dll 1 is immobilized on the antibodies thus avoiding the alteration of its biological activity by separating it from the solid surface. A visualization of the Dll 1 gradients was performed by binding a rabbit anti-Dll-1 antibody and then introducing a colloidal gold-conjugated secondary antibodies. Several Dll 1 gradients with different slopes and end points were obtained depending on the plasma Aac pulse width adopted during the plasma polymerization (Fig. IV.6) [331]. During the same year, the first cell tests on plasma gradients were performed by Wells et al. using mouse embryonic stem (ESC) cell lines E14 and R1 in order to examine their pluripotency [332]. OD/Aac gradients were deposited on coverslips using the same setup described by Parry et al. [319]. The degree of cell spreading was studied in function of COOH concentration. Alkaline phosphatase staining showed that cell capacity of self-renewal is preserved when the cell spreading is still below 120 μm^2 [332]. In 2012, in an attempt aiming to make a sweeping statement about this result, Harding et al. [333] used polyethylene oxide (PEO) that is well-known in the biomaterials field to limit protein adsorption and thus cell adhesion and spreading, together with Aac to produce two counter gradients. A RF apparatus consisting of a cylindrical glass chamber was used for the plasma copolymerization. As a first step, an OD layer then an Aac layer were deposited on the substrate since a unique Aac deposition resulted in the coating dissolution in water. Then a mask 12° titled in respect to the surface was employed to deposit a PEO-like gradient by using the monomer diethylene glycol dimethyl ether (DG) as a precursor. A successful fabrication of AA-DG plasma polymer gradient was revealed by XPS, profilometry and infrared microscopy mapping. The gradient could be easily altered by changing the plasma process parameters. Mouse ESCs were cultured on the gradient surfaces, then immunocytochemical stainings of the stem cell markers Oct4 and alkaline phosphatase were performed. Results showed a low cell adhesion and colony formation on the DG rich end and an increased colony size and decreased stem cell marker expression on the COOH rich end, thus supporting the hypothesis stating that

cellular spreading influences the fate towards cell differentiation or self-renewal [333].

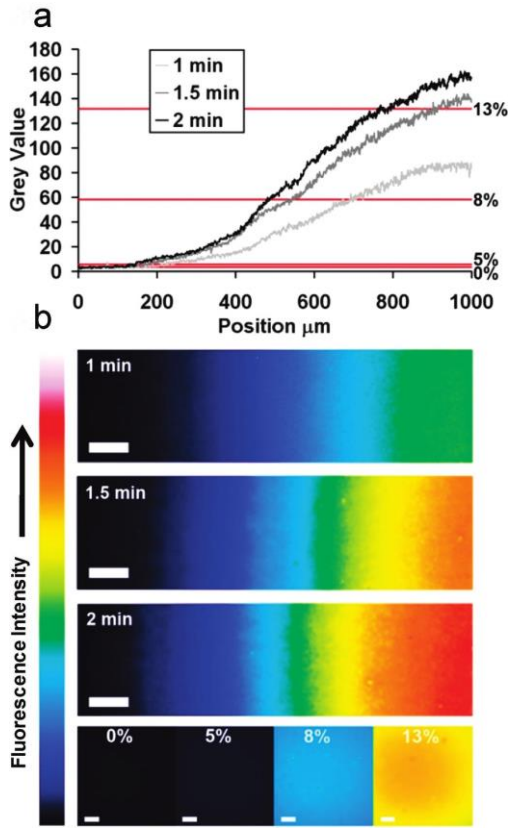

Fig IV.6. *a) Densitometry results of 9E10 antibodies immobilized on the gradient surface (3 different Aac pulse durations) and visualized by FITC-conjugated secondary antibodies. Red lines show the results of homogeneous surface treatments B) False color heat maps of the 9E10 antibody gradients. Homogeneous surfaces are presented for comparison. Scale bars: 100 µm [331].*

The same method using a tilted mask was then applied by Wang et al. [334] in 2014 to create the same Aac-DG gradients but also Aac-OD gradients by firstly depositing OD uniformly then using the tilted mask to deposit Aac. Attachment and differentiation of rat BMDSCs into adipogenic and osteogenic lineages were investigated on both gradients. After 24h of cell culture, a gradient in cell density was observed on the substrate with a decreased cell adhesion on DG and OD rich ends. The obtained cell density gradient vanished on Aac-OD

gradient after 6 days but not on Aac-Dg gradient, thus suggesting the long-term efficacy of the later gradient. Cell colonies containing bone nodules were detected on this gradient especially on the Aac rich ends but not on the DG rich end. Moreover, proteins and calcium were not secreted on the DG end implying that osteogenic differentiation is influenced by local cell densities. However, the induction of the cells towards an adipogenic lineage showed that this differentiation is cell density insensitive [334].

IV.4.2. Surface plasma polymer gradient of amine functionalities

In addition to COOH functionalities, NH_2 groups were also shown to be very powerful in influencing a wide range of particular cell type performances such as adhesion, proliferation, migration and differentiation. Therefore, when the research community started investigating surface gradients, a distinctive focus was directed towards the production of amine gradients and their use in several biomaterial and TE applications [335]. To the best of our knowledge, all COOH plasma polymer gradients described so far were only deposited on flat substrates, however some amine plasma polymer gradients were deposited on 3D scaffolds. For instance, in 2006 Barry et al. [336] thought of generating an amine gradient on PDLLA 3D porous scaffolds in order to solve the common problem of the highly disproportionate cell colonization on the scaffold periphery in comparison to the hardly accessible scaffold center that remains poorly colonized and supplied by nutrients. This issue was solved by plasma polymerizing hexane, known to be resistant to cellular adhesion, on the periphery of the scaffold while generating an amine plasma polymer coating on the central surface. To do so, a first plasma polymerization step using Aam monomers as precursors was performed, then a second polymerization using the cell-repellent hexane was achieved at lower deposition rate. XPS measurements throughout the whole scaffold showed that when the second hexane polymerization step is absent, a decrease in amine functionalities is observed towards the center. However, when hexane polymerization is introduced, the nitrogen concentration is reduced by 1 to 2 % in the periphery thus creating a reversed gradient. After seeding 3T3 fibroblasts on the treated scaffolds, X-ray micro-computed tomography and SEM revealed a uniform cell distribution throughout the whole scaffold with well spread cells in the center associated with a high production of ECM components [337]. The use of hexane and Aam to create amine gradients was also considered by Zelzer et al. [338] in the subsequent year, but this time on flat glass coverslips. The idea behind the study was to compare between mammalian cell interactions

on gradient and on uniformly treated surfaces. A T-shaped borosilicate RF reactor was used to plasma polymerize uniformly an amine coating on glass coverslip using Aam as precursors. Afterwards, a poly-hexane was deposited on the poly-Aam coated surface after placing a mask either directly or making use of a spacer clamping the mask at a distance of 0.04 mm from the surface. The direct positioning of the mask resulted in steep gradients while the use of a spacer gave more shallow gradients. Wettability gradients were detected by WCA measurements showing a gradual decrease from 93 ° to 66 °, thus correlating with the gradual increase of N/C ratio. NIH 3T3 fibroblasts cultured on the gradients surfaces were preferentially adhered and proliferated on the N-rich end with a gradual cell density decrease towards the poly-hexane rich end. Surprisingly, experiments performed on uniform surfaces revealed significant differences in cellular behavior compared to the gradient surfaces, leaving question marks on the use of gradients for high throughput screening. The cell signaling and the protein synthesis might be different between gradient and uniform surfaces since the cell neighboring environment differs [338]. Several subsequent studies involving amine plasma polymer gradients and their general results are summarized in table IV.1.

Since the biological systems *in vivo* are much more complex than *in vitro* assays, some authors considered a closer mimicking of the real systems by designing, instead of one dimensional or single protein gradients, 2 protein and 2 dimensional gradients. For instance, in 2009 Vasilev et al. [330] created an Aam-OD gradients on SPRchips or on silicon wafers based on the method described by Whittle et al. in 2003 [329]. Afterwards, polyethylene glycol (PG), known to be resistant to protein adsorption, was grafted on the amine gradient thus generating a PEG density gradient. The obtained density gradient was then benefited to control the deposition of 2 proteins, namely the large protein fibrinogen and the small protein lysozyme, by differential passive adsorption. A first incubation with the larger protein led to its adsorption on low PEG density regions, then a second incubation with the small lysozyme led to its adsorption only where there is still a "room" for it to adsorb since the previous fibrinogen adsorption passivated gradually the surface. As a result, 2 reversed gradients of 2 proteins could be designed and the method could be generalized to other pairs of small and large proteins (Fig. IV.7) [330].

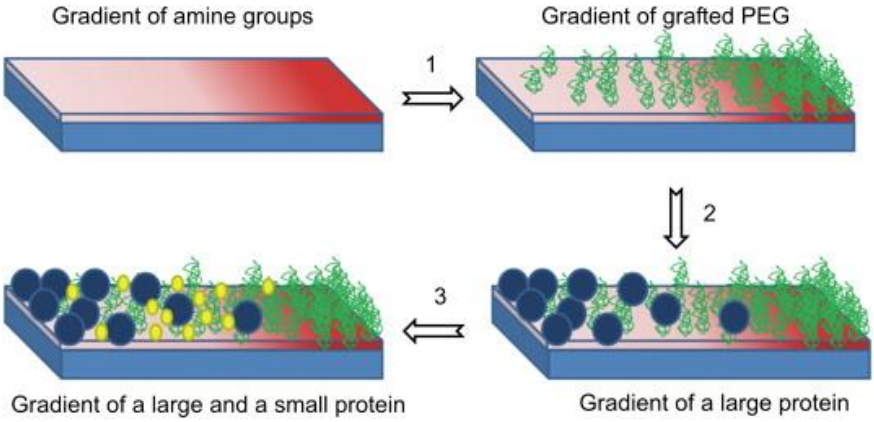

Fig IV.7. *Schematic representation of the creation of two-protein gradient. Step 1. PEG grafting on the amine plasma polymer gradient to generate a PEG density gradient. Step 2. Large proteins adsorption. Step 3. Small protein adsorption [330].*

In 2013, Mangindaan et al. [318] designed a 2 dimensional amine gradient by performing firstly a plasma polymerization of Aam on a propylene membrane while a mask is placed on top with a gap distance of 1 mm. Subsequently, the same procedure is repeated but after rotating the sample by 90 °. WCA measurements showed that both gradients were well controlled by varying the plasma treatment exposure time in each step. L-929 fibroblasts seeded on the treated surfaces adhered and grew proportionally with the amine content on the 2 dimensional gradient with a predominant effect of the gradient created during the initial plasma deposition [318].

Table 2. *Overview of literature on amine gradient obtained by plasma polymerization and not discussed in the text.*

Authors (year): Plasma reactor/ monomers used	**Gradient formation method**	**Surface chemical properties**	**Biological assay/ cell type**	**Bioresponsive properties**
Robinson et al. (2008): Cylindrical RF reactor/ Aam- OD [317]	Moving slot with a simultaneous change in the monomer mixture composition	Gradual increase in N/C ratio over a distance of 14 mm	Adsorption of heparin that mimics the heparan sulfate proteoglycans found in all tissue types	-Gradual increase in heparin adsorption parallel to the increase in N/C ratio. -Heparin functionality not correlated with the

				continuous increase in heparin adsorption
Robinson et al. (2010): T-shaped RF reactor/ Aam- OD [339]	Moving slot with a simultaneous change in the monomer mixture composition	Gradual increase in N/C ratio on washed and unwashed samples highlighting the stability of plasma polymer gradient surfaces	——	——
Harding et al. (2013): T-shaped RF reactor/ Aam- OD [306]	Moving slot with a simultaneous change in the monomer mixture composition	Gradual increase in N/C ratio over a distance of 12 mm	D3 murine embryonic stem cell line culture	-Maximum cell adhesion on the N-rich end -Inverse increase in stem cell marker expression towards the lower N/C ratio. -Correlation between the presence of stem cell markers and the formation of more multilayered and compact cell colonies.
Mangindaan et al. (2013): RF reactor/ Aam [335]	Use of a mask with a 1 mm gap on a polypropylene substrate	-Wettability gradient with WCA varying from 15˚ to 90˚. - Gradient over 1 cm of nitrogen content from 5.8 to 16.0 % and amine content from 1.98 to 4.03 per 100 carbons.	L-929 fibroblast culture	Continuous increase in the cellular density with more than 2-fold density on N-rich end
Delalat et al. (2014): RF reactor/ Aam-OD [340]	Moving slot with a simultaneous change in the monomer	Gradient over 12 mm of nitrogen content from 0 to 12.0 %	Mouse embryoid body cell culture	-Highest cell adhesion on the gradient central regions -Increased cell proliferation

	mixture composition			towards the Aam end. -Cell differentiation towards mesodermic and ectodermic lineages on high nitrogen content regions -No correlation between amine content and endodermal differentiation
Liu et al. (2015): RF reactor/ Aam-OD [341]	Moving slot with a simultaneous change in the monomer mixture composition	-Wettability gradient with WCAs varying from 90° to 70° -Gradual increase in N/C ratio over a distance of 12 mm - Unchanged surface topography	-Adsorption of fluorescein isothiocyanate-labeled bovine serum albumin (BSA) and rhodamine-labeled fibronectin (FN) -Human adipose-derived stem cell culture	-Gradual decrease in the amount of adsorbed BSA from OD towards Aam sides. -Gradual increase in the amount of adsorbed FN from the OD towards the Aam sides. -Increased cell adhesion and spreading towards the Aam side -No difference in cell performances in the absence of serum -Increased osteogenic cell differentiation towards the Aam side -Decreased adipogenic differentiation towards the Aam side.

IV.5. Conclusion

In this chapter, a quite extensive overview has been given on the literature involving plasma surface activation and polymerization of surfaces in a gradient way. These particular treatments were mainly applied on 2D sheets using complex designs of the used plasma reactors. For instance, automated stepper motors moving the samples

during the treatment, complex gas flow systems, reshaped electrodes and shielding covers were implemented for this purpose. In the next few years, more attention should be given on designing simple reactors and treating complex 3D and porous scaffolds, such as the inner wall of NGCs, in a gradient way. This would lead to significant advancements in several TE applications.

Chapter V. Sterilization of Polymeric Scaffolds

V.1. Introduction

In the last few decades, biodegradable polymeric scaffolds have revolutionized the evolving TE field holding great promise to restore damaged tissue functions while overcoming the restrictions faced in conventional transplantations. Researchers were focused on engineering the ideal scaffold by optimizing its mechanical, chemical, topographical and cyto-responsive properties to match those of the tissue to be regenerated [103]. The focus on the optimization of the tissue-engineered scaffolds has led researchers to often neglect a crucial and final prerequisite for their use *in vitro* and *in vivo*: the material sterility [96, 97]. In fact, the clinical use of unsterilized materials can result in serious patient nosocomial infections and morbidity/mortality concerns [342]. Sterilization refers to the process by which a material becomes free of contamination from any form of living microorganisms including viruses, bacteria and yeasts. Several heat, chemical and irradiation-based techniques are used for this purpose [343]. The selection of the best technique maintaining the biochemical, mechanical and structural properties of the designed scaffolds is problematic because of the high sensitivity of biodegradable polymers compared to other medical devices [344]. Due to the lack of specific techniques intended for such scaffolds, the conventional sterilizations customized for clinical applications such as ethylene oxide (EtO) and gamma radiation, become the first choice. Unfortunately, some of these standard techniques were shown to be unsuccessful on biodegradable polymers and others with reasonable performances are associated with several drawbacks [343, 345]. In what follows, the mechanisms underlying the microorganism inactivation are described for each technique with a brief overview on the post-sterilization effects on polymeric scaffolds.

V.2. Heat treatments

Nowadays, two heat treatments are extensively considered for sterilization: dry heat and steam treatments. They are performed by either subjected the product to be sterilized to hot air of 160 °C for 2 h or to saturated steam of around 130 °C for 20 min [343]. Many advantages are associated with these treatments such as high efficiency, simplicity, fast procedure and absence of any induced toxic residues [346]. Moreover, the penetration depth of heat treatments is one of the best compared to other sterilizations with a complete elimination of all forms of viable microorganisms [343, 347]. During steam sterilization, a destruction of the metabolic and structural

components essential for the replication occurs thus killing the microorganisms. In the dry heat sterilization, the killing mechanisms are mainly due to the direct heat exposure and oxidation effects [348]. Nevertheless, since glass transition temperatures (Tg) of most biodegradable polymers are rather low, the use of heat sterilization for TE scaffolds is tricky. Furthermore, the water vapor present in case of steam sterilization has been detected to trigger hydrolytic degradation of polymers [343-345, 349]. In order to obviate the undesirable effects, Rozema et al. altered the steam sterilization process by introducing individual cycles entailing separate phases of air removal, sterilization and steam elimination. In spite of this, an extensive reduction in the molecular weight of PLA scaffolds was still observed, together with an increase in the mechanical strength because of the polymer recrystallization [350]. In the same way, Gogolewski et al. appended an inert gas atmosphere or a vacuum during the dry heat process to lower the temperature while treating PLA scaffolds. However, a decrease in the bending strength and an increase in the molecular weight were detected after all [351]. One can therefore conclude that the use of heat treatments to sterilize polymeric scaffold is very limited since it is associated with big risks of alterations in mechanical and molecular properties as well as damages in the morphological structure such as melting and softening of the polymer.

V.3. Irradiation methods

As alternative to heat treatments, radiation methods come to offer several benefits such as low temperature process, short operational time and relatively lower process cost [343].

V.3.1. Gamma irradiation

Gamma (γ) irradiation is an electromagnetic sterilization technique that is mostly obtained from a ^{60}Co source and generated in a dose range of 10 to 30 kGy/h [352]. When irradiating a material, an energy transfer to valence electrons occurs triggering their ejection from the material. This causes the DNA and RNA strands of the present microorganisms to break and leads to the generation of reactive oxygen species (ROS) altering other crucial cellular components. ROS have also the capacity to cleave the phosphodiester bonds of DNA molecules causing their degradation [343, 353]. Gamma rays are able to inactivate both gram-positive and gram-negative bacteria as well as most viruses, yeasts and some bacterial spores [354]. While γ radiation sterilization is effective, rapid and simple, it was shown to be also associated with

alterations in scaffold chemical properties, decreased molecular weights and compressive mechanical properties as well as increased degradation rates [113, 355, 356]. For instance, after examining the effects of γ irradiation on the tensile strength of PCL, Cottam et al. found out a considerably higher yield point for the treated samples compared to the unsterilized ones, thus indicating an extensive damaging of the mechanical features [357]. Hooper et al. reported similar effects when γ irradiating PLLA scaffolds that degraded faster than unsterilized samples, lost their mechanical strength and retained less than half of their initial molecular weight post-sterilization [358]. Valente et al. detected changes in the WCA of electrospun PLA fibers after being subjected to γ irradiation, which suggests surface chemical and roughness changes [344]. In addition to the importance of the bulk properties of TE scaffolds, their surface properties affects to a higher extend their cytocompatibility. Therefore, the use of γ irradiation to sterilize biodegradable scaffolds leaves some question marks concerning the success of the implant.

V.3.2. Ultraviolet irradiation

Ultraviolet (UV) irradiation is a newer approach to sterilize polymeric scaffolds while potentially preserving their features. It is typically used for transparent scaffolds and material surfaces [148, 343, 345]. UV exposure causes electron excitation and photoproduct accumulation known to damage DNA molecules and prevent their replication thus inactivating the living microorganisms [353]. Vegetative bacteria and enveloped viruses are completely killed by UV, while bacterial spores are more resistant and not easily destroyed. The sensitivity of microorganisms to UV irradiation depends on the process parameters such as UV exposure time and wavelength as well as the type of the microorganisms to be killed. It has been stated that wavelengths between 200 and 280 nm are the most effective with a particular supremacy of 254 nm being the most lethal wavelength [343]. The duration of UV irradiation appears to also be a key parameter influencing the polymeric scaffold properties. For instance, Fischbach et al. subjected biodegradable poly (D,L-lactic acid)-poly(ethylene gycol)-monomethyl ether diblock (Me.PEG-PLA) copolymer films to UV irradiation of different exposure times. Results revealed that after 2 h of exposure, the film molecular weight distribution and topography remained unchanged. However, longer UV irradiation times of 5 h up to 24 h elicited drastic alterations in the surface chemical and topographical properties that were illustrated by extensive depletion of PEG chains and marked smoothening [345]. In a study conducted by Yixiang et al., electrospun PLGA and poly(L-lactide-co-ε-caprolactone)

(PLLA-CL) nanofibers were also UV irradiated for different intervals. Results showed no significant morphological changes for UV exposures up to 2h and 8h respectively, as visualized by SEM analysis (Fig. V.1). Although no obvious damages were observed for short exposure times, a reduction in molecular weight and tensile strength of both polymers was perceived already after 1 h of UV irradiation [359].

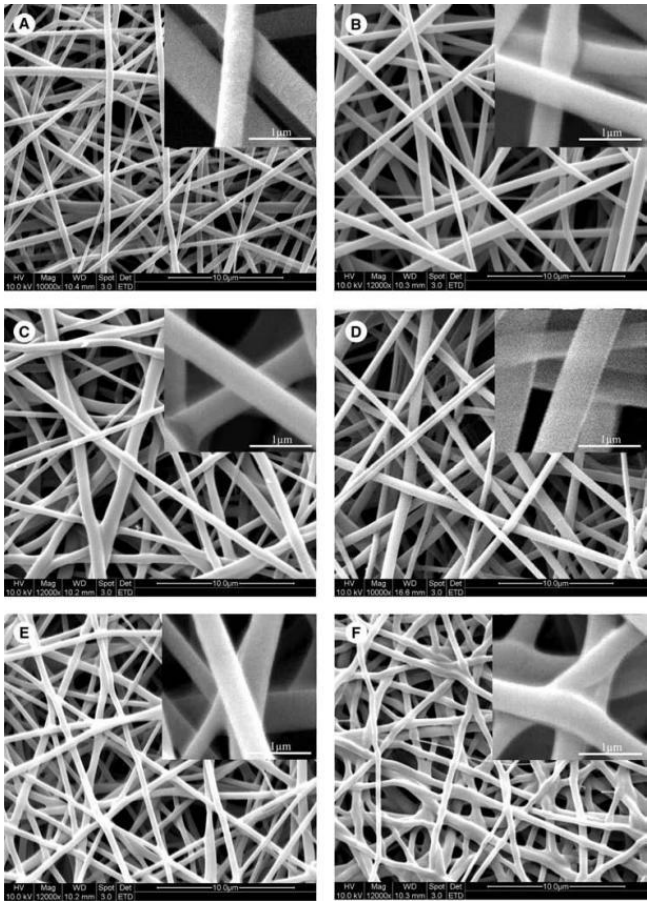

Fig. V.1. *SEM images of electrospun nanofibers subjected to UV irradiation of different exposure times. A: Unsterilized PLGA fibers; B: PLGA fibers irradiated for 2 h; C: PLGA fibers irradiated for 6 h; D: Unsterilized PLLA-CL fibers; E: PLLA-CL fibers irradiated for 8 h; F: PLLA-CL fibers irradiated for 48 h [359].*

Conversely, Valente et al. exposed aligned and random electrospun PLA fibers to a UV irradiation of 1 h and did not notice any remarkable alterations in mechanical, thermal and morphological properties. An *in vitro* study revealed that UV sterilization allowed a good adhesion and

proliferation of osteoblasts on the fibrous meshes with a perfect interaction and growth shape following the underlying aligned or random fiber arrangement [344]. Dai et al. subjected electrospun PCL fibers to a 30 min UV irradiation and did not discern any changes neither in the fibrous sheet wettability nor in the fiber morphology and dimension [360]. Similarly, Rainer et al. revealed that UV exposure of 20 min preserved the chemical and morphological features of electrospun PLA microfibers [113]. This disparity in literature suggests that the optimal process parameters vary between different polymers and structural morphologies and therefore should be carefully investigated according to the polymer features and final application.

V.4. Chemical sterilization

V.4.1. Ethylene oxide

EtO is frequently employed to sterilize clinical and medical products, such as plastic and rubber materials, given its low temperature conditions and wide range of antimicrobial efficacy [342, 361]. The mechanisms of action of this sterilization technique are illustrated by the ability of EtO to trigger an irreversible alkylation of cell molecules that contain carboxyl, amino, hydroxyl, amide and thiol groups. This leads to an everlasting repression of cell metabolic activity and mitosis [351]. Vegetative gram positive and gram negative bacteria, spores, RNA and DNA viruses, naked and enveloped viruses and fungi are easily deactivated by EtO [362]. The effectiveness of EtO sterilization depends on the process parameters such as temperature, exposure time, EtO concentration and relative humidity [342]. Several studies have investigated the influence of EtO on polymeric scaffolds intended for TE applications. Valente et al. sterilized electropsun PLA fibers with EtO and found out a morphological change from cylindrical to ribbon-like fibers with an increase in PLA crystallinity up to 28 % (Fig.V.2) [344]. Peniston et al. subjected molded PLA to EtO sterilization and did not notice any significant change in molecular weight or *in vitro* degradation up to 12 weeks post sterilization. A small increase in WCA of the sterilized samples was discerned suggesting a shielding of surface polar end groups after reactions with EtO molecules [363]. Hooper et al. sterilized PLLA films and the following 4 different biodegradable tyrosine-derived polycarbonates films using EtO: poly(DTE carbonate), poly(DTB carbonate), poly(DTH carbonate) and poly(DTO carbonate). Poly(DTO carbonate) was the only polymer to degrade faster than its unsterilized counterpart post-sterilization. EtO did not influence the degradation rate, surface chemistry,

mechanical properties, molecular weight and polydispersity of PLLA and the other polycarbonates. These results show that the sterilization method that should be selected for polymeric scaffolds strongly depends on the nature of the base material [358]. Moreover, the architecture of the sample has also a big influence on the choice of the appropriate sterilization method since films, fibrous electropun mats or porous 3D scaffolds of the same base material respond differently to one sterilization method. This was directly highlighted by Phillip et al. who subjected films, 3D scaffolds and fibrous mats of different poly(ethylene glycol) (PEG) to EtO sterilization. The films were prepared by compression molding, the 3D scaffolds were fabricated by solvent casting/porogen leaching and the fibers were electrospun. Overall, results showed that porous scaffolds collapsed and electrospun fibers fused together and lost their shape. The films were less affected by EtO and only underwent a mild smoothening [364]. It is worth mentioning that EtO is cytotoxic and only small amount of residual EtO remaining in the scaffold post-sterilization can greatly affect their cytocompatibility. The aeration of the sterilized scaffolds prior to *in vitro* and *in vivo* studies is therefore mandatory [343, 365].

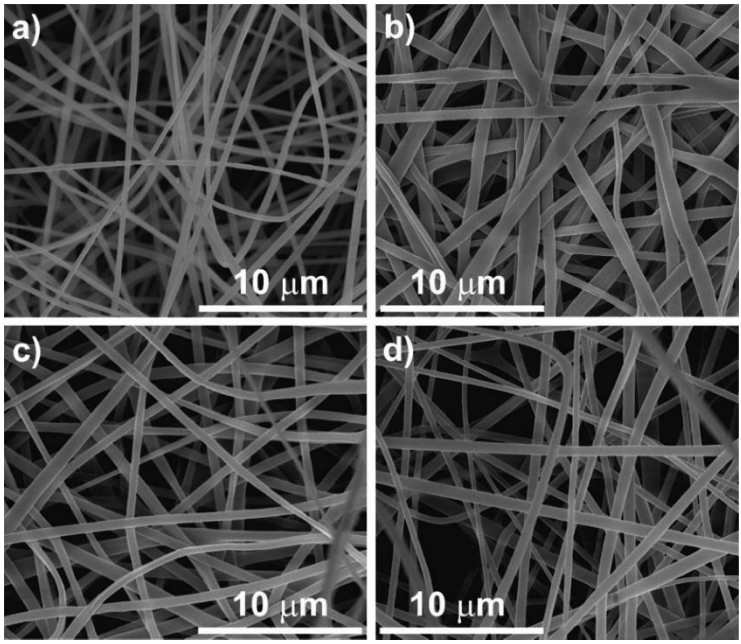

Fig. V.2. *SEM images showing the morphology of electrospun PLA fibers subjected to different sterilization methods. A: Unsterilized fibers; B: Fibers sterilized by EtO; C: Fibers sterilized by UV radiation; D: Fibers sterilized by γ irradiation [344]*

V.4.2. Ethanol

Several studies have used ethanol to decontaminate biodegradable scaffolds prior to *in vitro* and *in vivo* experiments because of its practical, easy, low-cost and ambient temperature operative conditions [21, 80, 96, 366]. However, a major concern in the use of ethanol is the restricted ability to kill all forms of microorganisms [113]. Ethanol triggers protein denaturation, dissolution of the cell membrane lipids and cellular dehydration leading to the inactivation of some microorganisms [343, 367]. Ethanol concentrations between 60 and 80 % can inactivate acid-fast, gram-negative and gram-positive bacteria as well as lipophilic viruses, whereas bacterial spores and hydrophilic viruses are ethanol resistant [343]. The effects of ethanol on the properties of polymers remain controversial. For instance, on the one hand, soaking PLGA hollow fibers and scaffolds in 70 % ethanol was documented to drastically alter their mechanical and structural properties, reduce scaffold porosity and induce surface wrinkling [368]. On the other hand, ethanol treatment was detected to have no influence on the molecular weights and structures of PLGA scaffolds [369].

V.5. Plasma sterilization

In addition to its ability to modify surface properties, non-thermal plasma treatment has been proven as an effective process to destroy microorganisms. Polymeric scaffolds can therefore benefit from simultaneous enhancement of cell-material interaction and sterilization when plasma-treated using optimized parameters [343, 370]. This unconventional sterilization technique operates in nontoxic gases and under relatively low temperatures which limits chemical and thermal damages to polymeric substrates. Furthermore, plasma treatment can provide effective disinfection and sterilization within a short time that can be restricted to only a few seconds. Besides its capacity to inactivate microorganisms, plasma can also eliminate dead microbial debris from the surfaces of the sterilized scaffolds [371-373]. Several studies aimed at evaluating the plasma-induced effects on different microorganisms showed the very wide inactivation range of plasma being able to even kill bacteria in biofilms, antibiotic resistant bacteria and spores [372-376]. For instance, Joshi et al. subjected biofilms of Escherichia coli and multidrug-resistant Staphylococcus aureus to different plasma treatments using a floating electrode DBD operating in air at atmospheric pressure. Live-dead staining assay showed a significant decrease in the surviving bacteria (green) or in

other terms an increase in the dead bacteria (red) as plasma exposure duration increases (Fig V.3) [374].

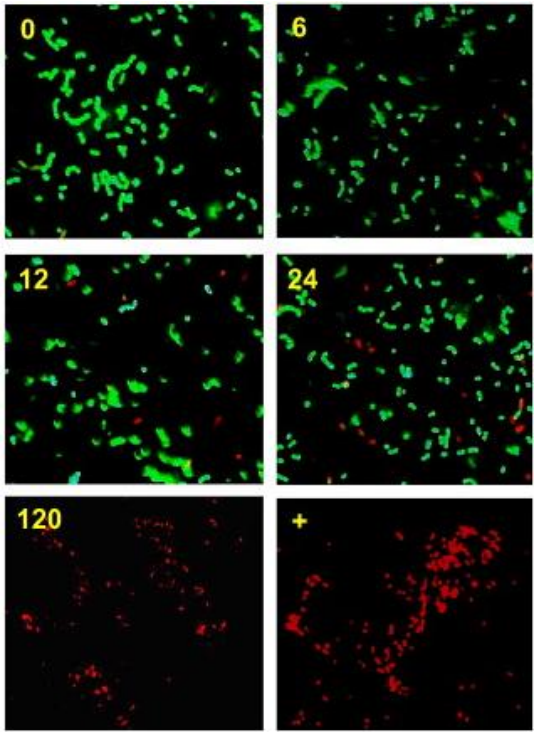

Fig. V.3. *Fluorescent micrographs after live-dead staining of meticillin-resistant Staphylococcus aureus biofilms subjected to plasma. The number in each image refers to the plasma exposure duration in seconds and the sign (+) is the positive control corresponding to a 70 % ethanol treatment [374].*

Rossi et al. exposed spores of Geobacillus stearothermophilus to a plasma treatment using an inductively coupled plasma discharge operating in air at low pressure. SEM images visualized a significant reduction in the spore size after 2 min of plasma exposure thus indicating the successful inactivation of the spores (Fig.V.4) [372].

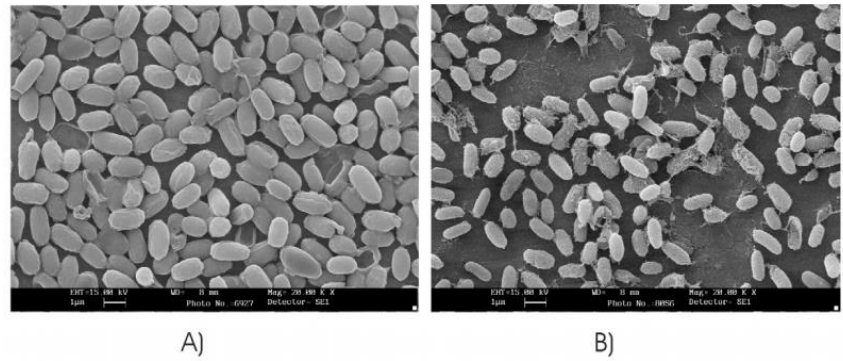

Fig V.4. *SEM images of Geobacillus stearothermophilus spores. A: Untreated spores; B: Oxygen plasma-treated spores [372].*

The mechanisms by which plasma triggers microorganism inactivation remain not fully understood. This is mainly due to the complexity of the different plasma discharges that can produce high fluxes of several ionized and neutral species on top of the energetic photons dynamically interacting with the treated materials. The precise contribution and function of each of these components depend on various intermingling parameters such as the applied power, the pressure, the gas flow, the excitation frequency, the reactor geometry and the nature of the microorganisms to be inactivated. This makes the comparison of the different studies using several experimental configurations very complex leading to controversy in the mechanisms playing a key role in the plasma/microorganism interactions [370-372]. Nonetheless, based on the published works, 2 major pathways of decontamination and sterilization are involved in non-thermal plasma treatments:

1) The first pathway relies on the physicochemical inactivation of the microorganisms mainly via etching effect by chemically active species primarily involving oxygen or via energetic ion sputtering. A recently suggested pathway is the assisted chemical etching combining the effects of reactive radicals and ion sputtering. Many studies have indeed shown that oxygen plasma is by far much more effective in the sterilization process than helium or argon gases for instance due to the strong oxidative and etching effects of oxygen reactive species physically destroying the pathogens [343, 371, 372, 375]. Laroussi et al. conducted a study in which Bacillus spores were subjected to an atmospheric pressure DBD treatment operating in pure helium or in a mixture of 97 % helium and 3 % oxygen as a proof of concept. In the case of the helium discharge gas, minor concentrations of reactive

species deriving from impurities are anticipated. However, when oxygen is added to helium, oxygen species such as O3 and O are largely produced. A comparison between the kinetics of spore inactivation was performed in both cases (Fig. V.5). In pure helium plasma, a high amount of surviving spores (70%) remained after 10 min of treatment, whereas a significantly higher spore killing rate was detected when helium/oxygen plasma is used [373].

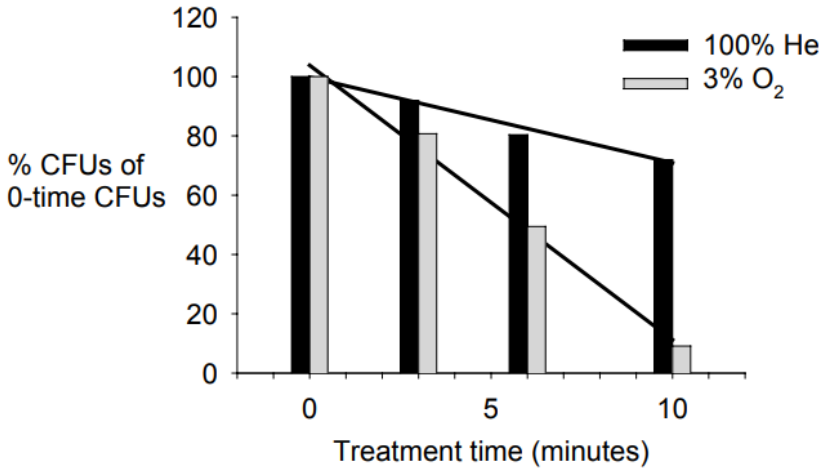

Fig. V.5. *Amount of surviving Bacillus spores after plasma treatment in pure helium or in helium (97 %) /oxygen (3 %) mixture in function of the plasma exposure time. CFU: colony-forming unit [373].*

Lerouge et al. selected a plasma gas mixture of oxygen and CF_4 to inactivate bacterial spores as this gas combination is known for its high efficacy in etching polymers. The number of live spores was considerably reduced from 10^6 to 10 per cm^{-2} due to the etching of the outer membrane and the physical destruction of the spores' components. Indeed, SEM images visualized spores not only reduced in size but also broken into pieces Fig. V.6) [375].

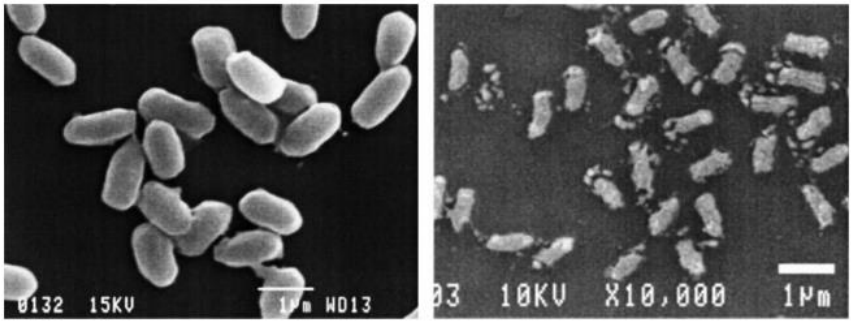

Fig. V.6. *SEM images of untreated (left) and O_2/CF_4 plasma treated (right) bacterial spores [375].*

2) The second pathway involves the alteration of the structural and chemical properties of the pathogens by the UV irradiations present in the plasma [372]. A first example is the alteration of the DNA molecules in bacterial spores by the emission of UV photons in plasma discharges thus suppressing the pathogen biological activity [377]. Another example involves the biological inactivation of bacterial endotoxins by the influence of vacuum UV irradiation that modifies their chemical structure [378]. In fact, non-thermal plasmas are a source of UV irradiation having different wavelengths. Nonetheless, only wavelengths between 200 and 300 nm with doses of several mJ/cm^2 are known to lethally damage cells. Low pressure plasma discharges, in contrast to atmospheric discharges are capable of providing UV radiation in the effective range of wavelengths. Therefore, the UV impact in sterilizing materials is considered to be a crucial contributor in vacuum plasmas and to have insignificant outcome in atmospheric plasmas [371, 379, 380]. However, a few authors stated that UV photons have a potential in atmospheric pressure plasma sterilization, but the majority of the arguments are incomplete or not fully persuasive [371, 381, 382]. The role of UV irradiation in plasma sterilization at atmospheric pressure is thus still forming a debate, and additional experiments should be conducted to solve this controversy.

Unfortunately, both pathways entail certain drawbacks in the sterilization of polymeric scaffolds. On the one hand, the physicochemical destruction of pathogens is very efficient but is associated with a big risk of polymer cross-linking or degradation leading to compromised mechanical properties. The scaffold integrity can be dramatically affected by the etching effect especially when the etch rate of the polymer is higher than the one of the microorganisms to be killed. On the other hand, the pathway based on the sterilization

by UV photons generally have a trivial effect on the microorganisms, but this is mainly counterbalanced by extensively increasing the plasma exposure time to enhance the sterilization effectiveness [343, 370, 372]. Holy et al. subjected PLGA scaffolds to a radio-frequency glow plasma discharge of high power (100 W) and operating in an inert argon gas at low pressure. Therefore, UV irradiation is anticipated to play the most potent role in sterilization. A complete sterility was obtained after 4 min of treatment. However, a longer exposure duration of more than 10 min with a lower power (33 W) drastically altered the 3D structure of the scaffolds [369]. Therefore, one can conclude that the plasma parameters should be delicately fine-tuned to sterilize polymeric scaffolds while preserving their features.

Three decades ago, an efficient sterilization system based on H_2O_2 germicidal effect and low-pressure plasma technology was commercialized under the name of Sterrad® 100 [375, 383]. The sterilization cycle of this apparatus includes the application of a high vacuum followed by an H_2O_2 diffusion phase and a final plasma phase induced by a generator with electromagnetic wave (Fig. V.7) [384]. Many studies were conducted to check for the relative efficacy of the H_2O_2 phase compared to the plasma phase in killing microorganisms. It was found that the chemical phase using the strongly oxidative H_2O_2 is responsible for the whole sterilizing effect. The plasma phase is mainly involved in the breakdown of the remaining peroxide and is therefore only playing a detoxifying role [370, 375, 384, 385]. Hence, although referred to as H_2O_2 plasma (HP) sterilization, the process is not a "real" plasma sterilization.

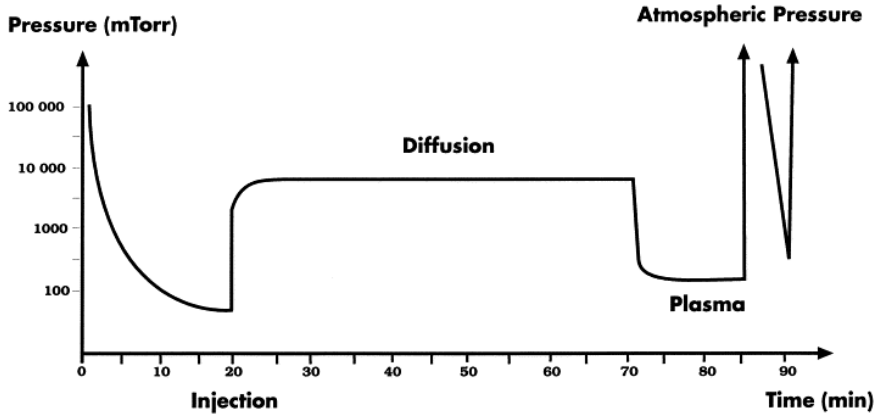

Fig. V.7. *H_2O_2 plasma sterilization cycle [384].*

Besides its frequent use in sterilizing medical devices, HP sterilization was successfully applied to biodegradable polymeric scaffolds intended

for TE applications. For instance, Rainer et al. showed that HP sterilization of PLLA electrospun microfibers did not modify their morphological and chemical properties [113]. Moreover, Dai et al. revealed that HP sterilization did not cause any damage to electrospun PCL fiber morphology and structural integrity. However, a decrease in the WCA was observed post-sterilization due to the plasma-induced incorporation of hydrophilic functional groups on the sample surface. This enhanced wettability played a favorable role as it significantly improved the osteogenic differention of pre-osteoblasts when seeded on HP sterilized fibers compared to fibers sterilized with UV or ethanol [360].

Chapter VI. Materials and Methods

VI.1. Biofabrication methods

VI.1.1. Spin coating: PCL films

PCL films are prepared by spin coating using the SPS Polos machine (SPIN150i/200i infinite). Commercially available PCL granules (MW =80000 g/mol) and THF were purchased from Sigma-Aldrich (Belgium) and used to prepare a 4% (w/w) solution. Glass cover slips having diameters of 12 mm (for subsequent cell culture tests) and 25 mm are used as substrates. A volume of 445 µl is deposited on a glass cover slip and spin coated for 70 s, at a spin speed of 3000 rpm and a spin acceleration of 500 rpm/s. Afterwards, PCL films are allowed to dry overnight to remove any residual solvent.

VI.1.2. Electrospinning: PCL fibrous sheets

The Nanospinner 24 (Inovenso, Turkey) is the electrospinning device that is employed to generate PCL fibers. It consists of 4 major components: a high voltage power supply, a programmable syringe pump, a copper tip and a large metallic cylinder (length = 28 cm, radius = 5 cm) which is used in the initial experiments as electrically conductive collector. In a next step, the collector is replaced by a home-made cylinder (length = 1 cm) having the same radius (5 cm) as the original collector for the remaining experiments. The device is conceived in a way allowing the jet to be sprayed in an ascending track towards the collector that is placed above the tip (Fig. VI.1 A).
Commercially available acetic acid (AA) and formic acid (FA) are supplied by Sigma-Aldrich (Belgium) and used as received, without any further purification. PCL (MW = 80000 g/mol) is dissolved in a mixture of AA/FA (1:9 v/v) to attain one of following polymer concentrations: 14 %, 20 %, 24 % and 28 % (w/v). Complete PCL dissolution is then achieved making use of a magnetic stirrer thoroughly mixing the solution at room temperature for 3 hours. The electrospinning process is performed at a temperature of 25 +/- 2 °C, a voltage of 32 kV and a solution flow rate varying between 0.5 and 0.7 ml/h. In order to obtain different fiber alignments, the rotational speed (RS) of the two collectors is varied between 100 and 3000 rpm. Different tip-to-collector distances (TCD) are also tested: 10, 12.5, 15 and 20 cm. Moreover, the influence of the humidity is also evaluated by introducing a humidifier inside the electrospinning chamber to achieve a RH of 35, 45, 55, and 65 % with an error range of +/- 2 %. PCL fibers are collected on glass cover slips (diameter = 12 mm) fixed on an aluminum sheet covering the collector.

VI.1.3. Electrospinning: PA conduits

Electrospun NGCs are fabricated at MERLN Institute (Maastricht University) using a custom-made electrospinning apparatus maintaining the temperature at 25 °C and the RH at 30 %. It is designed in a way allowing the jet to be sprayed in a descending track towards a tubular collector (diameter: 2 mm. length: 30 mm) placed below the spinneret (diameter: 0.8 mm) that is mounted on a metallic plate. A schematic representation of the device is illustrated in Fig. VI.1 B.

PA was purchased from PolyVation B. V. (Groningen, Netherlands) in the form of 300PEOT55PBT45 that follows the annotation aPEOTbPBTc where a is the molecular weight (in g/mol) of the base polyethylene glycol (PEG) segments used during polymerization while b and c represent the weight ratio between PEOT and PBT respectively. PA is dissolved overnight in the solvent system chloroform ($CHCl_3$, Sigma-Aldrich-The Netherlands)/ 1,1,1,3,3,3-hexafluoro-2-propanol (Bisolve, The Netherlands) at a ratio of 7:3 v/v. The electrospinning process is performed at a solution flow rate of 1 ml/h and a voltage of 20 kV that is applied through a DC high voltage supply (Gamma High Votage Research, USA). A distance of 13.5 cm is fixed between the collector and the spinneret that is programmed to translate in a back and forth motion along the axis of the tubular collector (120 mm/min) in order to ensure a homogeneous fiber deposition over the NGC length. An even wall thickness is safeguarded by rotating the mandrel at a speed of 50 rpm. After electrospinning, the collector is detached from the machine and placed in 70 % ethanol for an easy removal of the nerve guide without any residual fibers on the mandrel. The NGCs are then left to dry in ambient air.

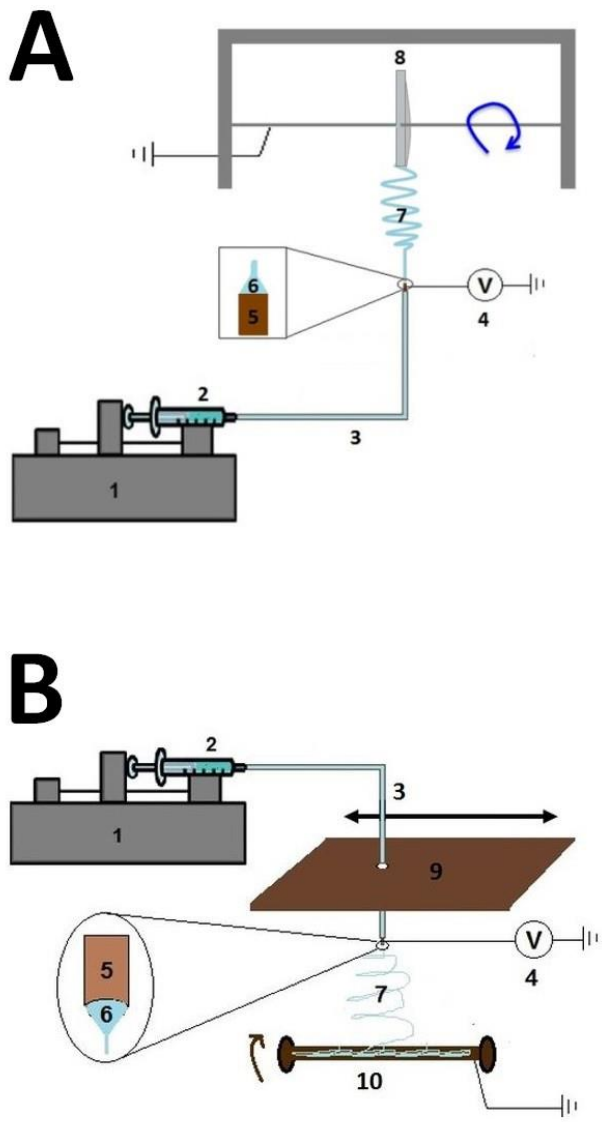

Fig. VI.1. *Schematic illustration of the electrospinning devices used to generate PCL fibrous sheets (A) and PA conduits (B) (1: syringe pump; 2: syringe containing the polymer solution; 3: capillary tube; 4: high voltage power supply; 5: copper tip; 6: Taylor cone; 7: polymer jet; 8: cylindrical collector; 9: Moving metallic plate; 10: Tubular mandrel).*

VI.2. Plasma treatments

VI.2.1. Dielectric barrier discharge

The DBD reactor used to treat PCL films, PCL fibers and PA NGCs consists of two main parts: a power supply and a plasma chamber fed with controlled gas flow and connected to a pump. A schematic view of this setup is presented in Fig. VI.2. Plasma is generated in the plasma chamber (cylindrical enclosure) between two circular copper electrodes (diameter= 4 cm), both covered with a square (25.0 cm^2) ceramic plate (Al_2O_3) (thickness =0.7 mm) serving as dielectric. The superior electrode is connected to a high frequency (50 kHz) AC power source and the inferior electrode is connected to the earth through a resistor R (50 Ω) or a capacitor C (10.4 nF) used to electrically characterize the discharge. The discharge gap between the two electrodes is set to 4 mm. As a preplasma phase, the sample is fixed on the inferior ceramic plate, and the discharge chamber is pumped down by a rotary vane pump below a pressure of 0.6 kPa. Afterwards, the plasma reactor is filled with the discharge gas (air or argon) at a rate of 3 standard liters per minute (slm) until a sub-atmospheric pressure (90 kPa) is reached. In order to reach a reproducible gas composition in the plasma chamber, the working gas is kept at a rate of 3 slm for 3 min to flush the chamber. This purging step constitutes the end of the pretreatment phase and the plasma treatment is performed for various treatment times at a medium pressure of 5.0 kPa and a gas flow of 1 slm.
Air and argon Alphagaz 1 are purchased from Air Liquide (Belgium).

In order to electrically characterize the DBD, the high voltage and the discharge current are measured and the current-voltage waveforms are acquired:

- The high voltage applied to the reactor is measured using a 1000:1 high voltage probe (Tektronix P6015A) connected to the superior electrode.
- The discharge current is monitored by measuring the voltage over the resistor of 50 Ω connected in series to the ground.
- The current-voltage waveforms are visualized using Picoscope 6 software after being recorded with a digital oscilloscope (Picoscope 3204A).

To determine the discharge power of the DBD, Lissajous figures are acquired. The resistor is thus replaced by a capacitor of 10.4 nF. The voltage across this capacitor is directly proportional to the charge stored on the copper electrodes. Lissajous figures are constructed by

plotting the charge as a function of the applied voltage, and the discharge power is calculated by multiplying the electrical energy consumed per voltage cycle with the frequency of the feeding voltage (50 kHz) knowing that the electrical energy is equal to the area enclosed by the Lissajous figure [386].

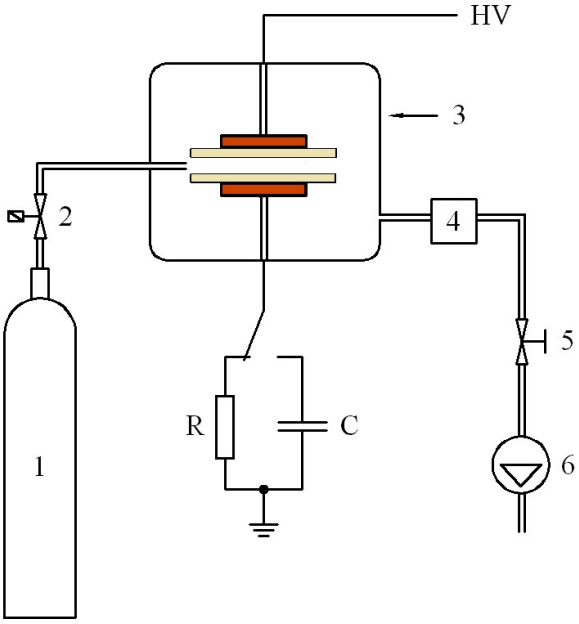

Fig. VI.2. *Schematic illustration of the DBD set-up (1: gas cylinder; 2: mass flow controller; 3: plasma reactor; 4: pressure gauge; 5: valve; 6: pump.*

VI.2.2. Plasma jet

In addition to the plasma treatment of PA conduits using air and argon DBDs, a direct plasma penetration inside the conduits is performed using an atmospheric pressure plasma jet (APPJ) operating in argon. The aim of this treatment is to create a chemistry gradient on the inner wall surface. The setup consists of a quartz capillary containing a needle electrode and encircled on the outside by a ring-shaped electrode. The capillary has an outer diameter of 3 mm and inner diameter 1.3 mm. The needle electrode that is connected to a high AC voltage source is made up of a tungsten wire having a diameter of 0.5 mm with a halfsphere-shaped tip. The ring-shaped grounded electrode is 10 mm long, made of copper and located at a distance of 35 mm from the needle electrode. The distance between the copper ring center and the capillary edge is fixed at 20 mm (Fig. VI. 3). An argon flow running

inside the capillary is regulated by a Bronckhorst El-flow controller at a rate of 1 slm. When applying a high voltage to the tungsten electrode, plasma appears in the inter-electrode gap and outflows from the capillary to propagate in the surrounding air and form the so-called effluent plasma. This plasma jet is produced at a fixed frequency of 60 kHz and a peak-to-peak amplitude of 7 kV that is measured making use of a high voltage probe (Tektronix P6015A) connected to the needle electrode. The discharge current is simultaneously determined through a current transformer (Pearson Current Monitor Model 2877). The voltage-current waveforms, recorded using a Picoscope 3204 A digital oscilloscope, are used to calculate the average discharge power W according to the equation VI.1 where T corresponds to the discharge period.

Eq. VI.1: $W = \frac{1}{T}\int_{t}^{t+T} I(t)V(t)dt$

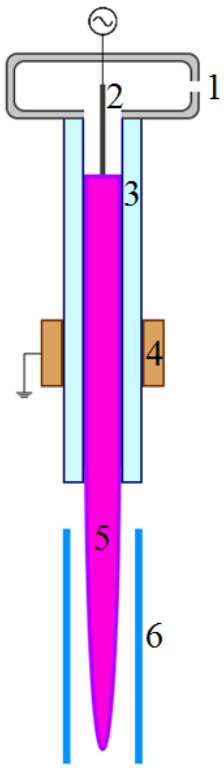

Fig. VI.3. *Schematic illustration of the APPJ set-up (1: gas flow; 2: high voltage electrode; 3: quartz capillary; 4: grounded electrode; 5: plasma jet; 6: conduit).*

The process parameters used in this thesis give a discharge power of 3.1 W. During the treatment, PA conduits are placed in tubular holes perforated in a transparent thermoplastic poly(methyl methacrylate) (PMMA) holder to safeguard for an accurate and precise penetration inside the conduits. A distance of 2 mm is set between the end of the capillary and the conduits that are exposed to plasma at different time intervals.

VI.3. Characterization techniques

VI.3.1. Static water contact angle

In order to get an insight on the surface wettability of the untreated and plasma-treated PCL films and fibrous meshes, static WCA measurements are performed at room temperature. The commercial Krüss Easy Drop optical system (Germany, Krüss Gmbh) is used for this purpose. Distilled water drops are deposited on the sample surface, after which an instantaneous determination of the drop profile is carried out using Laplace-Young curve fitting.

VI.3.2. X-ray photoelectron spectroscopy

In order to assess the surface chemical composition of PCL films, PCL fibers and the inner wall of PA conduits, XPS measurements are performed making use of the PHI 5000 Versaprobe II spectrometer. The samples are excited, over an area of 200 µm, with a monochromatic Al K_α X-ray source ($h\nu$ = 1486.6 eV) operative at a power of 50 W. The XPS specimen chamber is continually held, during the assessment process, at a pressure of minimum 10^{-6} Pa. The detection of photoelectrons is achieved by a hemispherical analyzer tilted 45° with respect to the normal of the fibrous mesh surfaces. All binding energies are adjusted relative to 285.0 eV being the hydrocarbon component of the C1s spectrum. Survey scans are recorded at a pass energy of 187.85 eV and analyzed to inspect the different surface elements. Quantification of the detected elements is carried out via Multipak software (V 9.6) using a Shirley background while considering the relative sensitivity parameters assigned by the XPS device manufacturer. High-resolution C1s peaks are also recorded with a pass energy of 23.5 eV and Multipak software is again used to curve fit these peaks. The energy scale is calibrated with respect to the hydrocarbon component of the C1s spectrum (285.0 ev). Afterwards, Gaussian-Lorentzian peak shapes (100-80% Gaussian) are utilized for the deconvolution of the peaks and

the full-width at half maximum (FWHM) of each line shape is restricted below 1.6 eV.

XPS micro-mapping is also performed on PA conduits to study the exact distribution of oxygen over the whole inner wall surface after DBD and APPJ treatments. The XY position of the sample is calibrated by a scanning X-ray induced secondary electron image camera allowing a precise navigation (resolution of 5-10 µm) over the sample surface. The conduits are cut open along their length and XPS mapping is therefore done over an area of 19 mm x 3.5 mm. Each XPS measurement spot (50 x 50 pixels) is selected at 10 µm intervals vertically and horizontally thus giving a total of 38 x 7 measurement points. Individual high resolution C1s and O1s spectra are recorded at each measurement spot with step size of 0.4 eV and a pass energy of 93.9 eV. XPS map figures are generated by stitching together all oxygen percentage results using Multipak software.

VI.3.3. Atomic force microscopy

Besides the chemical characterization, physical properties are studied through the examination of PCL film surface topography and roughness using an XE-70 atomic force microscope (Park Systems). A silicon cantilever (Nanosensors™ PPP -NCHR) scans the PCL surface in a non-contact mode. 15 µm images are recorded and analyzed using XEP software after their modification with an X and Y plane auto-fit procedure.
In order to determine the thickness of PCL films, a scratch is gently done on the film to locally remove it from the glass plate. AFM images covering the scratched and the unscratched areas on both sides, are recorded. XEP software is used to measure, without image flattening, the height difference between the two areas, which is the thickness of the film. The average of 10 measurements gives a thickness of 600.2 nm with a standard deviation of 13.3 nm, thereby indicating that the films are uniform.

VI.3.4. Scanning electron microscopy

PCL fibers and PA conduits are visualized using a scanning electron microscope (JSM-6010PLUS, JEOL, Japan) and SEM images are captured for further morphological analysis. Beforehand, the samples are sputter coated with a thin layer of gold making use of a JFC-130 autofine coater (JEOL, Japan) after which SEM images are acquired at an accelerating voltage of 7 or 10 kV.

VI.3.4.1. Fiber diameter

The average fiber diameter is calculated over 50 or 100 fibers taken from 2 different samples of the same condition by measuring the size of each fiber perpendicularly to its long axis. ImageJ (National Institutes of Health, USA) analysis software has been used for this purpose.

VI.3.4.2. Fiber alignment (Fast Fourier Transform)

A quantification of the fiber alignment in function of different electrospinning parameters is implemented by applying the fast Fourier Transform (FFT). This function transforms the data present in an original image from "real" space into a "frequency" space that is mathematically defined. The obtained output representation is comprised of grayscale pixels having a specific distribution that reflects the fiber alignment degree of the initial SEM image. When the fibers are randomly deposited, the resulting FTT image shows symmetrically distributed pixels having a circular shape (Fig. VI.4 B). This circular distribution stems from the fact that the frequency at which a particular pixel intensity arises in the original image is similar in any direction. Conversely, when the fibers are aligned, the resulting FTT output image shows non-randomly distributed pixels having an elliptical shape. This is due to the preferential assembly of the pixel intensities in a particular orientation (Fig. VI.4 B). A graphical representation of the FTT output image can be acquired by setting a circle on the FTT frequency distribution and running a radial sum of the pixel intensities for every degree in 1° increment. The obtained pixel intensity value can then be plotted in function of the direction (Fig. VI.4 D). The pixel intensities are analyzed between 0° and 360° but plotted only between 0° and 180° because of the symmetric FTT image with respect to the horizontal axis. The degree of alignment is reflected by the shape and the height of the overall distribution.
For FTT analysis, SEM images of PCL fibers are resized to 256 x 256 pixels and converted to TIF 8-bit grayscale files while SEM images of PA fibers are resized to 360 x 360 pixels and converted to TIF binary 8-bit files. Afterwards the images are processed with ImageJ analysis software.

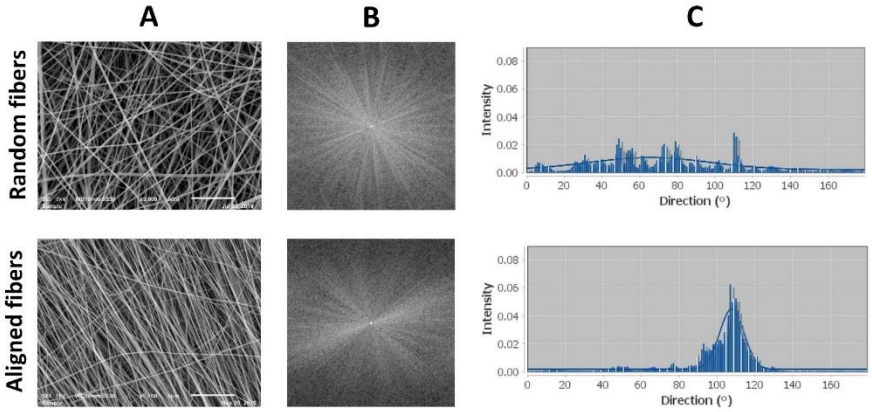

Fig. VI.4. Quantification of electrospun fiber alignment via FTT function. (A: SEM image of the aligned and random fibers (scale bar: 5 µm); B: FTT output image; C: Pixel intensity plot in function of the direction of the fibers).

VI.3.4.2. Conduit diameter and wall thickness

In order to visualize the cross section of PA conduits, an immersion in liquid nitrogen is done prior to the sectioning and imaging to avoid fiber damaging and conduit compressing during the cutting procedure. In this way, precise and unbiased measurements of the conduit diameter and the wall thickness can be done using ImageJ analysis software.

VI.3.5. Tensile measurements

In order to determine the mechanical properties of PCL fibrous meshes, rectangular samples (3 cm x 1 cm) of electrospun PCL are detached from the aluminum sheet and mounted between rubber coated grips at a distance of 1 cm in a universal testing machine (LRXplus, Lloyd Instruments, Bognor Regis, UK). Beforehand, the thickness of each sample is measured using a digital outside micrometer (Mitutoyo, Kruibeke, Belgium) on five different spots and averaged. Tensile testing is performed at a rate of 5 mm/min at room temperature (21°C). Samples with aligned fibers are loaded in the direction of the fiber alignment. The Young's modulus, which describes the tensile elasticity, is calculated as the slope of the linear part of the obtained stress-strain curves. Porosity is not taken into account in this study.

VI.4. Sterilization

Three different sterilization methods are applied to the untreated and plasma-modified PCL films and electrospun samples after placing them in 24-well polystyrene plates.

VI.4.1. Ethylene oxide sterilization

The samples are first wrapped in sterilization pouches (Steriking S6; Wipak medical) and then subjected to an EtO sterilization which is performed in the AZ Sint-Jan Brugge hospital (Belgium). The EtO exposure phase is achieved at a temperature of 38 ℃ and followed by an aeration phase of 48 h to get rid of the residual toxic EtO.

VI.4.2. H_2O_2 plasma sterilization

HP sterilization is performed using the STERRAD 100 Sterilizer (Advanced Sterilization Products; Johnson & Johnson) of the Ghent University hospital (Belgium). The samples are sealed in pouches and placed in the sterilizer. A 55-min cycle, during which a chemical phase corresponding to an exposure to vaporized H_2O_2 diffusing in the chamber and followed by a plasma phase, is carried out at temperatures not surpassing 55 °C.

VI.4.3. UV sterilization

The samples are irradiated by a commercial UV lamp (Sylvania, 15 W) at a wavelength of 254 nm for 3 h with an effective UV intensity of 300 $\mu W/cm^2$. The sample-to-lamp distance is fixed at 45 cm.

VI.4.4. Sterility test

To check for the efficacy of each sterilization method, ten sterilized samples of each sterilization method are immersed in a soybean casein digest broth, purchased from Sigma Aldrich (T8907), for the cultivation of fastidious microorganisms. After incubation at 37 ℃ for 5 days, the samples are checked. An efficient sterilization is approved when the broth preserves its original appearance for the 10 samples. However, clouding of the broth, for at least one sample, is a sign of contamination depicting an inefficient sterilization.

VI.5. *In vitro* cell tests

VI.5.1. Cell culture and seeding

VI.5.1.1. Adipose derived stem cells

Adipose tissue deriving from subcutaneous fat of Wistar rat cadavers (approved by the Ethical committee of Ghent University, Project EDC 13/14) is dissected, grinded and incubated in 0.1 % collagenase type I solution (Gibco, 17100-017) while shaking for 2 h at 37°C. The cellular suspension is then filtered making use of a cell stainer (70 µm) and centrifuged at 1200 rpm for 5 min. Thereafter, the cells are resuspended in DMEM Glutamax (Gibco™; Invitrogen) appended with 10% foetal calf serum (FCS) and 1% penicillin/streptomycin. Afterwards, the cells are cultured at 37°C in a humidified environment containing 5% CO_2. The medium is first changed after 24 h to get rid of the unattached cells and is subsequently refreshed every 3 to 4 days. When attaining 80-90% confluence, the cells are subcultured. For adhesion tests, ADSCs of passage 3 are seeded on PCL films and nanofibers at a density of 50 000 cells/100 µl per sample in a 24-well plate. For proliferation tests, the density of the cells is lowered to 20 000 cells/100 µl or 10 000 cells/100 µl. Additional medium is added 4 h after the seeding, which is a time dedicated to allow the attachment of the cells. The adhesion and proliferation of the cells are assessed after 3 h and after 1, 3 and 7 days respectively. Cells are also cultured on tissue culture plastic (TCP), following the same procedure, to serve as a positive control.

VI.5.1.2. Schwann cells

Primary SCs are harvested from sciatic nerves of neonatal Wistar rat pups, via dissection and digestion of the nerves, following the cell isolation and purification method described by Kaewkhaw et al. [387]. This method is based on the use of a selective culture medium simultaneously inhibiting fibroblast growth and favoring SCs survival and proliferation. Briefly, the harvested nerves are chopped and digested using a 0.05% (wt/vol) collagenase solution in 5% CO_2 for 60 min at 37 °C. The obtained cell suspension is then filtered via a 40µm cell strainer and centrifuged for 6 min at 400g. Afterwards, the supernatant is removed and the cell pellet is washed with DMEM containing 100U/ml penicillin/streptomycin and 10% fetal bovine serum (FBS). Cells are centrifuged once more for 6 min at 400 g and the supernatant is discarded. Finally, SCs are resuspended and cultured in DMEM Glutamax (Cell Culture Technologies)

supplemented with 10% (v/v) FBS, 0.25 µg/Ml amphotericin B, 1% (v/v) N2 supplement (R&D Systems), 20ug/mL bovine pituitary extract, 1% (v/v) penicillin/streptomycin and 5uM forskolin (Sigma Aldrich). Cell cultures are kept at 37°C in a humidified environment containing 5% CO_2. The medium is refreshed every 3 days and SCs are subcultured once they get to 80 % confluency.
Before cell seeding, UV-sterilized PA conduits are longitudinally cut open in two to generate flat electrospun sheets. Each sheet is placed in a rectangular well (8 mm x 1.9 mm) made up of polydimethylsiloxane (PDMS) from Sylgard 84 elastmer kit (Dow Corning). In order to create the PDMS wells, a mixture of the elastomer and the curing agent is prepared at a ratio of 10/1 (w/w) and filled inside rectangular molds having the desired dimensions. Afterwards, the mixture is degassed in a vacuum chamber. The curing process is done in an oven at a temperature of 80 °C for 1 h. The resulting PDMS casts were removed from the molds and dry-sterilized in an over at a temperature of 160 °C for 4 h. In order to prevent cell attachment on the PDMS casts and constrict it on the nerve conduits, a solution of 0.5 % Pluronic F127 is poured in each PDMS well. After 30 min incubation, the wells are washed 2 times with PBS.
Once the untreated and plasma-treated PA conduits placed in the PDMS wells, an incubation in DMEM supplemented with 10 % FBS is done overnight. The medium is then removed and the conduits are washed 2 times with PBS. SCs of passage 6 and 7 are seeded, at a density of 30000 cells/ cm^2, on the NGCs and on coverslips (diameter; 12 mm) serving as positive control. Two sets of experiments are performed in which SC culturing is done using either a medium without FBS or in a medium containing 10 % FBS. The common constituents of both media are the following: DMEM Glutamax, 1 % horse serum, 2 % N21-MAX supplement (R&D Systems), 100 ng/Ml of recombinant human NGF-ß (Sigma Aldrich) and 1 % penicillin/streptomycin. Cellular behavior is evaluated at day 1, 3 and 7 after seeding. Both sets of experiments are repeated 2 times each and in all 4 sets, 2 samples per condition are considered for every measurement.

VI.5.1.3. Schwann cells/ PC12 co-culture

PC 12 cells (DSMZ) are cultured in a proliferative medium containing RPMI 1640 solution (Thermo Fisher Scientific) appended with 10% horse serum and 5% FBS (Sigma Aldrich) and maintained in a humidified environment containing 5% CO_2 at 37°C. PC 12 cells of passage 26 and 27 are co-cultured with SCs of passage 6 and 7 on the NGCs at densities of 20 000 cell/ cm^2 and 30 000 cell/ cm^2 respectively in the following way:

- For the first set of experiments (FBS-free medium), the co-culture is directly performed after the immersion of NGCs in DMEM/ 10% FBS, using the same medium employed for the SC culture. Cellular behavior is assessed 3 days after cell seeding.
- For the second set of experiments (FBS-containing medium), SCs are first solely seeded on the NGCs as described previously. At day 7, the medium is removed and PC12 are seeded on the SC-cultured NGCs using the FBS-free medium. Cellular behavior is assessed 3 days after PC12 seeding.

VI.5.2. Live-dead staining (CaPi) and fluorescent microscopy

The evaluation of ADCSs viability and attachment to PCL films and fibers is made possible by performing a live-dead staining assay. First, the supernatant is gently aspirated and the samples are rinsed with phosphate buffered saline (PBS). Afterwards, 1 ml of PBS appended with 2 µl (1 mg/ml) of calcein acetylmethoxyester purchased from Anaspec (89201) and 2 µl of propidium iodine procured by Sigma-Aldrich (P4170) is used to stain the samples. The incubation is run in the dark at room temperature for 10 min after which the samples are rinsed again with PBS and imaged by means of an Olympus IX 81 fluorescent microscope.

VI.5.3. MTT assay

The quantification of the metabolic activity of ADSCs adhering and proliferating on PCL films and fibers is carried out by a colorimetric MTT assay. A yellow tetrazolium 3-(4,5-dimethyldiazol-2-yl)-2,5-diphenyltetrazolium bromide (MTT, Merck Promega) dye turns into purple-bleu formazan after the mitochondrial dehydrogenases of the living and metabolically active cells cause its reduction. In order to allow the occurrence of this reaction, the cell culture medium is replaced by the MTT solution (0.5 mg MTT/ml of medium), and cells are incubated for a duration of 4 h at 37°C. For the sake of dissolving the water insoluble formazan, the MTT reagent is removed and a lysis buffer, consisting of 1% Triton X-100 in isopropanol/0.4% HCl, is added and kept for 30 min at 37°C. Next, 200 µl of the solubilized formazan solution is transferred to a 96 well-plate. The absorbance of the color developed solution is assessed at 580 nm making use of a Universal microplate reader EL 800 (Biotek Instruments) spectrophotometer. The solution optical density of the PCL fibers is communicated as a ratio with respect to TCP.

VI.5.4. PrestoBlue assay

The proliferation of SCs cultured on PA NGCs and on coverslips is indirectly quantified by the PrestoBlue® Cell Viability assay (Life Technologies) at days 1, 3 and 7 post-seeding. PrestoBlue® reagent contains a blue cell-permeant resazurin-based compound that is not fluorescent in solution. When added to the cell medium, the reagent is taken up by the cells straightaway and converted to a strongly red-fluorescent dye by the reducing environment of the viable cells. Following the manufacturer's protocol, SCs are incubated for 1 h in culture medium containing 10% (v/v) PrestoBlue reagent at 37 °C, 5% CO_2 and away from light. Afterwards, 2 aliquots of 100 µL per sample are transferred to a black 96-well plate. The fluorescence signal is then measured in each well making use a spectrophotometer (CLARIOstar microplate reader, BMG Labtech) at an excitation wavelength of 560 nm and an emission wavelength of 590 nm. Blanks of PrestoBlue solution are monitored to correct the background fluorescence. A statistic evaluation of the presented data is done using one-way Anova and Turkey post-hoc tests. Welch and Brown-Forsythe tests are considered when the homogeneity of variances is violated. The significance level is $P < 0.05$

VI.5.5. Actin cytoskeleton staining

In order to visualize the actin cytoskeleton of the ADSCs and hence the cytoplasmic remodeling and morphology on different electrospun PCL fiber conditions, a phalloidin-rhodamin staining is performed. First, the samples are fixed with a solution of 4% paraformaldehyde (PFA) for 20 min and washed 3 times with PBS. The cell permeabilization is then carried out by soaking the samples in 0.5% Triton X-100 (Sigma-Aldrich; T8787) in distilled water for 5 min, after which a washing step with PBS is again done. Next, actin cytoskeleton is stained by incubating the cells in rhodamine-phalloidin (Thermo Fisher Scientific; R415; 1/100 in PBS) for 10 min. A final wash with PBS is executed before mounting the samples with Vectashield Antifade mounting medium with DAPI (Vectorlabs; H-1200) in order to stain the nuclei.
Actin staining images are then used to quantify the cell alignment in function of the different plasma-treated fiber conditions. The analysis is performed using the FFT function of ImageJ analysis software.
This software is also used to assess the circularity of the cell nuclei on the different fiber conditions using DAPI stained images. A circularity value of 1 designates a perfect circle. Decreasing the value and approaching 0 indicates an increasingly elongated polygon. The presented data are statistically analyzed using one-way Anova and

Turkey post-hoc tests. Welch and Brown-Forsythe tests are conducted when the homogeneity of variances is violated. The significance level is fixed at $P < 0.05$

VI.5.6. Immunofluorescent staining

Cells cultured on PA NGCs are fixed with 4 % (v/v) paraformaldehyde (Sigma Aldrich) in PBS for 20 min at a temperature of 4 °C. Afterwards, the permeabilization of the fixed cells is done using 0.1 % TritonX (Sigma Aldrich) for 15 min at ambient temperature. A blocking step follows by immersing the samples in a solution of 5 % goat serum for 1 h at room temperature. SCs cultures are then incubated in a primary antibody solution of rabbit anti-S100 antibodies (1:1000; Sigma Aldrich) for 12 h at a temperature of 4 °C. SCs/PC12 co-cultures are incubated in a solution containing both rabbit anti-S100 antibodies and chicken anti-neurofilament antibodies (1:1000; Sigma Aldrich). The samples are subsequently incubated for 1 h at ambient temperature with anti-rabbit Alexa 488 antibodies and anti-chicken Alexa 647 antibodies produced in goat (Invitrogen). Individual images are then acquired at a magnification of 20x on different zones of the NGCs using a fluorescent microscope. An automated stitching of overlapping images (12 x 1; 10x magnification) is also performed in order to visualize the cells on the whole NGC length.

VI.5.7. Protocol of cell fixation for SEM analysis

The morphology of the cells adhering and proliferating on PCL and PA fibers is analyzed by SEM. Prior to SEM analysis, the cells are washed with PBS and fixed with 2.5 % glutaraldehyde in 0.1 M cacodylate buffer for 1 hour. Afterwards, the cells on the nanofibers are dehydrated through immersion in increasing alcohol series (10 min immersion in each solution): 50%, 70%, 85%, 95% and 100% ethanol. The immersion in 100% ethanol is performed 2 times using a fresh solution the second time. After dehydration, the cell-containing nanofibers are transferred to a 100% hexamethyldisilazane (HMDS) solution where they are stored for 10 min. HMDS is subsequently replaced by a fresh HMDS solution which is left to evaporate under the fume hood. The nanofibrous samples with fixed cells are then coated with gold and viewed with SEM at an accelerating voltage of 10 kV.

Chapter VII. Effects of Different Sterilization Methods on the Physico-Chemical and Bioresponsive Properties of Plasma-Treated PCL Films

The results of Chapter VII were published in the following international peer-reviewed journal:

Ghobeira, R., Philips, C., Declercq, H., Cools, P., De Geyter, N., Cornelissen, R. & Morent, R.
Effects of different sterilization methods on the physico-chemical and bioresponsive properties of plasma-treated polycaprolactone films
Biomedical Materials, *12* (1): 015017 (2017).

VII.1. Introduction

Despite the sterilization drawbacks affecting the surface properties of polymers, few studies have investigated these properties when polymers are subjected to a previous surface modification. Furthermore, no study, to the best of our knowledge, has tackled the sterilization effects on plasma- activated PCL. The aim of this chapter is thus to perform a beneficial plasma surface modification of PCL films and to investigate the potential of this plasma treatment to sterilize the films. A second objective is to analyze the effects of different non-plasma sterilization methods on the physico-chemical properties and the cellular response of the plasma-treated films.
To do so, a medium pressure DBD operating in air and in argon is used to modify the surface of spin-coated PCL films. Plasma activated films are then subjected to UV, HP or EtO treatments, after which the sterility of the films is evaluated. Three surface analysis techniques are utilized in order to assess the physico-chemical modifications occurring on the surface: WCA goniometry, XPS and AFM. Besides surface characterization, live/dead staining and MTT assay are also performed to evaluate the adhesion and proliferation of ADSCs on PCL films.

The word "sterilization" is to some extent ambiguous because it mainly implies the initial killing of all forms of living microorganisms, which is not always the case in the treatments employed in this thesis. Therefore, the term "sterilization" used in the following parts might refer to "decontamination" in some cases.

VII.2. Experimental conditions

All experimental details can be found in Chapter VI. The parameters that are specifically used in this chapter are summarized in table VII.1.

Table VII.1. *Experimental conditions*

Base material	• PCL
Biofabrication method	• Spin coating
Plasma treatment	• Air DBD: - Power= 1.40 W • Argon DBD - Power= 1.07 W
Characterization techniques	• WCA: - 1 µl-drops of distilled water

	- Reported value: average of 10 values measured on 2 different samples. • XPS: - Reported value: average of 8 values measured on 2 different samples. • AFM: - Reported roughness value: average of 6 values measured on 2 different samples.
In vitro cell tests	• ADSC culture: - 50 000 cells/100 µl per sample for adhesion tests - 20 000 cells/100 µl per sample for proliferation tests • MTT assay: - Performed in triplicate.

To compare differences in adhesion and proliferation between plasma treatments and sterilization methods, one-way ANOVA followed by *post-hoc* Tukey (equal variances) or one-way ANOVA followed by *post-hoc* Dunnett's T3 (unequal variances) are performed using SPSS 23.0 software. Values of $p < 0.05$ are considered statistically significant.

VII.3. Results and Discussion

The results of this chapter are divided into two parts: the first part is dedicated to study the effect of the plasma treatment on the surface properties of PCL films while the second part mainly focuses on the effect of the sterilization on the properties of the plasma-treated films as well as on their bioactivity.

VII.3.1. Plasma treatment

VII.3.1.1.Electrical characterization of the DBD discharge

In order to evaluate the mode in which the DBD is operating, electrical properties of the different discharges are characterized. The voltage-current waveforms of the DBD operating in air and argon are visualized in Fig. VII.1. For the air plasma treatment, the discharge current shows several spike-like pulses with nanosecond duration at certain sections

of every half cycle of the applied voltage. Every current pulse corresponds to a series of microdischarges, clearly indicating that the DBD sustained in air operates in a filamentary mode [386]. Despite this non-uniform microdischarge activity, previous results showed a homogenous surface modification after plasma treatment [388]. For the argon discharge, at every half cycle of the voltage, only one wide peak is distinguished on the current waveform. This demonstrates that the argon discharge operates in a glow mode which guarantees a homogeneous treatment [389].

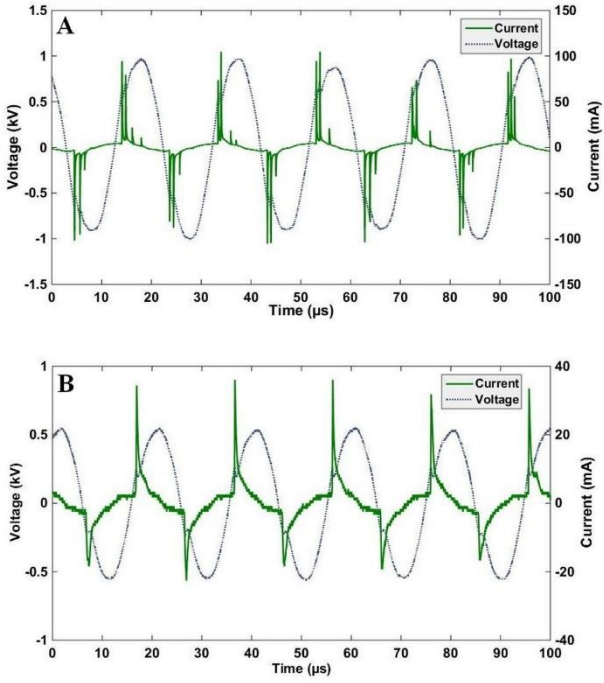

Fig. VII.1. *Current-voltage waveforms of the DBD sustained in air (A) and argon (B).*

VII.3.1.2. Water contact angle measurements

WCA measurements present a straightforward and highly sensitive technique to evaluate the wettability of the untreated PCL films and those subjected to air or argon plasma treatment. Since the discharge power and the plasma exposure time are different for both working gases, the evolution of WCA values is presented in function of energy density (Fig. VII.2). This value is obtained by multiplying the discharge

power by the plasma exposure time divided by the area of the electrodes.

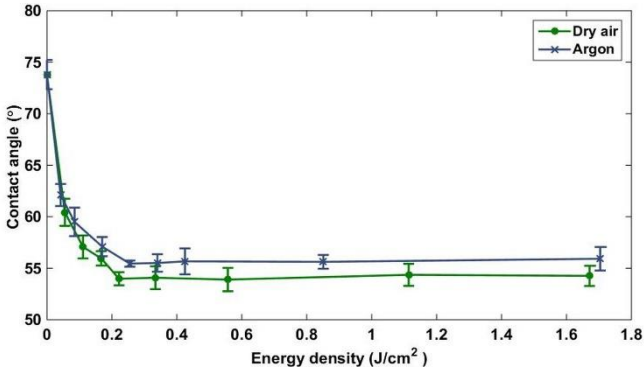

Fig. VII.2. *Water contact angles as a function of energy density for air and argon plasma-treated PCL.*

At zero energy density, corresponding to a non-exposure to plasma, the WCA of the PCL films is situated around 74 °. When applying a plasma treatment, the WCA decreases, clearly showing an increased wettability due to the increased number of oxygen-containing groups incorporated on the surface [390]. A saturation of the treatment effect is observed at a certain energy density, above which the WCA does not decrease any further, suggesting that a longer plasma exposure does not provoke further surface chemical modifications. In the case of the argon plasma treatment, the lowest contact angle value of 55.5 ° is obtained at an energy density of 0.25 J/cm², corresponding to a treatment time of 3 s. For PCL samples treated in dry air, a plateau is reached for a slightly lower WCA value of 54 ° at an energy density of 0.22 J/cm², which corresponds to a treatment time of 2 s. Surprisingly, when the energy density is increased above 2 J/cm², this plateau is no longer maintained and the WCA decreases again progressively reaching a value of 42 °for an energy density of 26.75 J/cm² (Fig. VII.3). This decrease in WCA value at high energy densities is not observed for the argon treated samples as an almost unchanged value of 56 ° is observed at an energy density of 25.55 J/cm². Air plasma treatment at high energy densities, is presumably causing a degradation of the PCL chemical structure observed trough XPS measurements, in line with the deterioration of the topographical and morphological surface characteristics examined via AFM imaging. These chemical and topographical changes are responsible for the extensive decrease in WCA value. For long plasma treatment times, many chain scissions

occur, leading to polymer degradation. This phenomenon is reinforced in the presence of oxygen; that is why it is not seen in the case of argon treatment where oxygen is only present as impurity [391]. Moreover, air treatment is operating in a filamentary mode while argon treatment is operating in a glow mode. This results in the fact that at high energy densities, the local microdischarges of the filamentary air treatment, provoke strong local oxidations degrading the polymer resulting in etching that increases the surface roughness and thus lower the WCA value [392, 393]. For argon treatments, a small decrease in WCA is detected at an energy density of 80 J/cm^2 and drastic changes in WCA begin to be observed only for energy densities above 100 J/cm^2. For example, a WCA of 27 +/- 19.5 ° is obtained at an energy density of 102.23 J/cm^2. The high standard deviations in these cases reveal the non-homogeneity of the polymer surface clearly indicating the degradation of the polymer.

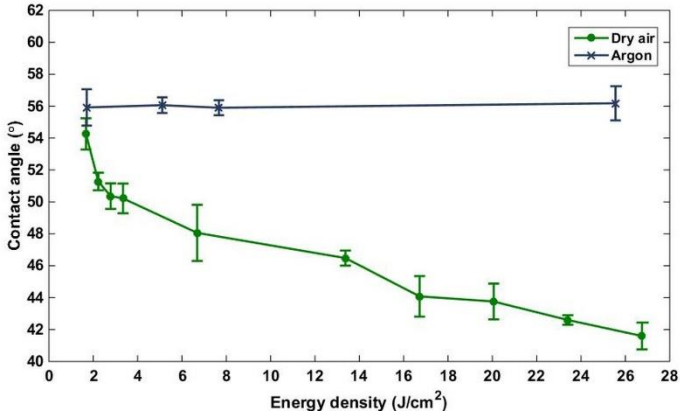

Fig. VII.3. *Water contact angles as a function of energy densities above 1.6 J/cm^2 for air and argon plasma-treated PCL.*

It is well-known that polymers exhibit a hydrophobic recovery after plasma treatment because of the tendency of the surface to recover to its original untreated state [394]. This so-called ageing effect is mainly attributed to the reorientation of the incorporated polar groups towards the bulk of the material, in order to create an energetically stable state and adapt the surface chemical structure to the environment. The ageing effect is investigated in this study because of the time needed to subject the samples to a sterilization method. The longest sterilization method among the 3 studied methods, is the EtO sterilization which is a 2 day cycle sterilization, followed by an extra 2 days of aeration to reduce to the maximum the residual toxic EtO. Consequently, all the

cell culture tests are done 4 days after the plasma treatment to ensure an objective comparison. Therefore it is important to find the plasma parameters resulting into a minimal ageing effect. After plasma treatment, the saturated air treated samples (0.22 J/cm^2) and argon treated samples (0.25 J/cm^2) are stored in ambient air at room temperature. The ageing behavior after 1 and 4 days is assessed by performing WCA measurements (Table VII.2). The WCA increases with ageing time and this increase is more pronounced for the air treated samples (62° after 4 days) compared to the argon treated samples (58° after 4 days). Morent et al. studied the ageing behavior of polypropylene, polyethylene terephthalate and PLA films and also found that the loss in treatment efficiency is higher for air than for argon treated samples [270, 395]. This result can be explained by the different cross-linking degrees of the air and argon plasma-treated surfaces. It was shown that air plasma treatment highly oxidizes polymer surfaces with a low cross-linking degree. However, argon plasma treatment forms an oxidized highly cross-linked structure. The high cross-linking degree limits the number of mobile groups that can migrate or re-orientate from the PCL surface into the material bulk, thus limiting the ageing effect.

In a trial aimed to minimize the ageing effect, the energy density is increased by increasing the plasma exposure time to 10 s, and the ageing behavior is then evaluated. Longer treatment times are not considered because of the risk of PCL degradation in the case of air plasma treatments. The increase in the plasma exposure time is shown beneficial for the air treated samples since a lower WCA (58°) is seen 4 days after the treatment of 10 s, compared to the WCA (62°) obtained at a plasma exposure time of 2 s. Most likely, longer treatment times exhibit a higher cross-linking degree.

An inverse effect is however observed for the argon treated samples as the WCA (61°) 4 days after the treatment is higher for a plasma treatment of 10 s compared to a plasma treatment of 3 s (58°). Slepicka et al. modified high-density polyethylene and poly (tetrafluoro-ethylene) surfaces using an argon plasma treatment and also found that the ageing effect is less pronounced when the polymers are treated at the shortest exposure time [396]. This is presumably due to a higher relaxation of the polymer chains for longer argon plasma treatment times, leading to different mechanisms of oxygen group rotations from the polymer surface to the bulk.

Table VII.2. *Water contact angles as a function of ageing time for air and argon plasma-treated PCL at different plasma exposure times.*

Treatment	Plasma exposure time (s)	Energy density (J/cm²)	WCA (°)		
			Ageing time (days)		
			0	1	4
Argon	3	0.25	55.4 +/- 0.3	56.8 +/- 0.8	58.3 +/- 1.0
	10	0.85	55.6 +/- 0.7	59.0 +/- 1.4	60.6 +/- 0.5
Air	2	0.22	54.0 +/- 0.6	60.1 +/- 1.6	62.0 +/- 0.6
	10	1.11	54.4 +/- 1.0	57.2 +/- 0.3	58.5 +/- 0.8

Based on the obtained results, a 10 s air plasma exposure and a 3 s argon plasma exposure are used to treat the PCL films for the subsequent sterilization study. The ageing behavior of the PCL films treated with the abovementioned parameters is studied for a storage time of 14 days (Fig. VII.4). The WCA increases with ageing time to reach a saturated value of almost 61 ° and 63 ° for the argon and air treated samples respectively. Despite increasing the plasma exposure time for the air treatment to minimize the ageing, the reached plateau value after approximately 9 days of ageing remains slightly higher compared to the argon treatment. However, the WCA values after 4 days of ageing are more or less the same for the air and argon plasma treatments (58 °). It is important to highlight that these values remain considerably lower than the value of the untreated PCL film (74 °) which means that a good wettability is maintained.

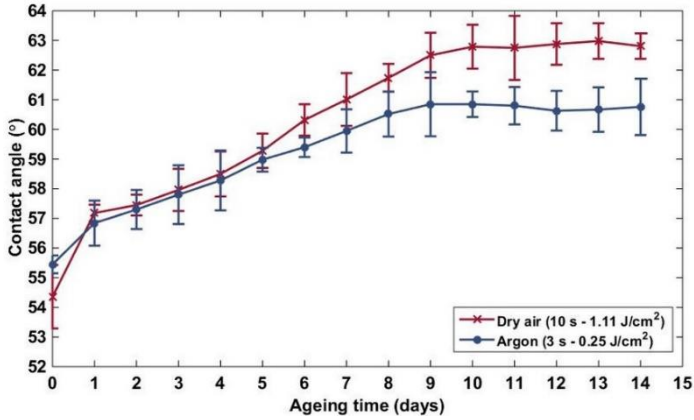

Fig. VII.4. *Evolution of the water contact angle as a function of ageing time for air and argon plasma-treated PCL.*

VII.3.1.3. XPS analysis

In order to explain the increased wettability after plasma treatment, XPS measurements are performed and PCL surface chemistry is analyzed. The atomic composition is obtained from the survey spectra, while the different chemical bonds between carbon and oxygen are determined by the curve-fitting of the high-resolution C1s peaks, since each bond has a different binding energy. In accordance to the literature, the C1s envelope of the untreated PCL can be decomposed into 4 components: a peak at 285.0 eV corresponding to hydrocarbon and carbon-carbon bonds (C-C / C-H), a peak at 285.5 eV corresponding to a secondary carbon bonded to an ester group (C-COO), a peak at 286.5 eV corresponding to a carbon single bonded to oxygen (C-O) and a peak at 289.1 eV corresponding to a carboxyl or ester group (O-C=O) [397]. Table VII.3 summarizes the obtained XPS results before and after plasma treatment at energy densities of 0.25 J/cm² and 0.22 J/cm², corresponding to the saturation point of argon and air treatments respectively. A schematic depiction of the curve fitting is observed in Fig. VII.5. It is found that the carbon and oxygen content of the untreated PCL, together with the concentration of the different bonds, are in accordance with its chemical structure. After argon and air plasma treatment, the O/C atomic ratio increases from 0.32 to 0.41 and 0.43 respectively, clearly indicating the presence of newly incorporated oxygen-containing groups. The increased oxygen content after argon treatment is attributed to the oxygen impurities remaining in the plasma chamber since it was not fully evacuated in addition to a post-oxidation. When taking a closer look at the surface chemical bonds, one

can find that the concentration of the C-C and C-H bonds decreases while the concentration of the C-O bonds increases. C-COO and O-C=O bonds have, as expected, more or less the same concentration and tend to slightly increase after plasma treatment. Moreover, a new peak appears at 287.7 eV corresponding to a carbon double bonded to oxygen (C=O). These results suggest that air and argon plasma treatments mainly attack the C-C and C-H bonds and form oxygen-containing bonds responsible of the increased wettability of the PCL surfaces. More precisely, literature agrees that it is the non-reactive species present in the plasma that can break the C-C and C-H bonds and thus can lead to the formation of polymer radicals. These radicals can subsequently react with the chemically reactive species of the plasma, which incorporates new atoms on the polymer surface [398].

Table VII.3. *Elemental composition and C1s curve fit results before and after plasma*

Treatment	WCA ( )	Atomic concentration (%)		C1s curve fit (%)				
		C	O	C-C/C-H 285.0 eV	C-COO 285.5 eV	C-O 286.5 eV	C=O 287.7 eV	O-C=O 289.1 eV
No	73.8 +/- 1.4	75.7 +/- 0.6	24.3 +/- 0.6	58.2 +/- 0.5	13.9 +/- 0.1	14.3 +/- 0.3	0	13.6 +/- 0.2
Argon (3s - 0.25 J/cm^2)	55.4 +/- 0.3	70.9 +/- 0.4	29.1 +/- 0.4	50.3 +/- 0.2	14.4 +/- 0.6	18.7 +/- 0.4	1.9 +/- 0.3	14.6 +/- 0.3
Air (2s – 0.22 J/cm^2)	54.0 +/- 0.6	69.8 +/- 0.5	30.2 +/- 0.5	49.1 +/- 0.8	15.0 +/- 0.4	17.9 +/- 1.0	2.2 +/- 0.1	15.9 +/- 0.4

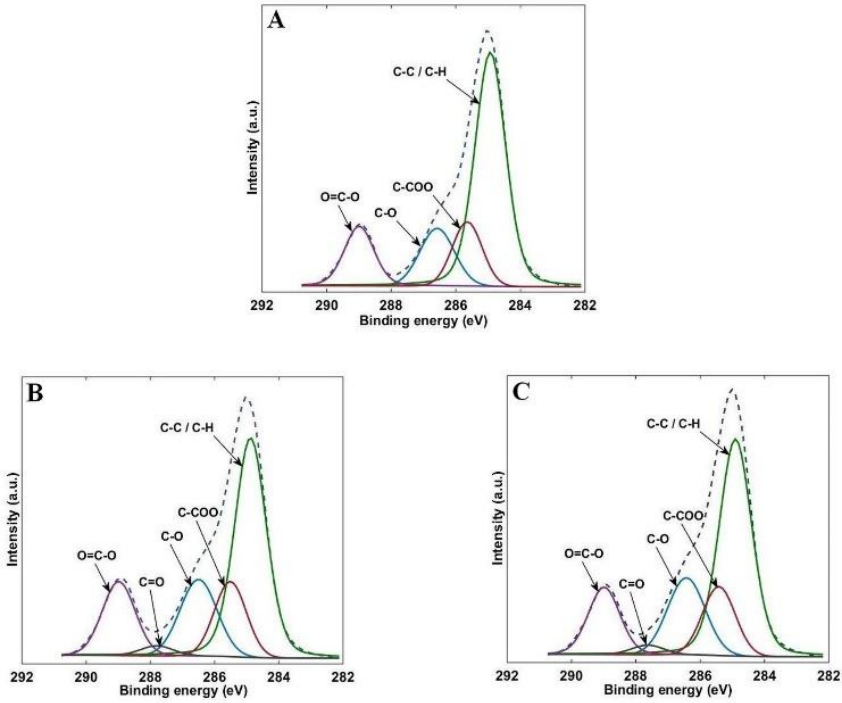

Fig VII.5*. High-resolution C1s peak of the untreated (A), argon (B) and air (C) plasma-treated PCL.*

To be able to understand the continuous decrease in WCA for long treatment times, observed in the case of air plasma treatment, the evolution of the surface chemistry in function of treatment time, is studied in this paragraph. For the air plasma-treated surfaces, plasma exposure times of 2 s and 10 s, show more or less the same atomic composition as well as the same concentration of the different chemical bonds. This is attributed to a saturation effect resulting in the highest concentrations of new oxygen-containing groups formed on the PCL surface. No further chemical modifications are thus expected to take place, however, plasma exposure times of 30 s and above, cause a progressive decrease in carbon content and an increase in oxygen content. Concerning the surface chemical bonds, a progressive decrease in C-C and C-H bonds as well as a progressive increase in C=O and O-C=O bonds are clearly observed. Fig. VII.6A shows the high-resolution C1s peaks of PCL after air plasma exposure time of 240 s. The increase in O-C=O concentration is accompanied with more or less unchanged

C-COO concentration, which can be explained by a random scission of the chains, consistent with the increase of free COOH groups (Table VII.4). The increase in C=O bonds and in free COOH groups is indicative of PCL degradation since it was observed by Domingos et al. when subjecting PCL to a degradation in basic solution [399]. Moreover, a PCL degradation was also observed when Pappa et al. treated PCL using air plasma at high power: C-C bonds decreased and C=O and O-C=O bonds increased significantly [278]. One can conclude that air plasma treatment at high exposure times is causing extensive chain scissions and thus degrading the polymer. The continuous decrease in WCA at high plasma exposure times is due to the increased oxygen content: the higher the oxygen concentration, the lower the WCA.

Table VII.4. *Evolution of the WCA and XPS results in function of plasma exposure time for air plasma-treated PCL*

Plasma exposure time (s)	Energy density (J/cm²)	WCA ( )	Atomic concentration (%)		C1s curve fit (%)				
			C	O	C-C/C-H 285.0 eV	C-COO 285.5 eV	C-O 286.5 eV	C=O 287.7 eV	O-C=O 289.1 eV
2	0.22	54.0 +/- 0.6	69.8 +/- 0.5	30.2 +/- 0.5	49.1 +/- 0.8	15.0 +/- 0.4	17.9 +/- 1.0	2.2 +/- 0.1	15.9 +/- 0.4
10	1.11	54.4 +/- 1.1	69.6 +/- 0.2	30.4 +/- 0.2	49.4 +/- 0.4	15.4 +/- 0.8	17.2 +/- 0.5	1.9 +/- 0.3	16.0 +/- 0.1
30	3.34	50.2 +/- 0.9	67.6 +/- 0.2	32.4 +/- 0.2	47.3 +/- 0.2	14.8 +/- 0.2	18.0 +/- 0.5	2.4 +/- 0.1	17.5 +/- 0.4
60	6.69	47.9 +/- 1.1	65.9 +/- 0.5	34.1 +/- 0.5	44.2 +/- 0.4	14.8 +/- 0.7	19.1 +/- 0.8	2.8 +/- 0.3	19.1 +/- 0.7
120	13.37	45.9 +/- 0.6	64.2 +/- 0.1	35.8 +/- 0.1	43.2 +/- 0.2	14.4 +/- 0.2	19.1 +/- 0.4	3.5 +/- 0.2	19.8 +/- 0.3
240	26.75	42.6 +/- 0.3	62.4 +/- 0.8	37.6 +/- 0.8	40.5 +/- 1.0	13.1 +/- 0.8	20.7 +/- 0.9	3.1 +/- 0.3	22.6 +/- 1.0

Increasing the plasma exposure time in the case of argon plasma treatment does not show the same effect. At a treatment time of 3, 10, 60 and 300 s, the surface atomic composition and the concentration of the chemical bonds remain the same (Table VII.5). This observation is in correlation with the unchanged WCA value. The surface is saturated after an argon plasma treatment of 3 s and no degradation is observed at higher exposure time. Fig. VII.6B shows the high-resolution C1s peaks of PCL after argon plasma exposure time of 300 s. As mentioned previously, it was shown that the presence of atomic oxygen enhances the polymer degradation [389]. During argon plasma treatment, only a small percentage of oxygen is left in the plasma chamber, which can explain why the polymer is not degraded.

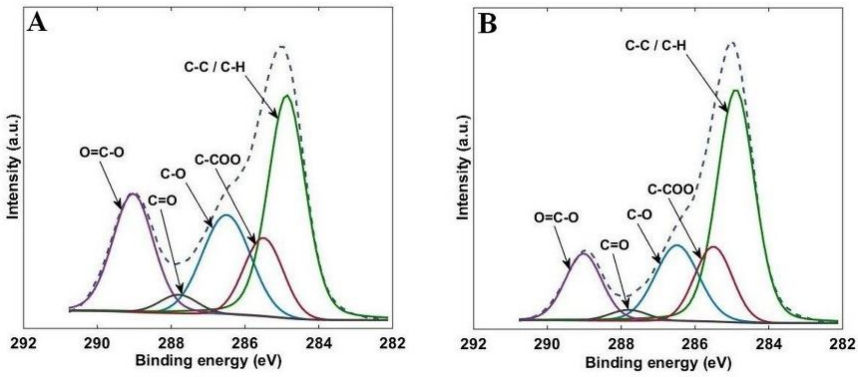

Fig. VII.6*. High-resolution C1s peaks of argon and air plasma-treated PCL. A: air (240 s - 26.75 J/ cm²), B: argon (300 s – 25.55 J/cm²).*

Table VI.5. *Evolution of the WCA and XPS results in function of the plasma exposure time for argon plasma-treated PCL*

Plasma exposure Time (s)	Energy density (J/cm²)	WCA ( )	Atomic concentration (%)		C1s curve fit (%)				
			C	O	C-C/-H 285.0 eV	C-COO 285.5 eV	C-O 286.5 eV	C=O 287.7 eV	O-C=O 289.1 eV
3	0.52	55.4 +/- 0.3	70.9 +/- 0.4	29.1 +/- 0.4	50.3 +/- 0.2	14.4 +/- 0.6	18.7 +/- 0.4	1.9 +/- 0.3	14.6 +/- 0.3
10	0.85	55.6 +/- 0.7	70.8 +/- 0.3	29.2 +/- 0.3	50.2 +/- 0.1	15.1 +/- 0.3	18.1 +/- 0.1	2.3 +/- 0.1	14.5 +/- 0.2
60	5.11	55.8 +/- 1.1	70.7 +/- 0.9	29.3 +/- 0.9	50.9 +/- 0.4	14.7 +/- 1.0	18.1 +/- 0.2	1.7 +/- 0.2	14.6 +/- 0.5
300	25.55	56.1 +/- 1.1	70.5 +/- 0.6	29.5 +/- 0.6	50.8 +/- 1.3	14.6 +/- 1.2	18.6 +/- 0.1	2.0 +/- 0.1	13.9 +/- 0.2

As all the measurements on the sterilized samples are done 4 days after the plasma treatment, it is necessary to execute an XPS analysis on non-sterilized and aged plasma-treated samples, to enable an accurate comparison. Therefore, PCL films subjected to 3 s argon or 10 s air plasma treatments are stored for 4 days in ambient air at room temperature, then XPS measurements are performed (Table VII.6). A decrease in O/C ratio and slight decreases in the oxidized carbon bonds are observed, compared to the non-aged samples. These findings confirm that polar groups induced by the plasma activation, re-orientate and move away from the surface. Despite the observed decrease in O/C ratio (0.38), it remains considerably higher than the O/C ratio (0.32) of the untreated PCL, meaning that a part of the oxygen induced during the plasma treatment is still on the surface.

VII.3.1.4. AFM imaging

AFM measurements are performed on both untreated and plasma-treated films in order to visualize the morphology and to quantify the roughness of PCL surfaces. Fig. VI.7 shows the AFM images of an untreated PCL film together with AFM images of air and argon plasma-treated films at different plasma exposure times. An unchanged PCL surface morphology is observed after air plasma exposure times of 2 s and 10 s and after argon plasma treatment. In contrast, extended air plasma exposure times significantly alter the morphology of the PCL surface and form microholes on it. This surface alteration is attributed to the PCL degradation which was already recognized in the WCA and XPS results. The root-mean-square roughness values quantifying the physical modifications, remain almost unchanged for the untreated, argon plasma-treated and air plasma-treated samples at short plasma exposure times. Increased roughness values are however detected for the PCL surfaces subjected to extended air plasma exposure (Table VII.7). The numerous chain scissions that occur at extended air plasma exposure lead to the formation of oligomers and desorption of volatile products from the PCL surface thus etching it. Literature agrees that oxygen mostly enhances this mechanism causing a pronounced etching effect [398]. Moreover, a comparison between glow and filamentary mode DBD plasmas shows that the filamentary mode, at high plasma power, provokes a more prominent etching damaging for example wool fibers, while the glow mode does not harm the same textile. The local microdischarges produced in the filamentary plasma treatment were found to cause strong local bombardments on studied fabric altering its surface [392]. This can explain the increased roughness and the modified morphology that are observed on the PCL samples only after air plasma treatment performed at high energy densities.

Table VII.6. *Elemental composition and C1s curve fit results of PCL samples 4 days after plasma treatment*

Treatment	WCA ( )	Atomic concentration (%)		C1s curve fit (%)				
		C	O	C-C/C-H	C-COO	C-O	C=O	O-C=O
				285.0 eV	285.5 eV	286.5 eV	287.7 eV	289.1 eV
Argon (3s - 0.25 J/cm²)	58.3 +/- 1.0	72.2 +/- 0.3	27.8 +/- 0.3	52.9 +/- 0.9	14.1 +/- 0.7	17.1 +/- 0.1	1.4 +/- 0.3	14.4 +/- 0.1
Air (10s - 1.11 J/cm²)	58.5 +/- 0.8	72.0+/- 0.6	28.0 +/- 0.6	51.9 +/- 1.1	15.1 +/- 0.4	17.3 +/- 0.7	1.2 +/- 0.1	14.4 +/- 0.3

Table VII.7*. Root-mean-square roughness values of the untreated, air and argon plasma-treated PCL*

Treatment	Plasma exposure time(s)	Energy density (J/cm^2)	Roughness (nm)
No	0	0	24.5 +/- 2.5
Air	2	0.22	24.1 +/- 2.3
	10	1.11	24.5 +/- 2.8
	30	3.34	28.1 +/- 3.0
	60	6.69	30.7 +/- 3.5
Argon	3	0.25	25.1 +/- 1.7
	60	5.11	24.0 +/- 2.7

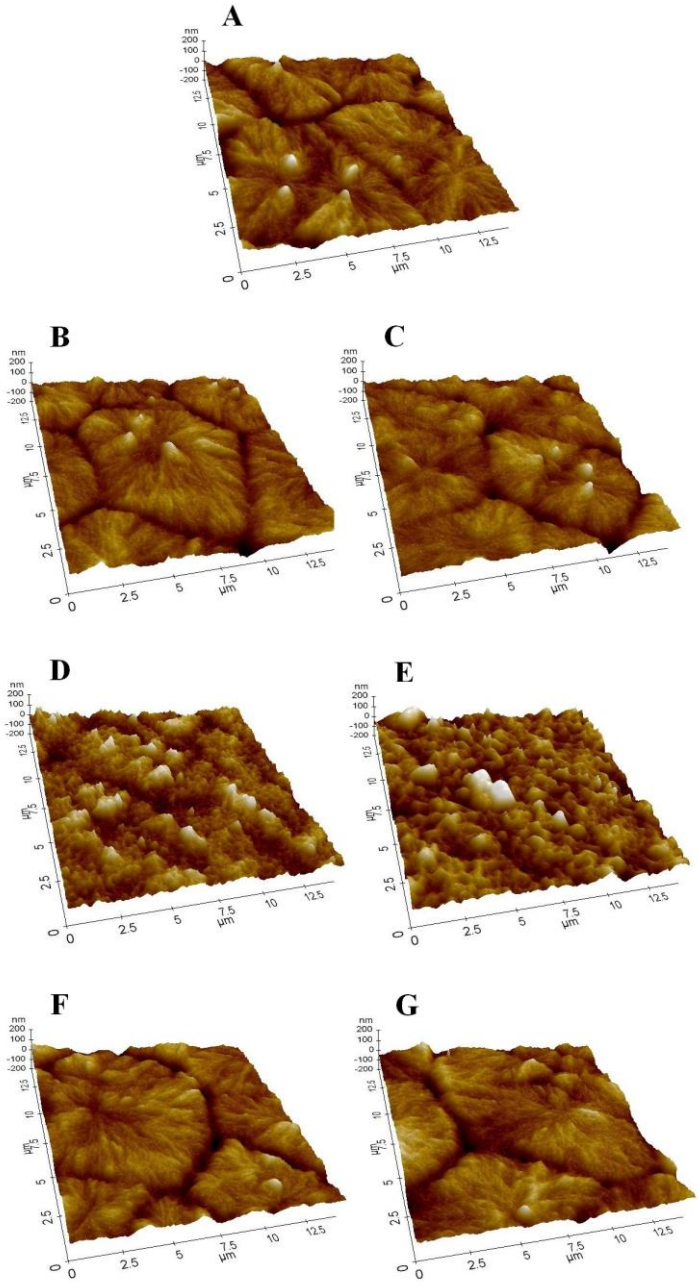

Fig. VII.7. *AFM images of untreated, air and argon plasma-treated PCL. A: Untreated, B: air (2 s – 0.22 J/cm²), C: air (10 s – 1.11 J/cm²), D: air (30 s – 3.34 J/cm²), E: air (60 s – 6.69 J/cm²), F: argon (3 s – 0.25 J/cm²), G: argon (60 s – 5.11 J/cm²).*

VII.3.2. Sterilization

VII.3.2.1. PCL sterility

The potential of plasma treatment to serve as a sterilization method is evaluated by testing the sterility of PCL films treated at different plasma exposure times (Table VII.8). In order to allow a beneficial surface modification and to avoid the degradation of the polymer while aiming to sterilize it, a limited range of plasma treatment times is considered. For argon plasma treatment, 5 treatment times ranging between 3 and 900 s are studied while for air treatment, 2 treatment times of 2 s and 10 s are evaluated. The aforementioned results revealed that higher treatment times exhibit a degradation of the PCL films.

Table VII.8. *Sterility of PCL films subjected to plasma, EtO, HP and UV treatments*

Sterilization treatment	Plasma exposure time (s)	Energy density (J/cm^2)	% Sterility (n=10)
Air plasma	2	0.22	30
	10	1.11	60
Argon plasma	3	0.25	40
	60	5.11	70
	300	25.55	80
	600	51.11	90
	900	76.67	80
EtO			100
HP			100
UV 1h			50
UV 2h			80
UV 3h			100

Results show that the percentage of sterility increases with increasing plasma exposure time. This can be explained by the prolonged time needed for the plasma to sterilize PCL films, since, as already mentioned in the introduction, 3 phases are involved: destruction of the genetic material by the UV irradiation generated by the plasma, erosion of the microorganisms by photon-induced desorption and etching in presence of oxygen. Moreover, the UV dose is proportional to the exposure time. Argon treatment shows that at some point, increasing the treatment time becomes inefficient: 80% sterility after 300 and 900 s and 90% after 600 s. This is probably due to the limited

etching effect of the argon treatment. It was demonstrated that this effect erodes the microorganism surface and thus facilitates the passage of UV photons through it, allowing them to reach and destroy the DNA [400]. As a consequence, the studied argon treatment times fail to attain 100% sterility, and thus to sterilize PCL films. Air treatment shows the same result because of the short treatment times studied. For that reason, the sterilization of the PCL samples after plasma treatment becomes an unavoidable step. Three sterilization methods are adopted: UV, EtO and HP. PCL films are tested for their sterility after being subjected to these sterilizations (Table VII.8). Sterility is 100% achieved after HP and EtO sterilizations. Concerning the UV sterilization, different exposure times are tested and it is found that 100% sterility is reached after 3 hours. Therefore, plasma-treated films are sterilized by EtO, HP or 3h UV irradiation immediately after plasma treatment. Surface characterization and cell tests are performed 4 days after the sterilization, to keep the results accurately comparable.

In the following experiments, plasma exposure times of 3 s and 10 s are adopted for argon and air treatments respectively, as previously mentioned.

VII.3.2.2. Water contact angle measurements

Fig.VII.8 shows the WCA results of untreated, air and argon plasma-treated samples before and after the 3 different sterilization methods.

After EtO sterilization, the WCA increases from around 74 ° to 77 ° for the untreated samples, and from 58 ° to 65 ° for air and argon plasma-treated samples. Peniston et al. also found a slight increase in WCA of PLA subjected to an EtO sterilization. The decreased wettability is presumably due to the modification of the PCL chain ends reacting with the EtO molecules. The short and strained C-C bonds of the EtO molecule can cause an easy opening of the ring, thus making it very reactive. Therefore, the following reactions between EtO and COOH or C-OH end chains can occur:

$CH_2CH_2O + R\text{-}COOH \longrightarrow R\text{-}COO\text{-}CH_2CH_2OH$ (1)

$CH_2CH_2O + R\text{-}OH \longrightarrow R\text{-}O\text{-}CH_2CH_2OH$ (2)

The obtained structure from the reaction with the carboxylic group, is shielding this highly polar bond while exposing a hydroxyl group. This phenomenon is contributing to a more hydrophobic surface since C-OOH bonds were shown to be more hydrophilic than C-O bonds. The termination entity of the structure resulting from the reaction with the

hydroxyl group is also a hydroxyl group, thus this reaction does not change the surface hydrophilicity [363].

The increase in WCA is more pronounced for the plasma-treated samples. This can be explained by the fact that the plasma-treated surfaces contain more carboxyl group end chains so more C-OOH bonds are shielded.

HP sterilization causes a slight decrease in WCA of the untreated samples from around 74 ° to 70 °. Several studies also showed an increased WCA of polymeric materials after HP sterilization [363, 383, 385]. This is due to a surface oxidation adding polar groups to the surface and thus increasing its wettability. The oxidation occurs during the chemical phase corresponding to the exposure to the highly reactive H_2O_2 and during the plasma phase. However, it is believed that most of the surface modifications are produced during the chemical phase because the plastic bag wrapping the samples limits the number of plasma active species to reach the PCL surface [383]. This can explain why the observed decrease in WCA is relatively small after HP sterilization.

HP sterilization of the air and argon plasma-treated samples causes however an increase in WCA value from around 58 ° to 68 °. The results are indicative of a decreased wettability due to a depletion of hydrophilic chemical groups. One of the complex chemical alterations provoked by the highly reactive H_2O_2 and the plasma active species is presumably the scission of the polar bonds generated in the previous air and argon plasma activation.

After UV sterilization, the WCA remains constant for both untreated and plasma-treated samples, demonstrating that a UV exposure of 3h does not provoke surface chemical modifications. XPS results, showed in the following paragraph, confirm this finding.

For all sterilization methods, no significant differences in WCA values are observed between the air and the argon plasma-treated samples.

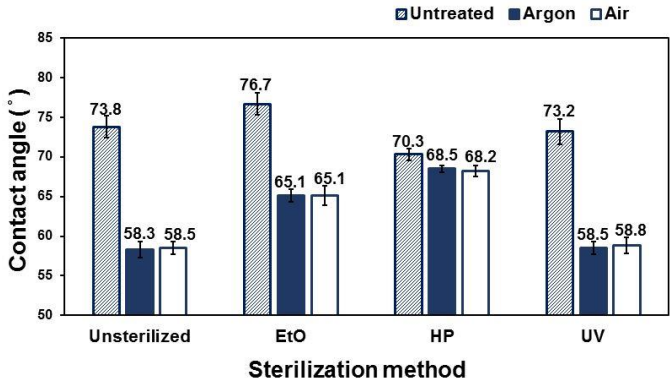

Fig. VII.8. *Water contact angles of untreated, air and argon plasma-treated PCL before and after EtO, HP and UV sterilizations.*

VII.3.2.3. XPS analysis

XPS analysis is performed on the untreated, air and argon plasma-treated samples before and after the 3 different sterilization methods, in order to investigate the changes in surface chemical composition induced by these sterilizations. Fig. VII.9 and Fig. VII.10 show the results obtained from the survey spectra and from the curve-fitting of the high-resolution C1s peaks respectively.

No significant changes in atomic composition and in the concentrations of the different chemical bonds are detected after EtO sterilization, whereas WCA measurements revealed a decreased wettability due to the reaction with EtO molecules modifying the chain ends of PCL. This can be explained by the limited ability of the EtO to penetrate into the polymer. EtO molecules react only with the top layers of PCL, knowing that WCA and XPS techniques have different depth of analysis: WCA is affected by the first atomic layers while XPS has a deeper penetration (≈ 10 nm).

After HP sterilization, a slight increase in oxygen content of the untreated samples is observed, while a decreased oxygen content is detected in the case of argon and air plasma-treated samples. These findings are in accordance with the WCA results. The oxidation of the untreated samples occurring during the chemical H_2O_2 phase and the plasma phase is confirmed by a decrease in the C-C/C-H bonds accompanied by a slight increase in the concentration of C-O groups as

well as a small incorporation of C=O groups. H_2O_2 is thus revealed to exhibit a better penetration compared to EtO. It is qualified to have a moderate-to-good penetration being able to penetrate as great as 1 mm in various plastics.[385] An inverse effect is observed for the plasma-treated samples, where the concentration of C-C/C-H bonds increases while slight decreases in C-O, O-C=O and C=O groups are detected. This observation supports the suggestion stating that one of the chemical processes occurring during HP sterilization is the scission of the weak oxygen-containing bonds induced by the previous plasma treatment.

XPS results show that a UV exposure of 3 hours does not cause any chemical alteration of the untreated, argon and air plasma-treated samples, and this finding is in correlation with the unchanged WCA.

It is also important to mention that the surface chemical composition of argon and air plasma-treated samples after each sterilization method is nearly identical, which is in agreement with the WCA results described in the previous paragraph.

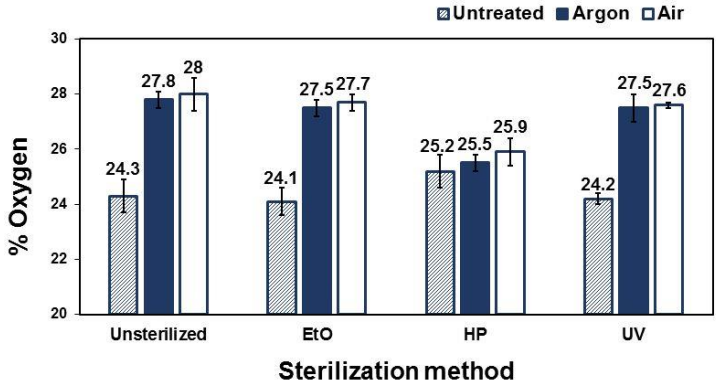

Fig. VII.9. *Surface oxygen content of untreated, air and argon plasma-treated PCL before and after EtO, HP and UV sterilizations.*

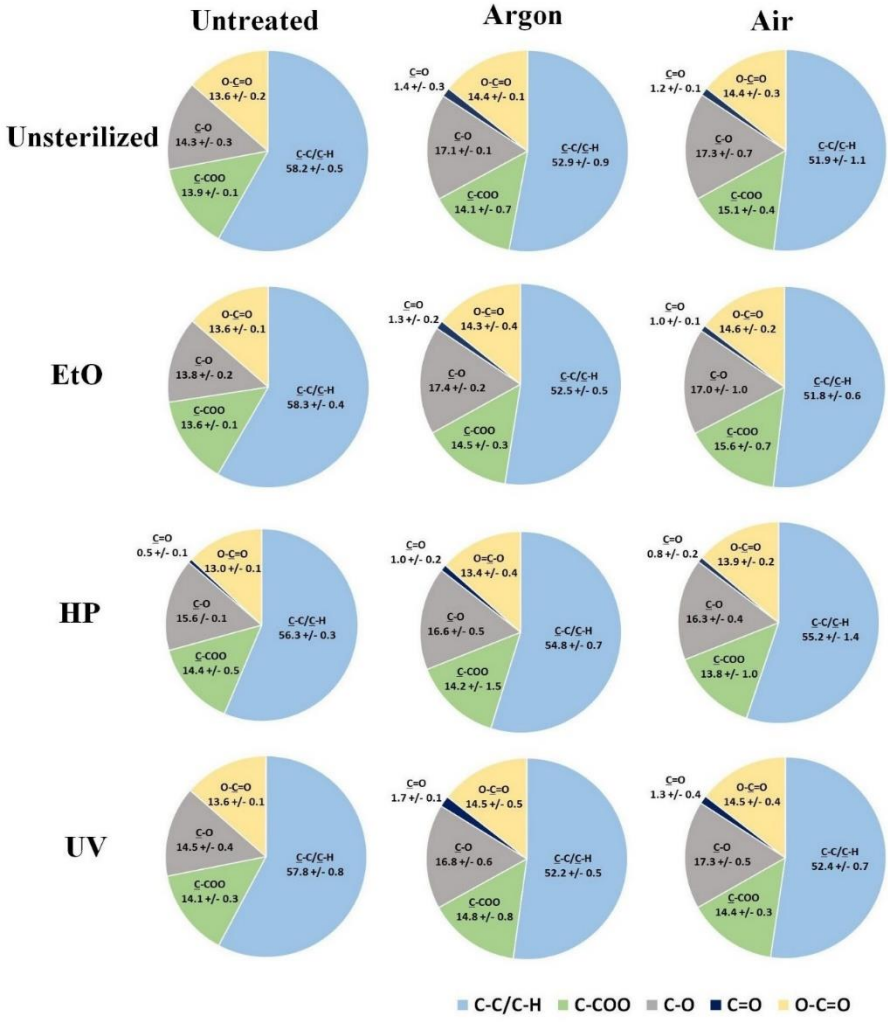

Fig. VII.10. *C1 curve fit results of untreated, air and argon plasma-treated PCL before and after EtO, HP and UV sterilizations.*

VII.3.2.3. AFM imaging

Surface physical properties of untreated, air and argon plasma-treated samples before and after the 3 sterilizations are examined via AFM imaging. Table VII.9 contains the obtained root-mean-square roughness values, while Fig. VII.11 shows the acquired AFM images. EtO sterilization does not alter the morphology of the untreated, argon and air plasma-treated samples. Moreover, no significant differences in roughness values are observed before and after the sterilization.

Therefore, EtO is shown to preserve the surface topography and structural integrity of the films.
HP sterilization is however causing drastic changes to the surface morphology of the PCL films as seen in Fig 12. Lerouge et al. also showed certain alterations in the surface appearance and topography of polymeric medical devices subjected to HP sterilization [383]. These surface modifications suggest a surface erosion by the highly reactive H_2O_2 molecules followed by a surface etching induced during the plasma phase. The roughness increases after HP sterilization and reaches average values of 31.7, 36.3 and 39.4 nm for the untreated, argon and air plasma-treated samples respectively. Higher roughness values are thus observed in the case of plasma-treated samples. This is probably due to additional chain scissions of the polar bonds generated during the previous plasma treatments, leading to the formation of more volatile compounds and thus to a greater surface etching. Moreover, plasma treatments are weakening PCL surfaces which as a result become more fragile and thus prone to supplementary alterations when subjected to HP sterilization. Particularly, air plasma-treated samples are extensively damaged after HP sterilization resulting in non-homogenous surfaces with roughness values ranging between 20 to 65 nm. This phenomenon can be explained by the fact that air plasma treatment, unlike the argon treatment, is operating in a filamentary mode giving cause to strong local microdischarges bombarding PCL surface non-homogenously and thus creating weak local spots.
An exposure to UV irradiation of 3h does not provoke morphological and topographical modifications to the PCL surfaces. No significant changes in surface roughness values of untreated, air and argon plasma-treated PCL samples are detected. Fischbach et al. also observed no changes in surface roughness of PLA films subjected to 2h of UV irradiation, however after extended exposure times a smoothening of the surface was noticed [345].

Table VII.9. *Root-mean-square roughness values (in nm) of untreated, air and argon plasma-treated samples before and after EtO, HP and UV sterilizations*

Treatment	Untreated	Argon	Air
Unsterilized	24.5 +/- 2.5	25.1 +/- 1.7	24.5 +/- 2.8
EtO	24.1 +/- 3.7	23.4 +/- 1.7	22.7 +/- 2.3
HP	31.7 +/- 2.1	36.3 +/- 1.8	39.4 +/- 14.1
UV	23.8 +/- 2.0	23.7 +/- 2.7	25.3 +/- 2.3

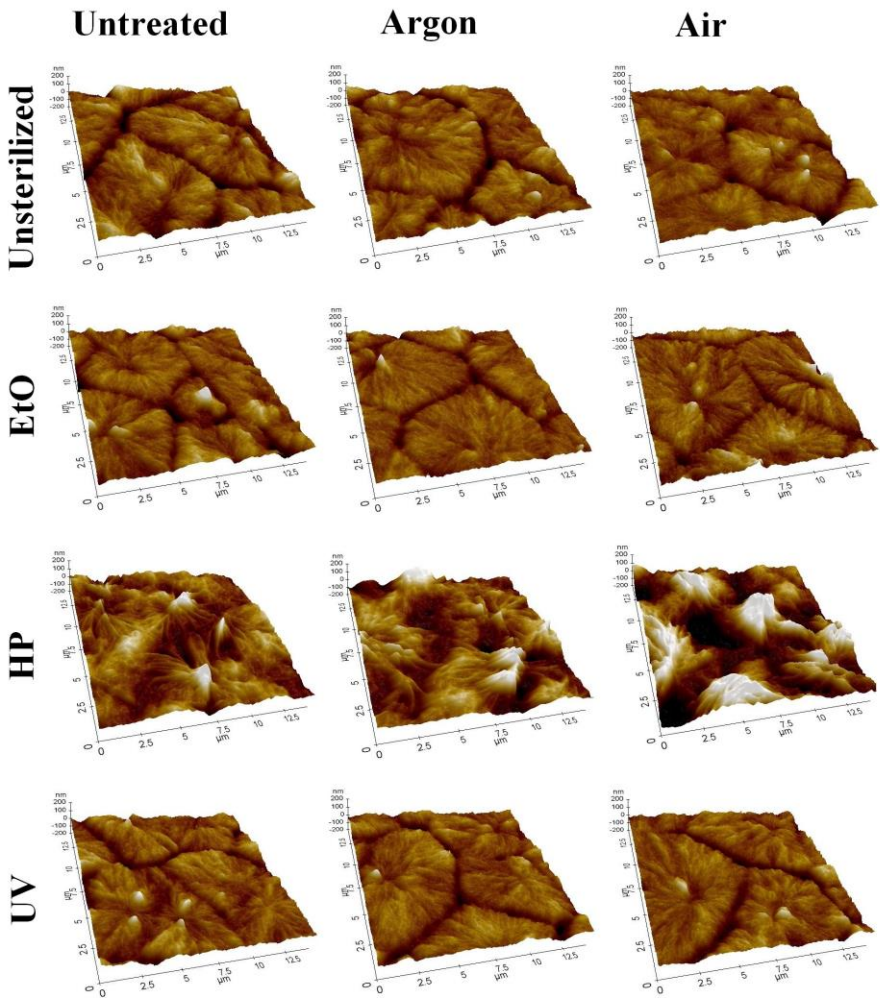

Fig. VII.11. *AFM images of untreated, air and argon plasma-treated PCL before and after EtO, HP and UV sterilizations.*

VII.3.2.4. Adhesion, proliferation and morphology of ADSCs

It is well known that cell-material interactions are largely influenced by the chemical and topographical features of the material surface. Thus, the ultimate goal of plasma treatment is the improvement of PCL surface properties to favor the cellular performance. In order to validate the effect of the plasma surface modification and evaluate the influence of the different sterilizations on the PCL bioactivity, cell culture tests

are performed using ADSCs. Both after 24 h and 7 days, the overall cell number is higher on plasma-treated samples as evaluated by MTT assay, regardless of the sterilization method (Fig. VII.12). These results are confirmed by the live/dead staining, showing a significantly greater cell attachment on plasma-treated samples compared to the untreated ones. Moreover, the ADSCs attached on plasma-treated surfaces exhibit an elongated morphology indicating a relative strong attachment and spreading, while the cells on the untreated surfaces are round which is a sign of poor attachment (Fig.VII.13 and14) [401]. This difference can be explained by the higher amount of oxygen-containing functionalities on the plasma-treated samples leading to an increased wettability promoting the protein adsorption and thus the initial cell attachment. Furthermore, oxygen-containing groups are correlated with an enhanced cellular growth, as reported in literature [114].

For the untreated samples, however, there are important differences between sterilization methods. There is a significantly higher attachment and proliferation of ADSCs after HP sterilization compared to EtO and UV sterilization, almost reaching the level of tissue culture plastic. The roughness of the untreated samples increases after HP sterilization, leading to a closer mimicking of the nanoarchitecture of natural ECM and thus favoring, together with the slightly increased wettability, the cell attachment and proliferation [402].

The effect of the sterilization methods is slightly different on plasma-treated samples. Attachment on both argon and air plasma-treated PCL films is higher after EtO and UV sterilization compared to HP sterilization. This can again be correlated to the wettability of the samples. HP sterilized samples have the highest WCA (68°) in this case compared to EtO and UV sterilized samples (WCA of 65° and 58° respectively). Furthermore, for air plasma treatment, there is a big variance in cell number between samples after HP sterilization. This is attributable to the non-homogeneity of the air plasma-treated films resulting in different cell adhesion patterns. Interestingly, despite the good initial attachment, the cell number on EtO sterilized samples falls below the level of tissue culture plastic after 7 days of proliferation for both plasma treatments. This can be due to the toxicity of the residual EtO causing the death of some cells during the lag-stage. The lag-stage is the period following the adhesion stage and corresponding to the adaptation of the cells to their environment. The cells that remain alive during this period, undergo the proliferation process [403]. HP and UV sterilized samples on the other hand clearly outperform tissue culture plastic in terms of proliferation. Especially for the argon plasma-treated samples sterilized by HP, the combination of a hydrophilic

surface and higher roughness seems to have beneficial effects on cell numbers. Ahn et al. also reported that the mutual effect of a hydrophilic and rough surface enhances the adhesion and proliferation of ADSCs [401]. These beneficial effects are less pronounced on air plasma-treated samples because of the non-homogenous surface, but are still present.

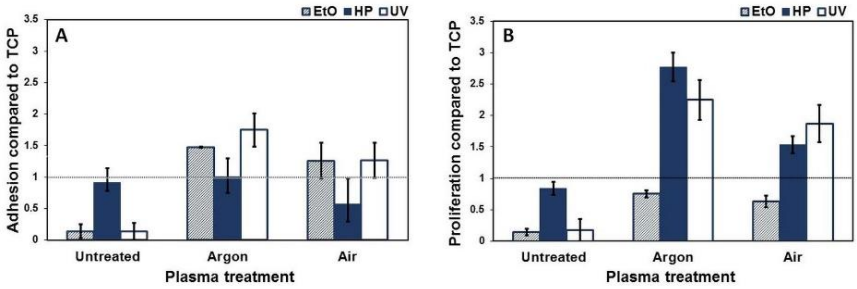

Fig. VII.12. *Ratio of cells attached to PCL films after (A) 24 h and (B) 7 days compared to tissue culture plastic (TCP). Error bars equal 95% confidence interval. The dotted line represents the TCP value.*

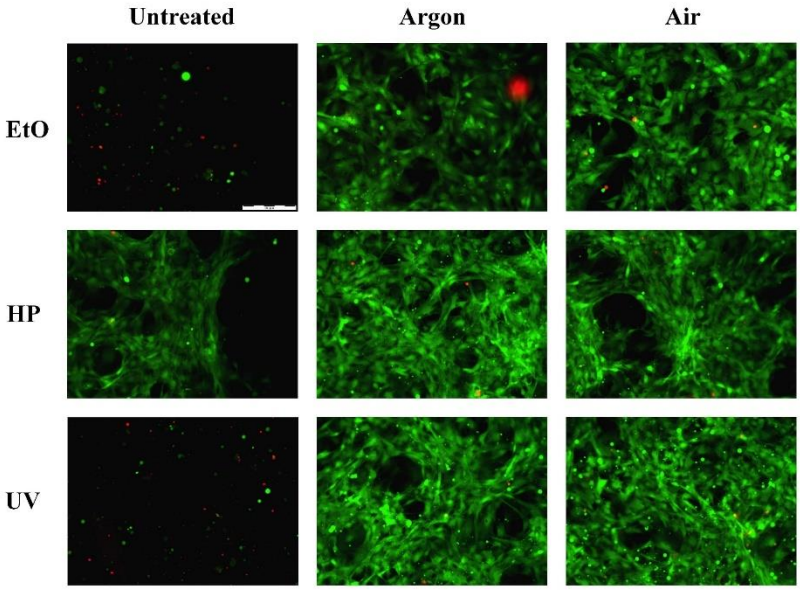

Fig. VII.13. *Live/dead staining of ADSCs on PCL films after 24 h. Scale bar = 200 μm (green: living cells; red: dead cells).*

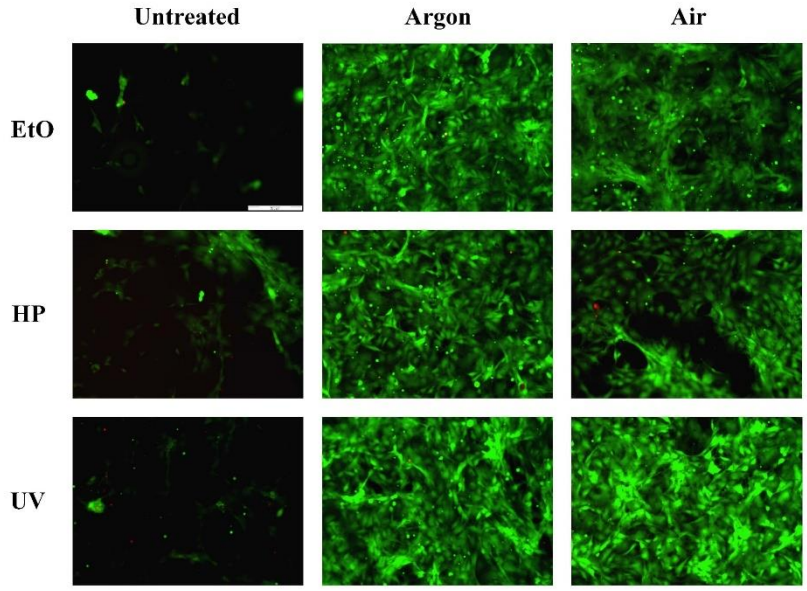

Fig. VII.14. *Live/dead staining of ADSCs on PCL films after 7 days. Scale bar = 200 µm (green: living cells; red: dead cells).*

VII.4. Conclusion

This chapter describes the physico-chemical surface changes and the bioreponsive properties of plasma-treated PCL films subjected to different sterilization methods. The results are divided into 2 parts: plasma surface modification of the PCL films on the one hand and sterilization of these plasma-modified samples on the other hand. For the surface modification, it can be concluded that air and argon plasmas are excellent treatments enhancing PCL wettability by incorporating oxygen-containing functionalities onto the surface. After storage in air, some of these induced groups tend to re-orientate from the surface into the bulk. This so-called ageing effect is more pronounced for the air plasma-treated samples compared to the argon plasma-treated samples, due to the higher cross-linking degree induced during the argon treatment. Therefore, in a trial to minimize the ageing effect, increasing the treatment time is shown beneficial for the air treated samples since it increases the cross-linking degree and thus limits the polymer chains movements. PCL surface morphology remains unchanged after plasma treatment. However, extended plasma

exposure times cause a surface etching leading to PCL degradation that is enhanced in the case of air plasma treatment. Besides the beneficial surface modification, the potential of plasma to sterilize PCL is studied by varying plasma exposure times in a range that ensures a good surface modification while avoiding PCL degradation. Although an increased percentage of sterility is observed with increasing plasma exposure time, PCL films remain incompletely sterile. Therefore, plasma-modified PCL films are subjected to UV, HP and EtO sterilizations. For the three sterilizations, an improved cell adhesion and a higher proliferation rate are observed on plasma-treated films compared to the untreated ones. An increase in WCA is observed after EtO sterilization, due to the modification of the PCL chain ends reacting with EtO molecules. These chemical modifications, together with EtO toxicity, lead to the lowest cell proliferation rate compared to the other sterilizations. HP sterilization provokes a decrease in WCA of the untreated samples attributable to a surface oxidation occurring during the exposure to the highly reactive H_2O_2 and during the plasma phase. However, an increase in WCA is detected for the plasma-treated samples, presumably due to the scission of some of the hydrophilic bonds generated during the previous air or argon plasma treatment. Moreover, HP sterilization increases the roughness and modifies the morphology of the films, in particular a drastic alteration was observed for the air plasma-treated samples. The increased roughness of the HP sterilized samples is shown to enhance the cellular proliferation, but the physical alterations might interfere with the structural integrity when it comes to 3D scaffolds. Overall, of the three sterilizations, UV is revealed the most effective for plasma-treated PCL films, since no physico-chemical surface alterations are noticed after an exposure of 3h and good cellular performances are detected. A subsequent study will examine whether UV sterilization will also be the most suitable for plasma-treated PCL nanofibers compared to HP and EtO.

Chapter VIII. Comparative Study of the Surface Properties and Cytocompatibility of Plasma-Treated PCL Nanofibers Subjected to Different Sterilization Methods

The results of Chapter VIII were published in the following international peer-reviewed journal:

Ghobeira, R., Philips, C., De Naeyer, V., Declercq, H., Cools, P., De Geyter, N., Cornelissen R. & Morent, R.
Comparative study of the surface properties and cytocompatibility of plasma-treated PCL nanofibers subjected to different sterilization methods
Journal of Biomedical Nanotechnology, 13(6): 699-716 (2017).

VIII.1. Introduction

After studying the effects of sterilization methods on plasma-treated PCL film, this chapter will further advance in complexity and transfer from 2D films to 3D electrospun fibers. In this way, an examination of different polymeric topographies will be completed to check if the delicate structure of nanofibers is more or equally prone to sterilization-induced damages compared to films. PCL nanofibers are therefore subjected to a plasma treatment using a DBD operating in air and argon at medium pressure. The influence of plasma exposure time is delicately analyzed since the fibrous nanostructure should not be compromised. Finally, the plasma-treated nanofibers are sterilized by UV, HP and EtO and surface properties are characterized by means of WCA goniometry, XPS and SEM. Live/dead staining and MTT assays are also performed to assess the interaction between ADSCs and the nanofibers.

VIII.2. Experimental conditions

All experimental details can be found in Chapter VI. The parameters that are specifically used in this chapter are summarized in table VIII.1.

Table VIII.1. *Experimental conditions*

Base material	• PCL
Biofabrication method	• Electrospinning: - Collector: cylinder (length = 28 cm, radius = 5 cm) - RS: 100 rpm - TCP: 20 cm - RH: 50 - 60%.
Plasma treatment	• Air DBD - Power= 1.45 W - Filamentary mode • Argon DBD: - Power= 1.47 W - Glow mode
Characterization techniques	• WCA: - 3 µl-drops of distilled water - Reported value: average of 6 values measured on 6 different samples. • XPS: - Reported value: average of 6 values measured on 2 different samples.

	• SEM: - Accelerating voltage: 10 kV. - Reported fiber diameter value: average calculated over 50 fibers
In vitro cell tests	• ADSC culture: - 50 000 cells/100 µl per sample for adhesion tests - 20 000 cells/100 µl per sample for proliferation tests • MTT assay: - Performed on 5 samples/condition.

The fiber diameter, represented as the average of 50 fiber diameters, is calculated for 3 different samples spun at different times at the considered temperature range (20-25 °C). The obtained values (153.7 +/- 23.9, 195.3 +/- 24.6 and 188.5 +/- 27.6 nm) are not statistically different when taking into account the standard deviations. For accurate subsequent comparison, the average of all the 150 obtained diameter values is calculated giving an average diameter of 184.5 +/- 33.5 nm. A nanometer scale is thus successfully reached with fibers uniformly distributed over the entire sample surface.

VIII.3. Results and Discussion

VIII.3.1. Plasma treatment

VIII.3.1.1. WCA measurements

In order to measure the degree of hydrophilicity and thus to evaluate the effect of plasma treatment on the surface wettability of the nanofibers, WCA measurements are performed before and after plasma treatment. The evolution of the WCA values as a function of plasma exposure time is depicted in Fig. VIII.1. The starting contact angle is approximately 139 ° revealing the highly hydrophobic characteristics of the untreated PCL nanofibers. When subjecting the nanofibers to a plasma treatment of 2 s, the WCA slightly decreases to around 132 ° and 133 ° for air and argon gas discharges respectively. This indicates the beginning of a surface chemical modification induced by the plasma treatment. When the plasma exposure time increases to 4 s, the water drop rapidly spreads out and penetrates into the nanofibrous mesh resulting in a large decrease in WCA reaching values of 31 ° and 34 ° for

air and argon plasma treatments respectively. This sudden decrease in WCA after plasma treatment of PCL nanofibers was also previously observed in a few studies [88, 114, 262, 276, 277]. The incorporation of polar groups on porous and high surface-to-volume ratio structures is responsible for the instantaneous penetration of water leading to the observed large and sudden increase in wettability [88, 262, 266, 278, 281, 285]. At exposure times above 6 s, only minor changes in WCA values are detected suggesting a saturation effect of the plasma modification process. Air plasma treatment achieves a lowest WCA value of 25 ° at a treatment time of 10 s while an almost similar effectiveness is noticed for the argon plasma treatment giving a lowest value of 26° for a treatment time of 6 s. However, it is worth noting that a comparison, on the basis of WCA analysis, between the 2 different discharge gases and between the different plasma exposure times is not very reliable when the differences are minor, given the highly porous and non-smooth structure of the nanofibers. When comparing the WCA measurements of PCL fibers with those previously performed on PCL films, it is found that for almost similar plasma parameters, the fibers (≈ 25°) display a significantly higher hydrophilicity than the films (≈ 55°) [404]. Moreover, a gradual decrease in WCA was observed for the PCL films which is not the case for fibers having a nanoscopic roughness significantly affecting the surface wettability. Therefore XPS analysis, a more precise and reliable surface chemical characterization technique for the nanofibers, is also performed in this work and the obtained results will be described in the following section.

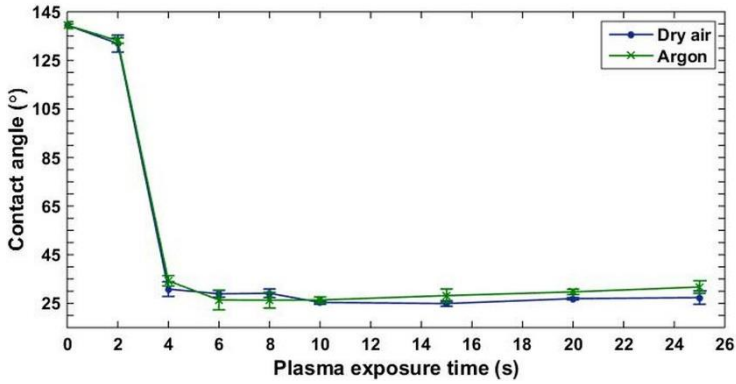

Fig. VIII.1. *Evolution of the WCA values as a function of air and argon plasma exposure time.*

VIII.3.1.2. XPS analysis

The elemental surface composition is assessed by performing XPS measurements on the nanofibers in order to more precisely elucidate the chemical modifications induced by the plasma treatment. An oxygen amount of almost 25 % is detected for the untreated PCL. This percentage gradually increases when subjecting the nanofibers to progressively ascending plasma exposure times, reaching a maximum of approximately 28 and 29% for air and argon discharges respectively. Hence the percentage of carbon decreases proportionally in both cases, since no nitrogen or other elements are incorporated during or after the treatment. Fig. VIII.2 shows the evolution of the oxygen percentage relative to the plasma exposure time. These findings confirm the suggestion stating that the incorporation of new oxygen-containing functionalities on the nanofibers is responsible for the detected enhancement of their surface wettability. Many studies performed in the past have also showed an oxygen incorporation in the form of hydroxyl, carbonyl and carboxyl groups on argon and air plasma-treated PCL [88, 278, 405, 406]. To be able to understand the obtained oxygen evolutions, it is important to clarify the influence of the discharge atmosphere on the active species bombarding the nanofibers. It is well known that 2 types of active species present in the plasma are involved: the non-reactive species break the C-C and C-H bonds and thus generate polymer radicals while the chemically reactive species such as O_2 and $O^{\cdot}$ add new atoms to the nanofibers surface. Argon plasma treatment, not containing oxygen species, normally triggers cross-linking and double bond creation on the polymer surface. The implantation of oxygen-containing functionalities in this study is thus due to a post-treatment oxidation or due to the presence of oxygen impurities in the plasma reactor. These impurities can originate from the residual air remaining in the reactor since it cannot be fully evacuated before the actual plasma treatment or can originate from gaseous products such as H_2O and O_2 that the plasma desorbs from the chamber walls [398, 406]. A saturation of the argon plasma treatment effect is perceived for a plasma exposure time of 15 s where a plateau retaining the maximal value of 29% of oxygen is reached. This suggests that prolonged argon plasma exposure does not elicit supplementary chemical modifications. When taking a closer look to the air plasma treatment, no saturation is however sensed. After the progressive increase in the amount of oxygen attaining a value of 28 % at a treatment time of 8 s, a sudden decrease followed by an irregular curve shape is then observed with big standard deviations. The reactive molecular oxygen species, in addition to atomic oxygen and oxygen radicals present in the air plasma incorporate oxygen-containing groups when reacting with the radicals on the surface of the nanofibers,

and can explain the higher incorporation of oxygen at short treatment times compared to the argon discharge where oxygen is only present as minorities. When exposed to prolonged treatment times in air, the nanofibers are disposed to numerous chain scissions occurring on their surface from where volatile compounds are desorbed and oligomers are formed. This phenomenon etches the surface leading to polymer degradation which explains the irregular curve shape and the big standard deviations observed at extended treatment times. No degradation of the PCL chemical structure is however induced by the argon plasma treatment since the etching effect is mainly reinforced in the presence of oxygen existing only as minorities in this case [398].

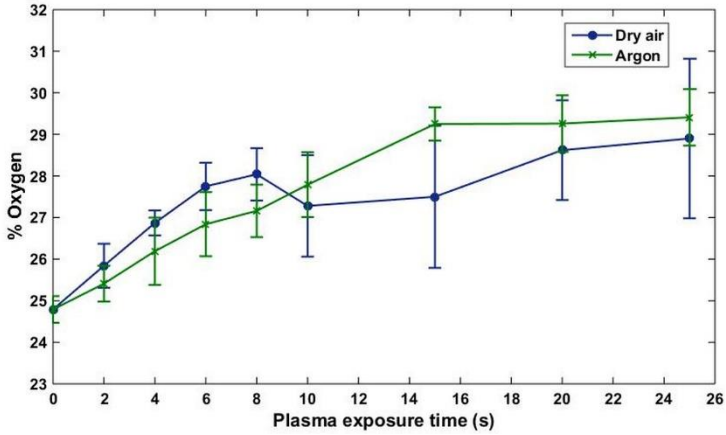

Fig.VIII.2. *Evolution of the surface oxygen content as a function of air and argon plasma exposure time.*

VIII.3.1.3. SEM imaging

SEM is a potent analysis tool to follow the morphology of PCL nanofibers subjected to different plasma exposure times. Fig. VIII.3 and VIII.4 provide a series of SEM images visualizing fibers exposed to a plasma treatment operating in argon and air respectively. In the case of argon plasma treatment, the nanofibers retain their morphology without any flattening or melting behavior for exposure times up to 15 s. At this treatment time, the dimension of the fibers is still preserved since only a statically insignificant increase in fiber diameter from 184.5 +/- 33.5 to 203.5 +/- 30.3 nm is detected. Mild morphological alterations are however observed when the plasma treatment time is increased to 20 and 25 s, such as melted joining points appearing all over the nanofibrous membrane. Nevertheless, the fiber diameter is preserved as

only insignificant decreases in diameters reaching values of 159.3 +/- 19.0 and 137.3 +/- 22.3 nm for exposure times of 20 and 25 s respectively are observed.

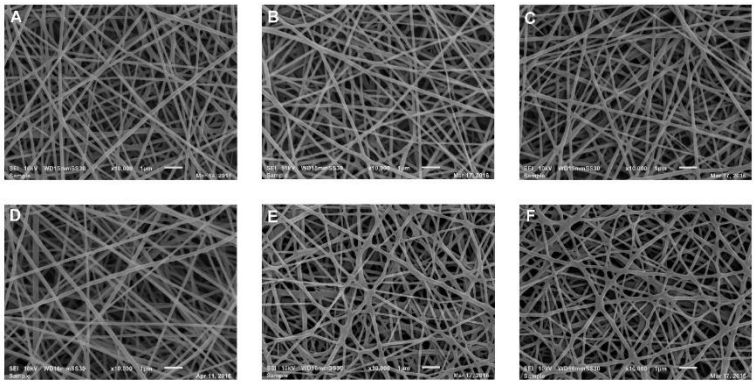

Fig. VIII.3. *SEM images of untreated (A) and argon plasma-treated PCL nanofibers at different plasma exposure times (B: 5 s, C: 10 s, D: 15 s, E: 20 s and F: 25 s).*

Concerning the air plasma treatment, a more drastic morphological deterioration of the fibers is observed starting at shorter plasma treatment times compared to the argon plasma exposure. Local damaged melted-like spots begin to be formed at a treatment time of only 8 s. In addition, the damage progressively worsens with increasing air plasma exposure time as can be seen by the enlargement and multiplication of the damaged spots, which gradually lose their nanofibrous structure. Therefore, air plasma treatment is shown to be only efficient at treatment times up to 6 s as no structural damages, in terms of fiber integrity, shape, uniformity and dimensions (average diameter = 194.8 +/- 31.5) are distinguished. At extended treatment times, the high energy bombardment of the plasma active species on the nanofibers can lead to a surface erosion (so-called etching effect) [272]. As already mentioned in the section above, etching is specifically enhanced in the presence of oxygen which can explain the early and aggressive damage observed on the air plasma-treated samples compared to the mild changes perceived on the argon plasma-treated ones. Moreover, the DBD sustained in air operates in a filamentary mode while the argon DBD operates in a glow mode. El Zeer et al. reported that the filamentary mode provokes a more pronounced etching and this was confirmed by a more prominent damage of wool fibers when subjected to a filamentary plasma treatment compared to a glow mode treatment. In the filamentary DBD, the fibers are exposed to a nonhomogeneous plasma consisting of local microdischarges strongly bombarding the PCL surface

causing local oxidation and etching. This can explain why the nanofibers are mostly locally damaged by the air plasma treatment. Plasma in the glow mode is uniformly generated all over the electrode surface which might become heated at extended plasma exposure times. Heating of the electrodes might cause a melting of the thermo-sensitive nanofibers as observed by the melted joining points. It is believed that the synchronic effect of heat and mild etching is the leading cause to the small morphological changes observed on the argon plasma-treated fibers at extended exposure times. Since the microdischarges in the filamentary mode are of short duration and only take up a small volume, the electrodes are believed to be only locally heated in case of air plasma treatment [407]. This can explain the absence of melted point-bonded junctions outside of the damaged spots on the air plasma-treated samples. Therefore, the strong etching in the filamentary air treatment combined with local heating is locally damaging the fibers leading to a polymer degradation that was also recognizable from the XPS measurements. These results are consistent with our previous results on PCL films showing an increased roughness and altered morphology of the PCL films treated with air plasma at extended treatment times, whereas no morphological alteration was observed for the argon-treated samples. As nanofibers have a more delicate structure than films, mild alterations are however detected in this work for the argon-treated nanofibers.

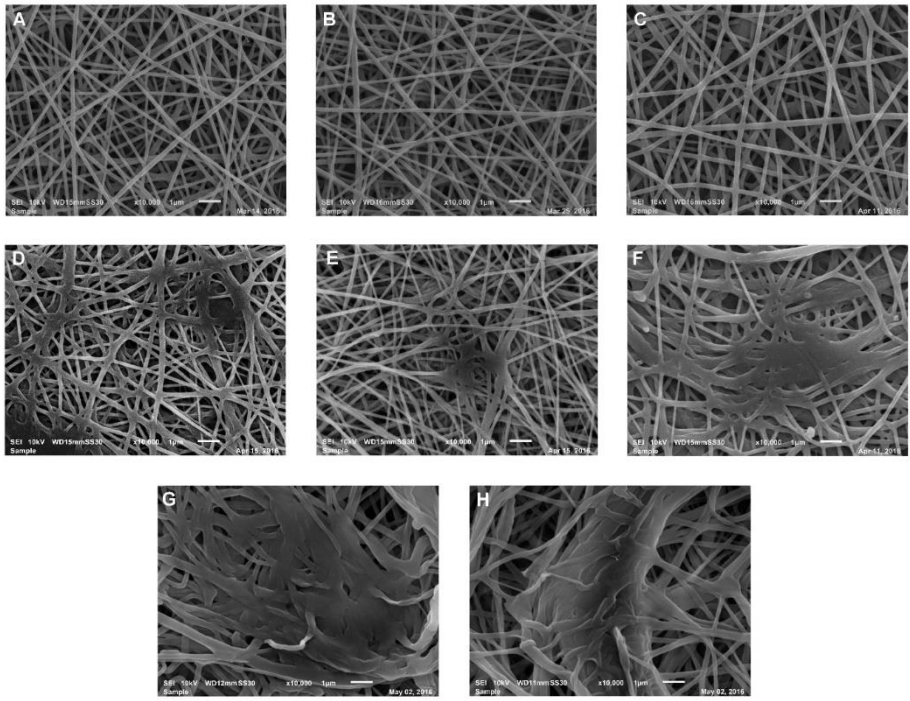

Fig. VIII.4. *SEM images of untreated (A) and air plasma-treated PCL nanofibers at different plasma exposure times (B: 5 s, C: 6 s, D: 8 s, E: 10 s, F: 15 s, G: 20 s, and H: 25 s.*

VIII.3.1.4. Ageing effect

Since it is crucial to preserve the structure of the nanofibers providing an ECM-like appearance while adding polar groups on their surface, argon and air plasma treatments of 15 s and 6 s are respectively considered for the subsequent sterilization experiments. In these experiments, all the cell tests, WCA, XPS and SEM measurements are performed 4 days after the plasma treatment. This period of time corresponds to the longest sterilization method which is EtO, and is adopted for all samples to ensure an adequate comparison between the 3 studied sterilization techniques. EtO sterilization is followed by an 48 h of aeration but an extra 48 h are implemented before performing the cell tests to minimize to the maximum the residual EtO molecules which are known to be highly toxic. It is well known that induced plasma treatment effects are not permanent over time since the treated surfaces undergo a hydrophobic recovery to the untreated state upon

storage in air. This phenomenon, also known as ageing effect, can be interpreted in terms of 2 reasons. First, the grafted chemical groups tend to re-orientate towards the bulk of the material to attain a more energetically favorable position. Secondly, post-plasma reactions between the treated surfaces and the atmospheric minorities such as CO_2 and H_2O might occur, leading to the neutralization of the implanted polar groups [266]. Therefore, it is also important to investigate this phenomenon in this study, in order to examine how the surface will vary within 4 days after the plasma treatment. For this purpose, PCL samples plasma-treated in air and argon at the determined optimal exposure times, are stored in ambient air at room temperature for 4 days. WCA and XPS measurements are then performed (Table VIII.2). For both treatments, an increase in WCA value of approximately 4 ° and a small decrease in oxygen content of approximately 1% are detected. After this mild ageing process, the WCA values are still considerably lower and the percentages of oxygen considerably higher than the corresponding values of the untreated sample. Previous results showed that the ageing is more pronounced for PCL films compared to PCL nanofibers. This is probably due to the fact that the fibrous network is less exposed to ambient air as each fiber is protected by neighboring fibers. Indeed, Dolci et al. did not even detect any surface modifications on plasma-treated PLA nanofibers after different storage times, thus demonstrating that no ageing effect is present, up to at least 5 days [266].

Table VIII.2. *WCA and oxygen content of PCL nanofibers immediately and 4 days after plasma treatment in air and argon*

	Dry air (6 s)		**Argon (15 s)**	
Ageing time (days)	0	4	0	4
Contact angle (°)	28.9 +/- 1.4	33.1 +/- 2.0	28.2 +/- 2.8	32.5 +/- 0.8
% Oxygen	27.7 +/- 0.6	26.5 +/- 0.6	29.2 +/- 0.4	28.4 +/- 0.4

VIII.3.2. Sterilization

VIII.3.2.1. Nanofibers sterility

The reported sterilizing effect of plasma alone in literature has first led us to an examination of the sterility of the plasma-treated nanofibers before subjecting them to any sterilization method [370, 408]. The

sterility test however shows clouding of the broth within 5 days following immersion of the samples, thus indicating the inability of the plasma treatment itself to serve as a sterilization method. Previous results also revealed the inefficiency of the plasma to sterilize PCL films even at very extended plasma treatment times. The air plasma-treated PCL films were degraded before attaining 100% sterility, as the etch resistance of the microorganisms is higher than the resistance of PCL. Argon plasma treatment, engendering a mild etching effect, did not damage the films but failed to also destroy all microorganisms [404]. Regardless, increasing the treatment time is not an option in the case of nanofibers, since their delicate structure will then be compromised as previously reported. Therefore, an extra sterilization process of the plasma-treated nanofibers becomes inevitable. Three sterilization methods are investigated in this work: EtO, HP and UV and the efficiency of each method is examined by performing the sterility test. This test shows that EtO and HP sterilization achieve a complete sterility of the nanofibers. In case of UV sterilization, irradiation times of 1 and 2 h are shown to be insufficient but complete sterility is however detected after an irradiation time of 3 h. As a result, a UV exposure of 3 h is adopted in the rest of this work.

VIII.3.2.2. SEM analysis

In addition to its effectiveness, the sterilization should also preserve the structural integrity of the PCL nanosized fibrillar arrangement as well as the functional integrity that is partly affected by the structural integrity but also by the surface chemical composition. Therefore, at a first glance, the morphology of the sterilized fibers is analyzed via SEM measurements before going deeper into the study of the surface chemical properties. Fig. VIII.5 shows SEM images of untreated and plasma-treated nanofibers after subjecting them to EtO, HP and UV sterilizations, while table VIII.3 contains the corresponding fiber diameters.

EtO sterilization modifies neither the appearance nor the diameter of the untreated nanofibers. However, when it comes to the plasma-treated samples, EtO transforms the fiber cylindrical morphology to a ribbon-like appearance associated with an increase in fiber diameter, showing that fibers have collapsed on top of each other. The same ribbon-like morphology has also been observed after EtO sterilization of PLA and polyethylene terephthalate (PET) nanofibers [344, 409]. This finding suggests that the functional groups grafted on the plasma-treated fibers are involved in this morphological change. Indeed, the instability of the EtO molecule provokes an easy opening of its three-membered ring allowing it to react with hydroxyl and carboxyl end

chains present on plasma-treated surfaces [363, 409]. Pillip et al. have subjected in the past different polymers belonging to the polyethylene glycol (PEG) family and having different types of structure to EtO sterilization. The results showed that the polymers containing groups susceptible to interact with EtO such as COOH groups undergo significant morphological changes. These structural modifications are attributed to the combined effect of EtO reacting with functional surface groups on the surface and the relatively high humidity and low temperature and pressure in the EtO chamber, softening the polymers. To confirm that EtO is really implicated in these alterations, Phillip et al. also placed the fibers under severe chamber conditions without the presence of EtO and did not found any structural changes [364]. This conclusion can also explain the observed unchanged morphology of the untreated nanofibers, probably not containing OH or COOH end chains, thus not reacting with EtO molecules. Moreover, the damage on the argon plasma-treated samples is more pronounced than the damage on the air plasma-treated samples which can be attributed to the fact that more oxygen is incorporated after the (longer) argon plasma treatment, meaning that more polymer end chains predisposed to react with EtO are present on the argon treated nanofibers. In addition to the significant increase in average fiber diameters of air and argon plasma-treated nanofibers after their sterilization, bigger standard deviations are also obtained highlighting the big differences in the level of damage between the fibers. Our previous results on PCL films showed no morphological alterations after EtO sterilization even for the plasma-treated samples. Thus, in addition to the chemical composition of the samples, the architecture is also a primordial condition influencing the structural integrity, which is in agreement with previous results where it was also shown that PEG films containing COOH groups are not damaged after EtO sterilization while PEG fragile fibers are damaged [364].

Arriving to the HP sterilization, drastic structural alterations are detected as the fibrillary arrangement is completely lost and a film formation is. Moreover, HP sterilization induces a color change of the samples from white to transparent. This dramatic change is presumably due to the thermo-oxidative degradation of PCL since HP sterilization is performed at temperatures that might exceed 55 ℃ and in the presence of H_2O_2 known as an aggressive oxidizer. Literature agrees that thermal degradation of polymers is accelerated in the presence of oxidants: in inert atmospheres, polymers tend to degrade at higher temperatures than in the presence of oxidants [410]. On the other side, possible chemical reactions between a polymer and a strong chemical agent might be slow or even might not take place at ambient temperatures, whereas at elevated temperatures these reactions are

accelerated with the emergence of new reactions. Therefore, the conditions of the HP sterilization are favorable for thermal oxidation which involves polymer chain scissions liberating molecular segments from entanglements thus causing conformational changes. The molecular segments rearrange by adopting lower energies to attain an equilibrium state thus changing the material irreversibly. The modifications in the material appearance can be more or less prominent such as color change, total structural loss, surface cracking, contraction or flaking [411, 412]. In the case of the untreated samples, the HP sterilization forms a film from where some fibers slightly protuberating can barely be visualized. The damage of the plasma-treated samples is even more pronounced as no fibers at all can be identified in addition to the presence of holes over the complete film surface. The incorporation of functional groups on the plasma-treated PCL surface is the reason for this extensive damage because it was shown that branching can markedly increase the proneness of a polymer chain to undergo a thermo-oxidative degradation. This is due to the high reactivity of the tertiary carbons involving numerous chain initiation reactions at the branch points of the polymer which, if untreated, would be probably subjected to one end-chain initiation [410]. Alterations in surface roughness and morphology were also observed on PCL films after HP sterilization, with a more prominent change on the ones previously plasma-treated. Moreover, Lerouge et al. also detected a color change and the occurrence of micro-cracks on polymeric devices sterilized by HP [385].

Finally, the last sterilization technique, UV sterilization does not provoke any morphological alterations on the untreated nor on the plasma-treated fibers and also the fiber diameters are retained. This unchanged morphological appearance and dimension was also detected after UV sterilization of PLA, PLGA and PET nanofibers [195, 344, 409] as well as on PCL films [404].

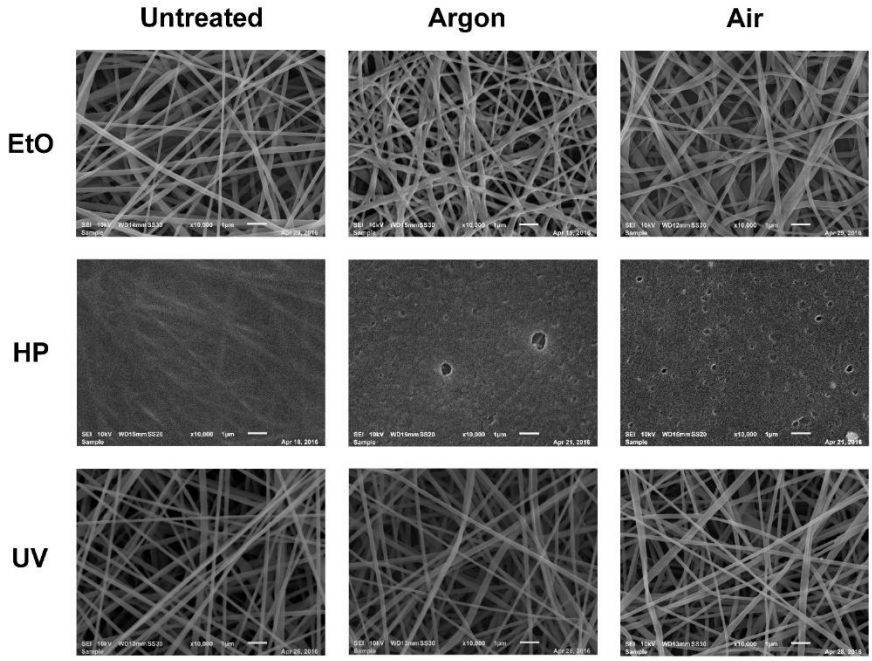

Fig. VIII.5. SEM images of untreated, argon and air plasma-treated PCL nanofibers subjected to EtO, HP and UV sterilizations.

Table VIII.3. Average fiber diameter (nm) of untreated, argon and air plasma-treated PCL nanofibers before and after EtO, HP and UV sterilizations.

	Untreated	Argon	Air
Unsterilized	184.5 +/- 33.5	203.4 +/- 30.2	194.8 +/- 31.4
EtO	203.1 +/- 33.6	320.8 +/- 104.7	291.0 +/- 107.3
HP	*	*	*
UV	198.6 +/- 35.3	200.1 +/- 38.3	193.7 +/- 38.7

*No fibers

VIII.3.2.3.WCA measurements

After checking how the different sterilizations affect the structural integrity of the nanofibers, their chemical surface properties are investigated by first studying their wettability. Fig. VIII.6 shows the WCA values of untreated, argon and air plasma-treated samples before and after subjecting them to each of the 3 studied sterilization methods.

EtO sterilization does not change the WCA of the untreated samples. However, an increase from 32° to 50° and from 33° to 43° is observed for the argon and air plasma-treated samples respectively. Our previous results on PCL films also showed an increase in WCA value after EtO sterilization [404]. The change towards a greater WCA is probably due to a chemical surface modification caused by reactions between EtO molecules and plasma-treated PCL chain ends. Indeed, the carbon-carbon bond of the EtO molecule is strained and short allowing an easy opening of the molecule ring, thus rendering it able to react with hydroxyl and carboxyl groups present on the plasma-treated samples, giving rise to the following chemical reactions:

$$CH_2CH_2O + R\text{-}COOH \longrightarrow R\text{-}COO\text{-}CH_2CH_2OH \quad (1)$$

$$CH_2CH_2O + R\text{-}OH \longrightarrow R\text{-}O\text{-}CH_2CH_2OH \quad (2)$$

The chemical structure obtained from the first reaction is exposing a hydroxyl group in its termination entity which is sheltering the carboxyl group. This phenomenon is involved in the shift to a more hydrophobic state, knowing that the hydroxyl group is less hydrophilic than the shielded carboxyl group. The second reaction leads to the creation of a chemical structure in which the hydroxyl group is sheltered by the same group, therefore it is not implicated in the wettability change [363]. Moreover, the morphological changes of the nanofibers after EtO sterilization might also have a small influence on the surface wettability. The increase in fiber diameter , lowering the surface-to-volume ratio as well as the surface roughness degree is known to have an impact on the liquid-solid interface thus changing the WCA [413].

Huge differences in WCA values are detected before and after subjecting the samples to HP sterilization. A decrease from 140 ° to approximately 75 ° is observed for the untreated samples, however an increase from 32/33 ° to 60 ° is perceived for the plasma-treated samples. This is due to the drastic damage destroying the nanofibrous structure leading to a film formation. For a hydrophobic material, an electrospun mat displays an enhanced hydrophobicity compared to a film, because of the high fibers surface-to-volume ratio in addition to the air

entrapment in the inter-spaces of the highly porous nanofibrous structure [413], which can explain the higher WCA value observed on the unsterilized untreated sample. However, for a hydrophilic material, the nanofibers exhibit an enhanced wettability as already mentioned, because in this case the porous structure favors the rapid penetration of water inside the material [266]. This conclusion can explain the lower WCA values obtained on the plasma-treated nanofibers before sterilization. After HP sterilization, the plasma-treated samples remain more hydrophilic than the untreated samples. The products of the reactions happening during the chemical phase and the plasma phase of the HP sterilization probably contain more hydrophilic groups in the case of the plasma-treated nanofibers because of their initial higher oxygen content compared to the untreated samples. Moreover, the micro-pores found on the plasma-treated samples after HP exposure might also lower the WCA.

Lastly, when looking at the WCA values before and after UV sterilization, no remarkable differences can be noticed for the untreated as well as for the plasma-treated samples. Dai et al. also found unchanged WCA values of PCL nanofibers before and after UV sterilization [360]. Since no morphological changes are detected as well, the unchanged WCA suggests that an exposure to UV irradiation of 3 h does not cause an alteration to the chemical surface composition which will be confirmed in the subsequent section on XPS measurements.

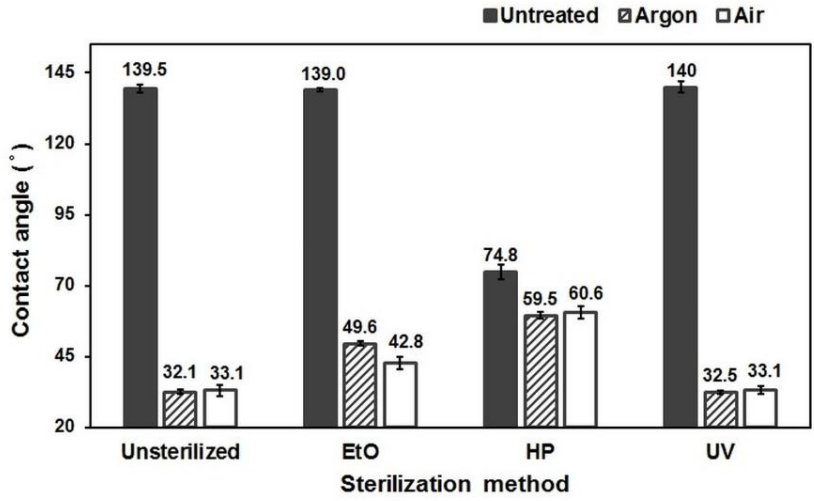

Fig. VIII.6. *WCA values of untreated, argon and air plasma-treated PCL nanofibers before and after EtO, HP and UV sterilizations.*

VIII.3.2.4. XPS analysis

The surface chemical composition is assessed by performing XPS measurements after subjecting the untreated and the plasma-treated samples to one of the three sterilization methods. Fig. VIII.7. displays the correspondent contents of oxygen obtained from the survey spectra. After EtO sterilization, an unchanged atomic composition is detected for the untreated samples. This finding is in correlation with the unchanged WCA value and unchanged morphology. Concerning the plasma-treated samples, the chemical reactions occurring between EtO molecules and PCL end chains should cause a slight decrease in the percentage of oxygen and hence an increase in the carbon content. However, this change in atomic composition is not so clearly seen in the XPS results compared to the remarkable WCA and morphology alterations. This is probably due to the low penetrability of EtO mainly reacting with the surface top layers, taking into account the difference in analysis depth between XPS and WCA: WCA measurements are influenced by the top surface while XPS has a larger penetration depth of approximately10 nm.

After HP sterilization, the surface chemical composition remains more or less the same for the untreated and air plasma-treated samples. Complex thermo-oxidative reactions involving chain scissions, cross-linking and molecular segment movements are probably taking place in the HP chamber predominantly during the chemical phase corresponding to the exposure to H_2O_2. These reactions can in some cases rearrange the molecular segments present on the polymer surface without any change in the atomic composition or the molecular size [412]. The second phase of the HP sterilization process involves a plasma exposure essentially serving as a detoxification step by breaking down the residual H_2O_2 in the chamber. The active plasma species known for their potential to modify the surface chemistry, react with the material of bags wrapping the samples and only a limited number can actually reach the PCL surface [383]. This can explain why the percentage of oxygen on the untreated and air plasma-treated nanofiber surfaces is not increased after HP sterilization. In the case of argon plasma-treated samples, the percentage of oxygen however decreases from 28.4 to 26.5%. It is known that argon plasma treatment oxidizes polymer surfaces with a high cross-linking degree. However, at relatively long plasma exposure times, a relaxation of the polymer chains occurs, lowering the cross-linking degree of the incorporated oxygen-containing groups thus weakening their chemical bonds. Our research group previously confirmed this mechanism, by obtaining a more pronounced ageing effect when subjecting PCL films to an argon plasma treatment of 10 s compared to a treatment time of 3 s [404].

Therefore, after an argon plasma treatment of 15 s, the incorporated oxygen groups probably undergo a relatively easier scission when subjected to a HP sterilization, which can explain the slight decrease in the oxygen percentage.
The slightly higher percentage of oxygen observed in the plasma-treated samples compared to the untreated ones is due to the fact that initially, before sterilization, the plasma-treated fibers already contain more incorporated oxygen.
Analogous to the WCA values, no remarkable difference in surface oxygen content of the untreated and plasma-treated nanofibers is detected before and after UV sterilization. Thus, UV sterilization does not provoke alterations in the surface chemical composition in this work despite the fact that some studies reported that UV irradiations having wavelengths around 250 nm can damage ester bonds [359]. The damage seems to depend on the material used as well as on the UV treatment time, which is shown to be a crucial factor influencing the surface chemical properties. For instance, Fischbach et al. demonstrated that 2 hours of UV exposure does not alter the chemical composition of poly(D,L-lactic acid)-poly(ethylene glycol)-monomethyl ether copolymer films, but extended UV irradiation of 5-24 h causes drastic chemical changes to the topography and the chemical composition [345]. In contrast, Dong et al. have reported that a very short UV exposure of 1 h can already exert drastic chemical alterations to PLGA and polylactide-co-ε-caprolactone nanofiber scaffolds [359]. In this work, it is however shown that a UV exposure of 3 h is very beneficial for the sterilization of PCL nanofibers since no chemical nor morphological alterations are observed. This conclusion has also been made in our previous paper focusing on plasma-treated PCL films [404].

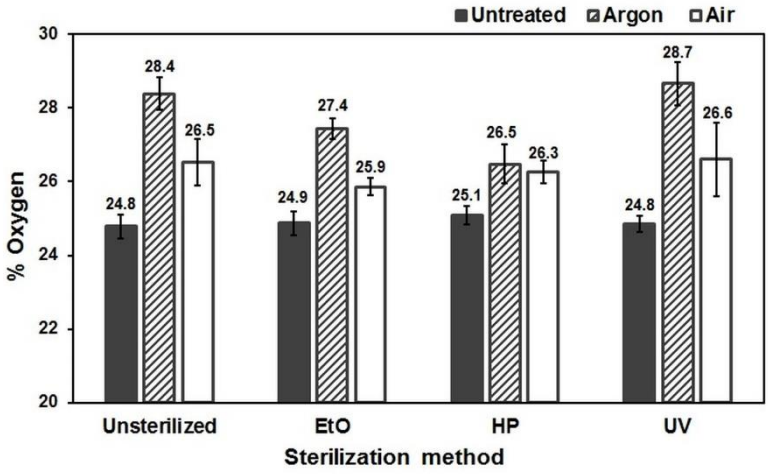

Fig. VIII.7. Surface oxygen content of untreated, argon and air plasma-treated PCL nanofibers before and after EtO, HP and UV sterilizations.

VIII.3.2.5. Cell tests

The ultimate goal of this study is to favor adequate cell-material interactions by providing convenient topographical and biochemical features and preserving them after sterilization. Therefore, the optimal material features, affected by the plasma treatment and the subsequent sterilization, are in this section validated by performing MTT assays and live/dead staining in line with imaging techniques in order to assess and visualize the cellular adhesion and proliferation.

- Adhesion of ADSCs

Fig. VIII.8 depicts the amount of viable ADSCs adhering to the untreated and plasma-treated samples sterilized by EtO, HP or UV, as revealed by the MTT assay. ADSCs cultured on tissue culture plate (TCP) serve as a positive control.

In the case of samples sterilized with EtO and UV, there is no significant difference between the number of viable cells attached to the untreated and to the plasma-treated nanofibers after 3 h of incubation. However, plasma activation leads to a slight increase in the amount of cells adherent on HP sterilized samples. Although plasma treatment does not exhibit significant or large differences in the cell number, great differences in cell morphology can be detected when visualizing the samples with fluorescent microscopy after live/dead staining and with SEM for more evident distinctions (Fig. VIII.9 and VIII.10). The cells

on the untreated nanofibers sterilized with EtO appear isolated and rounded with few having a star-like small bodies, suggestive of a poor cell affinity and attachment to the substrate. An almost similar cell appearance is observed on the untreated samples sterilized with UV, with slightly more star-like small cells. Some spindle-shaped cells are observed on the untreated HP sterilized samples, but the majority of the cells are rounded and clustered together. Regardless of the sterilization technique, the cells on the plasma-treated samples are however elongated and well spread with a significantly larger cell area indicative of a robust attachment [281, 401]. This enhanced adhesion might be attributed to the presence of more oxygen-containing groups on the plasma-treated samples, as many studies have reported their beneficial effect on cellular attachment [88, 114, 262]. The mechanism underlying the adhesion involves the binding of many receptors present on the cell surface to specific sites on the sample where proteins are adsorbed. Integrins constitute the most important class of receptors mediating the 2 adhesive phases: the arrest and the focal adhesion. Integrin clustering triggers the arrest phase. In the second phase, the receptors bind to the sample at focal adhesion sites, causing a change in their cytoplasmic domains associated with a modification of the cytoskeletal filament arrangement. In case of the untreated hydrophobic samples, the surface lacks bioactive sites suitable for the adsorption of proteins that bind to the receptors which results in a rounded cell morphology. As the focal adhesion occurs at rare binding sites, some of the cells appear to be slightly stretched. Plasma treatment promotes the hydrophilicity of the samples by incorporating oxygen-containing groups that can probably serve as binding sites for the cell receptors. Therefore, the adhesion occurs at numerous focal adhesive sites leading to a change in cell morphology from 3D-rounded cells to a 2D-planar and elongated cells [281]. Prabhakaran et al. reported an enhanced adhesion of SCs on air plasma-treated PCL nanofibers not only compared to untreated PCL, but also to PCL/collagen nanofibrous scaffolds, highlighting the importance of oxygen-containing groups in the cellular attachment [414]. For the HP sterilized samples, plasma treatment exhibits a better adhesion because of the synergistic influence of the slightly increased number of oxygen-containing groups along with the presence of holes increasing the roughness of the plasma-treated samples compared to the untreated ones [401].

In order to study the influence of the sterilization on the cellular performance, a comparison between the 3 methods is done, first for the untreated then for the plasma-treated samples. In case of the untreated samples, EtO sterilization seems to have a negative effect on cellular adhesion in terms of cell number and morphology. This is probably due

to the EtO toxicity, negatively affecting the cytocompatibility and causing the death of some cells as detected by the red staining in the fluorescent micrographs [343]. HP sterilization provokes an almost complete loss of the nanoscaled fibrous structure leading to a smaller surface area. A decreased surface area was previously shown to worsen the adhesion by reducing the interaction between integrins and the surface [272]. However, almost the same amount of cells adhering to PCL is detected after HP and UV sterilization. This is probably due to the super hydrophobic nature of the UV sterilized fibers hindering protein adsorption and therefore focal adhesion [344]. Therefore, the increased surface area of UV sterilized samples and the increased hydrophilicity of the HP sterilized samples help the cells to adhere with an amount reaching the amount of cells adhering to the TCP.

For the plasma-treated samples, EtO sterilization shows again the lowest cell adhesion, probably attributed to the EtO toxicity in addition to the changed fiber morphology and diameter. The adhesion on HP sterilized samples outperforms the adhesion on TCP as well as on UV sterilized samples despite the unchanged nanofibrous structure after UV sterilization. This is probably due to the difference in WCA between the HP ($\approx 60^\circ$) and the UV ($\approx 32^\circ$) sterilized samples. It is well known that surface hydrophilicity enhances protein adsorption and therefore the cellular adhesion, however super-hydrophilicity seems to have a limiting effect. Increasing the surface hydrophilicity increases the electrostatic force between water molecules and the surface making the displacement of adsorbed water more and more difficult thus reducing protein adsorption [272]. Indeed, Lee et al. showed that the best adhesion of different cell types (fibroblast, ovary and endothelial cells) was observed on surfaces having a WCA of 55° [261]. Moreover, another study investigating the adhesion of osteoblasts on surfaces having a WCA gradient between 12° and 98° revealed an optimal adhesion for a WCA of 64° [415]. ADSCs seem to adhere better on surface with moderate wettability (60°) as well.

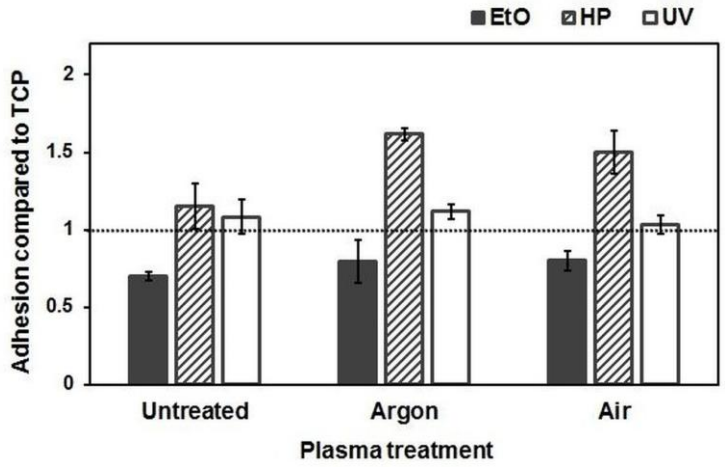

Fig VIII.8. *Ratio of viable ADSCs cultured for 3 h on untreated and plasma-treated nanofibers sterilized by EtO, HP and UV, relative to the TCP value (dotted line).*

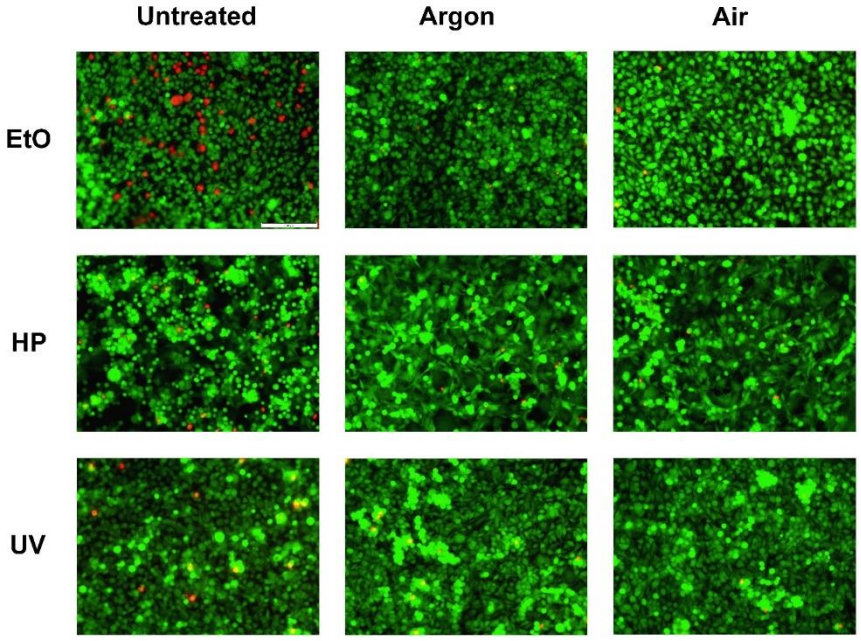

Fig. VIII.9. *Fluorescent micrographs after live/dead staining of ADSCs cultured for 3 h on untreated and plasma-treated nanofibers sterilized by EtO, HP and UV (Scale bar = 200 μm).*

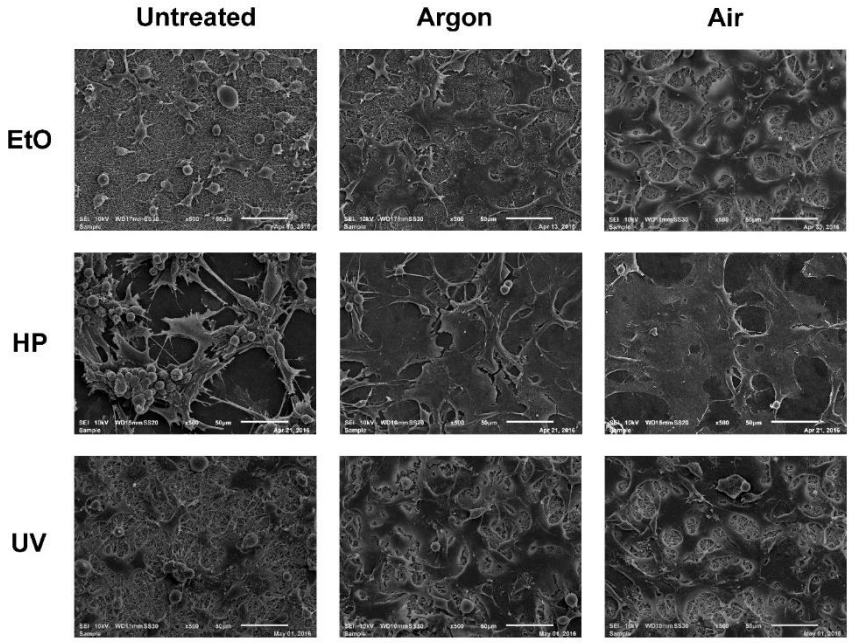

Fig. VIII.10. *SEM images of ADSCs cultured for 3 h on untreated and plasma-treated nanofibers sterilized by EtO, HP and UV (Magnification: 500 x).*

- **Proliferation of ADSCs**

After studying the adhesion of ADSCs, their proliferation is also investigated for culturing periods of 1, 3 and 7 days. Fig. VIII.11 represents the MTT results showing the rate of viable cells proliferating on the untreated and the plasma-treated samples sterilized with EtO, HP and UV. The plasma treatment clearly exhibits a positive effect on the cellular density in case of EtO and UV sterilization and this positive effect is still noticeable even one week after cell culturing on EtO and mainly on UV sterilized samples. However, no significant differences are observed between the untreated and the plasma-treated samples sterilized by HP. This finding suggests that cellular proliferation is not only influenced by surface chemistry but also by surface topography. Some authors showed the efficiency of oxygen and argon plasma treatments in improving adhesion and proliferation of different cell types on PCL nanofibers [88, 114, 272, 278, 405]. Oxygen-containing functionalities are proven to enhance the growth and proliferation of cells in addition to their important role in favoring cellular adhesion [262, 414]. Moreover, an initial good cellular adhesion triggers several signaling pathways in the cell leading to a

superior metabolic activity subsequently improving cellular growth and proliferation [405]. This mechanism takes place if the cells manage to adapt to their environment during the lag-stage following the adhesion stage [278]. The extensive morphological alteration after HP sterilization is postulated to have a negative effect on the adaptation of the cells and their subsequent proliferation because of the total loss of the ECM-like structure of the untreated as well as plasma-treated samples. Moreover, many studies have stated an enhanced proliferation on nanoscaled structures [88, 272]. A decrease in the cellular viability is mainly observed after 7 days as some of the cells that finally manage to proliferate, fail to find enough substrate because of the reduced surface area after HP sterilization. Despite the maintained nano-architecture after EtO sterilization, the cellular proliferation rate is decreasing over the days reaching values lower than the TCP even for the plasma-treated samples. This is again attributed to the toxicity of the residual EtO causing a progressive death of the cells. Moreover, the increased diameter and changed morphology of the plasma-treated nanofibers might result in a less suitable substrate for cellular growth and proliferation than unaltered nanofibers. Interestingly, excellent cellular proliferation is observed on the plasma-treated nanofibers sterilized by UV, as the rate of viable cells increases over the days to reach almost the double of the rate on TCP at day 7. Therefore, in addition to the plasma treatment effects, ADSCs proliferation is also deeply affected by the different sterilization methods which can extremely change the culturing conditions. Complementary results regarding the cellular morphology and viability at day 7 are also provided in this work by evaluating the fluorescent micrographs taken after live/dead staining and the SEM images (Fig. VIII.12 and VIII.13). In case of EtO and UV sterilizations, significant differences in the cellular density and morphology are observed between the untreated and the plasma-treated samples. The combined effect of the super-hydrophobicity of untreated nanofibers and the EtO toxicity leads to a decreased cell number and a rounded cell morphology. However, as UV sterilization does not leave toxic residues killing the cells, more cells are observed but as the hydrophobic surface does not provide an appropriate substrate, they tend to assemble together forming few clusters of cells. Elongated and well-spread cells are however observed on the plasma-treated surfaces after UV and EtO sterilization with an almost full coverage on the UV sterilized nanofibers that maintained their morphology and hydrophilicity. No obvious differences are detected on the untreated and plasma-treated samples sterilized by HP, as also found in the MTT results. After 7 days, the survived cells manage to spread on these surfaces having moderate hydrophilicity.

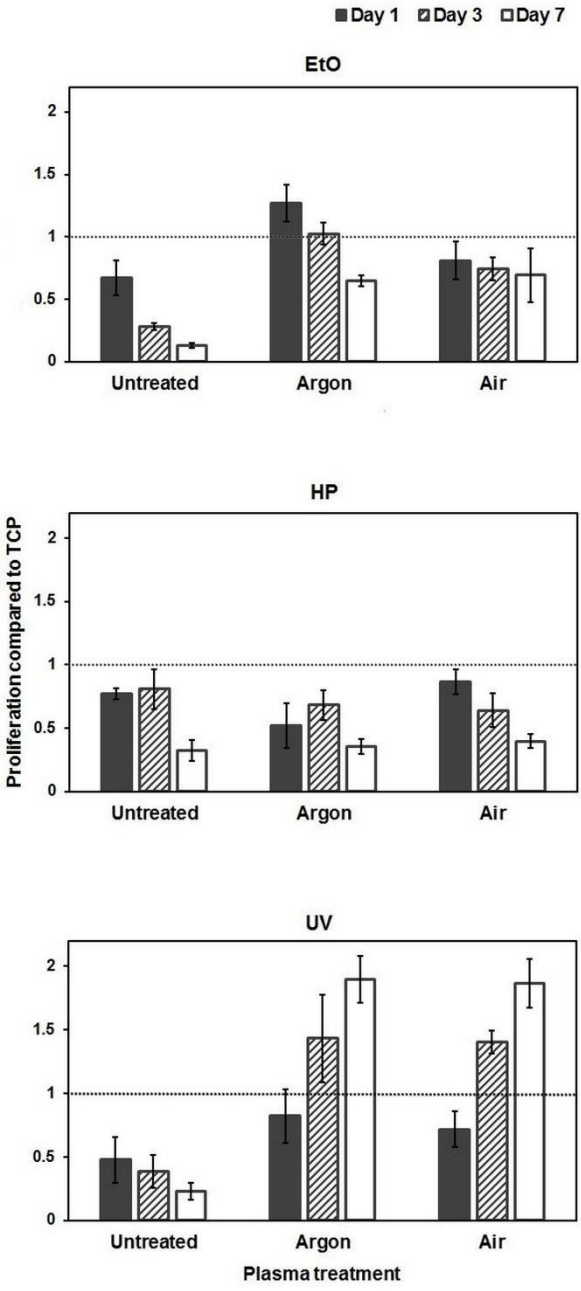

Fig. VIII.11. *Ratio of viable ADSCs cultured for 1, 3 and 7 days on untreated and plasma-treated nanofibers sterilized by EtO, HP and UV, relative to the TCP value (dotted line).*

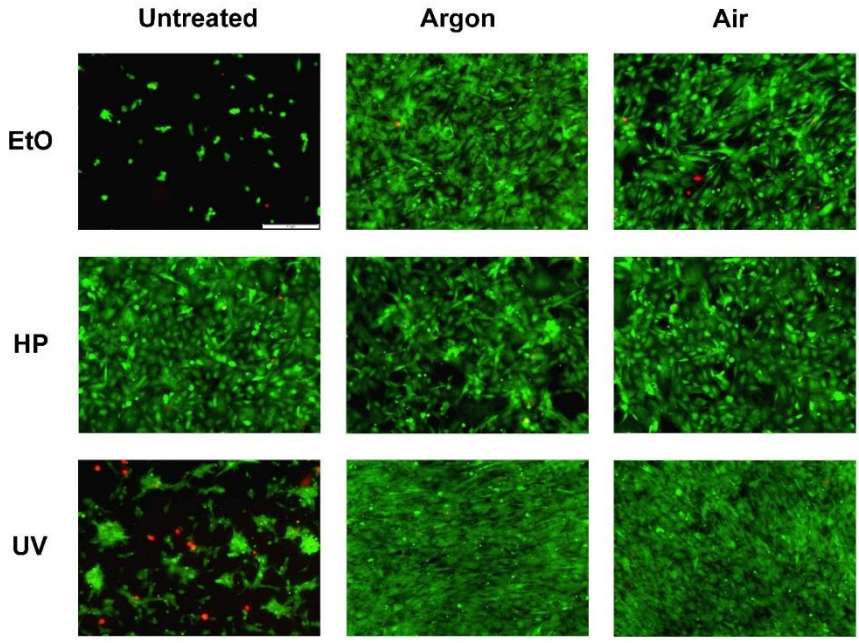

Fig. VIII.12. *Fluorescent micrographs after live/dead staining of ADSCs cultured for 7 days on untreated and plasma-treated nanofibers sterilized by EtO, HP and UV (Scale bar = 200 μm).*

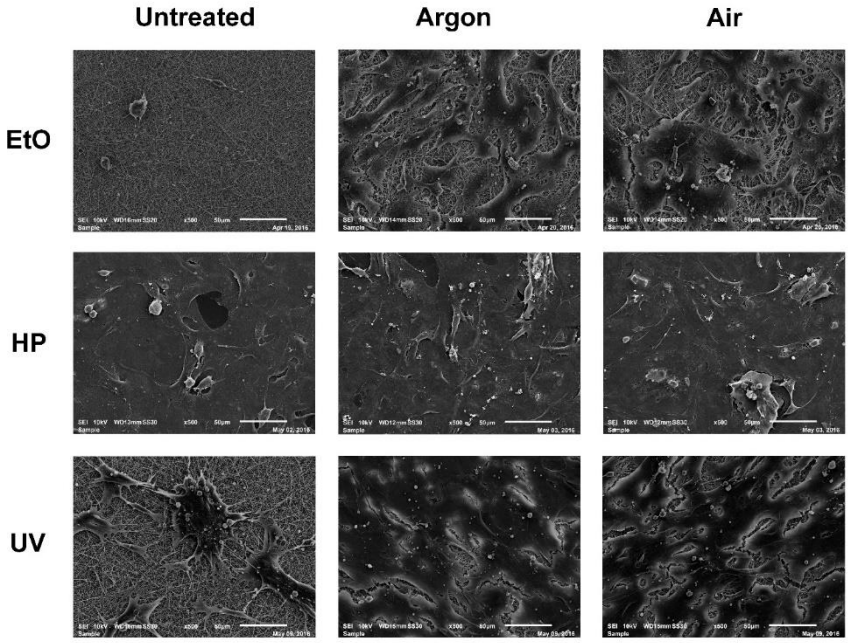

Fig. VIII.13. *SEM images of ADSCs cultured for 7 days on untreated and plasma-treated nanofibers sterilized by EtO, HP and UV (Magnification: 500 x).*

VIII.4.Conclusion

This chapter describes the simultaneous effect of non-thermal plasma treatment (air or argon) and subsequent sterilization (EtO, HP and UV) on the chemical surface properties, morphology and biological performance of PCL nanofibers. Firstly, bead-free PCL nanofibers mimicking the ECM are successfully electrospun and then subjected to a medium pressure plasma treatment in air and argon. WCA and XPS results show the great efficiency of air and argon plasma treatments in enhancing the nanofibers wettability by incorporating oxygen-containing functionalities on their surface. SEM analysis reveals that argon plasma treatment starts to cause mild morphological alterations such as melting at the nanofibers joining points from a plasma exposure of 20 s. From a shorter treatment time of 8 s, air plasma provokes more drastic but local alterations characterized by damaged melted-like spots progressively expanding in area and number. Non-damaged samples are sterilized and then rechecked for their structural integrity. The reactions occurring between EtO molecules and the grafted functional groups on the plasma-treated samples, in addition to the

EtO chamber conditions, change the morphology of the nanofibers from cylindrical to a ribbon-like appearance. Moreover, these reactions decrease the wettability of the plasma-treated samples. The thermo-oxidative reactions occurring during HP sterilization alters the samples drastically to a point where no more fibers are visualized and a film is formed. UV sterilization alters neither the morphology nor the surface chemical properties of the nanofibers. Regardless of the sterilization method, an enhanced adhesion of ADSCs is detected on plasma-treated nanofibers compared to untreated nanofibers. When it comes to cellular proliferation, a low cellular density with no distinction between plasma-treated and untreated samples is observed after HP sterilization, because of the total loss of the fibrillary nanostructure. In contrast, plasma treatment improves the proliferation of ADSCs on samples sterilized by UV and EtO. However, the cellular proliferation rate decreases over days in case of the EtO sterilized samples, mainly due to the EtO toxicity. An excellent proliferation is however perceived on the samples sterilized by UV since the cellular rate increases over time to reach almost the double of the rate on the TCP at day 7. Therefore, of the three investigated sterilization methods, UV sterilization is by far the best choice.

Chapter IX. Wide-ranging Fiber Diameter Scale of Random and Highly Aligned PCL Fibers Electrospun Using Controlled Working Parameters

The results of Chapter IX were published in the following international peer-reviewed journal:

Ghobeira, R., Asadian, M., Vercruysse, C., Declercq, H., De Geyter, N. & Morent, R.
Wide-ranging fiber diameter scale of random and highly aligned PCL fibers electrospun using controlled working parameters
Polymer, 157(2018): 19-31 (2018).

IX.1. Introduction

As already mentioned, PCL has known a massive rise mainly in the past decade, being immeasurably the most considered polymer in literature dealing with electrospinning [416]. This is due to the superior PCL viscoelastic and rheological properties rendering its electrospinning tailorable and relatively easy [83]. Furthermore, the extensive use of PCL in electrospinning is somewhat attributable to its solubility in numerous solvents. Chloroform is one of the most used solvents, however, it generates limited size range fibers since microfibers are electrospun rather than nanofibers [172]. Therefore, other relatively highly toxic single solvent systems have also been used such as dichloromethane (DCM), hexafluoropropanol and trifluoroethanol [101, 417-419]. Nevertheless, solvent solubility is not the only factor influencing fiber formation; solvent dielectric constant and boiling point are also key factors that determine to which extent a polymer solution is electrospinable. As a consequence, some binary and tertiary solvent systems exhibiting a good solubility-spinnability are recurrently adopted and cover nearly the whole extensive literature involving PCL electrospinning. The most used systems are highly toxic such as: dimethylformamide (DMF)/ THF, DCM/methanol, DMF/chloroform, DMF/DCM, chloroform/DCM/DMF and methylene chloride/DMF [420-426]. Since solvent properties were shown to considerably affect the fiber diameter, the selection of one of these toxic systems relies, in the majority of the cases, on the spawned fiber size. In 2011, Van der Schueren et al. introduced for the first time the solvent benign mixture acetic acid (AA) and formic acid (FA) in a study where other more toxic solvent systems were also tested. The solvent mixture gave, after varying the volume fraction of AA and FA, bead-free fine PCL nanofibers having diameters as low as 270 nm [172]. Despite the introduction of this advantageous solvent system, it was rarely observed in the PCL electrospinning literature that followed. (Fig. IX.1). Trials involving the use of one specific solvent system to obtain a wide fiber dimension range are largely unsuccessful and are therefore rarely conducted. Therefore, broadening the size range of PCL fibers electrospun from the alternative AA/FA benign solvent system by analyzing and varying different electrospinning parameters could represent a major breakthrough. In addition to the fiber dimension, tackling the fiber anisotropic alignment that is observed in native ECM of some tissues is very appealing for numerous applications. Researchers are trying to manipulate fiber alignment in the electrospinning process through specific mechanical effects such as varying the motion of a rotating collector or via certain electric field effects [427]. Nevertheless, a high degree of alignment is still problematic to achieve, and to the best of our knowledge, no study has

explored electrospun PCL fiber alignment when PCL is dissolved in a mixture of AA and FA.

Acknowledging the above, in this chapter, mechanical and electrical effects will be combined in a novel collector design generating highly aligned PCL fibers from the alternative AA/FA solvent system. A broad diameter range of random and aligned fibers will be precisely obtained by adjusting the polymer concentration, the TCD and the RH, parameters that were shown to be the most influential ones. Finally, the physico-chemical properties of the obtained fibers will be investigated by means of XPS, WCA, SEM and tensile strength measurements and comparisons will be made between different fiber orientations and diameters.

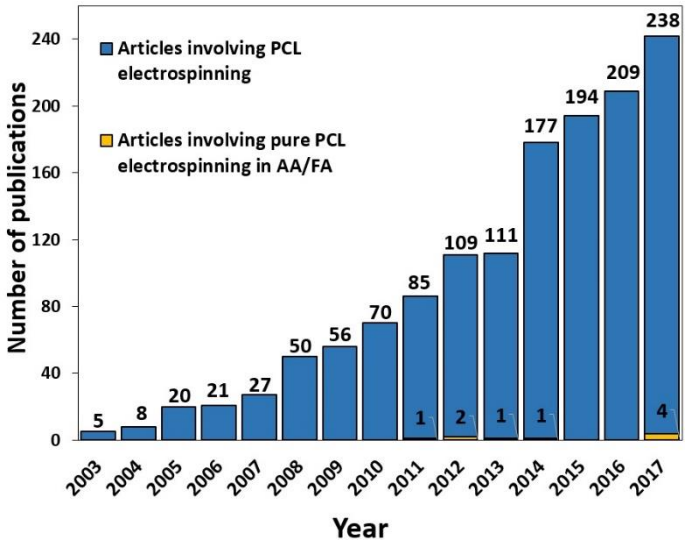

Fig. IX.1. *Total number of publications involving PCL electrospinning versus publications involving pure PCL electrospinning using the solvent system AA/FA, from 2003 until 2017. (Sourced from Web of Science®, topic keyword used during the search: "PCL electrospinning").*

IX.2. Experimental conditions

All experimental details can be found in Chapter VI. The parameters that are specifically used in this chapter are summarized in table IX.1.

Table IX.1. Experimental conditions

Base material	• PCL
Biofabrication method	• Electrospinning
Characterization techniques	• WCA: - 2 µl-drops of distilled water - Reported value: average of 6 values measured on 6 different samples. • XPS: - Reported value: average of 4 values measured on 2 different samples. • SEM: - Accelerating voltage: 7 kV and 10 kV. - Reported fiber diameter value: average calculated over 100 fibers on 2 different samples. • Tensile measurements: - Reported value: average of 5 values measured on 5 different samples.

The viscosity of the electrospinning solution is measured every 3 h over the 24 h following PCL dissolution. A DV2T EXTRA viscometer (Brookfield Engineering Laboratories, USA) operating at room temperature is employed for this purpose. The stated viscosities correspond to the average of 3 measurements per time point.

All the presented data in this chapter are communicated as means +/- standard deviations. One-way Anova and Turkey post-hoc tests are conducted. When the homogeneity of variances is violated, Welch and Brown-Forsythe tests are performed. The level of significance is set at $P < 0.05$.

IX.3. Results and Discussion

IX.3.1. Solvent system composition and PCL degradability

Defining an optimal solvent system composition providing the desired solubility and dielectric constant is one of the first primordial steps that should be achieved. Using AA or FA as single solvent does not accomplish the wanted electrospinability. AA has a low conductivity

and is therefore unable to produce fibrous material whereas the very polar FA is highly influenced by the electrical field which re-orientates the solvent molecules during the process and therefore gives fibers full of droplets [84, 172]. Consequently, mixing the two solvents becomes unavoidable. Based on the study performed by Van Der Schueren et al., we opted for a composition of 10 % AC and 90 % FA. Our selection stems from the finding stating that a minimum composition of 30 % FA and 10 % AA are required for a stable electrospinning process and that increasing the proportion of AA gives rise to inhomogeneous fiber diameters because of the non-uniform charge distribution in solvents with low conductivity [172]. The main downside of using AA and FA is PCL degradation which occurs in such an acidic medium thereby resulting in a decrease in molecular weight and thus in solution viscosity over time. In order to have control over this issue, PCL electrospinning is performed directly and 24 h after PCL dissolution. The lowest PCL concentration (14% w/v), an RH of 45 %, a TCD of 15 cm and a collector RS of 100 rpm are used for this test. In parallel, PCL degradability is quantitatively evaluated by assessing the viscosity of the solution over 24 h in 3 h increments. SEM images show a very good fiber quality when the electrospinning is performed directly after PCL dissolution which corresponds to 3 h post solution preparation time (Fig. IX.2A). This time frame is chosen as starting point since it matches up with the minimal time needed for complete dissolution of PCL in case of the highest concentration under study. In contrast, a mediocre quality of thinner and broken PCL fibers full of beads and droplets is obtained 24 h post-dissolution (Fig. IX.2B). This observation emphasizes the pronounced PCL degradation that is confirmed by the significant decrease in solution viscosity from around 780 to 240 cP only a day after PCL dissolution (Fig. IX.2C). The poor fiber quality is due to this reduced viscosity, rendering the solution not cohesive enough to undergo the strong deformations and to support the stresses developed during the spinning process. Lavielle et al. have also studied the degradation behavior of PCL when dissolved in an AA/FA mixture with a ratio of 50/50. An almost similar poor fiber quality was detected 168 h after PCL dissolution (25 % w/v). Good quality beaded-free PCL fibers were however still obtained 48 h after preparation of a 20 % (w/v) PCL solution [428]. This contradictory result compared to the current study can be explained as follows: The high dielectric constant of FA increases the net charge density of the solvent system containing more FA (90 %) as used in this study. As a consequence, the polymer jet undergoes stronger electrostatic repulsive forces thus leading together with the decreased viscosity to a more substantial thinning and quality reduction of the fibers. Moreover, a different solvent system composition can also lead to a different PCL degradation behavior. The

increase in the FA content, although beneficial for the generation of homogenous fibers, seems to have an intensified PCL degrading potential. This statement can be confirmed by Van der Scheuren et al. study that detected a stable solution viscosity after 3 h of PCL dissolution in 60:40 FA/AC [172]. However, when 90% FA is used, a small decline of about 100 cP is spotted for the same time frame (Fig. IX.2C). For that reason and in order to prevent PCL degradation, electrospinning is performed 3 h after solution preparation time (dissolution time counted) in all upcoming experiments and for all polymer concentrations. As such, an accurate comparison between the fibers electrospun with different conditions can thus be made.

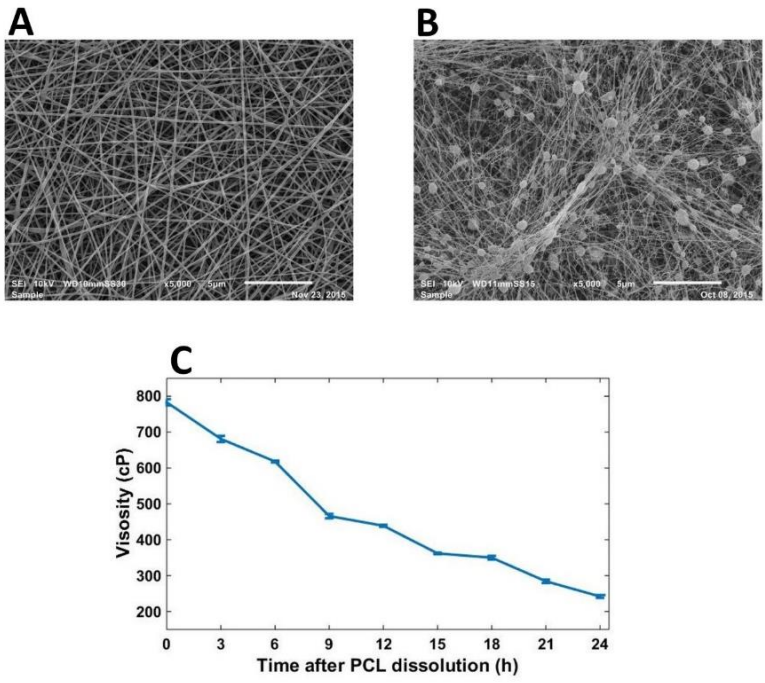

Fig. IX.2. *PCL degradability in AA/FA (10/90) solvent system. (A) SEM image of fibers electrospun directly after PCL dissolution (3 h post solution preparation time); (B) SEM image of fibers electrospun 24 h after PCL dissolution; (C) Solution viscosity as a function of time after PCL dissolution. (Non-varying parameters: C = 14%; TCD = 15 cm; RH = 45%; RS = 100 rpm).*

IX.3.2. Fixed parameters for a steady state electrospinning process

Prior to a deep exploration of the electrospinning parameters, it is of topmost necessity to permanently ensure a steady state process in all subsequent experiments. A steady state safeguards the high instability and the non-reproducibility that are known to be the 2 major challenges of electrospinning. Moreover, its guarantees the production of bead-free and uniform fibers. This state is reached when the Taylor cone becomes stable over time and when the quantity of polymer that is delivered from the needle is equal to that sprayed towards the collector per time unit [172]. After a visual check on the presence and the continuousness of the steady state over 20 min, a range of polymer concentrations and solution flow rates and a fixed voltage were opted for this study. The selected concentrations vary between 14 and 28 % (w/v) as an unstable jet is observed at lower concentrations. Concentrations lower than 14 % turn out to be below the critical concentration that allows minimal polymer chain entanglements indispensable for a stable jet and thus bead-free fibers. In contrast, at higher concentrations, the solution becomes too viscous to be easily electrospun and the polymer rapidly solidifies thus obstructing the tip. A voltage of 32 kV is kept constant in all experiments and is chosen since it results in a steady state condition for all used PCL concentrations. The solution flow rate is slightly varied during the experiments between 0.5 and 0.7 ml/h to ensure a permanent jet stability over the whole electrospinning period.

IX.3.3. Effect of collector design and rotational speed on fiber alignment

Since highly aligned fibers exhibit notable and numerous advantages in terms of mechanical properties and cellular behaviors and are very challenging to reach despite several described methods, one of our first goals is to achieve a good fiber alignment [102]. This allows, in a further step, to tackle the fiber diameter and other parameters of both random and aligned fibers and to make some comparisons. The common mechanical approach based on collecting fibers on rapidly moving cylinders is first tested. The mandrel RS is varied from 1000 to 3000 rpm in 500 rpm increments using first the large cylinder (length = 28 cm, radius = 5 cm). The lowest polymer concentration under study (14 % w/v) is selected for this test, since it was previously demonstrated that increasing polymer concentration improves the alignment degree,

so reaching the desired alignment with the lowest concentration guarantees a better or at least the same result with the higher polymer concentrations [427, 429]. This can be explained by the fact that the chaotic motion of the jet called bending instability or whipping motion decreases when increasing polymer concentration, so the jet travels in a more straight trajectory towards the collector creating more aligned fibers. An RH of 45 % and a TCD of 15 cm are also selected for this examination. Fig. IX.3 shows the used collector, the SEM images of the PCL nanofibers obtained at different RSs, the FTT output images and their corresponding pixel intensity histograms in function of the acquisition angle of the fibers. The degree of alignment is defined by the overall distribution of the data points: the higher and the narrower the peak is, the more accurately aligned the fibers are with respect to a specific orientation axis. The lower and the wider the distribution curve is, the more arbitrarily the fibers are deposited in random orientation axes and thus the less aligned they are. One can conclude from the FTT plots of Fig. IX.3 that increasing the mandrel RS improves the degree of fiber alignment. The maximal intensity values progressively rise from approximately 0.01 arbitrary units (a.u.) to approximately 0.025 a.u. when increasing the RS from 1000 to 3000 rpm. Simultaneously, the angle range of the majority of the fibers, designated by the width of the overall peak, shrinks from nearby the whole spectrum covering the full 180 ° to a significantly smaller range of 50 °. This observation is due to the mechanical RS force that leads to the stretching of the fibers and therefore their deposition in an aligned manner [424]. Despite the improved alignment at a RS of 3000 rpm, the fibers are still poorly oriented in a specific axis, which is generally observed when using this technique. Indeed, it has been stated that a high alignment degree demands very high RSs matching or exceeding the fiber production rate, otherwise the fibers adopt different orientations [430]. However, some studies, in return, also showed a rather low alignment despite the use of very high speeds of collection or the occurrence of multiple fiber breakages as a result of the fast movement [427, 431]. To deal with these issues, the electrical field effect was in some cases adopted to generate parallel fibers. To do so, two electrically conductive wires or substrates can be placed in parallel with an insulting gap or material in between thus allowing the charged fibers to be stretched perpendicularly to the substrates, spanning the gap to form uniaxially highly ordered fibers. The success of this method is however limited to only small inter-substrate distances, which in turn restricts the fiber production area [101, 432].

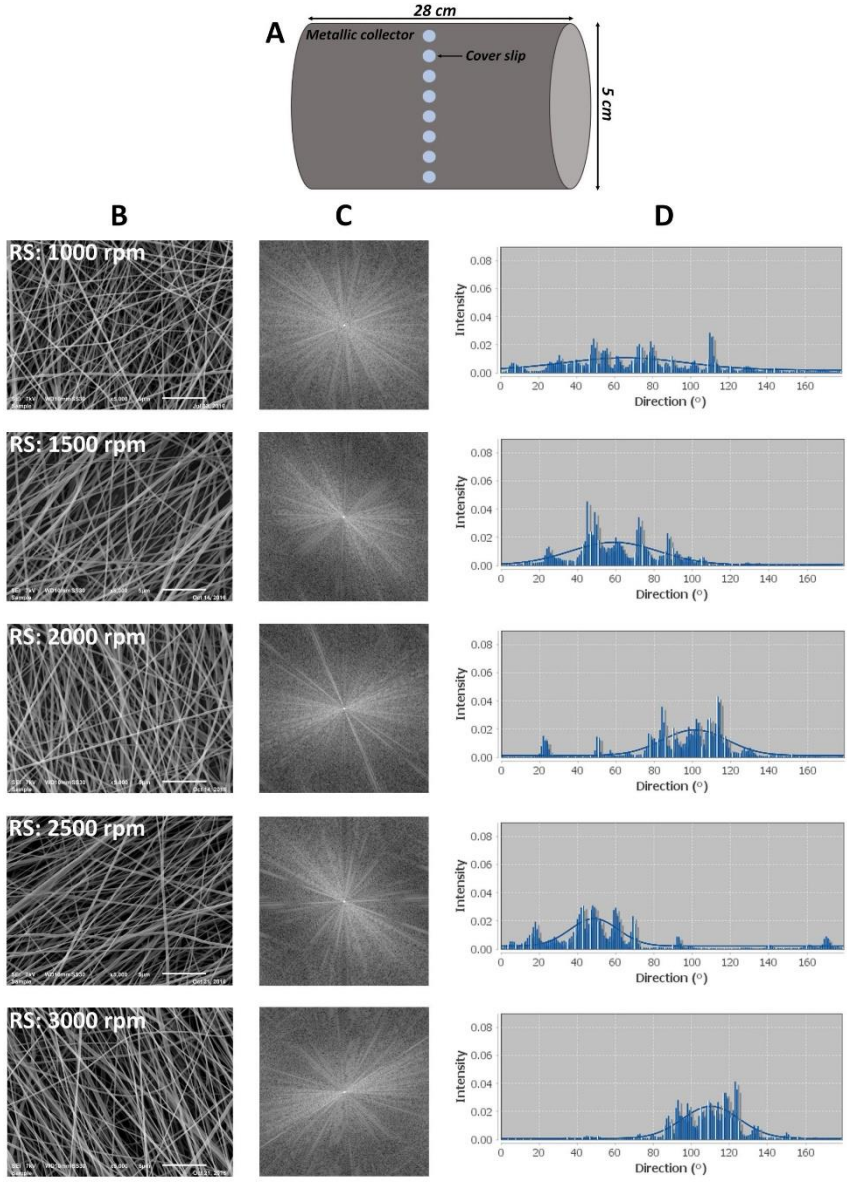

Fig. IX.3. *Effect of the collector RS on fiber alignment. (A: collector used; B: SEM images of the generated fibers (scale bar: 5 µm); C: FTT output images; D: Pixel intensity plots in function of the direction of the fibers).*

The initiation of a new method combining both mechanical and electrostatic forces in one collector is therefore also explored in this

study. As a first step, the metallic collector is covered with an insulating cellophane sheet, after which rectangular aluminum strips (3 cm x 1 cm) are placed in parallel between the cover slips on which the fibers are deposited (Fig. IX.4.A: C1). The newly designed collector is then used with a RS of 3000 rpm aiming to further improve fiber alignment by maintaining the mechanical effect while adding electrical forces. Based on the obtained SEM image and FTT plot (Fig. IX.4.B-D), a considerable improvement in the alignment degree is noted. A higher and narrower distribution curve is observed when comparing to the previously used collector (Fig. IX.3). This is presumably due to the synchronic effects of the rotation and the aluminum strips. In order to confirm this statement, the mechanical effect is almost eliminated by reducing the rotational speed to 500 rpm. In this case, random fibers are deposited as observed in the second SEM image and FTT plot of Fig. IX.4, showing an almost uniform fiber distribution on the different orientation axes. This observation thus confirms that the mechanical and electrostatic effects simultaneously lead to the improved fiber alignment and not only the addition of conductive strips. In a trial aiming to further ameliorate the alignment, smaller aluminum strips having a length of 1.2 cm, which is the diameter of the cover slips, are also used (Fig. IX.4.A: C2). This is based on the assumption that the fibers would be deposited on a more constricted width and therefore would be prone to less disorientation. Unfortunately, almost the same fiber alignment degree is observed as when the larger aluminum strips are used, which is probably due to a reduced electric field strength. Changing the base material of the strips is also thought to affect the electrical field and maybe the degree of alignment. Therefore, aluminum strips have also been replaced with copper strips (Fig. IX.4.A: C3), but, unfortunately also in this case no improvement in fiber alignment is noticed (Fig. IX.4).

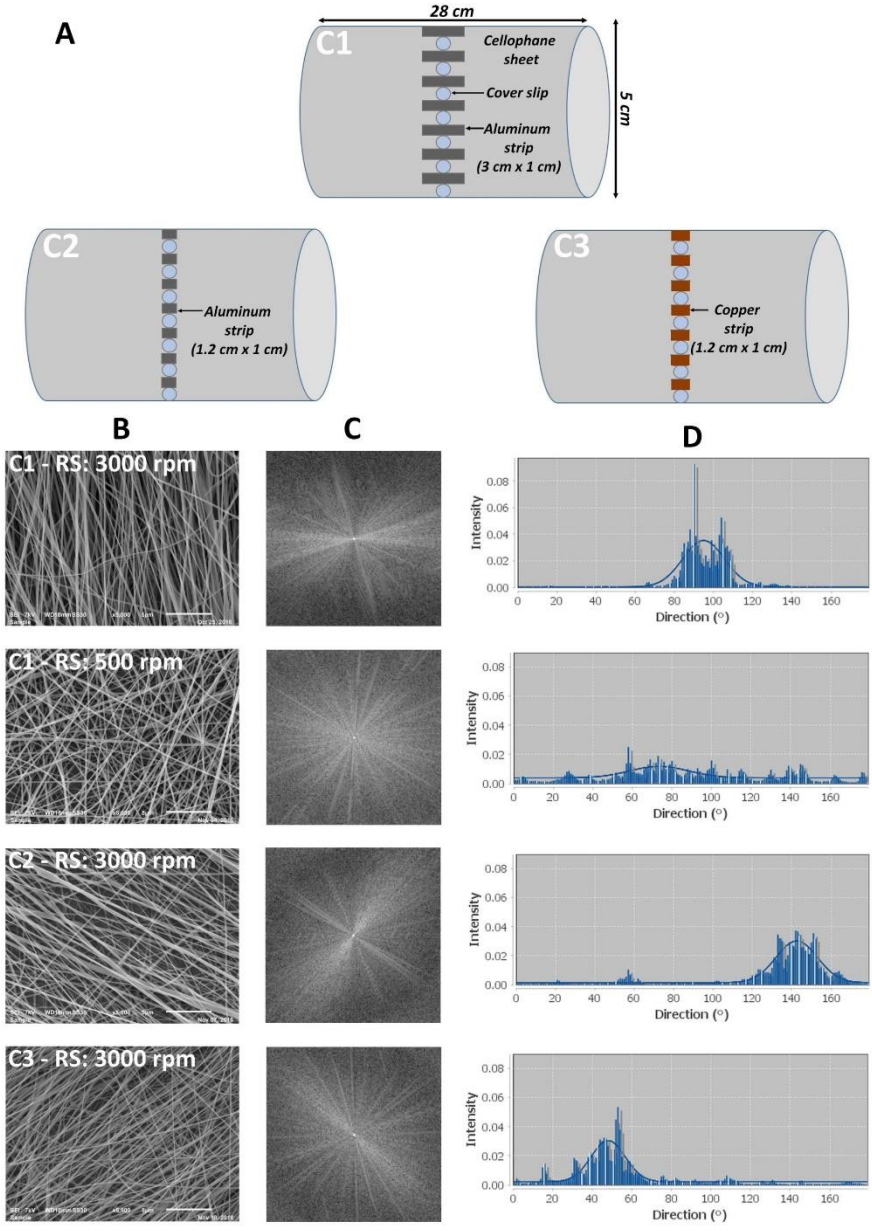

Fig. IX.4. *Effect of collector design and RS on fiber alignment. (A: collectors used; B: SEM images of the generated fibers (scale bar: 5 µm); C: FTT output images; D: Pixel intensity plots in function of the direction of the fibers).*

Based on the abovementioned results, an innovative collector consisting of a flat stainless steel cylindrical mandrel (length = 1 cm, radius = 5 cm) is fabricated on-site. Placing the cover slips on the reduced length cylinder is believed to mimic the conductive strips effect but with the generation of a more uniform electrical field. As such, the charged fibers may be stretched in a more constricted area and together with a RS of 3000 rpm, a better fiber alignment may be reached. This assumption was indeed confirmed by the SEM image of the nanofibers deposited on such a collector (Fig. IX.5). Moreover, the FTT output plot shows the highest maximal intensity (≈ 0.045 a.u.) and the narrowest distribution curve (the majority of the fibers delimited to an orientation range of around 25°) of all examined plots. Accordingly, this collector will be used in all upcoming experiments. A RS of 100 and 3000 rpm will be applied for the generation of random and aligned fibers respectively.

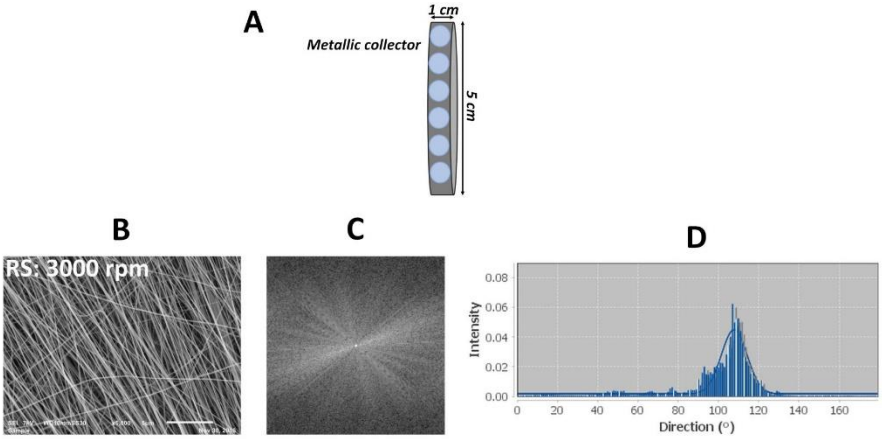

Fig. IX.5. *Effect of the novel collector design on fiber alignment. (A: collector used; B: SEM image of the generated fibers (scale bar: 5 µm); C: FTT output image; D: Pixel intensity plot in function of the direction of the fibers).*

IX.3.4. PCL fiber diameter

After addressing the challenging anisotropic properties of the fibers, tackling their topographical scale, which critically influences different cell type behaviors, becomes the focal issue of interest. Different electrospinning parameters are known to influence fiber dimensions and these parameters are mainly separated in three different subcategories: the solution-related parameters, the process-related

parameters and the environmental parameters [416, 426, 433]. In this study, only the most prominent parameters of the three subcategories will be varied:
- polymer concentration as solution parameter
- TCD as process parameter
- RH as ambient parameter

IX.3.4.1. Effect of polymer concentration on fiber diameter

Polymer concentration is the most important solution parameter since it affects both solution viscosity and surface tension having complementary effects on fiber size [426]. As already mentioned, 4 polymer concentrations, safeguarding a steady state electrospinning process, are tested in this study: 14, 20, 24 and 28 (w/v) %. A TCD of 15 cm and an RH of 45 % are fixed in this experiment. Both aligned and random fibers are generated by setting a collector speed of 3000 and 100 rpm respectively. Results show that increasing the polymer concentration from 14 to 28 (w/v) % leads to a statistically significant and progressive increase in fiber diameter from 131 to 1173 nm and from 155 to 1272 nm for aligned and random fibers respectively (Fig. IX.6 and Fig. IX.10.A). The proportional relation between fiber size and polymer concentration has already been widely observed in previous studies involving electrospinning [426, 433, 434]. This general trend is due to the fact that higher polymer concentrations lead to more entanglements between polymer molecular chains thus opposing jet stretching in the applied electrical field, which results in greater fiber diameters [100, 435]. When the polymer concentration is increased, a progressive increase in solution viscosity arises resulting in an intensified viscoelastic force which is the main factor limiting jet stretching [436]. Moreover, rapid solidification of the jet befalls with increasing polymer concentration and therefore the jet is prone to a shorter voltage-induced stretching time [172]. The obtained results also reveal that the diameter uniformity decreases with increasing polymer concentration but not to a significant level. This tendency was also observed by Beachly et al. after the electrospinning of PCL dissolved in DCM and methanol at different PCL concentrations [421]. To the best of our knowledge, no previous study has generated PCL fibers having diameters less than 200 nm and more than 1 µm when using the same solvent system. Moreover, regardless of the used solvent, producing micro-sized aligned fibers is normally challenging since the stretching force induced by the high collector RS results in thinning of the fibers additionally to their alignment. However, in contrast to what was frequently observed in literature, no reduction in fiber diameter is noticed in this study when increasing the RS for the PCL concentration

of 14 % (w/v). Furthermore, the aligned fibers produced from the polymer concentrations 20 and 24 % have significantly higher diameters than the corresponding random fibers. This is presumably due to the increased solvent evaporation rate provoked by the high collector rotational motion drying the fibers in the electrospinning chamber in an early stage of the travelling jet. The jet solidification is therefore accelerated and the liquid connection stretching induced by electrostatic forces is ceased earlier resulting in larger diameters compensating fiber thinning induced by mechanical stretching forces. This can explain the statistically non-significant difference between the diameter of random and aligned fibers when the PCL concentration is set to 14 %. When the concentration increases to 20 and 24 %, the effect of the high collector motion is more prominent. A faster jet solidification occurs, immediately ending the electrostatic stretching thus generating thicker fibers and masking the mechanical thinning effect. Moreover, as the solvent evaporates faster, the solution conductivity decreases leading to an additional increase in fiber diameter [437]. As a result, the generated aligned fibers present larger diameters than the randomly deposited fibers. When a critically high concentration is reached, the solution solidifies very rapidly regardless of the fast or slow collector motion and in this case the reduction in fiber diameter engendered by the stretching forces of the fast rotation can be seen. This is why aligned fibers are significantly thinner than random fibers when a PCL concentration of 28 % is used.

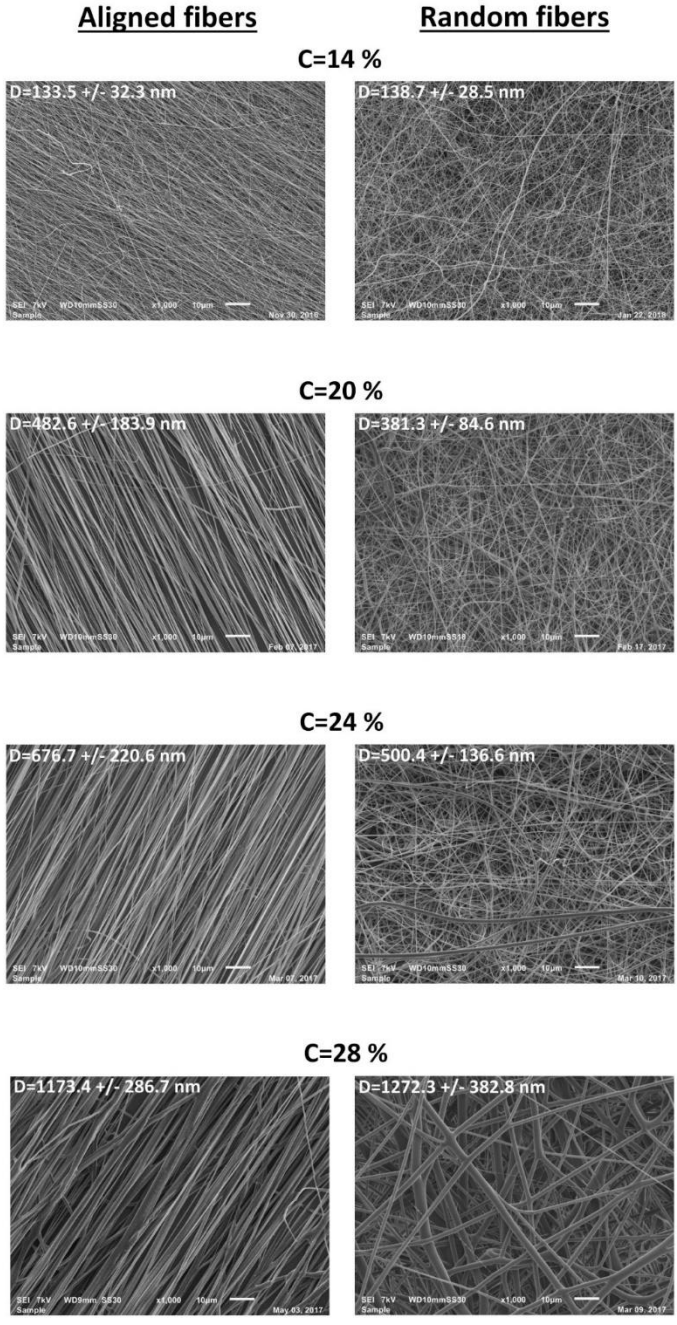

Fig. IX.6. *Effect of PCL concentration (C) on the fiber diameter of aligned and random electrospun PCL fibers.*

IX.3.4.2. Effect of TCD on fiber diameter

TCD is one of the major process-related parameters that has been substantiated to play an elemental role in determining fiber morphology and diameter. Small changes in this distance can significantly affect the fiber characteristics because of its influence on several other parameters such as fiber deposition duration, solvent evaporation, electrical field strength, bending instability interval or whipping motion [434, 438]. Moreover, the TCD effect was also shown to vary with the polymer-solvent system [437]. In order to evaluate the TCD effect on PCL fiber diameter, 4 different distances are tested in this study: 20, 15, 12.5 and 10 cm. The electrospinning process is performed using a polymer concentration of 20 % and under an RH of 45 % and both aligned and random fibers are produced. Results reveal that decreasing the working distance from 20 to 10 cm leads to a statistically significant and progressive increase in fiber diameter from 225 to 939 nm and from 232 to 837 nm for aligned and random fibers respectively (Fig. IX.7 and Fig. IX.10.B). After the polymer solution is ejected from the nozzle, it travels in a straight line for a certain space interval, then undergoes bending instabilities and whipping motion stretching and elongating the fibers before their deposition on the mandrel [439]. Therefore, the larger the TCD is, the more the fibers will elongate resulting in thinner fibers. The spatially restricted jet stretching in small TCDs is sometimes also accompanied with incomplete solvent evaporation at the moment of deposition leading to an additional increase in fiber diameter and conglutination of adjacent fibers [433, 440]. The imbalance between the complete and the inadequate PCL fiber drying within the jet can partly explain the considerable decline in fiber diameter uniformity with decreasing TCD. The inversely proportional relation between the TCD and the fiber diameter and their non-uniformity was previously observed by many groups [438, 440, 441]. However, discrepancies were also found in literature as some studies reported thicker diameters for larger working distances [439]. This can be explained by the fact that the electrical field strength increases with decreasing working distance, which leads to an intensification of the electrostatic force on the polymer jet facilitating fiber thinning [441, 442]. The controversial effects of decreasing TCD can also elucidate the high standard deviations in fiber diameter that are mainly detected for the smallest distance (10 cm). On the one hand, the unbalanced ejected polymer forces between surface tension, increased electrostatic repulsion and viscoelastic forces tend to result in the creation of thin non-homogeneous fibers [441]. On the other hand, the limited whipping motion and the incomplete polymer drying tend to produce thick non-

uniform fibers [440]. The slightly improved diameter uniformity in case of aligned fibers at the smallest TCD value is presumably due to the more complete solvent evaporation induced by the high collector motion at the deposition moment and the resulting reduced solution conductivity confining the effect of the stronger electrical field. The decreased solution electrical conductivity can also justify the similar or slightly higher fiber diameters of aligned fibers compared to random fibers despite the mechanical stretching effect of the high rotations resulting into fiber alignment.

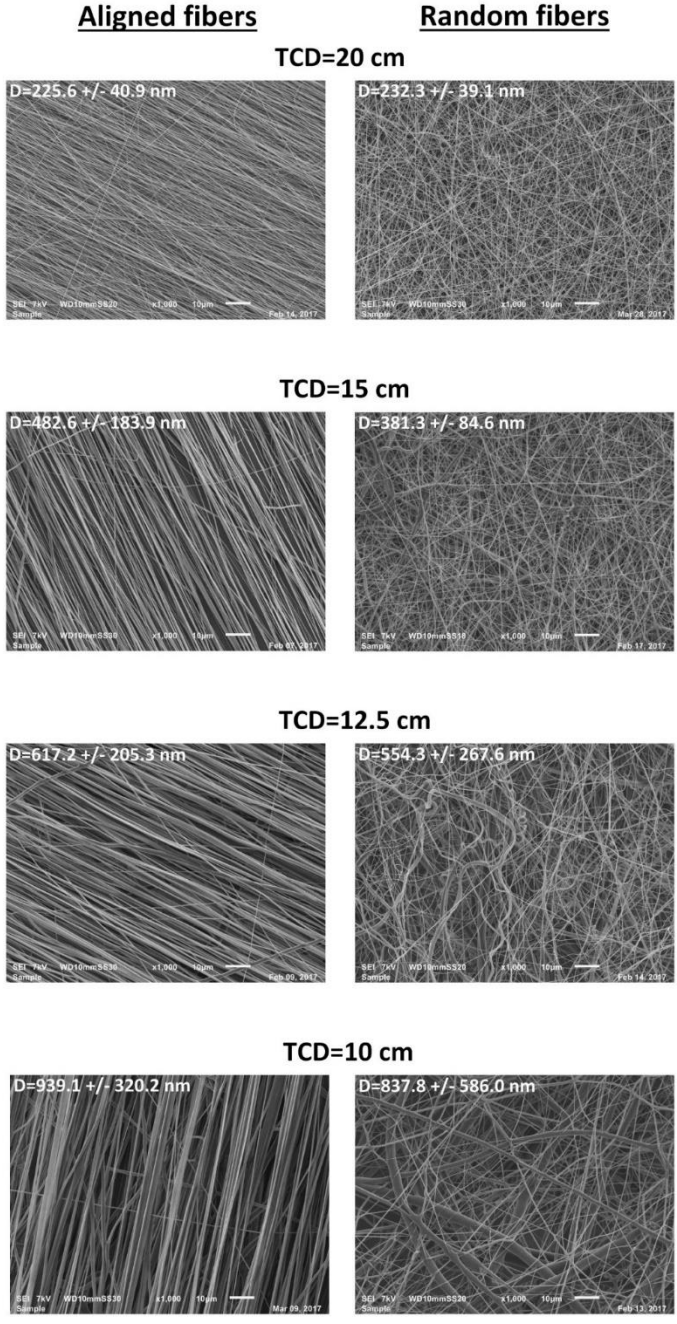

Fig. IX.7. *Effect of TCD on the fiber diameter of aligned and random electrospun PCL fibers.*

IX.3.4.3.Effect of relative humidity on fiber diameter

The role of ambient parameters is generally underestimated and only a few studies have monitored the impact of temperature on the electrospinning process while neglecting the relative humidity effect, which was also only very rarely explored. An unexpected considerable effect of the humidity on fiber diameter was however perceived from the available scant data. Therefore, scrutinizing its effect on PCL fibers turns out to be very valuable. To do so, the RH is varied from 35 to 65 % in 10 increments, while opting for a polymer concentration of 20 % (w/v) and a TCD of 15 cm. Aligned and random fibers are again electrospun. Results depict that increasing the RH from 35 % to 65 % leads to a progressive increase in fiber diameter from 249 to 841 nm and 279 to 514 nm for aligned and random fibers respectively (Fig. IX.8 and Fig. IX.10.C). Two reasons can explain this observed phenomenon. The first one stems from the fact that an increased humidity gives rise to a higher water vapor pressure and therefore to the presence of more water molecules between the tip and the collector. These water molecules lead to a decline in the total amount of excess charge on the polymer jet because of the induced molecular polarization. Consequently, the intensity of the electrical field is reduced and thicker fiber diameters are produced since the jet experiences weaker drawdown force and thus limited elongation [99, 443]. The second reason for this observation is the fast precipitation of PCL fibers due to the presence of water vapor acting as non-solvent. The higher the humidity, the faster the fiber precipitation occurs since more water molecules will be absorbed by the jet. This accelerated precipitation prohibits the jet elongation resulting in larger fiber diameters. The obtained results are in agreement with previous studies showing that increasing humidity has led to increased diameters of polysulfone, polyacrylonitrile and cellulose acetate electrospun fibers [98, 99]. However, divergence in literature was also noticed since a decrease in fiber diameter was in some cases the result of an increasing RH [100, 172]. The probable cause of this inverse manner turns out to be the plasticizing effect of the water vapor slowing the solidification of the jet that becomes prone to a longer period of thinning and stretching. In this study, an increasing RH led to a relatively slow increase in fiber diameter of random fibers with statistically insignificant fiber diameter differences when electrospinning at a RH 35 % or 45 %. One can therefore conclude that random fibers are probably affected to a certain level by the plasticizing effect of water. In contrast, a steeper increase in fiber diameter is noticed for aligned PCL fibers presumably owing to the high RS of the mandrel drying the fibers faster and thus compensating the plasticizing effect of water. Moreover, the accelerated

solvent evaporation in case of aligned fibers reduces the solution conductivity making the polymer jet, already neutralized by the water vapor, less stable and thus less uniform fiber diameters are observed compared to random fibers.

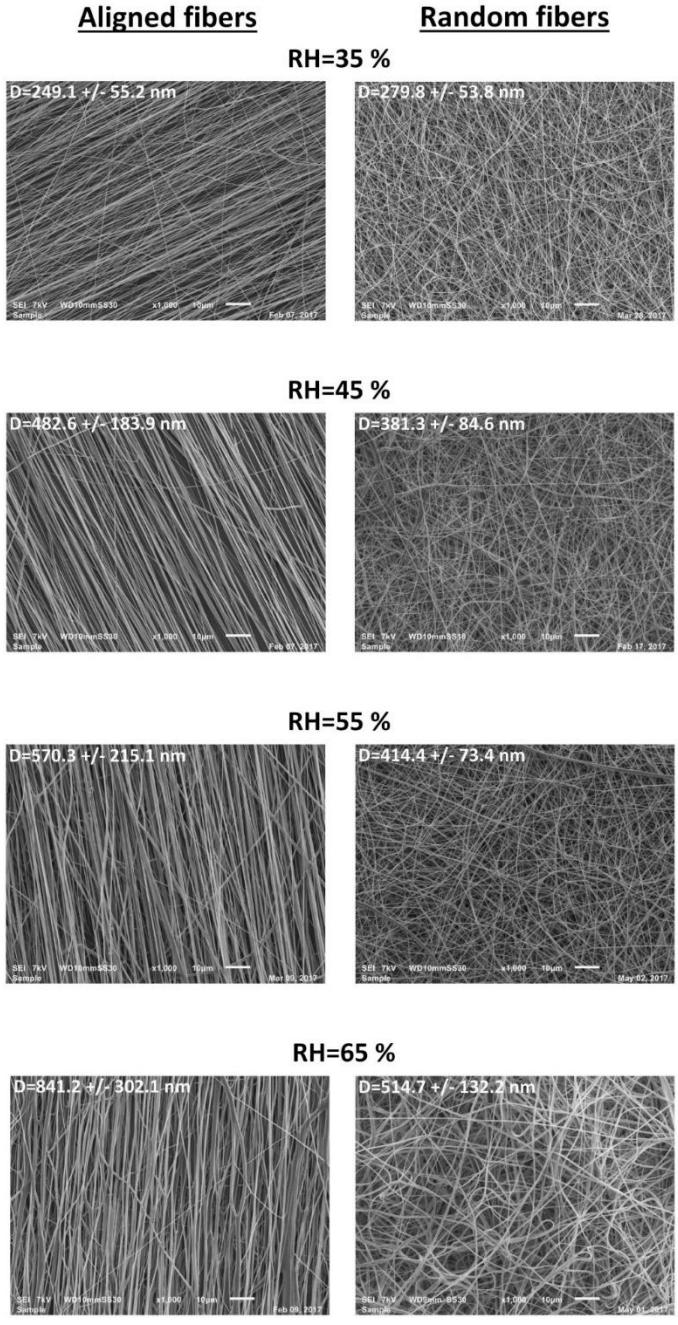

Fig. IX.8. *Effect of RH on the diameter of aligned and random electrospun PCL fibers.*

IX.3.4.4. Broadening the fiber diameter scale

Based on the analysis of the effect of polymer concentration, TCD and RH on the random and aligned PCL fiber diameters, all 3 parameters are also simultaneously varied to significantly broaden the attainable fiber size scale. The polymer concentration together with RH are increased while the TCD is concurrently decreased to end up with the following parameters combinations: D1) C = 14 %, TCD = 20 cm and RH = 35 %, D2) C = 20 %, TCD = 15 cm and RH = 45 %, D3) C = 24 %, TCD = 12.5 cm and RH = 55 %, D4) C = 28 %, TCD = 10 cm and RH = 65 %. These combinations are indeed capable of producing random PCL nanofibers with diameters as low as 94 nm to diameters as high as 1548 nm (Fig. IX.9 and Fig. IX.10.D). This achievement represents a major breakthrough since, to the best of our knowledge, the smallest good quality fiber size that could be attained so far when using the same solvent system is approximately 200 nm [172]. The fibers obtained in literature, although bigger than the fibers produced in this work, have led to the recent statement defining AA/FA as the solvent system that originates thin PCL fibers. This statement however becomes incomplete as PCL fibers having diameters of more than 1500 nm are also attained in this work, to be by far the thickest of the previously generated PCL fibers when using AA/FA as solvent mixture. The same fiber diameter trend is also observed for aligned fibers, which also present a wide diameter range going from 114 to 1408 nm (Fig. IX.9. and Fig. IX.10.D). To the best of our knowledge, aligned PCL fibers have not been previously electrospun with this solvent system. For both random and aligned fibers, an increasing fiber diameter is accompanied by a decrease in size uniformity but not to a significant level; the difference between the 4 diameters being statistically significant. In the next paragraphs, the physico-chemical properties of the 4 different aligned and random fiber sizes created in this section will be analyzed.

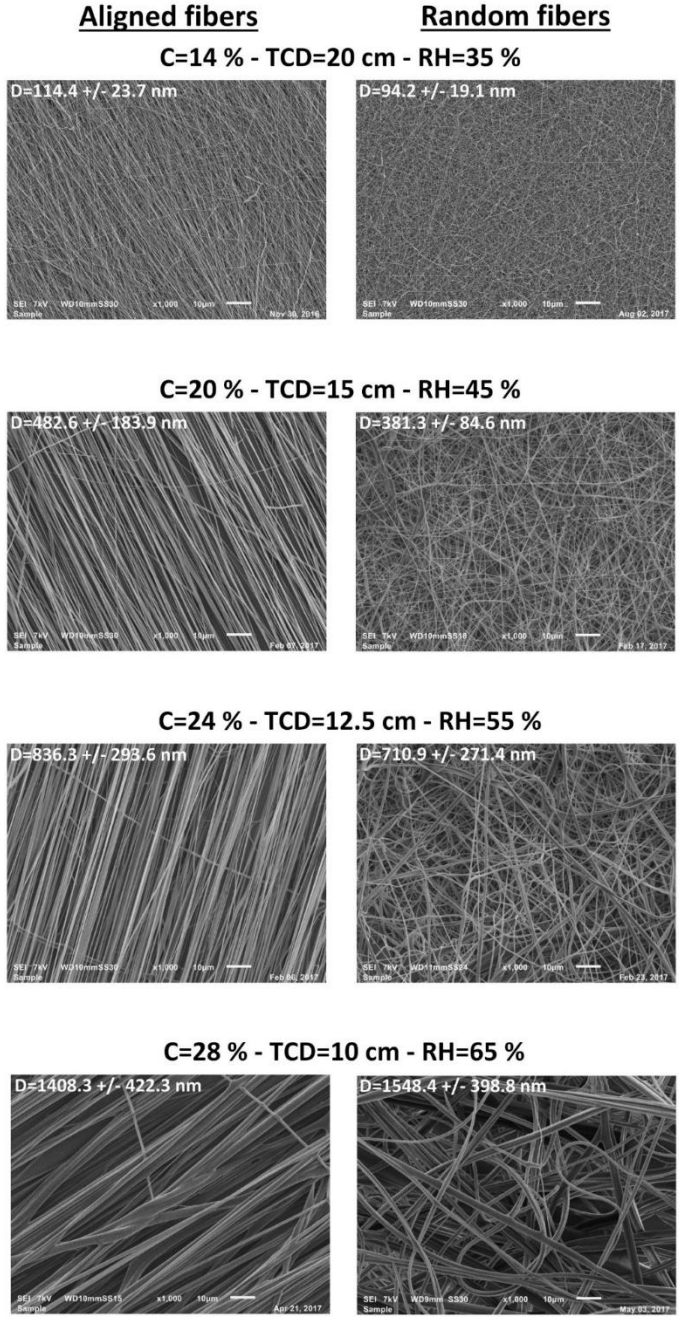

Fig. IX.9. *Effect of varying different parameters simultaneously on the fiber diameter of aligned and random electrospun PCL fibers.*

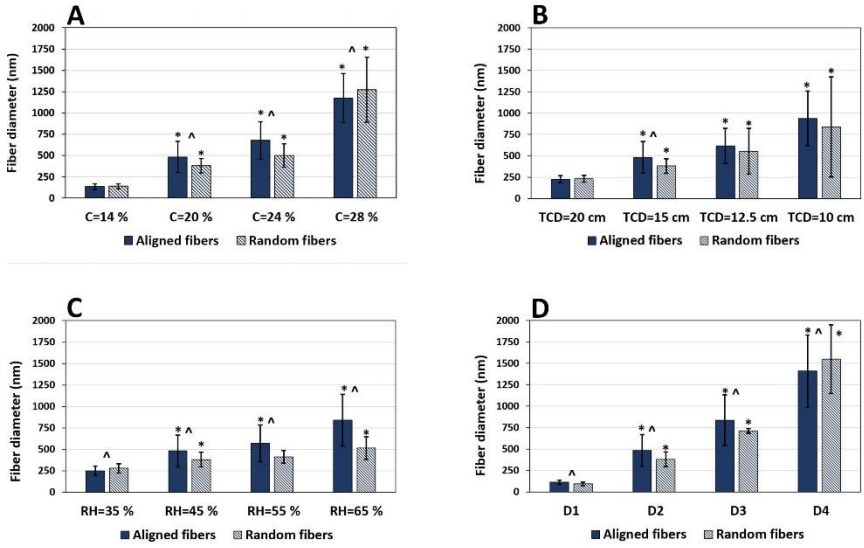

Fig. IX.10. *Effect of varying polymer concentration (A), TCD (B), RH (C) and all parameters simultaneously (D) on PCL fiber diameter. (*: statistically significant difference between fibers electrospun with 2 different and consecutive parameters within the same aligned or random fiber group; ^: statistically significant difference between aligned and random fibers electrospun with the same parameter; $P < 0.05$).*

IX.3.5. Physico-chemical properties of PCL fibers

In order to assess how the physico-chemical properties of electrospun PCL meshes are influenced by fiber size and orientation, XPS, WCA and tensile measurements are performed.

IX.3.5.1. X-ray photoelectron spectroscopy

Some studies have shown that the electrospinning process can favor the segregation or enrichment of specific chemical groups on the fiber surface over the fiber bulk. For instance, Deitzel et al. electrospun fibers from fluorinated polymers and noticed that the percentage of fluorine on the fiber surface is twice the percentage in the bulk [444]. Cui et al. electrospun PLA and PLA-poly(ethylene glycol) fibers and found out that chemical groups with lower bonding energy such as methyl groups are enriched on the fibers surface because of the electrospinning high voltage [265].

Therefore, evaluating the fibers surface elemental composition turns out to be essential in order to elucidate if different electrospinning parameters are leading to specific molecular rearrangements. To do so, XPS measurements are performed on aligned and random fibers electrospun using the parameters described in the previous section to obtain 4 different diameters for each of the 2 orientations. A carbon amount of approximately 76 % and an oxygen amount of approximately 24 % are detected on the fiber surface with no significant difference between the 8 examined electrospinning conditions (Fig. IX.11.A). In addition, the obtained percentages are in accordance with the PCL chemical structure and were previously detected on the surface of spin-coated PCL films [445]. One can thus conclude that the electrospinning process in this work is not causing any chemical group remodeling like the segregation of lower binding energy groups towards the surface.

IX.3.5.2. Water contact angle

Since most of the applications implicating the use of electrospun fibers are strongly dependent on very specific surface hydro-properties, appraising the fibrous mesh wettability helps to choose the appropriate fiber condition or the suitable surface modification for a certain utilization. Therefore, WCA measurements are conducted on the fibrous meshes displaying different fiber diameters and orientations. Values above 100 ° are perceived in all cases, thus placing the fibers between the hydrophobic and the super-hydrophobic categories (Fig. IX.11.B) Although displaying the same surface chemical composition as previously evaluated PCL films, the electrospun fibers show considerably increased hydrophobic characteristics; the WCA on the films being around 74 ° [445]. This observation reveals that, besides the surface chemistry, the topography has an extra strong influence on the liquid-solid interface. For a chemically hydrophobic material, the electrospun meshes exhibit an amplified hydrophobicity compared to films because of their highly porous structure triggering the air entrapment in the inter-fiber spaces, thus hindering the penetration of the water droplet that remains sitting on air [446, 447].

When taking a closer look to the different fiber conditions, significant variances in wetting behavior are detected. These differences in WCA are due to several complicated interacting factors such as mesh surface roughness, fiber diameter and mesh porosity [265, 448]. Several studies have shown that the fiber diameter dictates the mesh roughness in a proportional manner. For instance, Milleret et al. and Xu et al. assessed the roughness of polylactic-co-glycolic acid and PLA fibrous meshes respectively, and found rougher surfaces with increasing fiber diameter [448, 449]. Moreover, a markedly enhanced PCL fiber mat roughness

was recently correlated with an increased fiber diameter [450]. The results of this work show that the enhanced roughness of the aligned fibers leads to a statistically significant and progressive decrease in WCA from 137 ° for the thinnest fibers to 113 ° for the thickest fibers. Based on the Wenzel equation developed in 1936, one can deduce that the higher the roughness is, the lower the WCA becomes because of water penetration in the roughness grooves. This is referred to as "homogeneous wetting" [393]. However, the random fibers having 4 different diameters do not show significant differences in their WCA values except for the thickest fibers showing a reduced value of 127° in comparison to 135° for the other samples (Fig. IX.11.B). This is again due to the opposite effect of the enhanced fiber mesh porosity trapping air bubbles in the roughness grooves underneath the liquid [265]. This phenomenon is known as "heterogeneous wetting" [393]. As the fiber size increases, the pores become larger leading to more entrapment of air in the highly porous structure thus compensating the decrease in WCA resulting from increased roughness. This is in agreement with the recent study of Kim et al. who showed insignificant differences in WCA values of random PCL fibers having different fiber diameters [450]. Nevertheless, when a certain pore size is attained, the droplet of low tension cannot be held on the surface anymore, which explains the decreased WCA value for the thickest fiber diameter [446]. The aligned fibers are less affected by air entrapment because of their decreased porosity compared to random fibers [451]. The packing of fibers in one orientation becomes denser as the fiber diameter increases, thus hindering air entrapment. This can explain the observed WCA decrease with increased roughness.

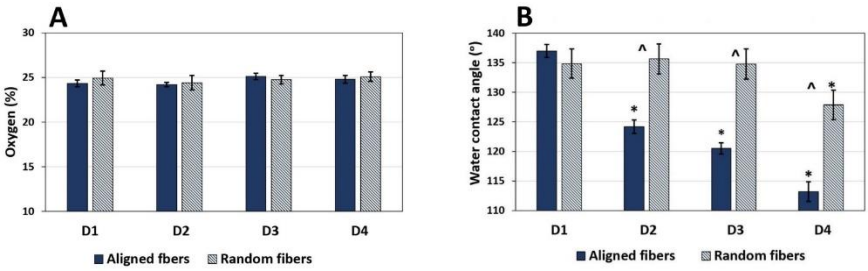

Fig. IX.11. *Effect of different fiber diameters and orientations on the surface oxygen content (A) and WCA (B). (*:statistically significant difference between fibers electrospun with 2 different and consecutive parameters within the same aligned or random fiber group; ^: statistically significant difference between aligned and random fibers electrospun with the same parameters; $P < 0.05$).*

IX.3.5.3. Tensile measurements

It is imperative that the mechanical properties of the fibers match the requirements of a specific end-application. For instance, different TE applications dictate different cell-type dependent responses that are greatly influenced by the scaffolds strength and elasticity. The importance of such properties can be obviously illustrated by the cell growth in tissues such as cartilage and blood vessels constantly exposed to shear stresses and compressions [452]. Hence, the mechanical properties of the PCL fibers generated in this work are assessed and analyzed based on the different fiber diameters and orientations. Results (Fig. IX.12.C) show that increasing the fiber diameter leads to a progressive and significant decrease in the fibrous mesh tensile strength from 58 to 31 MPa and from 28 to 6 MPa for aligned and random fibers respectively. Moreover, a decrease in Young's modulus from 217 to 155 MPa and from 52 to 31 MPa is observed between D1 and D2 of aligned and random fibers respectively (Fig. IX.12.D). When the diameter is further increased, a more gradual decrease in Young's modulus reaching values of 134 MPa for the aligned fibers and 19 MPa for random fibers is noticed. The ductility, which is defined by the strain at fracture, is also affected by the fiber size since it is shown to increase with increasing fiber diameter especially for random fibers (Fig. IX.12.A and B). These results are in accordance with previous studies conducted by Wong et al. and Kim et al. on PCL fibers where the same trends in tensile strength, stiffness and breaking strain are seen when increasing fiber diameter [450, 453]. The mechanical properties of the different fibrous meshes are dependent on the strength of an individual fiber on the one hand and on the bonding between different fibers on the other hand. When considering the distinctive fiber properties, one can think of the arrangement of macromolecules that need to adopt specific geometrical orientations for them to accommodate dimensional constraints in cylindrical shapes ranging from 100 nm to 1500 nm. The ordered or random macromolecular arrangement was shown to play an important role in delineating the fiber mechanical characteristics. The molecules in PCL, which is a semi-crystalline polymer, form a soft phase known as the amorphous phase providing the elastomeric properties and a hard phase or the crystalline phase marking the molecules dimensional stability [453]. For thin fibers to be electrospun, the polymer jet should stretch to a greater extent and should experience more whipping motion which results in a better orientation of the macromolecular chains. Moreover, the enhanced whipping motion encourages the complete crystallization of the polymer chains before reaching the collector leading to the formation of fibrils as the lamellar structure that is crystallized continues to undergo the stretching effect

of the fibers. This drawing phenomenon enhances the mechanical properties of fine fibers as the highly aligned and densely packed lamellar and mostly fibrillar structures afford an eminent resistance to tensile forces. For the fiber diameter to decrease, the polymer jet should experience less stretching and thinning effects which favors a less ordered arrangement of molecular chains. Furthermore, a complete crystallization might occur only after the jet has reached the collector which promotes the formation of a lamellar structure over an aligned fibrillary structure. The mediocre molecular arrangement is responsible for the decreased tensile strength and elasticity while the decreased crystallinity is responsible for the increased ductility [453-455]. Previous studies have shown that over a critical threshold diameter of approximately 500 nm, the mechanical properties start to decrease in a more progressive manner or even reach a plateau [453, 454]. The same trend is also observed in this work when taking a closer look at the Young's modulus values for D2, D3 and D4. When expanding the analysis and examining the fiber orientation within the whole fibrous mesh, one can clearly distinguish the considerable improvement in tensile strength and Young's modulus of aligned fibers over random fibers (Fig. IX.11). Yin et al. also perceived that the alignment of PLA fibers significantly enhances their mechanical properties [456]. This is owing to the highly porous structure of the random fibers interfering with the fibers mechanical properties to a great extent. Additionally, throughout the tensile loading, only the fibers that are positioned along the loading direction undergo stretching forces, whereas the perpendicular fibers are not subjected to any force [457]. In return, the diminished porosity and the increased packing density of aligned fibers trigger enhanced mechanical properties. Moreover, the ordered arrangement of the aligned fibers also play a role in the strengthening of the whole mesh in the same way as the orderliness of the molecular chains can affect the strength of a single fiber.

The random fibers also show a considerable increase in ductility compared to aligned fibers. This is presumably attributed to the possible movement of random fibers having room to align which increases the mesh extensibility. In contrast, the aligned fibers are densely packed which limits the fibers movement and therefore the mesh extensibility.

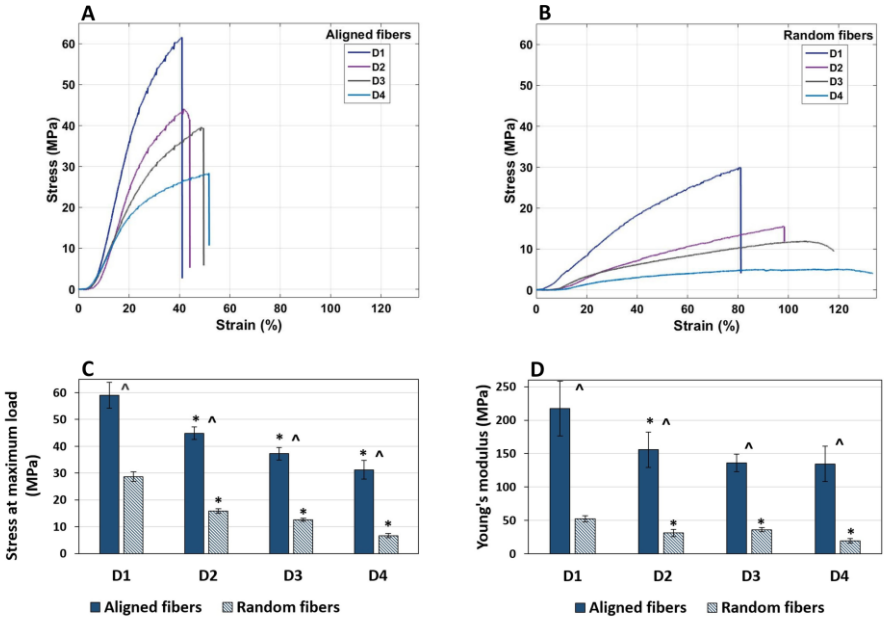

Fig. IX.12. *Mechanical properties of PCL fibers having different fiber diameters and orientations. (A: Stress-strain curves of aligned PCL fibers; B: Stress-strain curves of random PCL fibers; C: Histograms of stress at maximum load, D: Histograms of Young's modulus; *: statistically significant difference between 2 consecutive samples within the same aligned or random fiber group; ^: statistically significant difference between aligned and random fibers electrospun with the same parameters; $P < 0.05$).*

IX.4. Conclusion

This chapter describes the electrospinning of random and aligned PCL fibers with a wide scale of fiber diameters using the unconventional and benign solvent system FA/AA. The results are divided into 3 parts which deal with tackling the fiber alignment, broadening the fiber diameter range and analyzing the physico-chemical properties of the different generated fiber conditions. First, a profound study of the effect of the collector design and collector RS on fiber alignment has led to the fabrication of a novel collector consisting of a flat cylinder able to engender simultaneous mechanical and electrical effects leading to a high degree of fiber alignment. Secondly, the fiber diameter is addressed by varying and analyzing the influence of polymer

concentration, TCD and relative humidity. Increasing PCL concentration and RH and decreasing TCD has led to an increase in fiber diameter with some variances between aligned and random fibers. As a result of excessive fine-tunings of the above mentioned electrospinning parameters, a very broad range of fiber diameters going from 94 to 1548 nm and from 114 to 1408 nm is created for random and aligned fibers respectively.
XPS measurements have shown that the chemical composition on the surface of all sample conditions is similar and in accordance with the chemical structure of PCL, thus confirming that the electrospinning process is not causing any chemical group remodeling or segregation. Despite the unchanged surface chemical composition, considerable variances in WCA values are however detected. The hydrophobic behavior observed in all fiber meshes tends to amplify when decreasing the fiber size with a particular pronounced enhancement on aligned fibers. In addition, the tensile stress and Young's modulus are significantly higher for aligned fibers compared to random fibers. Moreover, within the same fiber orientation group, the mechanical properties increase with a decreased fiber diameter. Overall, the very flexible ability of FA/AA to cover a wide-ranging diameter scale of random and highly aligned PCL fibers is a major breakthrough compared to the other more toxic and less flexible solvent systems. Since every application demands a number of specific fiber properties, this paper represents a good reference on how to create PCL fibers having different orientations, diameters and physico-chemical properties from a unique and benign solvent system.

Chapter X. Synergetic Effect of Electrospun PCL Fiber Size, Orientation and Plasma-modified Surface Chemistry on Stem Cell Behavior

The results of Chapter X will be published in the following international peer-reviewed journal:

Ghobeira, R., Philips, C., Liefooghe, L., Verdonck, M., Asadian, M., Cools, P., Declercq, H., De Vos, W., De Geyter, N. & Morent, R.
Synergetic effect of electrospun PCL fiber size, orientation and plasma-modified surface chemistry on stem cell behavior
Applied Surface Science, 485(2019): 204-221 (2019).

X.1. Introduction

After studying the physico-chemical and bioresponsive effects of plasma activation on PCL films and electrospun fibers, this chapter comes to expand the investigations by tackling particularly different fiber sizes and orientations. The study will therefore pave the way towards a critical optimization of the previously designed biomaterials to obtain scaffolds being able to achieve the near-perfect complex ECM biomimicry. To the best of our knowledge, no study has dealt so far with the synergetic influence of PCL fiber size, orientation and surface chemistry on any cell type behavior; the few related studies found in literature were focused on only one or very rarely on two of the three factors [78, 79, 209, 278].
Therefore, this chapter is divided into 2 main parts: 1-plasma activation of highly aligned and random PCL fibers with 3 different diameters each using a DBD operating in argon at medium pressure; 2-in vitro study using ADSCs. The fiber morphology and surface chemistry are characterized by means SEM, XPS and WCA. An extensive comparative study is performed by subjecting the samples to different cell tests: MTT assay, live/dead staining, actin staining and dehydration followed by SEM imaging.

X.2. Experimental conditions

All experimental details can be found in Chapter VI. The parameters that are specifically used in this chapter are summarized in tables X.1 and X.2 and Fig. X.1.

Table X.1. *Experimental conditions*

Base material	• PCL
Biofabrication method	• Electrospinning: - Collector: cylinder (length = 1 cm, radius = 5 cm) - RH: 45 %
Plasma treatment	• Argon DBD: - Power= 1.47 W - Glow mode
Characterization techniques	• WCA: - 2 µl-drops of distilled water - Reported value: average of 4 values measured on 4 different samples.

	• XPS: - Reported value: average of 4 values measured on 2 different samples. • SEM: - Accelerating voltage: 10 kV. - Reported fiber diameter value: average calculated over 100 fibers on 2 different samples.
Sterilization	• UV: - Wavelength: 254 nm - Exposure time: 3 h
***In vitro* cell tests**	• ADSC culture: - 10 000 cells/100 µl per sample • MTT assay: - Performed on 5 samples/condition.

Table X.2. *Electrospinning parameters used to generate random and aligned fibers of different diameters*

Fiber orientation	**Random fibers**			**Aligned fibers**		
Concentration (%)	20	24	28	20	20	28
TCD (cm)	20	15	15	20	15	15
RS (rpm)	100	100	100	3000	3000	3000
Averge diameter +/- standard deviation (nm)	**232.3 +/- 39.1**	**500.4 +/- 136.6**	**1272.3 +/- 382.8**	**225.6 +/- 40.9**	**482.6 +/- 183.9**	**1173. 4 +/- 286.7**

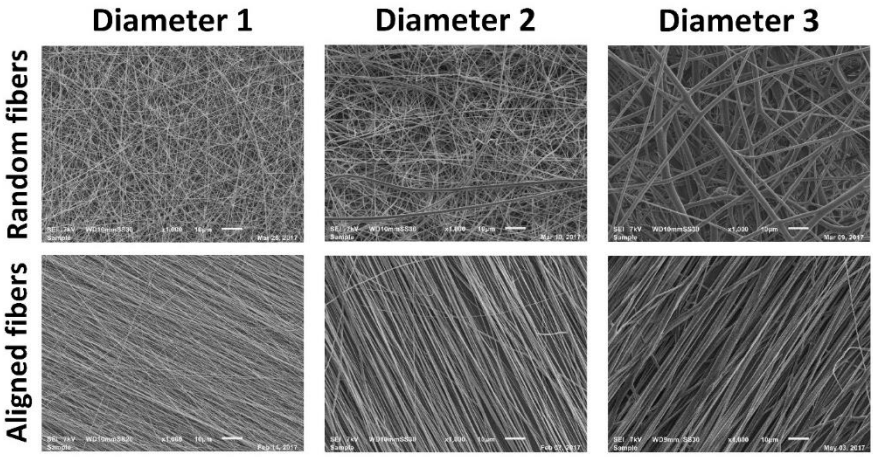

Fig. X.1. *The obtained PCL fibers.*

X.3. Results and Discussion

X.3.1. XPS analysis

A clear-cut evaluation of the surface elemental composition, based on XPS measurements, is first carried out on untreated fibers to check if the electrospinning process is not favoring the segregation of particular chemical functionalities on the fiber surfaces. This might induce a different surface chemistry which may be characteristic for a specific fiber orientation or fiber size since different electrospinning parameters are applied to produce each fiber condition. Nevertheless, XPS survey scan analysis shows that the surface oxygen (≈ 24%) and carbon (≈76%) content is nearly the same for all fiber conditions under study with no significant variations. Moreover, the detected fiber surface composition, which was also perceived on spin coated PCL films, is in conformity with the PCL chemical structure contrarily to what was observed in previous studies [445]. For instance, Martins et al. electrospun PCL fibers with chloroform and N,N-dimethylformamide (DMF) as solvent mixture and found an oxygen surface percentage of only 19% [88]. Ko et al. obtained an oxygen content of 22.6% on the surface of PCL fibers electrospun using acetone [458]. A remarkably lower surface oxygen amount of 9.7% was perceived by Yan et al. on PCL fibers after electrospinning using the solvent system chloroform/methanol [459, 460]. The chemical remodeling such as the enrichment of carbon on the fiber surface that occurred in former papers, is thus not taking place in the present study using acetic acid/formic acid as solvent system. The

effect of electrospinning on the rearrangement of lower binding energy groups on fiber surface was already investigated for several polymers such as PLA and PLA-poly(ethylene glycol) but not for PCL [265, 444]. Since different electrospinning parameters give the same surface chemistry on the different PCL fiber conditions, one can presumably conclude that the solvent system utilized to dissolve PCL is mainly influencing the chemical group remodeling which is pronounced with chloroform/methanol and not existing with acetic acid/formic acid.
After assessing the surface chemistry of the different pristine fibrous meshes, XPS measurements are also performed post-plasma treatment, in order to precisely detect the chemical modifications that are engendered. Fig. IX.2 depicts the oxygen percentage in function of argon plasma exposure time for the aligned and random fibers having different diameters. Although the treatment is sustained in an inert gas, a gradually ascending plasma exposure time is accompanied with a progressive increase in oxygen content attaining a maximum of approximately 30% for all fiber conditions. In return, the carbon content is proportionally decreasing as no other elements are incorporated on the surface throughout or after the plasma treatment. In order to obtain a clear insight on how oxygen-containing functionalities are implanted on PCL fibers, it is essential to elucidate the effect of the discharge gas on the different species reacting with the surface. Pure argon plasma contains several non-reactive species such as excited atoms, photons, electrons, molecules and non-reactive ions that are capable of breaking C-H and C-C chemical bonds and excite the PCL surface. Polymer radicals are thus formed which leads to the creation of a cross-linked network since these developed radicals tend to interact with other radicals of the neighboring polymer chains. Unlike air plasma treatment, argon plasma should only trigger this cross-linking and double bond formation since no chemically reactive species such as $O^{\cdot}$ and O_2 are present in theory. However, in fact, the working environment in the plasma reactor is not entirely pure. Oxygen impurities can emerge from gaseous components such as O_2 and H_2O that the plasma desorbs from the reactor inner walls during the treatment. Moreover, oxygen traces can also originate from an impure working gas or from the air lingering in the plasma chamber because of the incomplete pumping down and evacuation before running the treatment. These oxygen traces can then react with the polymer radicals induced by the plasma treatment to oxidize the surface through the implantation of certain bonds such as hydroxyl (C-O), carboxyl (O-C=O) and carbonyl (C=O). A post-treatment oxidation can also have an eminent influence on the incorporation of oxygen on the fiber surface [445, 461, 462]. The selection of argon as a discharge gas instead of air or oxygen stems from our previous study that showed PCL

fiber degradation after only 10 s of air plasma exposure [463]. The high quantities of oxygen species present in air plasma tend to etch the surface and damage the fiber morphology. The argon plasma treatment effect, in contrast, is saturated at an exposure time of 15s for all fiber conditions except R2 and R3 which already show a saturation of the plasma effect at 10s. This saturation is illustrated by a plateau holding on the maximum value (≈ 30%) of attained surface oxygen, signifying that a prolonged treatment time does not provoke additional chemical variations. This observation thus also shows that an argon exposure of at least 20 s is not degrading the fibers. Many studies carried out in the past have also detected an increase in oxygen content on PCL surfaces subjected to an argon plasma treatment[88, 459, 464]. However, the majority of these studies did not reach an oxygen amount of 30% especially when the initial amount is below 25%, thus highlighting the importance of the improved initial chemical properties of PCL fibers electrospun in this work.

When taking a closer look at the different fiber conditions, one can notice that although the difference in surface chemistry is negligible, the oxygen incorporation appears to develop in a slightly different trend. R2 and R3 fibers tend to incorporate a slightly higher percentage of oxygen at the different plasma treatment times with a saturation reached earlier (10 s) in comparison to the aligned and R1 fibers attaining a plasma saturation effect at 15 s. Moreover, the saturated R3 fibers show higher standard deviations in oxygen content suggestive of a less homogeneous fibrous mesh treatment. These observations are presumably associated with the distinct arrangement of macromolecules that are forced to follow certain geometrical positions for them to fit cylindrical fibers constrained in size. The electrospinning of thin nanofibers demands a pronounced stretching of the polymer jet that also experiences additional whipping motion resulting in more aligned and densely packed molecular chains. A polymer jet undergoing less stretching and thinning ends up with the deposition of bigger fibers made up of more randomly oriented molecular chains [453, 454]. The particular aligned chain assembly of thinner fibers probably makes the chemical bonds more protected by each other and less exposable to plasma. Moreover, a parallel organization of molecular chains gives rise to more Van der Waals interactions and hydrogen bonds between neighboring straight chains [465]. As a consequence, breaking surface chemical bonds to form radicals becomes harder and thus requires longer plasma exposure times. This elucidation is supported by the fact that PCL films which were previously subjected to an argon plasma treatment using the same DBD and process parameters, were saturated after a plasma exposure of only 3 s reaching a similar oxygen

content. This is due to the widely exposed macromolecules on the film surface [445].
When examining aligned fibers, the difference between the 3 diameters is trifling. This is due to the fact that the fibers are subjected to enhanced mechanical forces due to a high collector rotational speed stretching the fibers even more to ensure their deposition in an aligned modus. This leads to an improved alignment and adjoining packing of the molecular chains, making the implantation of oxygen tougher in comparison to random fibers [455, 466]. Moreover, aligned fibers can form more hydrogen bonds between each other as adjacent fibers are in contact along their whole length [465]. In contrast, the contact points between fibers in randomly deposited sheets are arbitrary and hence the formation of interfibrous chemical bonds is not homogenous throughout the fibrous membrane. Some locations can display more contacts where the fibrous network is dense and others can present more porous spaces and less fiber contacts, especially for the biggest fibers exhibiting larger interfibrous pores. This can possibly explain the relatively high standard deviations in oxygen content observed only for the saturated R3 fibers.

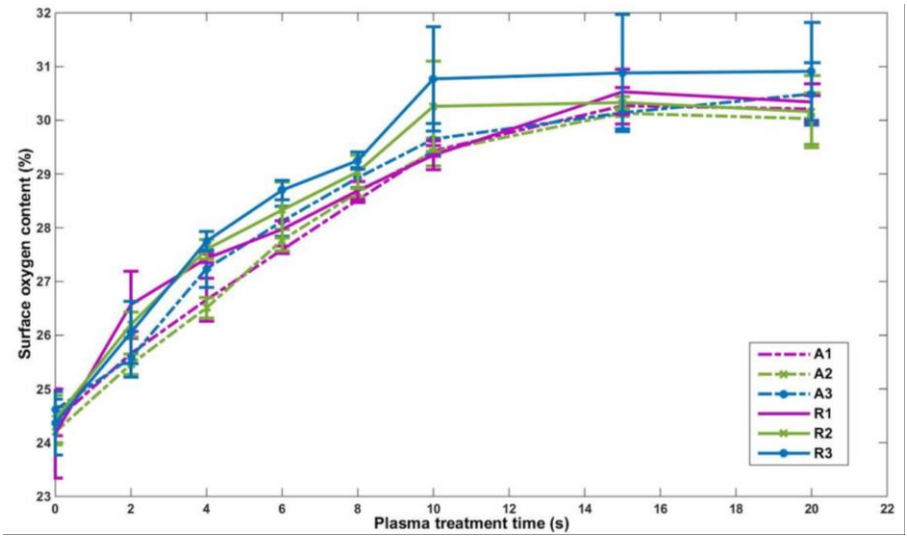

Fig. X.2. *Evolution of the surface oxygen percentage of PCL fibers in function of argon plasma exposure time.*

X.3.2. WCA analysis

The incorporation of oxygen-containing functionalities on the plasma-treated surface meshes, clearly beheld through XPS measurements, is known to enhance surface hydrophilicity thus leading to improved protein adsorption and subsequent improved cellular adhesion. However, this phenomenon is more complex than it appears. Very specific degrees of hydrophilicity tend to have tremendously different effects on how proteins adsorb onto a surface, resulting in the finding stating that each cell type favors a particular optimal WCA [261, 467]. Therefore, the hydro-properties of PCL fibers are also evaluated in the current work through WCA measurements since in addition to the surface chemistry, different mesh topographies engendered by the different fiber diameters and orientations, are known to markedly influence the solid-liquid interface. This is first proven by the fact that, untreated random and aligned fibers with different diameters display different WCAs despite possessing the same surface chemistry. WCAs of aligned fibers gradually decrease when increasing the fiber diameter (132° for A1; 127° for A2 and 119° for A3), however, random fibers show a more irregular trend with WCAs slightly fluctuating between different diameters (134° for R1; 128° for R2 and 132° for R3). In all cases, WCA above 100° are detected, thus situating the untreated PCL fibers between the super-hydrophobic and the hydrophobic classes. In contrast, a less hydrophobic state was previously sensed on untreated PCL films that showed a WCA of 74° [445]. A markedly enhanced hydrophobicity was also observed by Dolci et al. on PLA fibers compared to PLA films revealing a WCA of 121° and 90° respectively [447]. This shows that for the same structurally hydrophobic material, a boosted hydrophobicity is perceived on fibers compared to films due to the inter-fibrous pores triggering air entrapment and thus obviating the infiltration of water [446]. The behavior of air being trapped inside pores was already described by the Cassie-Baxter equation as "heterogeneous wetting" that leads to an amplified WCA. However, in 1936, an opposite trend portrayed by the Wenzel equation was formulated on the basis stating that an increased roughness leads to a lower WCA because of water infiltration in the roughness furrows. This is denoted as "homogeneous wetting". The rivalry between homogeneous and heterogeneous wetting which aims to minimize the Gibbs energy of the system and to accordingly define the resulting WCA of a rough surface, needs therefore to be understood [393]. Homogeneous wetting seems to surpass heterogeneous wetting in case of aligned fibers since the highly packing density of the parallel fibers tends to form roughness creases instead of well delineated pores thus leading to less air entrapment. This finding is reinforced by the

observed decrease in WCA on increasing mesh roughness which is dictated by broadening of the fiber diameters. Many studies have indeed depicted that the roughness of a fibrous surface proportionally follows the fiber size [448, 449]. For instance, Kim et al. measured the topological properties of PCL fibrous meshes and found out a markedly increased roughness associated with an increased fiber diameter [450]. Random fibers, in contrast, do not seem to follow homogeneous wetting since the increase in fiber diameter and thus in mat roughness is not accompanied with a WCA decrease. The drop in WCA stemming from the increased roughness is most likely compensated by the enlargement of the pore size that causes more air entrapment leading to more or less similar WCAs on different fiber diameters. A balance between homogeneous and heterogeneous wetting can thus be discerned and is also confirmed by previous studies which also obtained unchanged WCAs on PCL fibrous mats with different fiber diameters [450].

When inspecting plasma-treated samples, one can notice the pronounced effect of argon plasma causing the WCA to massively decrease to values below 25° and even attaining 0° in some cases (see Fig. X.3). This effect is attributed to the polar oxygen-containing groups that are incorporated on the fibers during and after plasma exposure causing PCL to become rather hydrophilic [445]. The massive inversion from super-hydrophobic to super-hydrophilic states was also perceived in a few studies using plasma as surface functionalization method for PCL fibers [88, 278, 416, 459, 463]. In contrast, a previous study conducted by our research group showed that the lowest WCA that a PCL film could reach after plasma treatment was 55° [445]. The more pronounced wettability enhancement of fibers compared to films is presumably accredited to the high fiber surface-to-volume ratio resulting in a relatively large surface area that can be treated. Moreover, when a certain threshold of chemical hydrophilicity is attained, porous structures tend to have a boosted wettability because of the penetration of water inside the pores. This is due to the fact that drops of very low tension start to overcome air entrapment by the incapability to be longer held on the surface [446]. Despite the fact that only slight differences in oxygen content occur between the different fiber conditions, differences in WCAs are plainly noticed and are portrayed as function of plasma treatment time in Fig. X.3. To the best of our knowledge, no other studies have yet compared the wettability of different plasma–treated fiber sizes and orientations. For random fibers, the WCA tends to strongly decrease at shorter plasma exposure intervals for smaller fiber sizes (for R1: sudden decrease from 134° to 44° at 2 s; for R2: sudden decrease from 118° to 24° at 6 s and for R3: sudden decrease from 110° to 0° at 10 s). This is probably due to the higher surface-to-volume ratio of smaller fibers leading to a bigger

surface area that is treated. This fact explains the faster penetration of water resulting in a large decrease in WCA at shorter plasma treatment times. As the fiber diameter increases, a smaller surface area is treated and the pore size increases enhancing the effect of inter-porous trapped air bubbles thus slowing down the decrease in WCA. After a certain treatment time (6 s for R2 and 10 s for R3), enough oxygen functionalities are however incorporated to overcome the effect of air entrapment and the WCA undergoes a sudden decrease. The WCA saturates at a value of 25° for R1 while it attains 0° for R2 and R3. This is due to the larger pore size in R2 and R3 causing the water drop to fully penetrate inside the mesh.

An opposite effect is observed for the aligned fibers. The WCA tends to decrease faster for larger fiber diameters (for A1: sudden decrease from 88° to 28° at 6 s; for A2: sudden decrease from 112° to 26° at 4 s and for A3: sudden decrease from 119° to 41° at 2 s). This observation is again due to the fiber alignment and high packing density resulting in a decreased porosity. Therefore, the effect of air entrapment in the pores is not influencing the WCA values to a large extend and the high packing density reduces the surface area exposed to the plasma treatment. Homogeneous wetting which is in close correlation with the mesh roughness remains the main actor of the system here. The increased roughness of larger diameters can explain the faster decrease in WCA values of A3 and the complete penetration of the water drop for the samples A2 and A3. In contrast, the decreased roughness and pore size of A1 fibers results in a WCA saturation value of 19° instead of 0°.

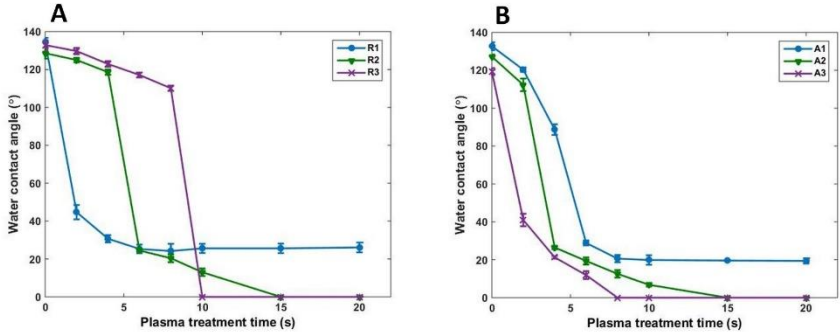

Fig. X.3. *Evolution of the WCA values in function of argon plasma exposure time (A: Random fibers; B: Aligned fibers).*

X.3.3. SEM analysis

Besides the beneficial surface chemistry modification, an extra decisive key approving plasma treatment effectiveness is its adeptness to prevent fiber morphological damage and scale variations. To examine this, SEM images are taken after a plasma exposure time of 15 s which coincides with the chemical saturation effect of all fiber conditions. The physical effects of extended treatment times are also evaluated by visualizing the fibers exposed to plasma for 1 min (Fig. X.4). All fibers are found to retain their morphological features without any melting or flattening after 15 s of plasma treatment. Moreover, a preservation of fiber scale is detected as almost similar diameter values are obtained pre- and post-plasma treatment. Therefore, 15 s of argon plasma exposure is capable to maximally functionalize PCL fibers of different diameters and orientations without affecting their topography. Sankar et al. also perceived no deformities on PCL nano- and microfibers after subjecting them to a mild argon plasma treatment [464]. However, extending the plasma treatment time to 1 min starts to lead to some physical alterations ranging from trifling to serious deteriorations that appear distinctively on the different fiber conditions. Two phenomena damaging and antagonistically changing the fiber diameter are initiated at longer plasma stages: melting and etching. On the one hand, the melting effect is characterized by the enlargement of fiber sizes, the occurrence of melted joining points and the collapsing of neighboring fibers. It is presumably due to the electrodes that get heated at prolonged plasma ignition time because of the high energy supplied by the plasma source. On the other hand, the etching effect or surface erosion, although mainly enhanced in oxygen plasmas, is also found to be induced by argon plasma and is illustrated by fiber thinning. This phenomenon is caused by the extensive amount of chain scissions that occur in a certain treatment interval, thus dictating the generation of oligomers and the desorption of volatile compounds from the fiber surface [445]. In addition to the visual SEM inspection, both described effects are also evidenced by the large standard deviations obtained when calculating fiber diameters. A conspicuous observation that also cannot be overlooked is the different damage intensity between random and aligned fibers. Random fibers are more severely altered as melted contact points are frequently occurring (R2-R3) and fibers are collapsing (R1), thinning (R2) and severely melting (R3). Aligned fibers only show some melted point-bonded junctions (A2) and trivial fiber thinning (A3), while the thinnest fibers do not show any sign of damage. This deep scrutiny led us to the conclusion that increasing fiber size is associated with a growing risk of drastic morphological alterations. In fact, the distinct molecular chain

arrangement, crystallinity and hence mechanical properties of different fiber conditions are responsible for these diverse responses to plasma. Nanofiber diameter and their resulting crystallinity are directly affected by whether a complete crystallization occurs before or after the polymer jet has reached the collector during electrospinning [454]. As already mentioned, the polymer jet experiences more whipping motion and extra elongation when generating thinner fibers. This leads, besides the formation of an aligned fibrillary structure of molecular chains, to a complete crystallization of the jet before attaining the collector. Moreover, the rise in the crystal phase is due to the increase in inter- and intramolecular interactions that contribute to securing the molecules in a compact conformation [465]. When the polymer jet undergoes less stretching, crystallization takes place only after reaching the collector and the molecular chains accommodating thicker fibers are deposited in a misaligned non-packed lamellar structure [453, 454]. First, the increased crystallinity of thinner fibers is associated with an increase in melting temperature rendering them less sensitive to heat [465]. Moreover, the locked molecules in a packed configuration have a limited degree of freedom to deform and are protecting each other from extensive chain scission. In contrast, the poor molecular arrangement, crystallinity and intermolecular interactions in larger fibers increase the molecules degree of freedom rendering them more susceptible to move and deform. Therefore, the most pronounced damage is observed for the thickest random fibers. When comparing between aligned and random fibers, some authors have noticed an increased crystallinity degree of aligned fibers [455, 465, 466]. The fiber deposition on high speed rotating collectors is shown to enhance the crystal phase owing to the extra stretching experienced by the macromolecules that concomitantly induces an additional improvement of molecular orientation. This partly explains the lower vulnerability of aligned fibers to melting and changes in their morphology. Furthermore, the decreased porosity of aligned fibers, together with the interfibrous chemical bonds along their length, strengthen their resilience against deformation.

Based on the obtained results, a plasma exposure time of 15 s is adopted in the following experiments as this exposure time is sufficient to improve the surface chemistry while maintaining an ECM-like appearance.

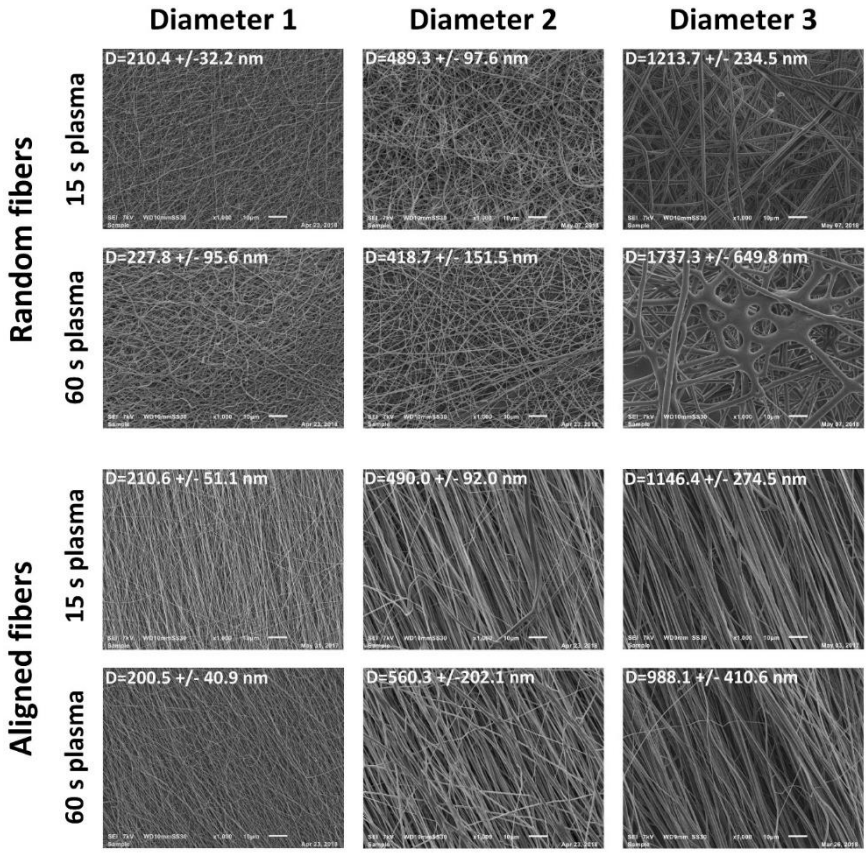

Fig. X.4. *SEM images of random and aligned PCL fibers subjected to argon plasma treatment of 15 s and 60 s.*

X.3.4. Ageing effect of plasma-treated fibers

After plasma treatment, the surface has a propensity to retrogress towards its untreated hydrophobic state over time [447]. In order to have control over this unfavorable phenomenon, so-called ageing effect, PCL fibers subjected to a 15 s plasma treatment are kept in ambient air at room temperature for 1, 3 and 7 days. The possible relapse of their surface chemistry is assessed by performing XPS measurements (Fig. X.5). These results reveal that the surface oxygen content slightly decreases over time with remarkably different decline profiles for the different fiber diameters and orientations. For instance, a small decrease in oxygen percentage (approximately 1%) is detected on A1

fibers 7 days post-treatment, whereas a more considerable drop (approximately 4%) is perceived on R3 fibers 7 days post-treatment. Overall, the obtained results clearly show that aligned fibers tend to withstand ageing more than random fibers. Moreover, a similar trend is observed with decreasing fiber diameters as less pronounced ageing behaviors are sensed on thinner fibers. An elucidation of the reasons underlying the ageing effect is essential for the subsequent in-deep understanding of the distinct behavior experienced by each fiber topography. Two previously described phenomena are envisaged to come into play. Firstly, the implanted polar groups have a tendency to re-orientate towards the fibers bulk in order to accommodate energetically more stable positions [270, 445]. The distinct molecular chain arrangement of the different fiber conditions is presumably intervening again in the practicability of chain movements inside the fibers and thus the ageing effect. The chains alignment and densely fastened conformation in aligned and thinner fibers hinders the movement and re-orientation of the incorporated functional groups towards the fiber bulk. In contrast, the randomness and the decreased packing density of molecular chains forming random and thicker fibers enables the plasma-induced polar groups to rotate and translate more easily. The second reason mediating the ageing behavior is the occurrence of post-plasma treatment reactions between the atmospheric surrounding minorities (e.g. CO_2 and H_2O) and the fiber surface neutralizing the inserted chemical groups [447, 463]. However, given the structure of fibrous networks, the treated fibers are not widely exposed to ambient air as neighboring fibers are shielding and protecting each other. The minor influence of post-plasma reactions can be confirmed by the negligible ageing of thin fibers undergoing a limited reorientation of their incorporated polar groups. In fact, previous results have shown that plasma-treated PCL fibers are less prone to age than PCL films as they are more exposed to air and composed of unpacked molecular chains [445, 463]. It is also worth mentioning that the oxygen content on all aged fibers remains considerably higher than on the corresponding untreated samples until at least 7 days post-treatment. Nonetheless, in order to minimize the ageing effect, plasma-treated samples are sterilized and seeded with cells directly after plasma treatment.

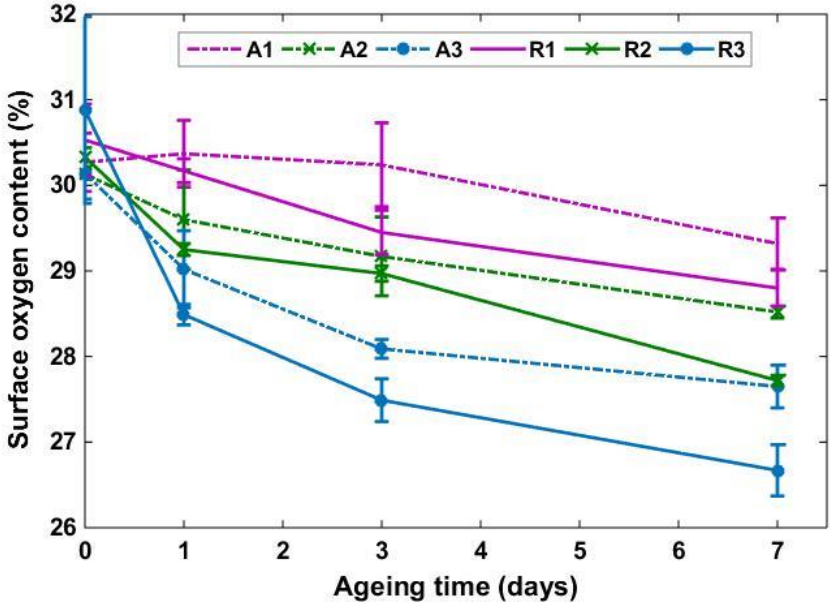

Fig. X.5. *Evolution of the surface oxygen percentage of PCL fibers as a function of ageing time (days) after plasma treatment.*

X.3.5. In vitro cell tests

After assessing the physico-chemical properties of PCL fibers, the behavior of ADSCs grown on the different fibers are investigated in this section. The coordinated effects of the fiber size, orientation and surface chemistry on the bioresponsive processes are profoundly studied. MTT assay (day 1, 3 and 7), live-dead staining (day 1 and 7), actin staining (day 3) and SEM imaging (day 1 and 7) are performed to evaluate the cell adhesion, proliferation, viability, cytoplasmic remodeling, morphology, orientation and infiltration. The cell alignment and nucleus circularity are quantified using the actin and DAPI stained images (day 3).

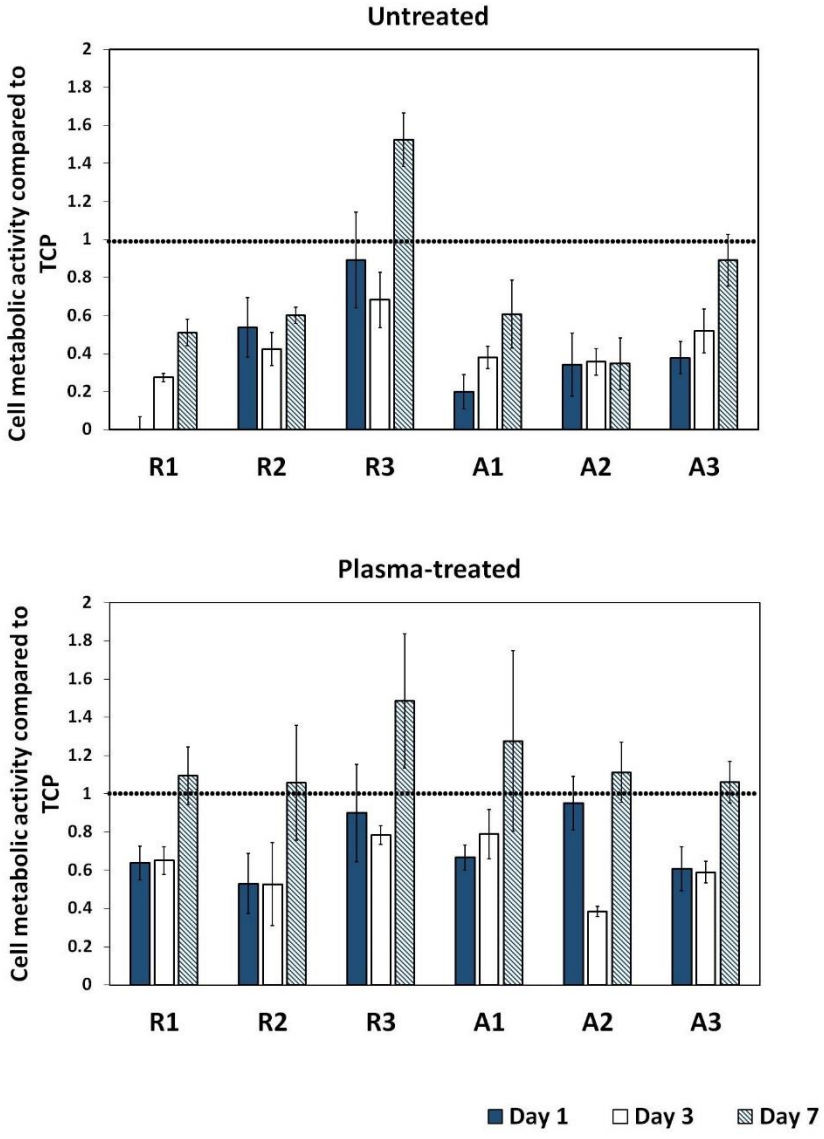

Fig. X.6. *Ratio of metabolically active ADSCs cultured for 1, 3 and 7 days on PCL fibers, relative to the TCP value (dotted line).*

- <u>ADSCs on untreated fibers of different diameters:</u> As a first step of this multifurcate cell study, one can already notice differences in cellular performances between untreated fibers of different sizes. This is quantitatively illustrated by MTT results (Fig. X.6) showing that the number of metabolically active cells adhering (day 1) and proliferating

(day 3 and 7) on the substrates increases with increasing diameter of random fibers. This trend is also present, but less distinguishable in case of aligned PCL fibers. These MTT results are in close correlation with the cellular morphology and cytoskeleton shape, as shown in Fig. X.7, X.8 and X.9. The quantitative gradual increase in cell attachment and proliferation on increasing fiber diameters is associated with gradual enlargement and spreading of the cytoplasm and regression of cell cluster occurrence. When surface properties are biologically inappropriate, cells tend to escape the surface by forming bunches and they prefer to attach to each other rather than on the substrate, as clearly discernable on the actin staining images of the thinnest fibers (Fig. X.7). In contrast, less cell clusters and some elongated cells can be detected on the thickest fibers. Nevertheless, it is worth mentioning that in case of untreated fibers, ADSCs performance remains defective even on the thickest fibers as poorly spread and rounded cells are still observed 7 days after cell seeding. The diverse cellular responses on different fiber conditions is presumably associated with the primary cell capture efficiency and cells/fibers contact in which cellular receptors, mainly the integrin proteins, play a primordial role [204, 463, 468]. The distinctive size of focal adhesion contacts of different cell types is presumably associated with their preference to specific topographical sizes [205]. Many studies have reported, in contrast to what is observed in this work, that the adhesion and subsequent proliferation of some cell types such as SCs, neural stem cells, fibroblasts and osteoblasts are enhanced when decreasing the fiber size [203, 204, 209]. This finding was linked to the fact that smaller fibers have larger surface-to-volume ratio and would probably bind more cell receptors. However, ADSCs seem to have relatively wide focal adhesion complexes in comparison to small-sized nanofibers. This gives rise to fewer anchor points weakening the complexes and leading to poor cell attachment on smaller fibers. When increasing the fiber diameter, an improved recruitment of integrins takes place directing the occurrence of more anchor points and resulting in more stable focal adhesion sites [211]. This can explain the superior cell adhesion, and spreading of ADSCs on larger fibers. The same trend was also previously detected when keratinocytes were seeded on different fiber sizes as they stayed spherical on the thinnest fibers and spread out on the thickest fibers [205]. Other important characteristics affecting cell adhesion are surface chemistry, wettability and roughness. A similar surface chemistry is detected on all untreated fibers causing super-hydrophobicity characteristics which negatively influence cell attachment. Therefore, one may think that the increased roughness on larger diameters is partly affecting and improving cell affinity. This preliminary conclusion is further confirmed by the study of Ahn et al.

showing that ADSCs that were seeded on roughness gradients of polyethylene films adhered better on rougher surfaces [467]. Nonetheless, a conspicuous observation that cannot be overlooked is the stagnation of the cells metabolic activity on the intermediate fiber diameter until day 7 and on the thickest diameter until day 3 only, which indicates relatively weak cellular processes after initial adhesion (Fig. X.6). This initial cell attachment is followed by a lag-stage phase during which the cells try to adapt to their surroundings. Cells that stay alive and that retain their activity during this post-adhesion phase manage to proliferate [445]. Therefore, ADSCs that attach to intermediate and thick fibers seem to be disturbed during this adaptation phase. This can be presumably attributed to the fibers depth or pattern height that were found, independently of the surface roughness, to be among the topographical factors influencing the long-term adhesion and the maturation of focal adhesions during the lag-stage [206]. The increased height of intermediate and thick fibers is thus slowing down the cell adaptation phase which causes a subsequent poor cell proliferation. Some studies have indeed reported boosted long-term cell adhesion and proliferation on lower height patterns [206, 207]. The metabolic activity of cells grown on the thickest fibers, contrarily to the intermediate fibers, again markedly increased at day 7. This can be due to the slightly lower cell sensitivity to fiber height on large fibers as SEM images (Fig. X.8-X.9) show that each cell tends to attach and elongate on a single fiber. Conversely, in case of the intermediate fiber diameter, each cell is adhering on multiple fibers, thus sensing more the fibers depth which retards its proliferation. Lastly, very few dead cells (red cells) are detected on live-dead staining images obtained 1 day after cell seeding and even fewer are seen 7 days after seeding which indicates the non-toxicity of untreated PCL nanofibers maintaining cell viability independent of their size and orientation (Fig. X.10-X.11).

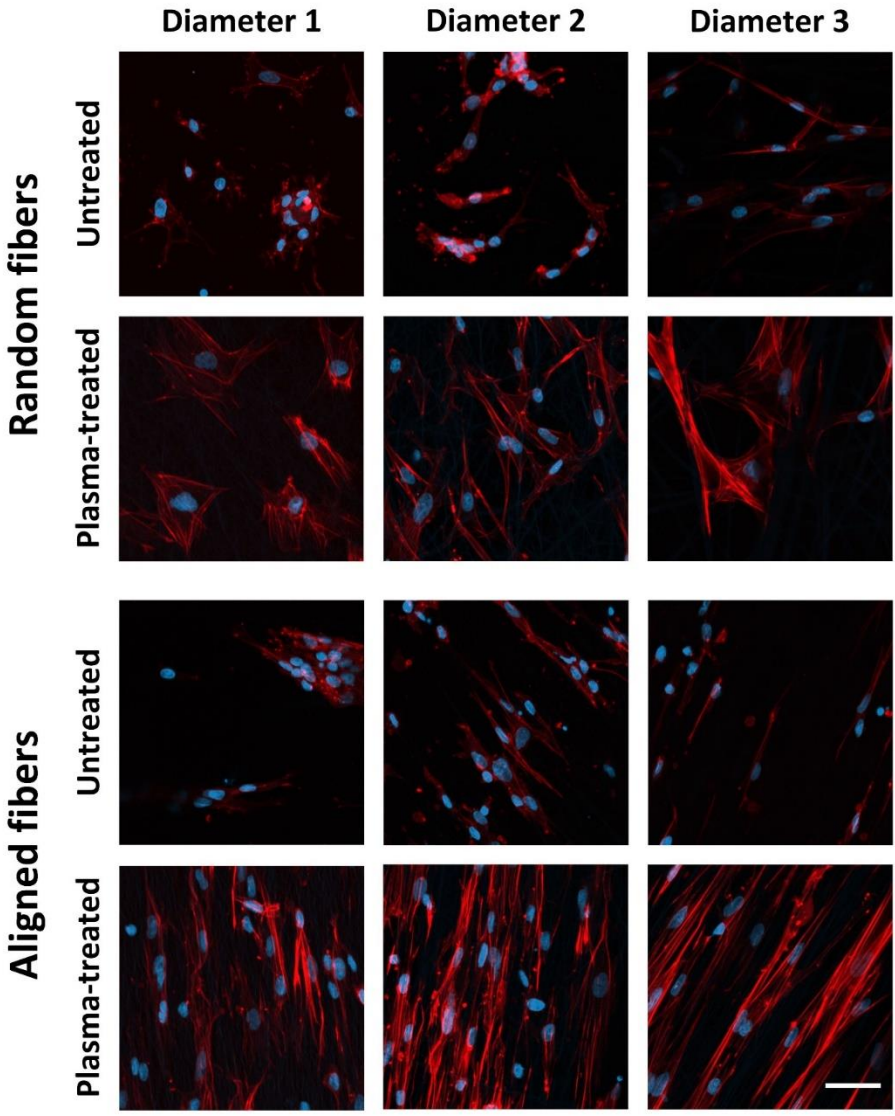

Fig. X.7. *Fluorescent micrographs after actin (phalloidin-rhodamin, red) and nuclei (DAPI, blue) staining of ADSCs cultured for 3 days on PCL fibers (Scale bar = 50 µm).*

- **ADSCs on untreated fibers of different orientations:** Beside the fiber size, cell test results evidently reveal the great influence of fiber orientation on ADSC adhesion, proliferation and particularly cytoskeletal reshape and morphology. First, MTT results point out a

generally higher number of metabolically active cells adhering and proliferating on random fibers compared to aligned fibers at day 1, 3 and 7 of cell culturing (Fig. X.6). Jahani et al. also found out an enhanced proliferation of MSCs on random PCL fibers compared to aligned fibers [469]. A possible explanation for this finding is the presence of more interconnected pores and multidirectional overlapping fibers forming numerous joining points on randomly deposited sheets. This random structure assists the formation of more focal adhesion complexes leading to a greater number of cells. Moreover, crossing multiple directions requires more cellular energy and thus an increased metabolic activity of ADSCs [469, 470]. Deviating from the previously mentioned trend, the metabolic activity on the thinnest fibers does not differ between random and aligned fibers. This is presumably due to the fact that the probability of encountering misalignments in aligned fibers is higher for smaller fiber diameters because of the increased whipping motion that is partly in charge of thinning the fibers during electrospinning [211]. Consequently, joining fiber contacts occur more frequently on the thinnest aligned fibers leading to a cellular response similar to the one perceived on random fibers. When taking a closer look to the cell morphology, one can already notice differences between aligned and random fibers despite the cell spherical shaping and clustering tendency on untreated samples (Fig. X.8-X.9). Actin staining and especially live-dead staining illustrate that the cells starting to spread out are aligned in the main axis direction of the aligned fibers while they are randomly oriented on random fibers (Fig. X.7, X.10, X.11). These observations emphasize the great potential of fiber alignment in providing cell contact guidance. Some other cell types such as neural stem cells, fibroblasts, embryonic stem cells and MSCs were also shown to elongate along the main axis of aligned fibers and to spread arbitrarily on random fibers [79, 211, 469, 470]. This is due to the alignment of focal complexes on aligned fibers during the focal adhesion phase described earlier. Moreover, a traction force is exerted on the actin cytoskeleton in the same direction of aligned fibers promoting protrusions and actin polymerization parallel to the underlying fibers. This reveals again the extremely precise interplay between the substrate and the cytoskeleton filaments, particularly the actin filaments as actin disrupting agents previously attenuated cellular alignment [203]. Live-dead staining results do not reveal any

differences in cell viability between random and aligned fibers (Fig. X.10-X.11).

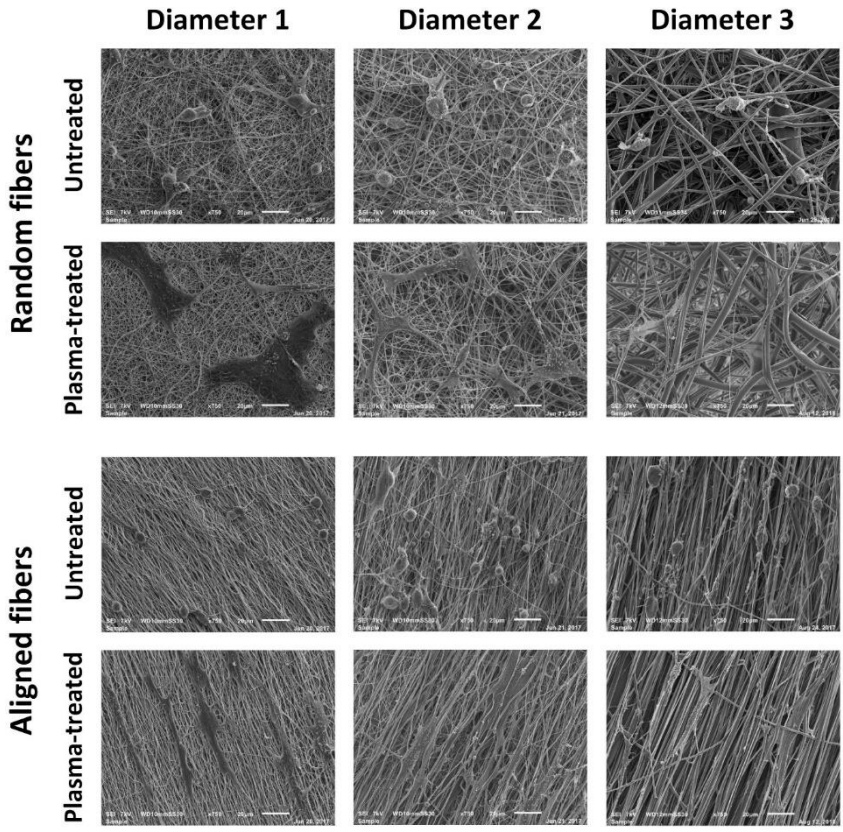

Fig. X.8. SEM images of ADSCs cultured for 1 day on PCL fibers of different conditions (Scale bar = 20 µm).

- <u>ADSCs on untreated versus plasma-treated fibers:</u> Plasma treatment strikingly transfigures ADSCs bio-response to PCL nanofibers of all topographical conditions. First, a significant increase in the number of metabolically active ADSCs is detected on the plasma-treated fibers with the smallest and intermediate diameters compared to their untreated counterparts (Fig. X.6). However, the number of viable cells adhering (day 1) and proliferating (days 3-7) on the thickest fibers does not significantly differ between untreated and plasma-treated samples, given that adhesion and proliferation were already improved when increasing fiber diameter (Fig. X.6). Chaurey et al. also detected a

greater enhancement of fibroblast adhesion on small fibers compared to thick fibers after surface functionalization by poly-L-lysine [211]. Although plasma functionalization does not exhibit large cell density differences on all fiber conditions, great differences in ADSCs morphology can however be detected even on the thickest fiber diameters. Actin staining images (Fig. X.7) clearly show the disappearance of cell clusters on treated fibers, which is the first sign of enhanced cell attachment to the surface. Moreover, cell shape and dispersion change markedly, as very well spread out and dispersed cells covering almost the entire surface are visualized: star-like and spindle-shaped cells are mainly detected on random fibers, while well-elongated and parallel cells are spotted on aligned fibers (Fig. X.7). More evident distinctions are noticed on the SEM images that show, regardless of the fiber condition, completely rounded 3D cells with tiny cell areas in close contact with untreated fibers and 2D planar and stretched out cells firmly fastened to plasma-treated fibers (Fig. X.8-X.9). Additionally, cells on the plasma-treated samples tend to infiltrate in the fibrous mesh especially in case of the thickest fibers. This enhanced ADSCs performance is attributed to the increased plasma-induced hydrophilicity that allows for the adsorption of more proteins without altering their natural conformation. Consequently, more cellular receptors can bind to the adsorbed proteins leading to numerous focal adhesive sites enhancing cell adhesion. Contrarily, the super-hydrophobicity of untreated fibers severely hampers protein adsorption and therefore limits the focal adhesion resulting in barely attached ball-shaped cells[445, 463, 464]. In-deep analysis elucidates that the introduced oxygen-containing functionalities responsible for the increased wettability are specifically correlated with the enhanced cell adherence and growth. Carboxyl, carbonyl and hydroxyl groups, that steadily bind proteins, recruit more integrins and act as a glue strongly connecting and stabilizing the anchor points of focal adhesive complexes [88, 459, 468]. Therefore, the few anchor points that might still arise on smaller fibers, as described previously, are strengthened which explains the markedly improved adhesion and subsequent proliferation. Moreover, it is known that tensile forces are generated by the cells to resist the fibers and that an isometric tension is boosted within the cell when its receptors bind to proteins. These forces alter the remodeling of cytoskeletal filaments causing their reassembly and changing the cell morphology from 2D to 3D after initial adhesion [468]. This can explain the long-standing 3D cell rounded shape on untreated fibers even after 7 days of cell culturing. Nevertheless, the stable focal adhesion sites induced by the oxygen-containing groups are probably hindering the cytoskeletal reassembly in case of plasma-treated fibers, which justifies the irreversible 2D planar shape of cells after their

adhesion. Prabhakaran et al. underlined the particular importance of plasma-induced surface oxygen groups by obtaining an improved SC adhesion on air plasma-treated PCL fibers, not only in comparison to untreated fibers, but also when comparing to PCL/collagen fibers [471]. Other studies also showed that the cytocompatibility of other cell types such as osteoblasts, embryonic stem cells, endothelial cells and chondrocytes is significantly boosted on plasma-treated PCL fibers [88, 459, 470, 472]. Lastly, plasma treatment does not seem to have a toxic effect on the cells as almost no dead ADSCs are detected on the live-dead staining images of day 1 and very few dead cells are perceived at day 7 (Fig. X.10-X.11). As plasma treatment is favoring cellular infiltration in-between the fibers, the presence of dead cells at day 7 might be due to the PBS inability to rinse away the infiltrated cells that did not survive during the lag-stage.

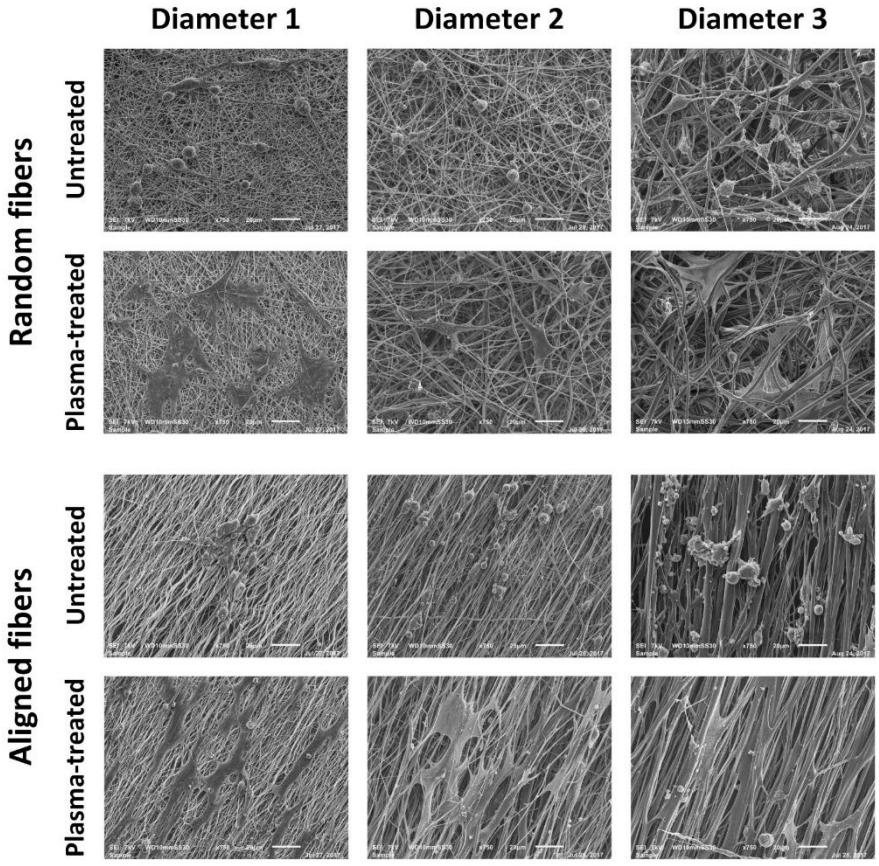

Fig. X.9. *SEM images of ADSCs cultured for 7 days on PCL fibers of different conditions (Scale bar = 20 μm).*

- **ADSCs on plasma-treated fibers of different diameters:** When taking a closer look at the plasma-treated fibers of different diameters, one can notice some variations in ADSCs behavior. As already mentioned, MTT results show a bigger post-treatment enhancement of cell density at day 1, 3 and 7 on the thinnest fibers as these fibers had the poorest cytocompatibility prior to the plasma treatment (Fig. X.6). This observation can be linked to the different surface wettability between the thinnest fibers on the one hand and the intermediate and thickest fibers on the other hand. After plasma treatment, A1 and R1 saturate at a WCA of 19° and 25° respectively, while larger fibers were fully penetrated by water, their WCA being 0°. Despite the positive effect of hydrophilicity in enhancing protein adsorption, the super-hydrophilicity of thick fibers seems to be a limiting factor. Protein adsorption takes place when proteins displace the water molecules adsorbed on the surface. This displacement becomes difficult on super-hydrophilic surfaces as they exhibit a greater electrostatic force at the water/solid interface [464]. This explains the minor ADSCs density improvement on thick fibers. In fact, previous studies have shown that each cell type favors a particular surface wettability. For instance, fibroblasts and endothelial cells adhere better on surfaces with a WCA of 55° while osteoblasts prefers a WCA of 64° [416, 463]. ADSCs were also noticed to behave better on polymer films with moderate hydrophilicity (≈ 60°) [445, 467]. Controlling the WCA of the PCL fibers to attain a moderate hydrophilicity while introducing a maximal amount of oxygen-containing groups is very difficult, if not impossible. Nonetheless, the increased surface area and roughness of the fibers compared to films comes to compensate the excessive fiber hydrophilicity as ADSCs were perceived to adhere better on rough surfaces.
  Similar to what is observed for the untreated fibers, a stagnation or even decrease in cell metabolic activity is distinguished on plasma-treated fibers at day 3. This observation can be attributed to the depth of the intermediate and thicker fibers negatively affecting the ADSCs during the lag-stage. However, in contrast to the untreated fibers, a remarkable increase in ADSCs metabolic activity is again seen at day 7 especially in case of the intermediate fibers, indicative of outstanding proliferation (Fig. X.6). Pappa et al. also obtained, based on MTT results of fibroblasts grown on plasma-treated PCL fibers, a decrease in metabolic activity at day 3 and subsequent increase at day 7 [278].
  Actin staining and SEM images (Fig. X.7-X.9) of plasma-treated random fibers visualize a gradual change from dilated and more circular cell shape to stretched out and more elongated cell shape on fibers with increasing diameters. ADSCs adhere on multiple fibers and

therefore extend multi-directionally on the smallest fibers. A different trend is observed for thicker fibers: cells continue to adhere on multiple fibers but extend along a few preferred fiber axes on R2 and along one preferred fiber axis on R3. Given the fact that the length of an R3 fiber in between crosslinks is relatively large compared to the ADSC dimension, a partial alignment of the cells is sensed. At some points where numerous fibers converge, ADSCs still stretch multi-directionally. These ADSCs morphologies are consistent with other cell types such as neural stem cells and SCs when seeded on random fibers of different sizes [204, 473]. An ADSC bipolar and parallel fashion is however observed on aligned fibers compared to the multipolar cell shape on random fibers. When increasing the fiber size, each cell tends to attach to fewer number of fibers to a point where one cell is not anymore distinguished from a fiber on the thickest diameters.
A distinction of the essence, clearly observed on the SEM images (Fig. X.8-X.9), is the infiltration of ADSCs in between the pores of plasma-treated R3 fibers, and to a lower extend of R2 fibers mainly at day 7. The synchronic effect of larger pore size and plasma-optimized surface chemistry resulted into this deep and complete cell colonization of the fibrous mesh.

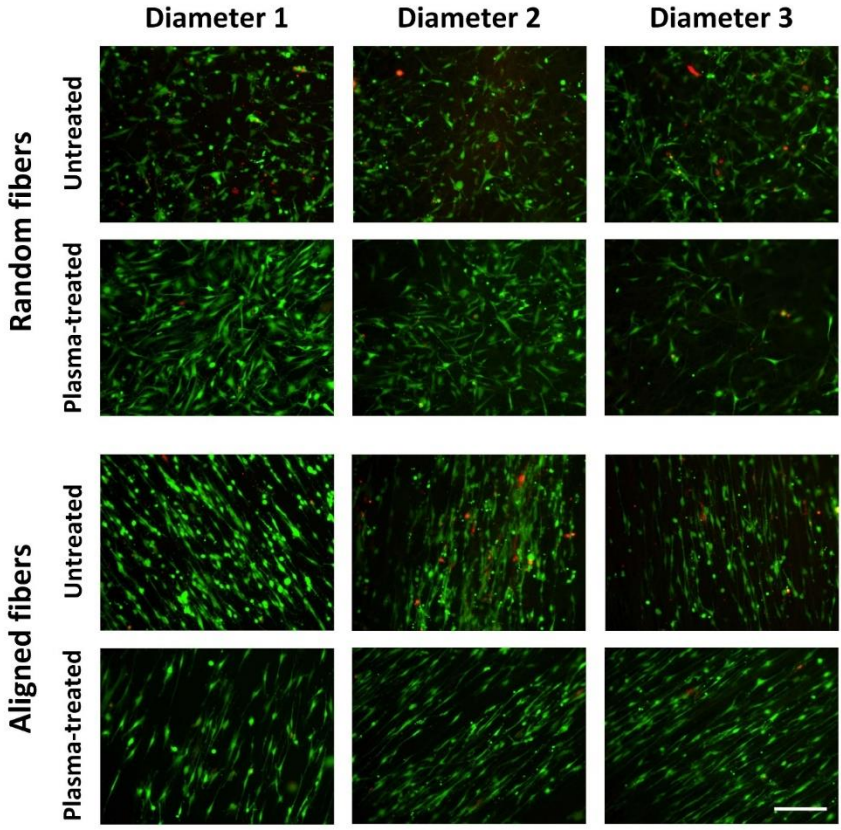

Fig. X.10. *Fluorescent images after live/dead staining of ADSCs cultured for 1 day on PCL fibers of different conditions (Scale bar = 200 μm).*

- **ADSCs on plasma-treated fibers of different orientations:** After subjecting the aligned fibers to a plasma treatment, significant differences in ADSCs metabolic activity are no longer perceived compared to random fibers (Fig. X.6). The presence of less fibrous joining points that reduces the amount of focal adhesion complexes on aligned fibers, is compensated by the incorporated polar groups strengthening these fewer adhesion sites. Therefore, similar adhesion efficiency and subsequent proliferation are detected on both fiber orientations. A more discernable difference in cell morphology is however visualized between aligned and random fibers after plasma treatment. In addition to live-dead staining images (Fig. X.10-X.11), SEM images also show the enhanced and complete alignment of ADSCs on aligned fibers and the absence of rounded cells (Fig. X.8-X.9). Actin

staining images come to corroborate these observations by highlighting the bi-directionally overextended cytoplasm of ADSCs on aligned fibers (Fig. X.7). In fact, a quantitative confirmation of this finding can be concluded from the pixel intensity histograms of the FTT output images plotted in function of the acquisition angle of the cells (Fig. X.12-A). The overall data point distribution shows higher and narrower peaks on the aligned fibers of different diameters in comparison to their random counterpart. This indicates that the cells are more accurately aligned on the aligned fibers with respect to the specific orientation axis of the underlying fibers. The low and wide distribution curve of random fibers reveals the arbitrary shape of cells grown on the multiple orientation axes of random fibers. An important distinction is the improved cell alignment on the biggest diameter of the aligned fibers proven by the further upgraded height and narrowness of the distribution curve. This can be explained by the increased probability of encountering misalignments on smaller fibers which deviates the cell that can continue growing in another direction. Moreover, each cell tends to attach to only one fiber of the biggest diameter leading to its overextension in the direction adopted by the neighboring cells growing on parallel fibers. The cell bipolar elongation can narrow the cytoplasm extensively to a point where the nuclei become compressed and therefore adopt a polygonal shape instead of a circular shape. This is visually discernable on the actin staining images of the plasma-treated aligned fibers. The nucleus circularity values on the different fiber conditions represent a quantitative affirmation of this observation (Fig. X.12-B). The cell nuclei on the untreated and plasma-treated random fibers have a circularity between 0.7 and 0.9 indicative of a more rounded shape because of the circular and multipolar cytoplasm. Rounded nuclei are still detected on untreated aligned fibers which shows the limited ability of the cell to extensively elongate. In contrast, a statistically different nucleus circularity value (around 0.5), indicative of a more elongated shape, is detected on the plasma-treated aligned fibers. This confirms again the positive effect of plasma in allowing a robust attachment and elongation of the cells that overextend to a point where their nuclei elongate as well.

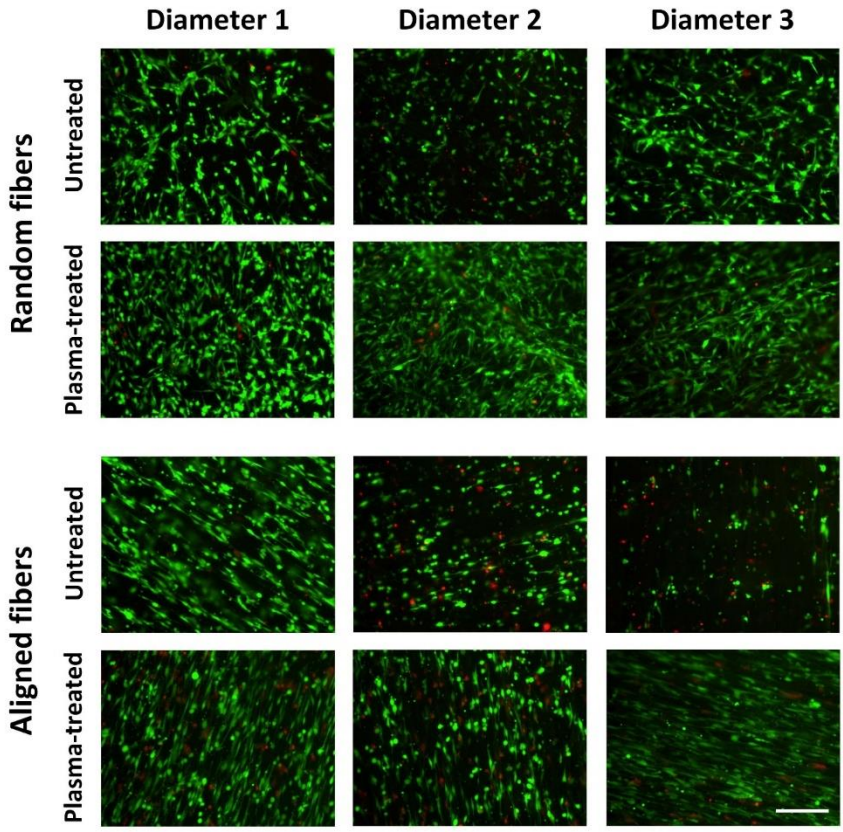

Fig. X.11. *Fluorescent images after live/dead staining of ADSCs cultured for 7 days on PCL fibers of different conditions (Scale bar = 200 μm).*

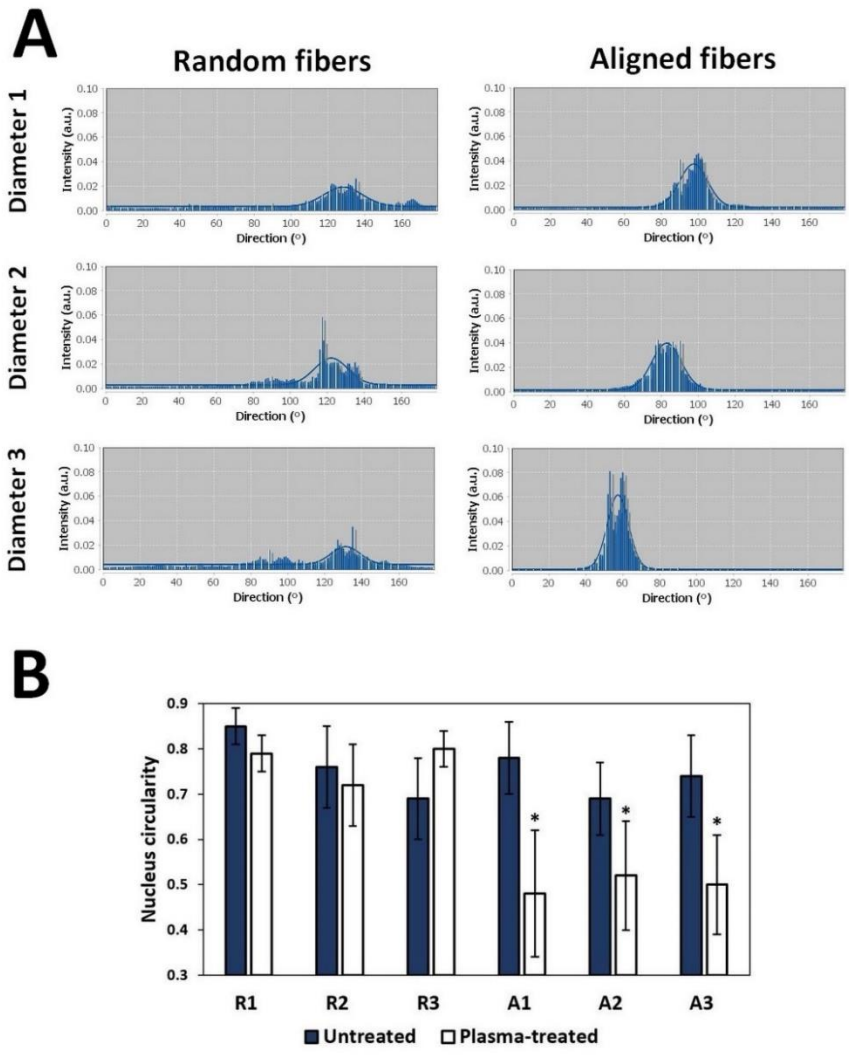

Fig. X.12. *FTT pixel intensity plots in function of the direction of the cells grown on plasma-treated fibers (A) and nucleus circularity of the cells grown on all fiber conditions (B) (*: statistically significant difference with respect to untreated fibers and random fibers).*

X.4. Conclusion

This present study highlights the synergistic effect of PCL fiber size, orientation and surface chemistry on the performance of adipose-derived stem cells. First, random and aligned fibers of 3 different diameters each are subjected to a DBD plasma treatment operating in argon at medium pressure, after which their physico-chemical properties are deeply examined pre- and post- treatment. XPS and WCA results reveal the prominent efficiency of plasma in enhancing the fibers hydrophilicity by grafting oxygen-containing polar groups on their surface. Despite the incorporation of approximately the same oxygen amount on all samples, WCA values significantly differ between the different fiber sizes and orientations thus emphasizing the outstanding influence of the fibrous mesh topography on the liquid-solid interface. SEM analysis shows that all fibers preserve their morphology and their scale after 15 s of plasma treatment which corresponds to the surface chemical saturation time. In contrast, an extended plasma exposure of 1 min starts altering the fibers morphological features with a growing risk of drastic damaging on thicker and random fibers compared to thinner and aligned fibers. The diverse responses to plasma stem from the distinct molecular chain arrangement and crystallinity of different fiber diameters and orientations. After analyzing the surface properties of untreated and plasma-treated fibers, ADSCs are also seeded on all samples under study. The bioresponsive processes arising from the interaction of the cell cytoskeleton and the fibers are profoundly examined based on the strongly coordinated interplay between fiber size, orientation and surface chemistry effects. Some distinctions in cell performance can already be distinguished on the untreated fibers of different diameters. A gradual increase in cell density and cytoplasm spreading is observed with increasing fiber diameter. This is presumably due to the wide focal adhesion complexes of ADSCs giving rise to fewer anchor points on small fibers leading to poor cell attachment and subsequent proliferation. Generally, the improved surface chemistry of plasma-treated fibers strikingly enhances the cell metabolic activity, adhesion, proliferation, cytoplasmic remodeling and morphology on all topographical conditions. ADSCs adhere on random fibers in a multi-directional fashion with a gradual change from dilated and more circular to stretched out and more elongated morphology on increasing diameters. In contrast, cells overextend and align in parallel and bi-polar fashion on aligned fibers with a tendency to attach on fewer fibers when increasing their size. An important distinction is the infiltration of cells in-between the pores of the thickest and plasma-treated fibers. Overall, non-thermal plasma technology constitutes a very promising surface treatment for successful fibrous implants of multiple TE

applications. As the desired ADSCs performance strongly depends on a specific end-application, appropriate fiber size and orientation can thus be selected accordingly. Therefore, this chapter represents an on-target reference paving the way towards the optimization of the previous generation of biomaterials.

Chapter XI. Plasma Treatment of Electrospun Polyactive® Nerve Guidance Conduits for Peripheral Nerve Regeneration

XI.1. Introduction

As already mentioned, the newly designed NGCs are up to the minute failing in promoting nerve regeneration within critical injury gaps and in attaining the functional outcome of autografts in all nerve gap sizes. Therefore, the goal of the final experimental study of this PhD dissertation is to design a novel NGC possessing ideal physical, chemical and cellular properties triggering potent regenerative capacity in severe PNIs. To do so, fibrous NGCs, made up of PEOT/PBT, are electrospun using optimized process parameters synergistically leading to the finest fiber diameter, alignment and porosity. Next to the significant importance of NGC topography, tailoring the surface chemistry is believed to play a pivotal role in the enhancement of glial and neural cell activities. Therefore, a surface functionalization is done via plasma technology that was, to the best of our knowledge, never applied to treat NGCs. A DBD operating in air or argon at medium pressure and a PJ operating in argon at atmospheric pressure are used with precisely fine-tuned parameters to reach and modify the NGC inner wall. In addition to a homogeneous surface treatment, a purposely engineered surface chemistry gradient with gradually increasing oxygen content is implemented along the conduit length. This is anticipated to boost nerve regeneration across critical gaps by favoring SC elongation and chemotaxis on the one hand and neurite sprouting and guidance on the other hand. The NGC morphology and surface chemistry are characterized by means of SEM and advanced XPS measurements. Finally, SCs are cultured on the NGCs as cellular cues to further promote nerve regeneration across long gaps. In addition to their active secretion of growth factors, SCs express cell adhesion molecules, build their own basal lamina and intensely assist, at a later stage, in the remyelination of growing nerve fibers [63, 66]. In fact, previous studies have revealed that scaffolds pre-seeded with SCs supported directed axons outgrows *in vitro* [246, 474]. Moreover, NGCs cultured with SCs prior to *in vivo* implantation considerably enhanced nerve regeneration compared to their acellular counterparts [64, 67]. A comparative *in vitro* study is thus performed to assess the behavior of SCs seeded on untreated and plasma-treated NGCs with homogeneous and gradient surface chemistries. After an overnight immersion of NGCs in FBS, two sets of experiments in which FBS is added or not to the culture medium are conducted. In this way, one can evaluate if cells would sense plasma-induced surface changes similarly in the absence or presence of proteins in the medium. Finally, PC12 are cultured on SC pre-seeded NGCs, as a proof of concept, to monitor their capacity in growing and extending neurites, hence in promoting nerve regeneration.

XI.2. Experimental conditions

All experimental details can be found in Chapter VI. The parameters that are specifically used in this chapter are summarized in table XI.1 and Fig. XI.1.

Table XI.1. Experimental conditions

Base material	• PA
Biofabrication method	• Electrospinning of NGCs
Plasma treatment	• Argon DBD: - Power= 1.47 W - Glow mode • Air DBD: - Power= 1.45 W - Filamentary mode • Argon APPJ: - Power= 3.1 W
Characterization techniques	• XPS: - Reported value: average of 4 values measured on 2 different samples. • SEM: - Accelerating voltage: 10 kV. - Reported fiber diameter value: average calculated over 50 fibers on 2 different samples.
Sterilization	• UV: - Wavelength: 254 nm - Exposure time: 10 min on each side of the NGCs (Total time: 20 min)
***In vitro* cell tests**	• SC culture: - 30 000 cells/cm^2 • SC - PC12 co-culture: - 30 000 cells/cm^2 - 20 000 cells/cm^2

XPS measurements and immunostaining imaging are performed on 4 different zones (0.5 cm each) of the NGCs. The zones of the plasma-treated NGCs are numbered based on the position of the conduits in the DBD and relative to the PJ: zone 1 and zone 4 being respectively the farthest and the closest from the DBD gas inlet or the PJ capillary end.

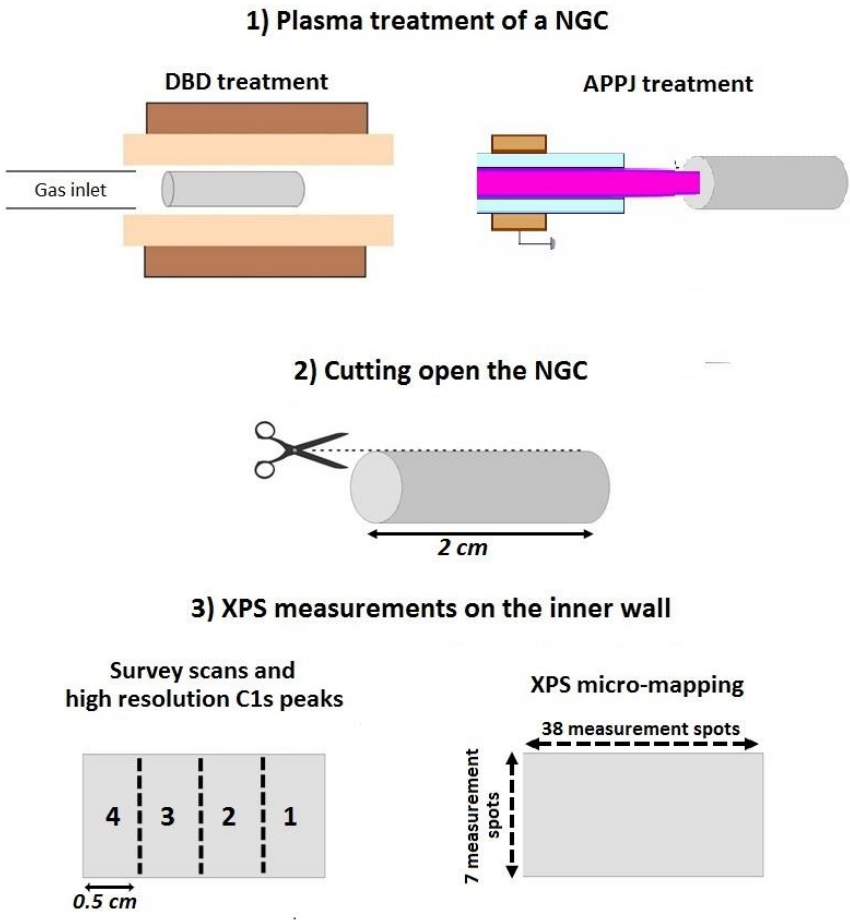

Fig. XI.1. *Schematic illustrations of the steps followed to perform XPS measurements on the inner wall of the plasma-treated NGCs.*

XI.3. Results and discussion

XI.3.1. Characterization of the electrospun PA NGCs

After electrospinning, the deposited PEOT/PBT fibrous network is successfully pulled out from the tubular mandrel to obtain a steady and well-formed conduit not showing any signs of collapse all over its 2 cm length (Fig. XI.2 A). The selected ratio of PEOT (55) to PBT (45) was shown by Santos et al. to generate electrospun NGCs with higher flexibility and resilience (Tensile strength: 2.6 MPa; Young's Modulus:

10.5 MPa) compared to other materials such as the electrospun PCL NGCs used by Yu et al. (Tensile strength: 4.6 MPa; Young's Modulus: 2.0 MPa) [21, 181]. In fact, well balanced strength and elasticity are primordial keys in the success of NGCs that should resist stretching and rearing forces while retaining a steady shape during the regenerative sequence. A second benefit of PEOT55PBT45 NGCs is their slow *in vivo* degradation rate that is essential to support regeneration in long gaps [21].

After examination under SEM, the electrospun NGCs show an inner diameter of 2 mm and a wall thickness of 200 µm (Fig. XI.2 B-C). The inner diameter is similar to the diameter of the mandrel used during electrospinning, thus revealing no shrinkage of the robust NGCs post-removal. This diameter is specifically picked since it is suitable for future *in vivo* tests using a rat sciatic nerve model. The wall thickness is purposely conceived to be almost 2 times bigger than the one considered in several previous studies [21, 181]. The reason behind the thicker wall is the bigger nerve defect (2 cm) that is intended to be repaired and that requires a steady bridging for a longer time. The inner wall fibers of PA NGCs were previously shown, after 4 months of *in vivo* implantation, to start detaching and invading the lumen because of the physical erosion of inter-fiber cross-links [21]. This unexpected and progressive occurrence of intraluminal fibers is beneficial as it serves as additional ECM-like structure guiding SC migration and axon regrowth. However, when the wall is not thick enough, all the fibers would fall apart and the bridging role of the NGCs might come to an end before the complete nerve regeneration.

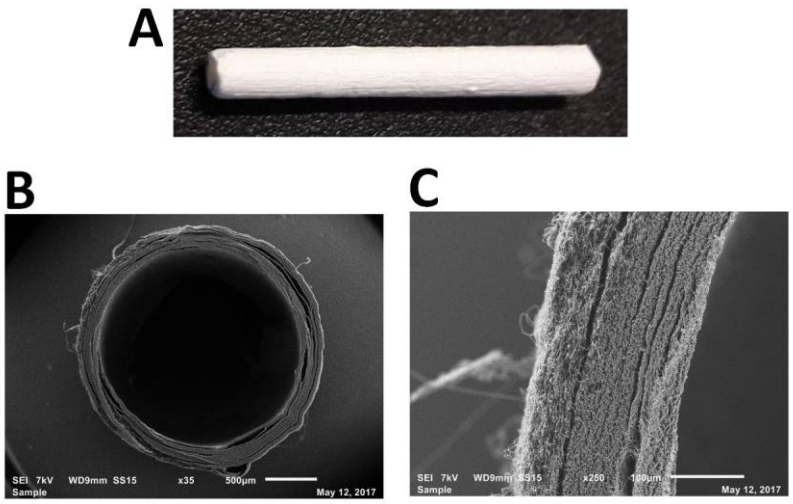

Fig.XI.2. *A: Photograph of the obtained NGC; B: SEM image of the NGC cross section; C: SEM image of the wall cross section.*

When taking a closer look at the inner and the outer walls, one can notice consistently well-shaped fibers with a smooth surface and diameters of 710 nm and 775 nm respectively (Fig. VI.3 A). PLLA fibers in the same diameter range (759 nm) were previously reported to exhibit the extension of the longest neurites form DRG explants compared to fibers with smaller (293 nm) and larger diameters (1325 nm) [475]. Next to the importance of the diameter, the fiber orientation also critically influences neural and glial cell behavior. After a qualitative inspection of the SEM images, one can visualize a clear difference between the inner and the outer walls: bundles of aligned fibers with random fibers in between compose the inner wall while more randomly deposited fibers form the outer wall (Fig. IX.3 A). This observation is quantitatively confirmed by generating the FTT output images and plotting the pixel intensity in function of the fiber direction (Fig. XI.3 B). Results show that the inner wall displays a significantly narrower and higher distribution curve compared to the outer wall, thus corroborating the considerable heightening of the inner fiber alignment and the outer fiber randomness. The inner fiber alignment plays a primordial role in enhancing nerve regeneration as it provides cell guidance contact and directional cues promoting neurite directed extension and SCs elongation and guided migration [22, 78-81]. However, the high packing density of aligned fibers reduces the porosity or even completely hampers the occurrence of pores cutting off the vital nutrient supply [476]. Therefore, the presence of random fibers with interconnected pores in between the aligned fibers on the inner wall comes to solve this issue. This beneficial inner wall architecture, synergistically enhancing a directed regeneration while allowing nutrient exchange, was never observed in any of the previously engineered NGCs. The unalike outer wall architecture presenting a higher porosity is expected to further intensify the influx of neurotrophic factors that are expected to concentrate more and more inside the conduit creating a regenerative microenvironment. This boosted nutrient inflow is extra-needed in long nerve gaps since the regenerative capabilities of the nerve ends are exceeded and the fibrin cable may not form adequately [21, 477] . Moreover, the random fibers of the outer wall safeguard for the steady bridging role of the NGCs thanks to their numerous joining points forming a robust fibrous network. This network strengthens the whole conduit structure and prevents the fibers from falling apart. A higher SEM image magnification (x 10 000) reveals that overlapping fibers of the outer wall are slightly fused together, thus consolidating more the NGCs (Fig. XI.3 A). This fiber fusion is presumably attributed to the retention of small solvent amounts that merge the fibers in contact and form a number of physical cross-links after complete evaporation. Another

advantage of the random deposition of fibers on the outer wall is the enhanced tear resistance that it appends to the entire wall. This makes the NGC more prone to withstand the surgical coaptation where a suture travels through the NGC wall multiple times to secure it to the nerve stump. When the whole wall is composed of aligned fibers, the NGC becomes predisposed to tearing along the direction of fiber alignment after frequent piercings [19].

The distinctive NGC double-layered wall obtained in this study is generated in a one-step electrospinning process with custom-tailored parameters. Since the goal is to align the inner fibers along the conduit length and not perpendicular to the tubular mandrel, a very low mandrel RS of 50 rpm is put into play during electrospinning. In this way, the mechanical forces caused by high RSs stretching and aligning the fibers in the same motion direction are cancelled out. Next to decreasing the RS, all the electrospinning device parts neighboring the mandrel are covered with an insulating tape, thus giving prominence to the metallic mandrel conductivity. Therefore, the charged fibers are driven by electrostatic forces to stretch and deposit in an aligned manner spanning the mandrel length. The more the metallic mandrel is covered by the non-conductive polymeric fibers, the less the electrical forces causing the alignment are intervening in the deposition. This can explain the randomly deposited fibers on the outer layers. In the previous literature involving the electrospinning of NGCs, few studies have also generated double-layered scaffolds of aligned and random fibers. However, the biofabrication was done in a 2 step process implicating a separate electrospinning of random and aligned fibrous membranes that are stacked on top of each other and rolled up to form a tube. The edges are then secured using glue, solvents or heating [19, 22]. In addition of being time-consuming, this fabrication strategy gives non uniform outer NGC wall. Moreover, the 2 layers might disconnect from each other and the risk of conduit opening because of inadequate fastening of the edges becomes high *in vivo*. In the studies where the electrospinning of NGCs is done on a tubular mandrel in a one-step procedure, walls composed of only random fibers are mostly formed [48, 169].

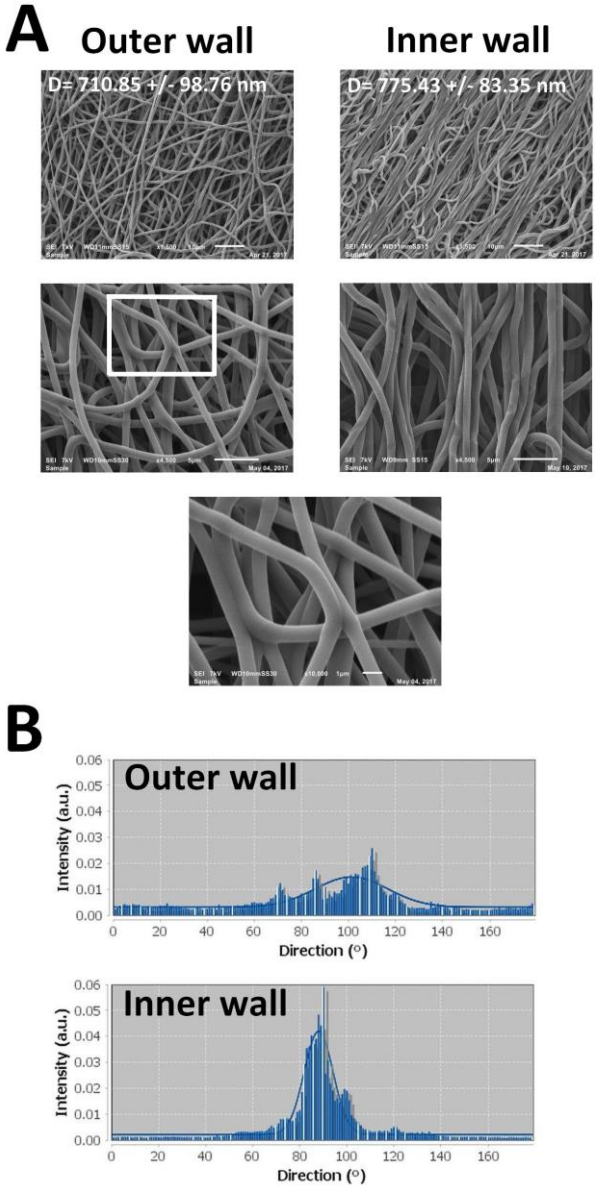

Fig. XI.3. *A: SEM images of the generated fibers on the inner and the outer NGC walls (magnifications: x 1500, x 4500 and x 10000); B: FTT pixel intensity plot in function of fiber direction on the inner and outer NGC walls.*

XI.3.2. XPS analysis pre- and post-plasma treatments

XI.3.2.1. Survey scans: elemental composition

After electrospinning, XPS measurements are carried out to assess the surface chemical composition of the generated NGCs. Since the regenerating nerves will be in direct contact with the NGC inner wall, the measurements that follow are only restricted to the inner conduit surface. XPS survey scan analysis reveals a surface oxygen content of 17.5 % and a carbon content of 82.5 % on the 4 different zones of the NGC thus indicating a homogeneous surface chemistry across the NGC length (Fig. XI.4). The obtained elemental composition is not in direct correlation with the PEOT/PBT structure that should theoretically give an oxygen content of 25.1 % and a carbon content of 74.9%. This finding is presumably attributable to the enrichment of lower binding energy functionalities such as methyl groups on the fiber surface over the bulk during electrospinning. The chemical remodeling and rearrangement of particular groups on the surface of electrospun fibers was previously observed in several studies. For instance, Cui et al. found out that methyl groups got enriched on PDLLA fiber surface because of the high electrospinning voltage [413]. Deitzel et al. also perceived a double fluorine content on the surface of electrospun fibers made up of the copolymer tetrahydroperfluorooctyl acrylate/methyl methacrylate compared their bulk [444].

In an attempt to enhance the surface chemical properties for an improved nerve regeneration, the NGCs are subjected to several plasma treatments. In a first set of experiments, a DBD operating in air or in argon at medium pressure is used for this purpose. In contrast to 2D surfaces, plasma modification of 3D scaffolds using a parallel plate DBD is a challenging task. Since the main goal is to modify the NGC inner wall surface, an efficient plasma penetration through the interconnected pores is therefore required. In order to precisely evaluate this plasma capacity to reach and modify the luminal wall, XPS measurements are again performed on NGCs exposed to different treatment times (Fig. XI.4). The results show that air and argon discharges lead to different chemical surface modifications along the NGCs. After 2 s of plasma exposure, almost no changes in the NGC surface chemistry are detected when argon is used as discharge gas. However, a significant increase in the oxygen content from 17.5 % to at least 20.9 % can already be detected when air is used as discharge gas, thus highlighting the fast penetration of air plasma inside the conduits. Nevertheless, the conduits are non-homogeneously treated since the oxygen percentage is shown to vary along the NGCs (zone 1: 22.4 %;

zone 2: 20.9 %; zone 3: 21.5 %; zone 4: 22.5 %). In return, surface carbon content decreases proportionally in respect to the oxygen increase since no other elements are incorporated on the fiber surface during or post-plasma treatment. When increasing the plasma exposure time to 4 s then 8 s, a sudden increase in the surface oxygen from 17.5 % to around 23.6 % then 24.7 % is perceived in case of the argon discharge. These results also denoted the penetration ability of argon plasma but with a delay compared to air plasma. Moreover, it is worth mentioning that argon plasma engenders a completely homogeneous surface modification illustrated by similar oxygen percentages on the 4 zones along the luminal wall. In the air discharge, the oxygen content continues to increase after 4 s and 8 s of treatment time but in smaller steps and with the same non-uniform trend across the NGC length. A plasma exposure time of 16 s marks a noticeably higher and uniform oxygen incorporation reaching around 28 % along the NGCs treated with argon. This percentage could not be attained with the air discharge where a gradient-like oxygen incorporation continues to be seen after a treatment of 16 s (zone 1: 25.7 %; zone 2: 25.3 %; zone 3: 25.8 %; zone 4: 27.4 %). At 32 s of plasma exposure, a saturation of the treatment effect is distinguished in both discharges as the NGC surface chemistry is completely analogous to the one detected at a 16 s treatment.

In order to get a clear understanding on how air and argon plasmas modified differently the NGC inner wall, it is essential to elucidate: 1) the mechanisms underlying plasma penetration throughout the NGC wall thickness and then 2) the effects of each discharge atmosphere on the different active species bombarding the fibrous surface. First, the active species of plasma generated between both DBD electrodes must have the chance to move to the intended reaction location which is, in our case, the inner NGC wall without losing their modifying capacity. This diffusive transport of particles is mainly influenced by their mean free path on the one hand and the fibers inter-distance or the wall porosity on the other hand. When the mean free path of the surface modifying particles is smaller than the typical distance between PA fibers, the particles are more prone to collide with each other rather than with the NGC. Therefore, the lifetime of the active species becomes very short which limits their transport to reach the luminal wall. However, when the mean free path is comparable to or bigger than the wall pore size, plasma species impact only with the NGC surface and the shortfalls of particles induced by excessive collisions are ignored [478, 479]. Since argon is denser than air and the mean free path of particles in the plasma phase is comparable to that in the gas phase, one can deduce that the active species in air plasma have bigger mean free paths than the ones in argon plasma. This can explain the

faster penetration of air plasma (2s) inside the NGCs. The pressure in which plasma is generated also plays a decisive role in the particle diffusive transport as it substantially influences the mean free path of plasma species. When decreasing the pressure, the mean free path increases, suggesting more efficient plasma penetrations in low-pressure systems [478]. In fact, Poll et al. demonstrated the complete inability of plasma to penetrate into textile fabrics at atmospheric pressure despite extended treatment times. Moreover, it was stated that the pressure range that is optimal for plasma modification of the whole thickness of multilayered textiles is restricted between 0.1 and 10 kPa [479]. Since the DBD plasma treatments performed in this study are done at a medium pressure of 5 kPa, the active species seem to attain sufficiently big mean free paths to be able to reach the luminal wall. This is why argon plasma could also modify the inner wall surface but with a slightly delayed primary effect (4s).

Once inside the NGC, 2 types of species are recognized to induce surface chemical changes: 1) non-reactive species break down C-H and C-C bonds spawning surface radicals and 2) chemically reactive species such as molecular and atomic oxygen insert new functional groups. Since one of the plasma treatment is sustained in pure argon, the grafting of oxygen containing functionalities should not theoretically occur and the generated radicals will instead interact with each other forming a cross-linked network [259, 398, 406]. In reality, the plasma chamber contains oxygen impurities sourced from: 1) gaseous components such as H2O and O2 that plasma desorbs from the reactor walls, 2) oxygen trace in the working gas, 3) air remaining in the plasma chamber because of insufficient pre-treatment pumping and evacuation. Moreover, post-treatment oxidation via secondary reaction pathways between the plasma-created radicals and oxygen molecules of the surrounding air is also anticipated to take place [91, 480].

For the sake of testing if plasma species have lost some of their surface modification ability during the penetration throughout the NGC wall, flat PA fibrous membranes are plasma-treated and a comparative XPS analysis is performed. Maximal oxygen contents of 28.4 % and 28.7 % are detected on the surfaces treated with air and argon DBD respectively. These results divulge the fact that air plasma is unable to modify the inner NGC wall with its full potential like argon plasma. The reason behind these distinctive consequences is presumably the different DBD modes being filamentary and glow in the air and argon discharges respectively. First, a higher concentration and more even distribution of surface modifying species and ions are normally present in the glow mode compared to the filamentary mode [392]. For instance, Massines et al. have indeed found higher amounts of exited species in a glow helium discharge compared to a filamentary helium discharge

that showed a 15 times less intense emission spectrum [481]. Therefore, even if some particle losses occurred during the movement throughout the NGC walls, a higher amount of species responsible for the surface modification will reach and concentrate in the lumen in case of the glow argon discharge. Moreover, it is know that a glow mode preferentially produces active species close to the cathode, while a filamentary mode generates active species in the whole discharge gap [481, 482]. Since the NGC lies on the electrode, the majority of the active species are initiated near the wall in the argon glow discharge. In contrast, the particle scattering in the air filamentary discharge causes less species to be created next to the NGC wall. When closer to the NGC, the species reach the lumen with higher surface modifying capacities, while when far away from the NGC, the species can already return to their fundamental level even before attaining the outer wall. This can explain why the middle NGC zone could only incorporate around 25 % of oxygen in the air discharge while 28 % of oxygen are incorporated in the argon discharge. Fang et al. have also uncovered that a glow DBD operating in air is more efficient in modifying polypropylene surfaces than the filamentary DBD that introduced less oxygen-containing groups [482].

The inhomogeneous surface modification of the air plasma-treated NGCs showing a higher oxygen content (27.4 %) on zone 4 is probably due to the side penetration of plasma through the conduit opening. This occurs only at the conduit side positioned next to the gas flow inlet. This "gradient-like" oxygen content created along the NGCs can be interesting in enhancing nerve regeneration as regrowing axons were shown to be driven by chemotactic signals distributed in a spatial concentration gradient [308, 309]. However, a "real" and steeper gradient with increasing oxygen content on each of the 4 zones is more likely to direct this beneficial effect. Therefore, in a trial aiming at generating such a gradient, the NGCs are subjected to a PJ treatment operating in argon at atmospheric pressure. In this way, the plasma jet or the so-called effluent plasma outflows from the jet capillary and directly penetrates inside the NGC through its opening. Ideally, a gradual decrease in the plasma intensity is supposed to occur across the effluent length leading, in theory, to a gradual decrease in the plasma modification efficiency along the NGC surface. Nevertheless, after 5 s of plasma exposure, the oxygen content increases in an arbitrary manner from 17.5 % to 22.4 %, 23.5 %, 26.8 % and 24.6 % on zone 1 to 4 respectively (Fig. XI.4). An unbalanced and non-gradient oxygen incorporation was also previously perceived when treating polyethylene tubes making use of an argon AAPJ [483]. This fluctuating behavior is probably due to very specific gas-dynamic processes occurring at the inlet region. Moreover, another explanation

might be related to the theory stating that the PJ discharges are particularly comprised of a train of ionization waves propagating at high speeds and known as "plasma bullets" [484]. Many studies have noted the complicated mechanisms underlying the propagation of "plasma bullets". One of the assumptions indicates that the electron density distribution, the electric field and the active species inside a bullet are nonhomogeneous [485-489]. When increasing the treatment time to 10 s, a gradient incorporation of oxygen is successfully attained along the NGC with a 9 % difference between the lowest and the highest amount (zone 1: 21.6 %; zone 2: 26.8%, zone 3: 29.5 %; zone 4: 30.5 %). This is presumably attributable to the plasma propagation that starts after a certain treatment time to follow a more controlled trend: the radius of the bullets increases progressively along the NGC path while plasma intensity decreases affecting less and less the surface [483]. When increasing more the treatment time to 15 s and 20 s, fluctuations is the oxygen amount are again perceived along the NGCs with an overall average drop. Most likely, this behavior could be correlated with the plasma etching effect that starts to cause at extended treatment times a random depletion of the plasma-induced oxygen-containing bonds and the bonds already present in the polymer backbone. Although mainly triggered by the presence of oxygen species, the etching effect was also observed in argon plasmas where UV etching is predominant rather than the oxidative degradation [91, 398, 490]. Riekering et al. also perceived a decrease in the O/C ratio when subjecting PEO/PBT films to an argon plasma treatment at a certain exposure time [490]. This outcome was linked back to the preferential etching the softer PEO regions of the copolymer that is also anticipated to take place during PJ treatment of the NGCs in this present study.

In what follows, the analysis will be restricted to the optimal plasma exposure times: argon DBD treatment of 16 s, air DBD treatment of 16 s and argon PJ treatment of 10 s.

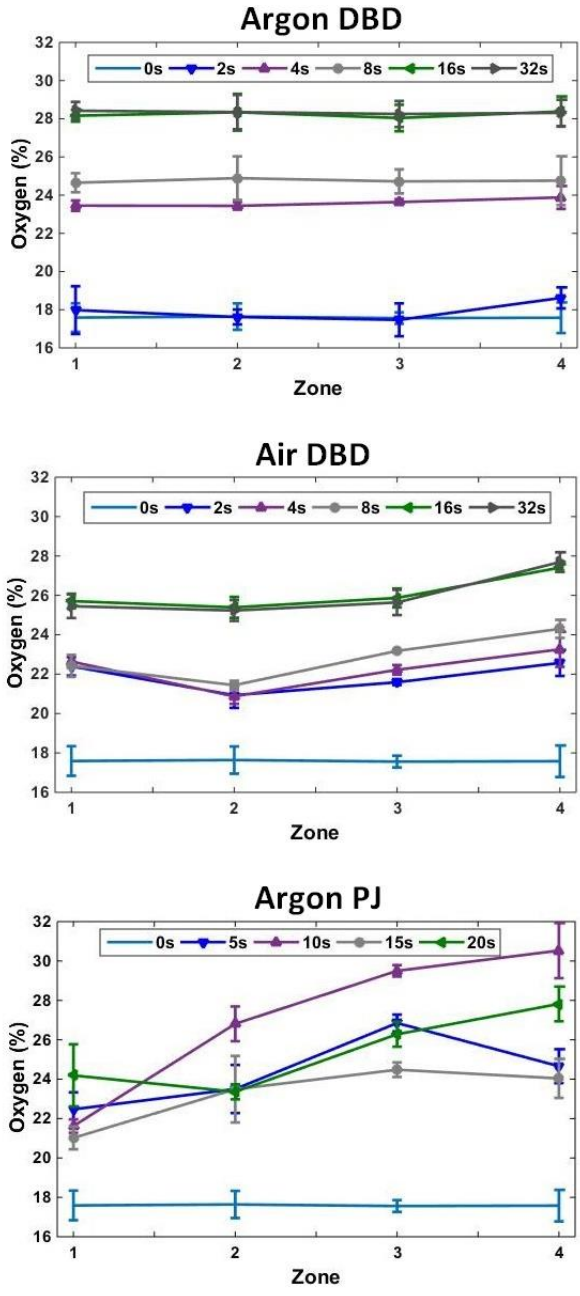

Fig. XI.4. *Evolution of the surface oxygen content on 4 zones of NGCs subjected to argon DBD, air DBD and argon PJ treatments as function of plasma exposure time.*

XI.3.2.2. XPS micro-mapping

After assessing the surface elemental composition on 4 different zones of the plasma-treated NGCs, an advanced and uncommon XPS micro-mapping is performed to visualize with very high precision the exact distribution of oxygen over the whole NGC inner wall surface. In this way, the homogeneous and gradient surface modifications induced by the different plasma treatments can be confirmed and further highlighted and deciphered. The obtained XPS micro-maps (1900 x 350 values) are displayed in Fig. XI.5. Since oxygen and carbon are the only elements present on the NGC surface, the maps showing the carbon content are not presented as they picture the reverse of the oxygen maps. Argon DBD is revealed to engender a completely homogeneous surface modification thus corroborating the previous zone-specific results. An overall lower and non-homogeneous oxygen incorporation is observed after air DBD treatment underlying again the reduced amount and efficiency of plasma species penetrating throughout the NGC wall and interacting with the inner surface. The map exposes a "gradient-like" distribution illustrated by a noticeable increase in the oxygen content on a quarter area at one side of the NGC. This particular observation ascertains our previous assumption concerning the side penetration of plasma through the NGC opening close to the gas inlet, leading to a more efficient surface modification on one extremity. Finally, a steep gradient map with increasing oxygen content along the NGC length is clearly discerned post argon PJ treatment to be in line with the previous zonal analysis. In this way, a new approach involving a simple PJ design is used to create chemical gradient in tubular scaffolds. Previous studies aiming at creating chemical plasma gradients on polymeric surfaces were rather using very complex and extensively redesigned plasma reactors involving for instance automated stepper motors moving the samples, reshaped electrodes and shielding covers [320, 323, 324, 327, 328]. A visual comparison between the 3 maps draws more attention to the big variances that can be induced by different working gases and reactor configurations in the plasma treatment of electrospun tubular scaffolds.

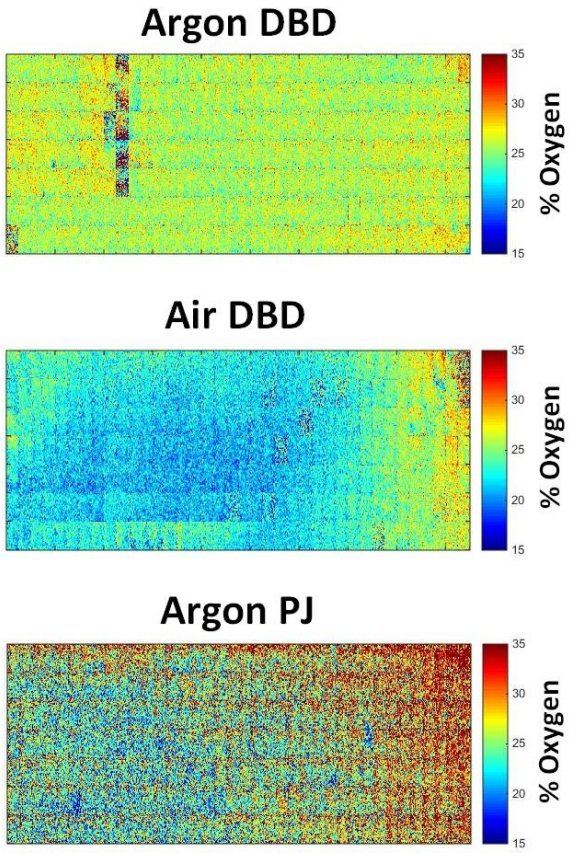

Fig. XI.5. *XPS micro-mapping images of the oxygen distribution on the whole inner surface of NGCs subjected to air DBD, argon DBD and argon PJ treatments.*

XI.3.2.3. C1s peak deconvolution: chemical bonds

In order to get an insight on the specific types and relative amounts of the plasma introduced oxygen-containing functionalities, high resolution C1s curves are deconvoluted for each of the 4 NGC zones. According to the molecular structure of PEOT/PBT and to literature, the C1s envelope of the copolymer encompasses 4 different peaks: a peak at 285.0 eV attributed to hydrocarbon and aliphatic or aromatic carbon bonds (C-C), a peak at 286.5 eV ascribed to hydroxyl groups (C-O), a peak at 287.7 eV accredited to carbonyl groups (C=O) and a peak at 289.1 eV corresponding to carboxyl groups (O-C=O) [90, 491]. Table XI.2 contains the quantitative results of the C1s fitting carried out for

untreated NGCs and for the 4 zones of NGCs subjected to air DBD, argon DBD and argon PJ treatments. Fig. XI.6 shows the high-resolution C1s curve deconvolution on only zone 4 of the untreated and plasma-treated NGCs. The relative amount of the peak at 285.0 eV on the untreated NGCs (69.3 %) is higher by around 5 and 9 % than the one previously detected on spin-coated and 3D printed 300PEOT55PBT45 respectively [90, 480]. In return, the total amount of the other oxygen-containing bonds is lower but their relative concentrations follow parallel proportions. This comparison comes to validate our aforementioned assumption stating the possible enrichment of low binding energy functionalities such as methyl groups on the fiber surface over the bulk during electrospinning. After argon DBD treatment, the relative concentration of all bonds changes substantially but similarly on all zones which is in agreement to the homogeneous oxygen incorporation on the whole NGCs. An average decrease of 11.9 % is noted for the C-C peak and increases of 6.9 %, 1.7 % and 3.3 % are detected for the C-O, C=O and O-C=O peaks respectively. These results suggests that argon plasma attacks C-C and C-H bonds and the formed radicals could interact with oxygen species rather than fully undergoing cross-linking. The C-O bonds are shown to be more easily incorporated than O-C=O and C=O bonds, which was frequently observed after argon plasma treatment of some other polymers [259, 398]. Air DBD treatment also induces noticeable variations in C1s curve fit but to a lower extent and in a non-homogeneous manner over the NGC length. As anticipated, zone 4 shows the biggest changes as it is affected by the side plasma penetration. A decrease range of 3.5 to 8.9 % is noted for the C-C peak and increase ranges of 2.5 to 5.9 %, 0 to 1.2 % and 1.3 to 2.5 % are detected along the NGCs for the C-O, C=O and O-C=O peaks respectively. Given the reduced potential of air plasma species in modifying the surface after crossing the NGC wall, C=O groups are not introduced at all on zones 1 to 3. This result is to be expected as a normal air DBD plasma treatment of flat PEOT/PBT films was previously shown to have a lower ability in incorporating C=O groups than an argon DBD treatment [480]. Moreover, Nandakumar et al. detected C-O and O-C=O bond incorporation without any C=O bond grafting on electrospun PA fibers subjected to an RF oxygen plasma treatment [491]. Interestingly, a remarkable gradual decrease in C-C bonds from 65.7 to 55.3 % and a prominent continual increase in O-C=O bonds from 4.8 to 11.1 % are detected along the NGCs subjected to argon PJ treatment. These ascending and descending percentages are in line with surface oxygen and carbon gradients revealed by the XPS survey scans and micro-mappings. No signs of C=O bond incorporation are detected on zone 1, while zones 2 to 4 show an average C=O increase

of 3.0 %. Despite the overall higher surface modification potential of the PJ compared to the DBD, the maximal C-O bond amount found after argon DBD treatment is not attained after PJ treatment. A non-homogeneous C-O increase ranging between 2.5 and 4.0 % and not following an ascending trend is discerned. Since PJ operates at higher power, this behavior is presumably linked to the preferential plasma etching of the softer PEOT segments causing the depletion of C-O bonds from the polymer backbone. This depletion is overcompensated by the incorporation of new C-O bonds that could not reach at the end the amount added during DBD treatment. This elucidation can be further approved by several studies showing a stagnation or even a decrease in C-O bonds on the surface of PEOT/PBT samples after plasma activation making use of reactors with higher powers [90, 480, 490].

Table XI.2. *C1s curve fit results of the untreated and along 4 zones of the plasma-treated NGCs*

Condition	Zone	C1s curve fit (%)			
		C-C/C-H 285.0 eV	C-O 286.5 eV	C=O 287.7 eV	O-C=O 289.1 eV
No treatment		69.23 +/- 0.54	24.02 +/- 0.51	2.69 +/- 0.18	4.04 +/- 0.25
Argon DBD (16 s)	1	57.19 +/- 0.24	30.64 +/- 0.34	4.45 +/- 0.01	7.69 +/- 0.13
	2	56.94 +/- 0.56	30.83 +/- 0.46	4.68 +/- 0.27	7.53 +/- 0.15
	3	57.68 +/- 0.27	30.96 +/- 1.17	4.18 +/- 0.80	7.15 +/- 0.63
	4	57.19 +/- 0.48	31.39 +/- 0.46	4.25 +/- 0.91	7.14 +/- 0.33
Air DBD (16 s)	1	63.97 +/- 0.30	27.29 +/- 0.59	2.62 +/- 0.44	6.08 +/- 0.07
	2	65.58 +/- 0.24	26.61 +/- 0.64	2.36 +/- 0.06	5.42 +/- 0.30
	3	63.15 +/- 0.80	27.47 +/- 1.04	3.00 +/- 0.35	6.34 +/- 0.26
	4	60.26 +/- 1.08	29.11 +/- 0.82	3.97 +/- 0.04	6.61 +/- 0.20
Argon PJ (10 s)	1	64.74 +/- 0.71	28.04 +/- 0.67	2.30 +/- 0.12	4.88 +/- 0.18
	2	59.37 +/- 1.71	27.44 +/- 0.98	5.58 +/- 0.56	7.56 +/- 0.85
	3	56.20 +/- 0.94	26.55 +/- 1.00	6.23 +/- 0.26	10.99 +/- 0.45
	4	55.33 +/- 1.48	28.02 +/- 0.99	5.51 +/- 1.41	11.11 +/- 0.76

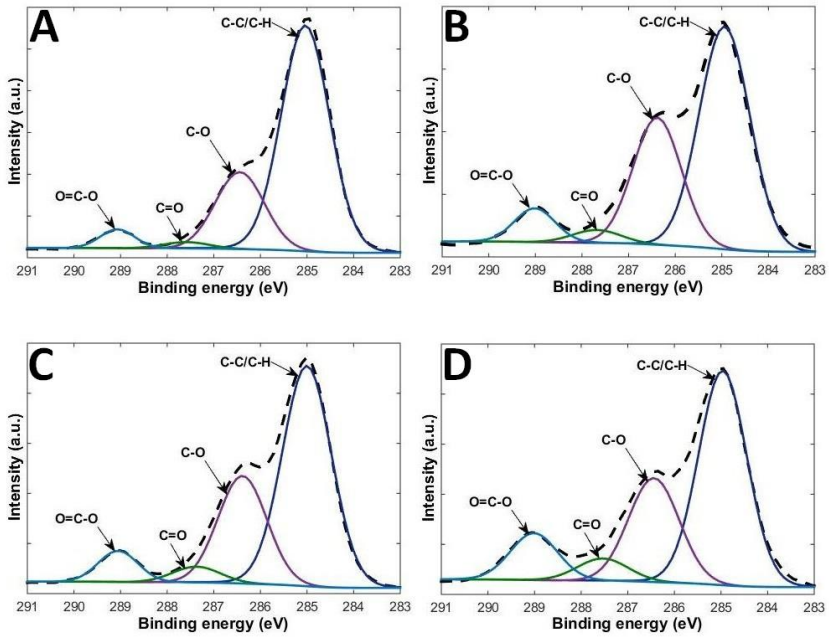

Fig. XI.6. *C1s peak deconvolution of the untreated and zone 4 of the plasma treated NGCs. A: no treatment; B: argon DBD (16 s); C: air DBD (16 s); D: argon PJ (10 s).*

XI.3.3. SEM analysis pre- and post-plasma treatments

Besides the advantageous surface chemical modification, the preservation of the fibrous morphology is an extra critical consideration to approve plasma treatment suitability for PA NGCs. Therefore, SEM images of the inner NGC wall are acquired before and after plasma treatment (Fig. XI.7). The analysis is restricted to zone 4 as it underwent the most pronounced chemical modifications in case of air DBD and PJ treatments and is therefore the most prone to plasma-induced physical damages. The 3 different plasma treatments are shown to exhibit no alterations in the morphological features of the fibers composing the NGC wall. Moreover, the particular fiber architecture illustrated by bundles of aligned fibers with random fibers in between is preserved. Since the fiber diameter is also a critical parameter influencing neural and glial performances, it is again measured post-plasma treatments. The obtained values do not reveal any statistical differences, which also points out the conservation of the fiber scale even in case of PJ treatment where a mild chemical etching

is probably taking place. In one of our previous studies, electrospun PCL fibers showed signs of melted joining points and more drastic morphological deterioration when subjected to the same argon and air DBD treatments respectively [91]. This highlights again the enhanced mechanical and thermal properties of PA fibers compared to other polyester fibers.

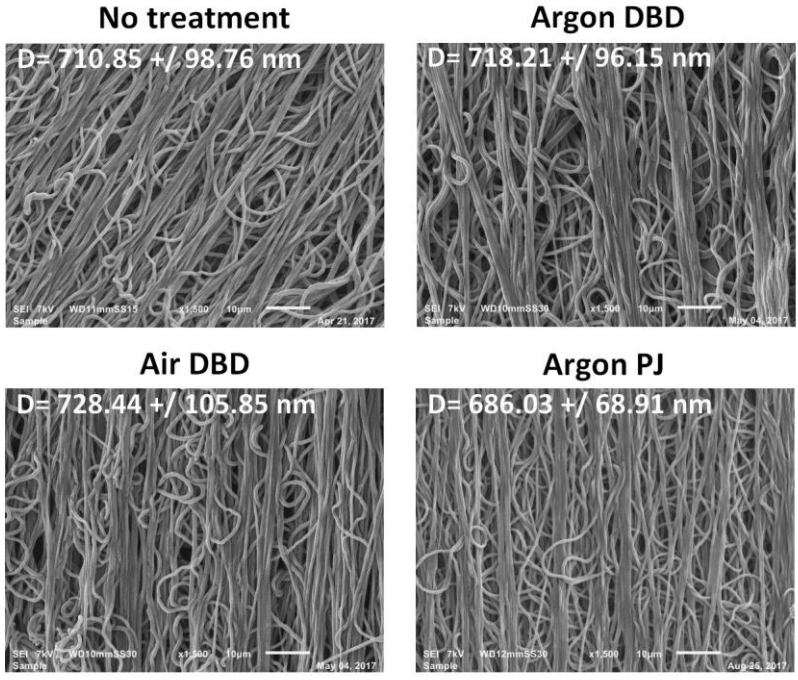

Fig. XI.7. *Inner wall SEM images of the untreated and zone 4 of the plasma treated NGCs (magnification: x 1500).*

XI.3.4. Comparative *in vitro* cell study on untreated and plasma-treated NGCs

The ultimate goal of implementing plasma-induced chemical features on the surface of NGCs is to promote glial and neural cell performances for an enhanced nerve regeneration across critical defects. Therefore, the final step of this chapter is to assess the bioresponsive properties of untreated and plasma-modified NGCs through a comparative *in vitro* study using SCs and PC12. Argon DBD treatment engendering a homogeneous surface oxygen incorporation and argon PJ treatment

creating surface oxygen gradient are only considered in the following tests.

XI.3.4.1. SCs-surface interaction along the NGCs

Since SCs are the primary glial cells of the peripheral nervous system playing a key role in nerve regeneration, they should adhere, proliferate and migrate effectively on the NGCs. In order to visualize the interaction of SCs on the whole untreated, homogeneously treated and gradient NGC surfaces, 12 overlapping immunostaining images are acquired along the inner wall and stitched together. Figures XI.8, XI.9 and XI.10 depicts the final stitched images of SCs cultured in the presence and absence of FBS for 1, 3 and 7 days respectively. Regardless of the culturing day and the presence or absence of FBS, untreated NGCs show a drastically lower cell density compared to plasma-treated NGCs. A uniform cell distribution is observed along the homogeneously plasma-treated NGCs. However, cell gradients towards increased surface oxygen contents are interestingly detected on the NGCs subjected to a gradient plasma treatment. These clear variations in cytocompatibility on the different NGCs highlight the importance of oxygen-containing functionalities in enhancing cellular behaviors starting from the initial attachment. In fact, hydroxyl, carbonyl and carboxyl groups were previously shown to steadily bind proteins without affecting their natural conformation [88, 114, 281]. The immobilized proteins serve as recognition sites for cell receptors of which the integrin family playing a key role in the primary cell capture efficiency by mediating 2 attachment phases: the arrest adhesion and the focal adhesive phase. When the cell senses its surrounding, the arrest phase is triggered by the integrin clustering or affinity modulation. The receptors bind to proteins adsorbed on specific sites of the NGCs. Focal adhesion sites comprised of adhesion receptors and cytoplasmic plaque proteins, mainly actin filaments, are then attached at the contact surface [91, 204, 281]. Since the surface of untreated NGCs contains considerably less polar groups and therefore less bioactive sites for protein adsorption, few cells end up attached on the surface. However, plasma-induced surface oxygen groups act as glue fastening proteins on the surface thus recruiting more integrins resulting in significantly increased number of cells adhering on the surface. Prabhakaran et al. also spotted an improved SC adhesion on air plasma-treated PCL fibers compared to untreated fibers but also to PCL/collagen fibers, thus underlining the exclusive importance of plasma-induced oxygen functionalities [138]. Since a gradient distribution of oxygen groups is detected on PJ treated NGCs, protein adsorption increases gradually along this gradient, proportionally

recruiting integrins and anchoring more and more focal adhesive complexes along the NGCs. This can explain how the density of SCs attached to the surface intensifies in parallel with the oxygen gradient. During the initial cell attachment, the formation of robust focal adhesion complexes on the plasma-treated NGCs leads to the phosphorylation of a focal adhesion kinase triggering several signal transduction pathways responsible for cell survival, cytoskeleton remodeling, proliferation, and other vital cell functions [281, 472]. This is mainly why, plasma-incorporated oxygen containing functionalities were proven in many studies to enhance cell growth and proliferation in addition to their crucial role in promoting cell adhesion [88, 114, 272, 278]. However, the mediocre level of initial cell adhesion on untreated NGCs hampers the proper occurrence of subsequent cellular activities thus maintaining the big difference in cell density with plasma-treated NGCs even after 7 days of culturing.

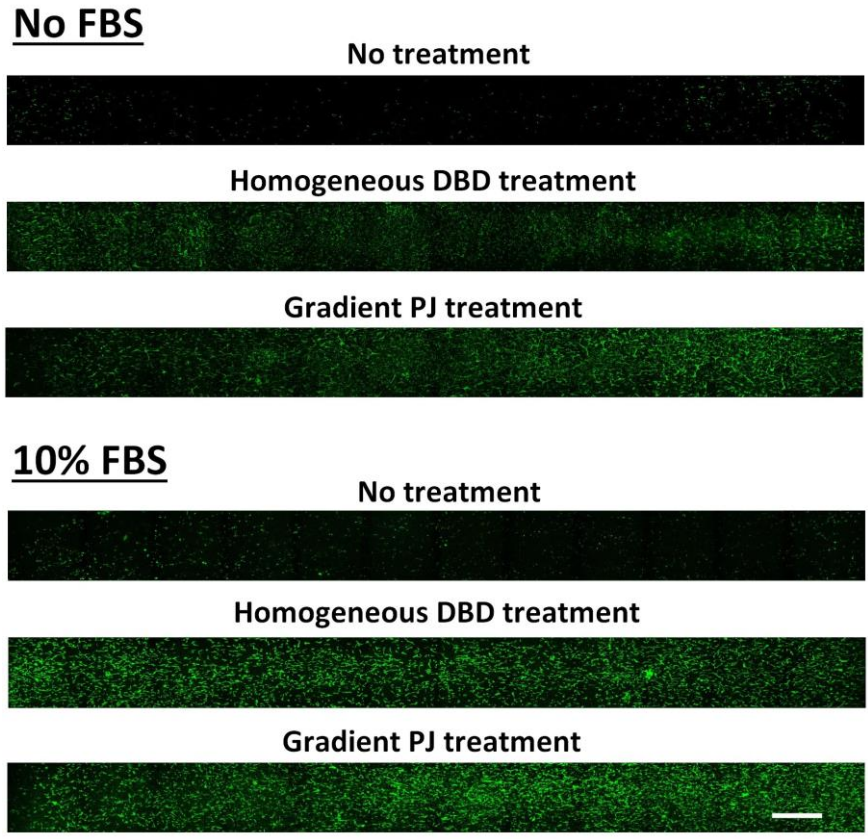

Fig. XI.8. *S100 immunostaining images of SCs on the whole NGC length after 1 day of culturing (scale bar: 1000 µm).*

The cell adhesion occurring in a free-FBS medium is due to the prior adsorption of proteins on the NGCs during their immersion in FBS the night before cell seeding. Nonetheless, regardless of the surface treatment, a higher cell density is clearly visualized when SCs are cultured with FBS in the medium. This is due to the fact that proteins present in the serum continue to attach to the surface during cell culturing, anchoring more focal adhesion complexes and therefore binding more cells. A noticeable stagnation and even decrease in the fluorescent intensity is observed over the culturing days when FBS-free medium is used. This suggests that the pre-adsorbed FBS proteins on the NGCs are not enough to maintain adequate cell survival, growth and division. The extra direct interactions between cells and proteins provided by the FBS presence in the medium are therefore essential for long term cell endurance.

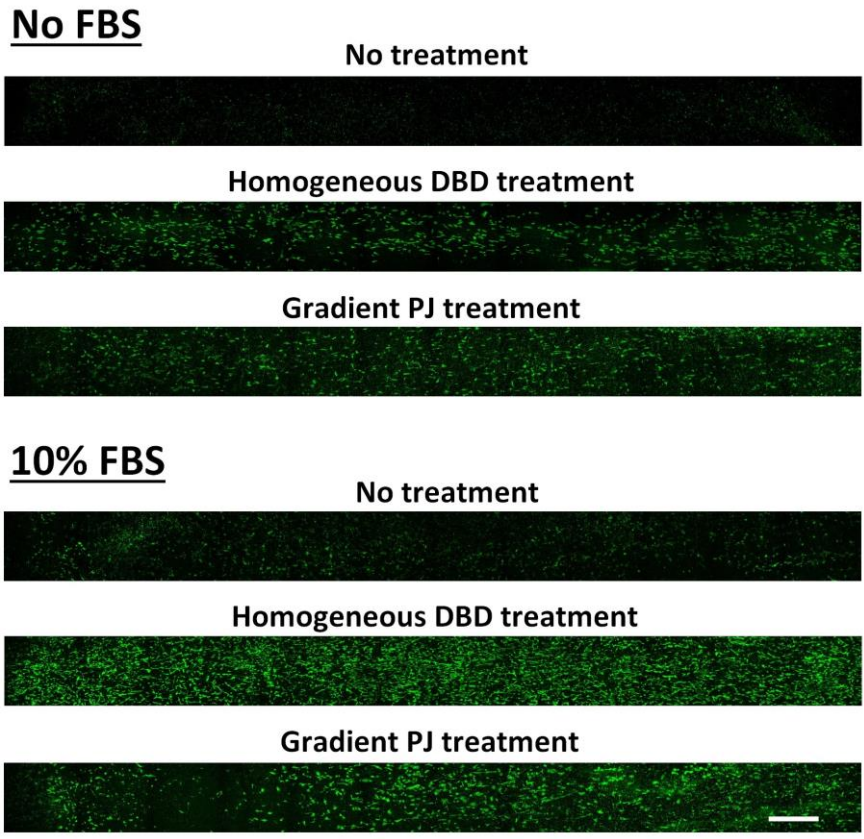

Fig. XI.9. *S100 immunostaining images of SCs on the whole NGC length after 3 days of culturing (scale bar: 1000 µm).*

When taking a closer look at the PJ-treated NGCs, some differences in the cell gradient notability and steepness can be visualized at different culturing days on the one hand and in the presence or absence of FBS on the other hand. At day 1, the cell gradient is less pronounced when FBS is present in the medium. This is presumably attributed to the extra amount of adsorbed proteins on the whole NGC, reducing the cell receptor ability to sense small differences in spatial ligand concentrations. A lower cell density can be still easily discernable on zone 1 compared to zone 4. However the optimal amount of adsorbed proteins seems to already be reached somewhere on the intermediate zones (Fig. XI.8).

At day 3, the cell gradient in the presence of FBS becomes more prominent and steeper, while the cell gradient in the absence of FBS becomes considerably less pronounced when comparing to day 1. In fact, after initial attachment, cells enters the lag-stage in which an adaptation to the surrounding microenvironment occurs. The cells that manage to survive during this stage undergo subsequent proliferation and migration [278]. The absence of FBS has probably led to the death of some cells and to the perturbation the other surviving cells causing the partial loss of the gradient cell dispersion. In contrast, in the presence of FBS, cells most likely undergo more smoothly and rapidly the lag-stage. The steeper and more prominent cell gradient is presumably engendered by 2 mechanisms: 1) a higher proliferation on the oxygen-rich end and as response to the better prior adhesion; 2) a directed cell migration towards higher surface oxygen content, hence higher adsorbed protein concentration. Some authors have indeed shown that cells tend to polarize unidirectionality on chemical gradients by redistributing their chemosensory signaling receptors and organelles towards higher ligand density side [492-494]. For instance, Warneken et al. and Arnold et al. have modulated the spatial distribution of integrins on the cell membrane leading to cell polarization after the implementation of defined surface peptide gradients [495, 496]. When the polarization persists in a unique direction owing to permanent gradient signaling, a contraction of cytoskeletal filaments pull the cellular body towards the leading edge and cell migration occurs in succession. Moreover, cells on chemical gradients tend to attach more tightly at one end. The resulting imbalance in the adhesive forces can lead to the movement in the direction of the boosted adhesiveness [492]. Puccinelli et al. found out that the directional migration of endothelial cells is considerably promoted on epidermal growth factor (EGF) gradients compared to non-gradient surface [497].

At day 7, an inverse gradient steepness is again detected. The cell gradient in the absence of FBS becomes more protruding when

comparing to day 3. This is presumably associated with one or both of the following assumptions: 1) the cells on the low oxygen content zones do not manage to survive while more cells on the rich-oxygen end stay alive given their initial stronger adhesion and the presence of more proteins, 2) after the lag-stage, the surviving cells also undergo a directional migration that is further facilitated by the initial lower adhesive forces compared to the tighter adhesion occurring in the presence of FBS. The cellular gradient is still clearly perceived in the presence of FBS where cells start to fully cover the oxygen rich extremity not leaving space for more cells to attach. Therefore, a lateral accumulation of the proliferating and migrating cells start to be noticed on the intermediate zones.

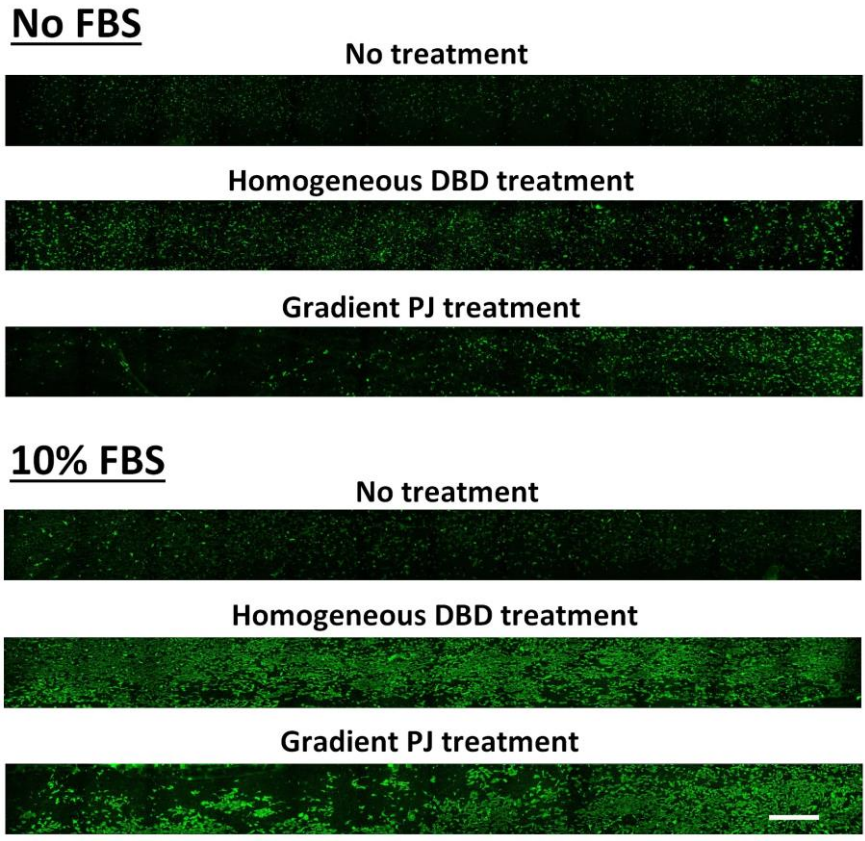

Fig. XI.10. *S100 immunostaining images of SCs on the whole NGC length after 7 days of culturing (scale bar: 1000 µm).*

Next to the immunostaining images, PrestoBlue® assay is performed to measure the amount of viable cells on the NGCs and therefore to quantitatively assess SC proliferation (Fig. XI.11). Despite the obvious visual variations in cell densities between untreated and plasma-treated NGCs, PrestoBlue® results do not reveal any statistical differences in the amount of SCs cultured without FBS on the distinct NGCs. However, when FBS is added to the culture medium, a statistically higher cell amount is detected on the DBD treated and PJ treated NGCs compared to the untreated NGCs but only after 7 days of cell culture. Results of day 1 and day 3 do not show any variations in SC amount on the different NGCs, thus also deviating from the previous imaging results. This can be presumably due to a low sensitivity of the assay not being able to detect inter-sample variations when the cell amount is below a certain threshold. The difference that could be sensed in the presence of FBS after 7 days of culturing, highlights the very efficient cell proliferation on plasma-treated NGCs leading to a considerably higher cell amount compared to untreated NGCs.

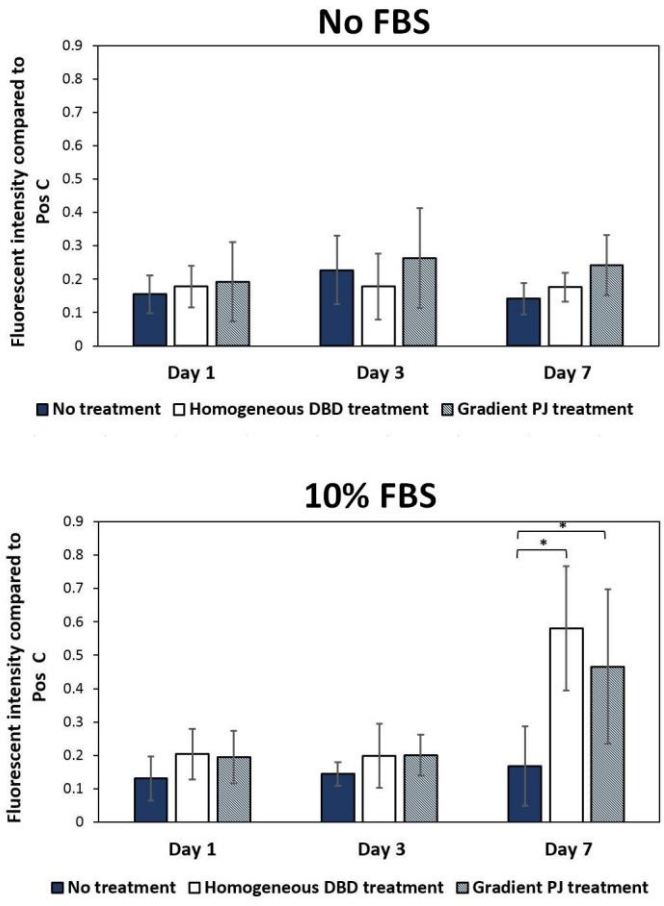

Fig. XI.11. *Ratio of viable SCs cultured on NGCs with and without FBS, relative to the positive control values.*

XI.3.4.2. Morphological studies of SCs on different zones of the NGCs

In addition to enhanced cell adhesion, proliferation and migration, SC morphology and directionality are two extra parameters playing a leading role in neurogenesis [498, 499]. Therefore, individual S100 immunostaining images of higher magnification are also acquired to closely visualize SCs cultured for 3 days without and with FBS on untreated and plasma-treated NGCs (Fig XI.12 and XI.13). The fluorescent images are complemented with SEM imaging for a more detailed scrutiny on how the cells are attached and shaped on the PA

fibers (Fig XI.14 and XI.15). A zone-specific analysis is only performed for PJ treated samples since untreated and DBD treated NGCs exhibited the same SC morphology and orientation on their whole length. An arbitrary image of one of the 4 zones is therefore only shown in case of untreated and homogeneously treated NGCs. Regardless of the presence and absence of FBS in the culture medium, SCs cultured on untreated NGCs remain rounded with very tiny body areas in close contact with PA fibers, thus indicating a poor cell adhesion. However, planar and completely spread out SCs are observed on plasma-treated NGCs: the homogeneous DBD treatment shows a relatively equal combination of star-like and spindle-shaped SCs while the PJ gradient treatment displays different cell morphologies along the 4 zones. A higher occurrence of star-like and tri-polar radially spread out SCs are visualized on low-oxygen content areas (zone 1). A gradual change to spindle-shaped bipolar morphologies befalls towards areas of increasing oxygen contents. Zone 4 shows therefore a higher incidence of aligned cells stretching out unidirectionally and overextending on longer distances. The rare focal adhesive complexes that succeed to form on untreated NGCs probably consist of few anchor points leading to scarcely attached rounded cells. However, plasma-treated NGCs attracting more proteins to adsorb on their oxygen-rich surface leads to the creation of numerous focal adhesion sites with stable anchor points spreading out the cells on the surface. Many other cell types were previously shown to adopt similar morphologies on untreated versus plasma-treated electrospun fibers [88, 114, 276, 472]. Both spindle-shaped and star-like morphologies adopted by SCs when spreading on plasma-treated NGCs can be linked back to the inner wall architecture made up of alternating bundle of aligned fibers and random fibers respectively. In fact, focal adhesion complexes are dispersed arbitrarily on the overlapping multidirectional random fibers ending up by the attachment of multipolar cells. However, aligned fibers are known to have a great ability in providing contact guidance aligning the cells. On the one hand, this is due to the aligned positioning of focal complexes on parallel fibers. On the other hand, traction forces are exerted on the cytoskeleton in the aligned fiber direction leading to protrusions and actin polymerization in parallel to the fibers [203]. Gupta et al. and Masaeli et al. have indeed shown that SCs grown on aligned fibers exhibit a bipolar morphology oriented along the fiber direction, while SCs seeded on random fibers adopt a multipolar morphology [78, 499]. The extra gradual elongation and orientation of cells perceived along PJ treated NGCs is driven by the oxygen gradient. MC3T3 osteoblasts were also seen to gradually change from a more circular shape to more elongated shape along a peptide gradient [495, 496]. This is due, as already mentioned, to the redistribution of the chemosensory receptors

towards the high protein density end, polarizing and aligning the cells. The synergistic influence of the aligned underlying fibers and the oxygen surface gradient accentuates the formation of SC columns mimicking the bands of Bùngner formed during nerve regeneration (Fig XI.12-14). In fact, the bands of Bùngner are composed of unidirectionally elongated SCs that selectively guide regrowing axons [498, 499]. The presumed mechanism underlying their formation is the polarized expression of specific adhesion proteins on the SC axis, which is close to what takes place on gradient surfaces [500].

When comparing SCs cultured with and without FBS, some differences in cell morphology can be also clearly perceived. In addition to the 3D ball-shaped cells observed on untreated NGCs in the absence of FBS, some star-like cells will small cell bodies are also attached when FBS is used. Moreover, DBD treated NGCs exhibit more spread out cells when FBS is present. This is again due to the occurrence of more bioactive sites created by the extra proteins present in the FBS. In case of PJ treated NGCs, the gradual elongation of SCs along the oxygen gradient is more pronounced when FBS is absent. Almost all cells become very elongated reaching a fibrous-like morphology on zone 4 (Fig. XI.12). Whereas when FBS is present, few multipolar and disoriented cells can be still observed on zone 4, and the other elongated cells are less stretched out (Fig. XI.13). This is presumably due to the lower spacing between adsorbed proteins on NGCs in the presence of FBS, reducing the cell ability to sense the differences between its back and front and therefore to orient itself in the gradient direction. In fact, few authors have revealed that cells elongate themselves along gradient surfaces only when the average distance between ligands is larger than a certain non-detectable small spacing [495, 496].

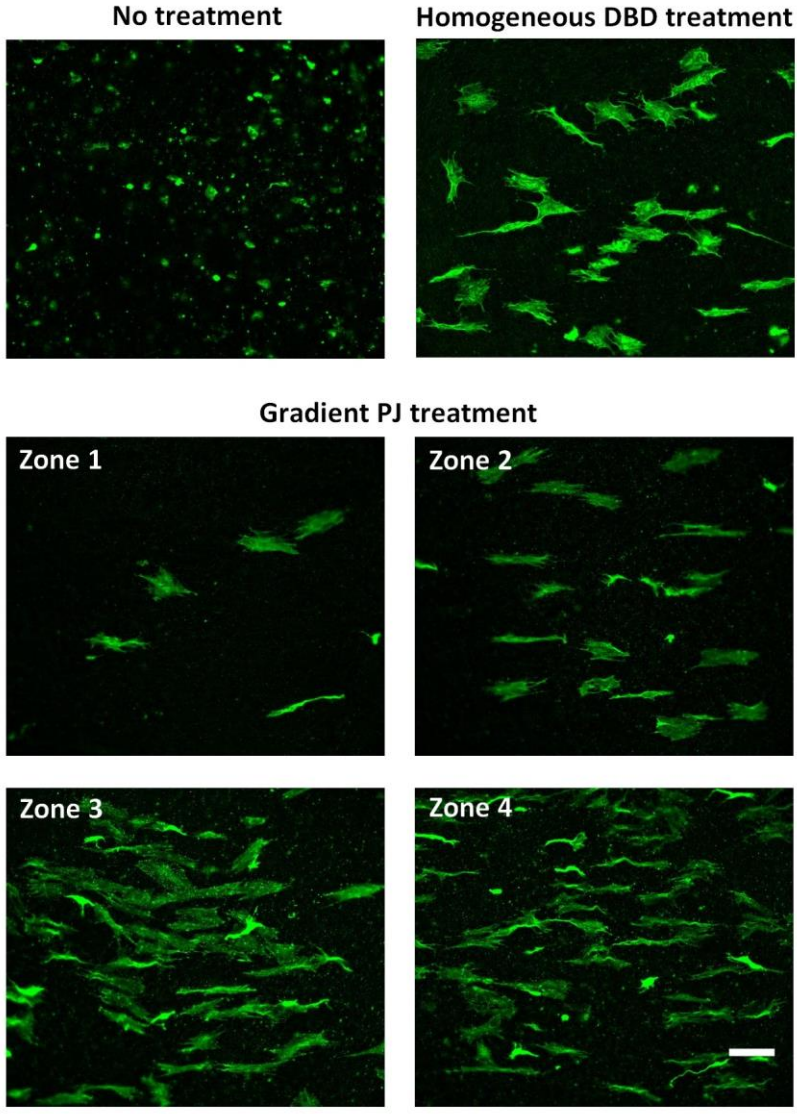

Fig. XI.12. *S100 immunostaining images of SCs cultured for 3 days without FBS on untreated, DBD treated and 4 zones of PJ treated NGCs (scale bar: 100 µm).*

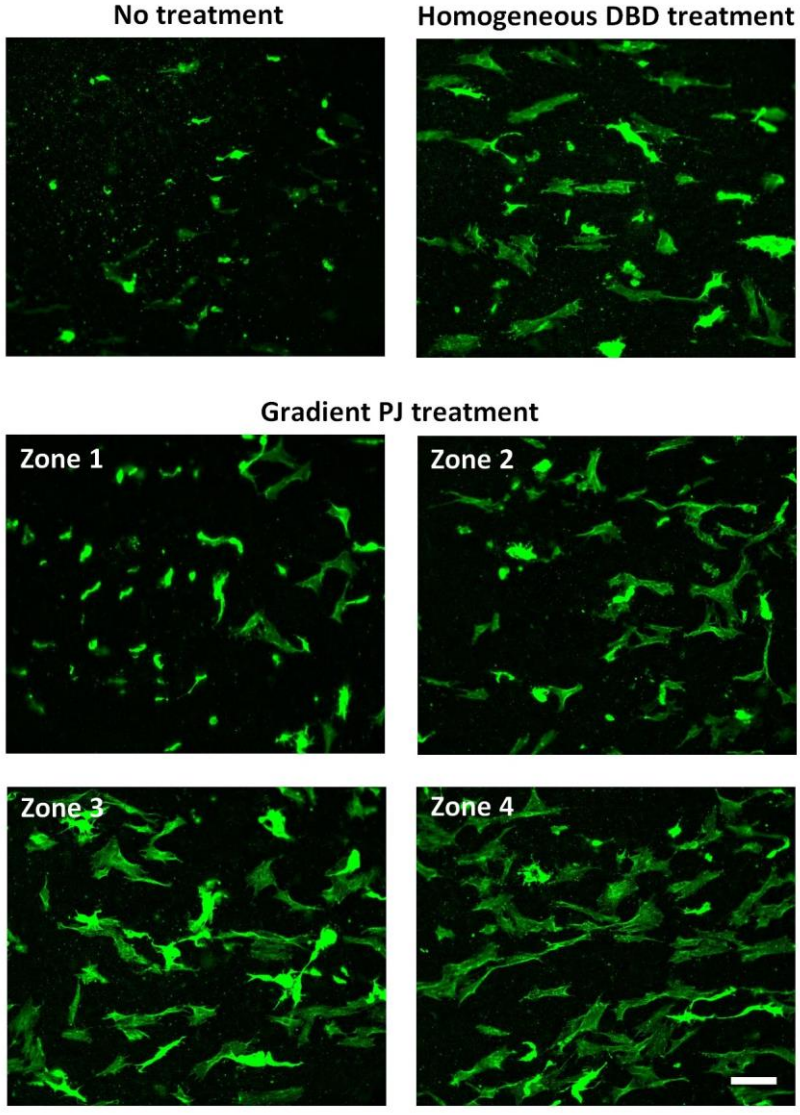

Fig. XI.13. *S100 immunostaining images of SCs cultured for 3 days with FBS on untreated, DBD treated and 4 zones of PJ treated NGCs (scale bar: 100 µm).*

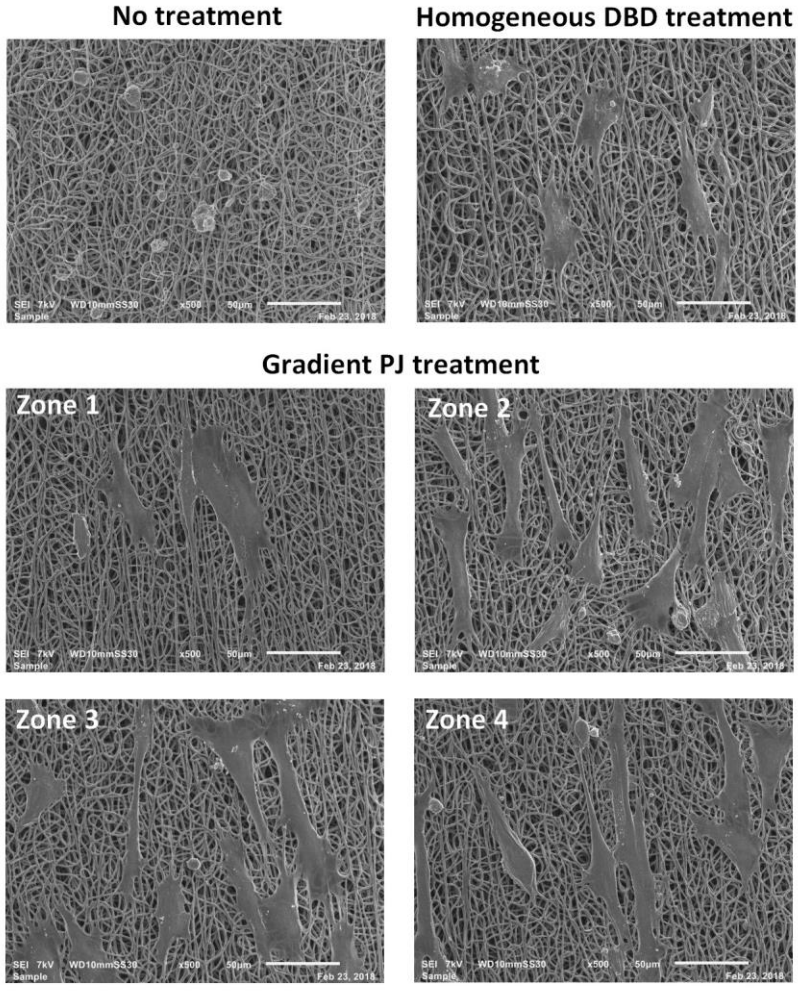

Fig. XI.14. *SEM images of SCs cultured for 3 days without FBS on untreated, DBD treated and 4 zones of PJ treated NGCs (scale bar: 10 µm).*

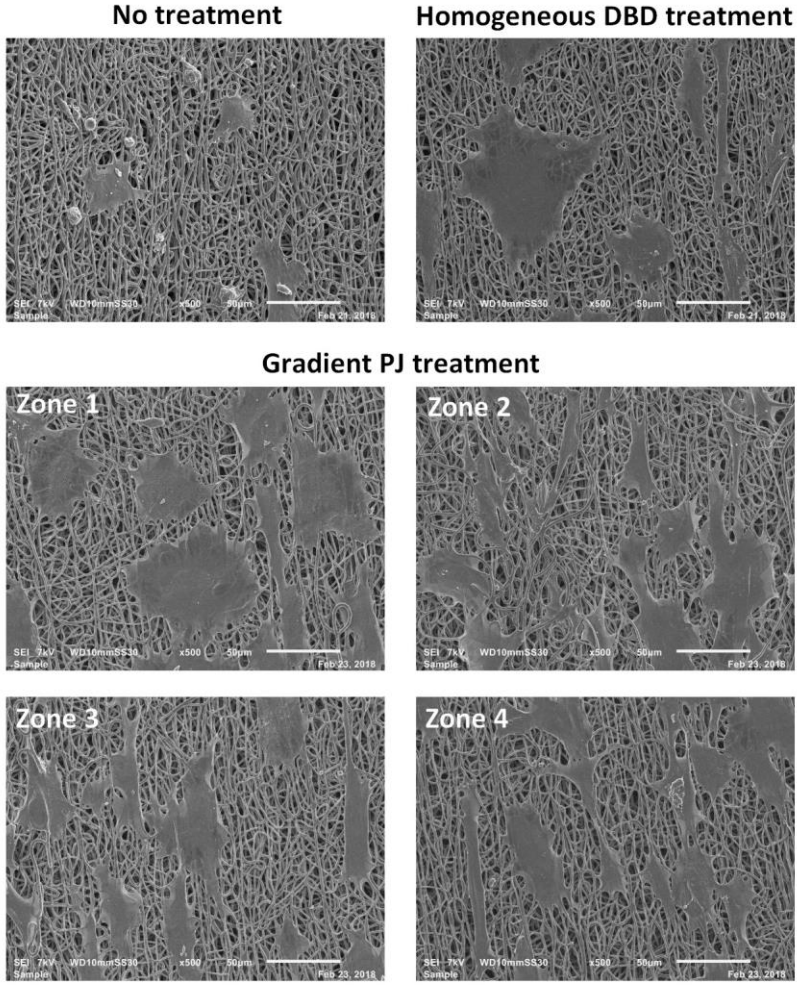

Fig. XI.15. *SEM images of SCs cultured for 3 days with FBS on untreated, DBD treated and 4 zones of PJ treated NGCs (scale bar: 10 μm).*

XI.3.4.3. Neurite extension on different zones of SC pre-seeded NGCs cultured with PC12

PC12 cells are cultured on the SC pre-seeded NGCs in order to assess their potential in triggering neurite outgrowth and elongation. S100 (green) /neurofilament (red) immunostaining images are therefore acquired 3 days after PC12 cell seeding. Anti-S100 antibodies seem to also bind to PC12 cells as they were stained in red and green. Nonetheless, a distinction between both cells can be made based on their clearly different morphologies. PC12 cells are rounded and tend to cluster together (Fig. XI.16 and XI.17). No signs of neurite outgrowth are perceived on all NGCs pre-seeded with SCs in the absence of FBS. However, neurite outgrowth is only detected on plasma-treated NGC pre-seeded with SCs in the presence of FBS. DBD treated NGCs display relatively short neurites extending in multiple directions. Conversely, PC12 cells seeded on PJ treated NGCs extend neurites that are mainly directed towards higher oxygen contents of the plasma gradient. Moreover, neurite length tends to increase on the oxygen-rich end. The results first suggests that neurite outgrowth is closely correlated with the presence of underlying SCs and their ability to offer or not a supportive environment. In fact, in addition to their secretion of neurotrophic factors, SCs are known to act as favorable substrate for neurite outgrowth via the expression of cell surface ligands and ECM components. Several regeneration-promoting cell adhesion molecules can be expressed on SC surface of which the neural cell adhesion molecule [474, 501]. This implies that PC12 cells lying on top of SCs are more prone to extend neurites than PC12 not in contact in SCs. When FBS is not present during culturing, SCs could not proliferate effectively to cover the whole NGC surface and PC12/SC contacts are less probable to occur. However, when FBS is present in the medium, an overall higher SC coverage is visualised on the plasma-treated NGCs but not on the untreated NGCs. This could explain to some extent the inability of PC12 cells to outgrow neurites on NGCs poorly covered with SCs. In a study conducted by Schnell et al., PC12 cells were cultured on PCL/collagen fibers pre-seeded with SCs. A tendency of neurites to grow directly on top of SCs rather than on the fibers was noticed [246]. Another study run by Thompson et al. also revealed that neurites are mainly observed on top of SCs in a neuron/SC co-culture. Moreover, neurons on SC monolayers extended more neurites than neurons on acellular substrates [474]. Another possible explanation is the inability of SCs cultured without FBS to maintain their specific activities that provide a regenerative environment such as the secretion of neurotrophic factors. The orientation of neurites towards the oxygen gradient is probably due to two factors: 1) SC alignment, that is more pronounced on PJ treated NGCs compared to DBD treated NCGs, is

probably providing an adequate guidance cue for outgrowing neurites. This unidirectional orientation of neurite outgrowth following SC alignment was also apparent is previous studies even in the absence of other directional cues [246, 474, 502, 503]. 2) The particular ability of growing neurites to sense chemical gradients promoting a directional orientation and elongation towards higher concentrations. Adams et al. placed DRGs in the middle of a grid containing peptide gradients and noticed that DRG growth cones could even turn and climb up towards the perpendicularly oriented gradients [504]. Few other studies have detected neurites directedness and gradual increase in length towards NGF gradients [311, 315, 316].
Both reasons implies an indirect communication of chemotactic signals and topographical cues from the NCGs via SCs to the growing neurites.

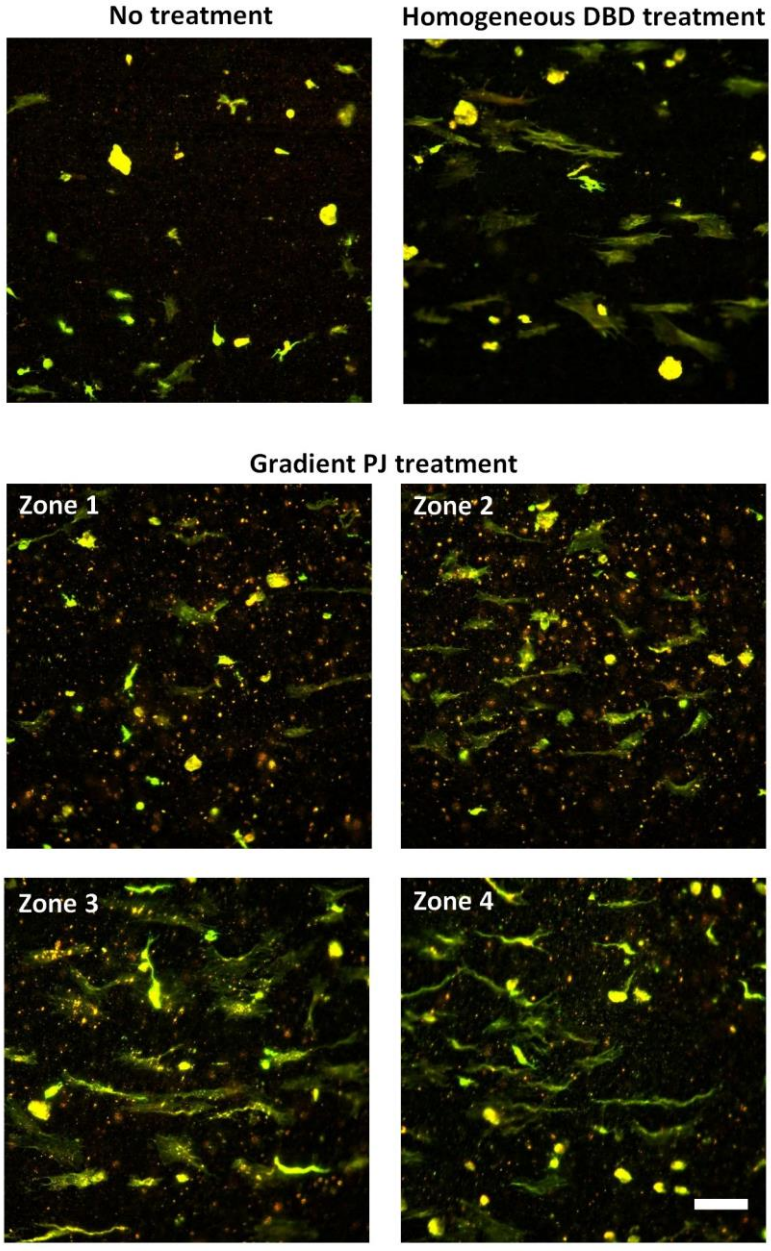

Fig. XI.16. *S100/neurofilament immunostaining images of SCs/PC12 cells co-cultured without FBS on untreated, DBD treated and 4 zones of PJ treated NGCs (S100: green; neurofilament: red; scale bar: 100 µm).*

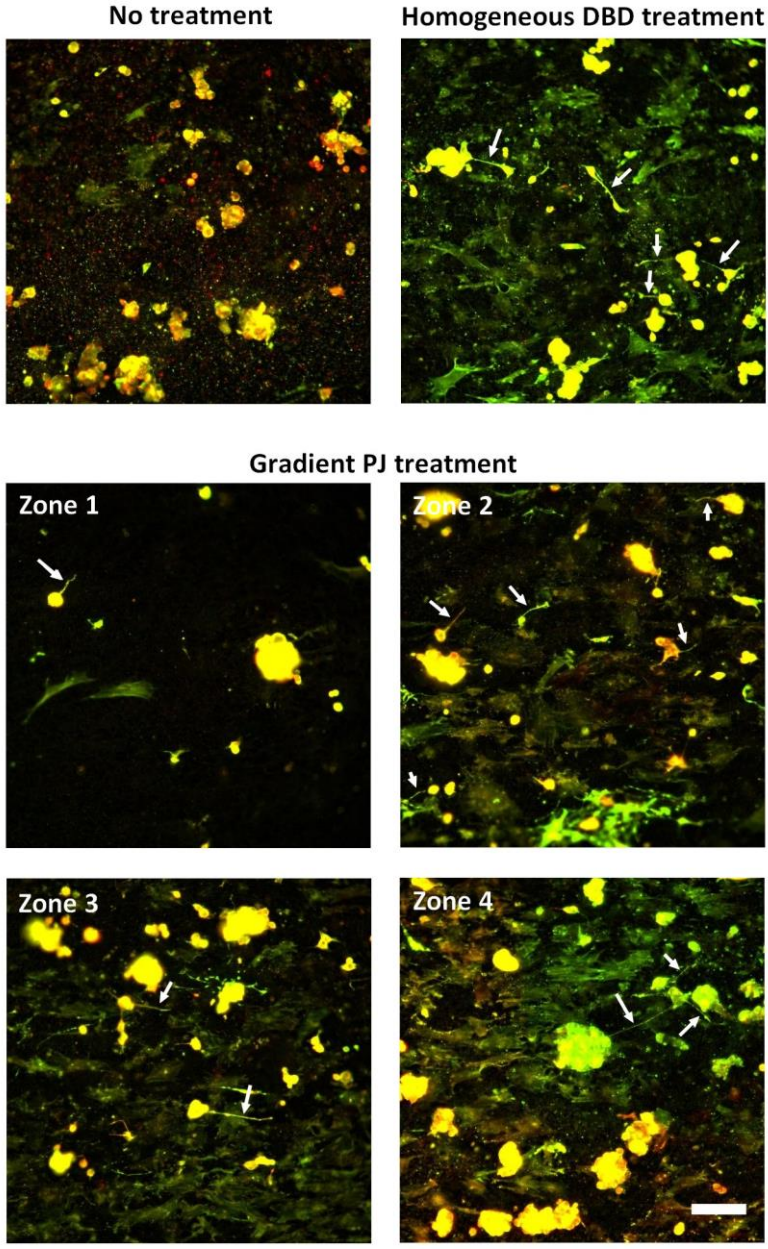

Fig. XI.17. *S100/neurofilament immunostaining images of SCs/PC12 cells co-cultured with FBS on untreated, DBD treated and 4 zones of PJ treated NGCs (The white arrows point at outgrowing neurites; S100: green; neurofilament: red; scale bar: 100 µm).*

XI.4.Conclusion

In this chapter, PA NGCs are electrospun using fine-tuned process parameters engendering an inner wall comprised of bundles of aligned fibers with random fibers in between and an outer wall fully composed of random fibers. The double-layered architecture is conceived to synergistically provide directional cues enhancing and guiding neurite extension while allowing sufficient nutrient supply. The NGCs are then subjected to different plasma treatments in order to promote the inner surface chemical properties for improved glial and neural cell performances. Medium pressure argon DBD treatment homogeneously increased the surface oxygen content from 17 % to 28 % by incorporating C-O, C=O and O-C=O groups, thus highlighting the plasma ability to penetrate through the porous wall. Atmospheric pressure argon PJ treatment created a gradient chemistry throughout the inner wall with an oxygen content gradually increasing from 21% to 30%. No fiber morphological alterations and scale variations are perceived post-plasma treatment. A significantly enhanced SC adhesion is observed on plasma-treated NGCs compared to untreated NGCs. A uniform cell distribution is observed along the homogeneously plasma-treated NGCs. However, cell gradients towards increased surface oxygen contents are interestingly detected on the NGCs subjected to a gradient plasma treatment. With time, the cell gradient becomes steeper and more prominent owing to the better cell proliferation on the oxygen-rich end and to a directed cell migration along the NGCs. SCs cultured on untreated NGCs remain rounded while planar and completely spread out SCs are observed on plasma-treated NGCs. A gradual change from a more circular shape to a more elongated shape is visualized along the oxygen gradient thus forming SC columns mimicking the natural bands of Bùngner structure. Finally, PC12 cells are cultured on SC pre-seeded NGCs to test their potential in triggering neurite extension as a proof of concept. Neurite outgrowth is only detected on plasma-treated NGC: DBD treated NGCs display relatively short neurites extending in multiple directions, while PJ treated NGCs show gradually longer neurites mainly directed towards higher oxygen contents. Overall, it can be concluded that plasma-treated PA NGCs have a great potential in nerve TE applications. Particularly, plasma-induced chemistry gradient along the inner wall is believed to strongly enhance the directed nerve regeneration thus paving the way towards critical nerve gap repair.

Chapter XII. General Conclusions and Outlook

XII.1.General conclusions

Despite the advances in peripheral nerve TE, the lately designed NGCs are still failing in repairing critical-sized peripheral nerve gaps. Tissue engineers are mainly focusing on optimizing the conduit design while overlooking its surface chemistry, an elemental parameter enhancing or halting cellular activities and thus neural regenerative capacity. Given the conduits' complex shape and narrow dimensions, reaching and changing the inner wall chemistry without damaging the subtle 3D structure remain challenging tasks. Therefore, the main goal of this thesis was to develop a novel NGC possessing in addition to refined topographical properties, a plasma-modified surface chemistry.

A step-by-step approach was adopted, all the way through this dissertation, to pave the way towards the generation of an optimized NCG. The joint or separate use of electrospinning and non-thermal plasma treatment marked each step as they constitute the biofabrication method and the surface engineering technique considered in the NGC generation respectively.

In order to prevent sterilization-induced damages of the engineered NGCs after the execution of all electrospinning and plasma treatment optimizations, the first step of this thesis was to select a suitable sterilization method for plasma-treated PCL surfaces. To do so, chapter VII was dedicated to study the effects of ETO, UV and HP sterilizations on the physico-chemical and bioresponsive properties of plasma-treated PCL films. Chapter VIII moved forward to a higher level in complexity and shifted from 2D films to 3D electrospun fibers. A clear scrutiny of different polymeric topographies was thus accomplished to check if they are equally affected by each sterilization. The trade-off between treatment stability/efficiency and affordability of the common low and atmospheric pressure treatments has led to the selection of a medium pressure DBD to plasma-treat the samples. WCA and XPS results showed the great efficiency of air and argon plasma treatments in enhancing the films and fibers wettability by incorporating oxygen-containing functionalities on their surface. Besides the beneficial surface modification, the potential of air and argon plasmas to sterilize PCL was first studied by varying plasma exposure times in a range that ensures a good surface modification while avoiding PCL degradation. Although an increased percentage of sterility was observed with increasing plasma exposure time, PCL films and fibers remained incompletely sterile. A decreased wettability is observed after EtO sterilization, attributable to the modification of PCL chain ends reacting with EtO molecules. A more drastic damage affected the fibers as their morphology also changed from cylindrical to a ribbon-like. HP

sterilization increased the roughness and modified the morphology of the films and radically altered the fibrous meshes to a point where no more fibers were visualized and a film was formed. This is presumably due to the complex thermo-oxidative reactions occurring between the strong oxidizer H_2O_2 and PCL in the HP chamber where temperature might exceed 55℃. UV did not affect the physico-chemical properties of the plasma-modified films and fibers which resulted in a considerably higher ADSC proliferation rate compared to EtO and HP sterilized samples. The first conclusion that can be drawn states that UV can be undoubtedly used to sterilize plasma-treated NGCs and other 2D and electrospun scaffolds intended for several TE applications.

In a second step, the focus shifted towards the electrospinning process itself. In fact, the ECM-like fibrous morphology created by electrospinning is not enough to achieve the near-perfect complex biomimicry. Very specific topographical features seem to be highly characteristic of a particular end application of which nerve TE. In reality, the ECM has a heterogeneous hierarchical nature since it is comprised of bioactive proteins structured to form randomly oriented or aligned fibers having dimensions ranging from a few nanometers to a few micrometers. Therefore, glial, neural and stem cells are critically influenced by changing the fiber diameter and orientation. To check for the optimal fiber characteristics, highly aligned and random PCL fibers with a wide scale of fiber diameters were first electrospun (Chapter IX). The overwhelming majority of studies involving PCL electrospinning implicated the use highly toxic solvent systems providing a good PCL solubility-spinability. Therefore, our goal was to use the unconventional and non-toxic solvent system acetic acid/formic acid, recently defined as the system producing ultra-thin PCL fibers, in a trial to outspread the size range and to tackle fiber alignment. A profound study of the effect of the collector design and collector RS on fiber alignment has led to the fabrication of a novel collector consisting of a flat cylinder able to engender simultaneous mechanical and electrical effects leading to a high degree of fiber alignment. Afterwards, the fiber diameter was addressed by varying and analyzing the influence of polymer concentration, TCD and RH. As a result of excessive fine-tunings, a very broad range of fiber diameters going from 94 to 1548 nm and from 114 to 1408 nm was successfully created for random and aligned fibers respectively. Overall, Chapter IX represents a good reference on how to create, using a unique and benign solvent system, PCL fibers having different diameters and orientations thus spanning the demands of every TE applications.

After electrospinning, random and highly aligned PCL fibers with 3 different diameters were selected and subjected to an argon DBD

plasma treatment. The synergistic influence of PCL fiber size, orientation and plasma-modified surface chemistry was then investigated on ADSC behavior (Chapter X). XPS and WCA results revealed the prominent efficiency of plasma in enhancing the fibers hydrophilicity by grafting oxygen-containing polar groups on their surface. Extended plasma exposure started altering the fibers morphological features with a growing risk of drastic damaging on thicker and random fibers compared to thinner and aligned fibers. The diverse responses to plasma stemed from the distinct molecular chain arrangement and crystallinity of different fiber diameters and orientations. The bioresponsive processes arising from the interaction of the ADSC cytoskeleton and the fibers were profoundly scrutinized based on the strongly coordinated interplay between fiber size, orientation and surface chemistry effects. The improved surface chemistry of plasma-treated fibers strikingly enhances the cell metabolic activity, adhesion, proliferation, cytoplasmic remodeling and morphology on all topographical conditions. ADSCs adhered on random fibers in a multi-directional fashion with a gradual change from radial to elongated morphology on increasing diameters. In contrast, cells overextended and aligned in parallel and bi-polar fashion on aligned fibers with a tendency to attach on fewer fibers when increasing their size. A mimicry of the natural bands of Büngner structure guiding axon extension during nerve regeneration was thus gradually observed, making from the aligned plasma-treated fibers promising candidates in the design of NGCs. A more general conclusion can be drawn: non-thermal plasma technology can constitute a very adequate surface treatment for fibrous implants of other TE applications as well. As the desired ADSCs performance strongly depends on the specific end-application, appropriate fiber size and orientation can thus be selected accordingly. Overall, Chapter X represents an on-target reference that can be used to optimize the previous generation of TE scaffolds.

The last experimental chapter directly tackled the core goal of this dissertation. Innovative double-layered PA NGCs were electropun in a one step process by using optimized working parameters. Bundles of aligned fibers with random fibers in between composed the inner wall while only random fibers were deposited on the outer wall. In this way, the inner wall can provide directional cues guiding neurite extension and can simultaneously allow nutrients to reach the lumen. The highly porous outer wall can further increase the nutrient supply while consolidating the whole NGC structure. After plasma treatment using a medium pressure argon DBD, the inner surface oxygen increased homogeneously along the NGC from 17 % to 28 %, thus emphasizing on plasma ability to penetrate through the porous wall. However, when NGCs were subjected to an atmospheric pressure argon PJ treatment,

a gradient chemistry with an oxygen content gradually increasing from 21% to 30% was perceived throughout the inner wall. SC adhesion was considerably enhanced on plasma-treated NGCs compared to untreated NGCs. A homogeneous cell distribution was visualized along the homogeneously plasma-treated NGCs. However, cell gradients towards increased surface oxygen contents were remarkably detected on the NGCs subjected to a gradient plasma treatment. With time, cell gradients became steeper and more prominent owing to the better cell proliferation on the oxygen-rich end and to a directed cell migration along the NGCs. SCs cultured on untreated NGCs remained rounded while completely spread out SCs were perceived on plasma-treated NGCs. SC morphology gradually changed from circular to elongated along the oxygen gradient thus forming SC columns mimicking the natural bands of Büngner structure. Finally, when PC12 cells were cultured on SC pre-seeded NGCs, neurite outgrowth was only detected on the plasma-treated NGCs. DBD treatment led to relatively short neurites extending in multiple directions, while PJ treatment exhibited gradually longer neurites mainly directed towards higher oxygen contents. Therefore, it can be concluded that a gradient plasma treatment of NGCs can boost SC elongation and migration and trigger directed neurite outgrowth that are essential for a successful peripheral nerve regeneration.

In summary, this thesis has first shown that UV sterilization is a suitable sterilization method for plasma-treated TE scaffolds of which NGCs. Moreover, the joint use of the electrospinning technique and the non-thermal plasma technology in the engineering of NGCs has a great potential in enhancing peripheral nerve regeneration. Particularly, plasma-induced chemistry gradient along the inner NGC wall offers high promises in bridging critical nerve defects and ensuring a complete functional recovery.

XII.2.Outlook

The results of this thesis revealed that homogeneous and/or gradient plasma activation of electrospun NGCs is a powerful tool in enhancing, glial, neural and stem cell performances *in vitro*. These NGCs are thus anticipated to promote nerve regeneration and functional recovery in critical nerve defects and to outperform the autograft. The next logical step is to transfer to *in vivo* tests to check our hypothesis. The *in vivo* implantation should involve both acellular and SC-seeded NGCs, to verify if plasma treatment alone would give similar results. Moreover, in order to obviate the drawbacks of the use of autologous SCs, deeper

in vitro investigations of the behavior of ADSCs and other stem cells cultured on plasma-treated NGCs should be run. Despite the enhanced regeneration observed when seeding undifferentiated ADSCs into NGCs, their definitive mechanisms of action are still questionable because of their multipotency. In this sense, the risk of differentiation towards unwanted cell types is relatively high. Therefore, the differentiation into glial or neural lineages prior to implantation is preferred. I believe that specific plasma-induced modifications could play an important role in stimulating and directing stem cells differentiation towards the desired cell type.

To broaden the functionalization spectrum and have more control on the grafted functional groups, future plasma polymerization of the NGCs is planned. Specific plasma polymers can be considered for a subsequent homogeneous or gradient immobilization of particular biomolecules such as NGF, BDNF, CTNF and GDNF. Several challenges are however foreseen as the process parameters should be very carefully tuned to obtain stable coatings using a low range of powers not compromising the delicate structure of NGCs. Moreover, applying a plasma coating on the inner wall and in a further step a plasma polymer gradient is way trickier than in the case of plasma activation.

More attention should be also given into the effects of the plasma-induced (bio)chemistry on the molecular processes taking place in different cell types via gene expression analysis. This will give more insights on how to specifically optimize the plasma process parameters enabling the studied cell type to enhance the regeneration of a targeted tissue such as peripheral nerves. For instance, plasma treatment optimizations based on correlations between the NGC plasma-modified surface and the SC expression of neurotrophic factors is believed to further promote axon regrowth.

A critical aspect that is mostly overlooked in the design of NGCs is their ability to support neovascularization in addition to nerve regeneration. In fact, the formation of new vessels in an injury site has been strongly correlated with the enhanced regeneration and functional recovery of the targeted tissue. Therefore, *in vitro* tests involving endothelial cell cultures and endothelial cell/glial cell co-cultures on plasma-treated NGCs should also be carried out.

Finally, future experiments can be conducted to test the potential use of plasma-treated conduits in the treatment of the more complex spinal cord injuries. Given the limited ability of the central nervous system to regenerate, more sophisticated conduits tackling heterogeneity in many aspects should be conceived.

References

[1] W. Daly, L. Yao, D. Zeugolis, A. Windebank, A. Pandit, A biomaterials approach to peripheral nerve regeneration: bridging the peripheral nerve gap and enhancing functional recovery, J. R. Soc. Interface 9(67) (2011) 202-221.
[2] D. Arslantunali, T. Dursun, D. Yucel, N. Hasirci, V. Hasirci, Peripheral nerve conduits: technology update, Medical Devices (Auckland, NZ) 7 (2014) 405.
[3] G.N. Panagopoulos, P.D. Megaloikonomos, A.F. Mavrogenis, The present and future for peripheral nerve regeneration, Orthopedics 40(1) (2017) e141-e156.
[4] P.-X. Zhang, N. Han, Y.-H. Kou, Q.-T. Zhu, X.-L. Liu, D.-P. Quan, J.-G. Chen, B.-G. Jiang, Tissue engineering for the repair of peripheral nerve injury, Neural regeneration research 14(1) (2019) 51-58.
[5] A. Quigley, K. Bulluss, I. Kyratzis, K. Gilmore, T. Mysore, K. Schirmer, E. Kennedy, M. O'Shea, Y. Truong, S. Edwards, Engineering a multimodal nerve conduit for repair of injured peripheral nerve, Journal of neural engineering 10(1) (2013) 016008.
[6] H. Koh, T. Yong, W. Teo, C. Chan, M. Puhaindran, T. Tan, A. Lim, B. Lim, S. Ramakrishna, In vivo study of novel nanofibrous intra-luminal guidance channels to promote nerve regeneration, Journal of neural engineering 7(4) (2010) 046003.
[7] X. Gu, F. Ding, Y. Yang, J. Liu, Construction of tissue engineered nerve grafts and their application in peripheral nerve regeneration, Progress in neurobiology 93(2) (2011) 204-230.
[8] P.J. Kingham, A.J. Reid, M. Wiberg, Adipose-derived stem cells for nerve repair: hype or reality?, Cells Tissues Organs 200(1) (2014) 23-30.
[9] S. Vijayavenkataraman, S. Thaharah, S. Zhang, W.F. Lu, J.Y.H. Fuh, Electrohydrodynamic jet 3D-printed PCL/PAA conductive scaffolds with tunable biodegradability as nerve guide conduits (NGCs) for peripheral nerve injury repair, Materials & Design 162 (2019) 171-184.
[10] E. Biazar, M.T. Khorasani, N. Montazeri, K. Pourshamsian, M. Daliri, M. Rezaei, M. Jabarvand, A. Khoshzaban, S. Heidari, M. Jafarpour, Z. Roviemiab, Types of neural guides and using nanotechnology for peripheral nerve reconstruction, International journal of nanomedicine 5 (2010) 839-852.
[11] R.M.G. Menorca, T.S. Fussell, J.C. Elfar, Nerve physiology: mechanisms of injury and recovery, Hand clinics 29(3) (2013) 317-330.
[12] R.M. Menorca, T.S. Fussell, J.C. Elfar, Peripheral nerve trauma: mechanisms of injury and recovery, Hand clinics 29(3) (2013) 317.
[13] M. Artico, L. Cervoni, F. Nucci, R. Giuffre, Birthday of peripheral nervous system surgery: the contribution of Gabriele Ferrara (1543–1627), Neurosurgery 39(2) (1996) 380-383.

[14] S.W. Mitchell, G.R. Morehouse, W.W. Keen, Gunshot wounds and other injuries of nerves. 1864, Clinical orthopaedics and related research 458 (2007) 35-39.
[15] A.D. Gaudet, P.G. Popovich, M.S. Ramer, Wallerian degeneration: gaining perspective on inflammatory events after peripheral nerve injury, Journal of neuroinflammation 8(1) (2011) 110.
[16] G.R. Evans, Peripheral nerve injury: a review and approach to tissue engineered constructs, The Anatomical Record: An Official Publication of the American Association of Anatomists 263(4) (2001) 396-404.
[17] S. Kehoe, X. Zhang, D. Boyd, FDA approved guidance conduits and wraps for peripheral nerve injury: a review of materials and efficacy, Injury 43(5) (2012) 553-572.
[18] E.W. Wang, J. Zhang, J.H. Huang, Repairing peripheral nerve injury using tissue engineering techniques, Neural regeneration research 10(9) (2015) 1393-1394.
[19] J. Xie, M.R. MacEwan, W. Liu, N. Jesuraj, X. Li, D. Hunter, Y. Xia, Nerve guidance conduits based on double-layered scaffolds of electrospun nanofibers for repairing the peripheral nervous system, ACS Appl. Mater. Interfaces 6(12) (2014) 9472-9480.
[20] A. Moradzadeh, G.H. Borschel, J.P. Luciano, E.L. Whitlock, A. Hayashi, D.A. Hunter, S.E. Mackinnon, The impact of motor and sensory nerve architecture on nerve regeneration, Experimental neurology 212(2) (2008) 370-376.
[21] D. Santos, P. Wieringa, L. Moroni, X. Navarro, J.D. Valle, PEOT/PBT guides enhance nerve regeneration in long gap defects, Adv. Healthc. Mater. 6(3) (2017) 1600298.
[22] J. Xie, M.R. MacEwan, A.G. Schwartz, Y. Xia, Electrospun nanofibers for neural tissue engineering, Nanoscale 2(1) (2010) 35-44.
[23] C. Cunha, S. Panseri, S. Antonini, Emerging nanotechnology approaches in tissue engineering for peripheral nerve regeneration, Nanomedicine: Nanotechnology, Biology and Medicine 7(1) (2011) 50-59.
[24] F. Ijpma, R. Van De Graaf, M. Meek, The early history of tubulation in nerve repair, Journal of Hand Surgery (European Volume) 33(5) (2008) 581-586.
[25] M. Sun, P.J. Kingham, A.J. Reid, S.J. Armstrong, G. Terenghi, S. Downes, In vitro and in vivo testing of novel ultrathin PCL and PCL/PLA blend films as peripheral nerve conduit, Journal of Biomedical Materials Research Part A: An Official Journal of The Society for Biomaterials, The Japanese Society for Biomaterials, and The Australian Society for Biomaterials and the Korean Society for Biomaterials 93(4) (2010) 1470-1481.

[26] P. Labroo, D. Hilgart, B. Davis, C. Lambert, H. Sant, B. Gale, J.E. Shea, J. Agarwal, Drug-delivering nerve conduit improves regeneration in a critical-sized gap, Biotechnology and bioengineering 116(1) (2019) 143-154.
[27] M.D. Sarker, S. Naghieh, A.D. McInnes, D.J. Schreyer, X. Chen, Regeneration of peripheral nerves by nerve guidance conduits: Influence of design, biopolymers, cells, growth factors, and physical stimuli, Progress in Neurobiology 171 (2018) 125-150.
[28] J.S. Belkas, M.S. Shoichet, R. Midha, Peripheral nerve regeneration through guidance tubes, Neurological research 26(2) (2004) 151-160.
[29] I.P. Clements, Y.-t. Kim, A.W. English, X. Lu, A. Chung, R.V. Bellamkonda, Thin-film enhanced nerve guidance channels for peripheral nerve repair, Biomaterials 30(23-24) (2009) 3834-3846.
[30] X. Jiang, S.H. Lim, H.-Q. Mao, S.Y. Chew, Current applications and future perspectives of artificial nerve conduits, Experimental neurology 223(1) (2010) 86-101.
[31] R. Deumens, A. Bozkurt, M.F. Meek, M.A. Marcus, E.A. Joosten, J. Weis, G.A. Brook, Repairing injured peripheral nerves: bridging the gap, Progress in neurobiology 92(3) (2010) 245-276.
[32] R.V. Bellamkonda, Peripheral nerve regeneration: an opinion on channels, scaffolds and anisotropy, Biomaterials 27(19) (2006) 3515-3518.
[33] V. Mukhatyar, L. Karumbaiah, J. Yeh, R. Bellamkonda, Tissue engineering strategies designed to realize the endogenous regenerative potential of peripheral nerves, Advanced Materials 21(46) (2009) 4670-4679.
[34] S. Itoh, K. Takakuda, H. Samejima, T. Ohta, K. Shinomiya, S. Ichinose, Synthetic collagen fibers coated with a synthetic peptide containing the YIGSR sequence of laminin to promote peripheral nerve regeneration in vivo, Journal of Materials Science: Materials in Medicine 10(3) (1999) 129-134.
[35] T. Toba, T. Nakamura, Y. Shimizu, K. Matsumoto, K. Ohnishi, S. Fukuda, M. Yoshitani, H. Ueda, Y. Hori, K. Endo, Regeneration of canine peroneal nerve with the use of a polyglycolic acid–collagen tube filled with laminin-soaked collagen sponge: a comparative study of collagen sponge and collagen fibers as filling materials for nerve conduits, Journal of Biomedical Materials Research: An Official Journal of The Society for Biomaterials, The Japanese Society for Biomaterials, and The Australian Society for Biomaterials and the Korean Society for Biomaterials 58(6) (2001) 622-630.
[36] T.T.B. Ngo, P.J. Waggoner, A.A. Romero, K.D. Nelson, R.C. Eberhart, G.M. Smith, Poly (l-lactide) microfilaments enhance

peripheral nerve regeneration across extended nerve lesions, Journal of neuroscience research 72(2) (2003) 227-238.
[37] Y.-C. Lin, M. Ramadan, M. Van Dyke, L.E. Kokai, B.J. Philips, J.P. Rubin, K.G. Marra, Keratin gel filler for peripheral nerve repair in a rodent sciatic nerve injury model, Plastic and reconstructive surgery 129(1) (2012) 67-78.
[38] F. Ding, J. Wu, Y. Yang, W. Hu, Q. Zhu, X. Tang, J. Liu, X. Gu, Use of tissue-engineered nerve grafts consisting of a chitosan/poly (lactic-co-glycolic acid)-based scaffold included with bone marrow mesenchymal cells for bridging 50-mm dog sciatic nerve gaps, Tissue Eng. Part A 16(12) (2010) 3779-3790.
[39] S. Yoshii, M. Oka, Collagen filaments as a scaffold for nerve regeneration, Journal of Biomedical Materials Research: An Official Journal of The Society for Biomaterials, The Japanese Society for Biomaterials, and The Australian Society for Biomaterials and the Korean Society for Biomaterials 56(3) (2001) 400-405.
[40] K. Matsumoto, K. Ohnishi, T. Kiyotani, T. Sekine, H. Ueda, T. Nakamura, K. Endo, Y. Shimizu, Peripheral nerve regeneration across an 80-mm gap bridged by a polyglycolic acid (PGA)–collagen tube filled with laminin-coated collagen fibers: a histological and electrophysiological evaluation of regenerated nerves, Brain research 868(2) (2000) 315-328.
[41] F. Stang, H. Fansa, G. Wolf, M. Reppin, G. Keilhoff, Structural parameters of collagen nerve grafts influence peripheral nerve regeneration, Biomaterials 26(16) (2005) 3083-3091.
[42] Y.-t. Kim, V.K. Haftel, S. Kumar, R.V. Bellamkonda, The role of aligned polymer fiber-based constructs in the bridging of long peripheral nerve gaps, Biomaterials 29(21) (2008) 3117-3127.
[43] M.D. Wood, M.R. MacEwan, A.R. French, A.M. Moore, D.A. Hunter, S.E. Mackinnon, D.W. Moran, G.H. Borschel, S.E. Sakiyama-Elbert, Fibrin matrices with affinity-based delivery systems and neurotrophic factors promote functional nerve regeneration, Biotechnology and bioengineering 106(6) (2010) 970-979.
[44] X. Hu, J. Huang, Z. Ye, L. Xia, M. Li, B. Lv, X. Shen, Z. Luo, A novel scaffold with longitudinally oriented microchannels promotes peripheral nerve regeneration, Tissue Eng. Part A 15(11) (2009) 3297-3308.
[45] G.E. Rutkowski, C.A. Miller, S. Jeftinija, S.K. Mallapragada, Synergistic effects of micropatterned biodegradable conduits and Schwann cells on sciatic nerve regeneration, Journal of Neural Engineering 1(3) (2004) 151-157.
[46] S. Panseri, C. Cunha, J. Lowery, U. Del Carro, F. Taraballi, S. Amadio, A. Vescovi, F. Gelain, Electrospun micro-and nanofiber tubes

for functional nervous regeneration in sciatic nerve transections, BMC biotechnology 8(1) (2008) 39.
[47] S.Y. Chew, R. Mi, A. Hoke, K.W. Leong, Aligned protein–polymer composite fibers enhance nerve regeneration: A potential tissue-engineering platform, Advanced functional materials 17(8) (2007) 1288-1296.
[48] W. Yu, W. Zhao, C. Zhu, X. Zhang, D. Ye, W. Zhang, Y. Zhou, X. Jiang, Z. Zhang, Sciatic nerve regeneration in rats by a promising electrospun collagen/poly (ε-caprolactone) nerve conduit with tailored degradation rate, BMC neuroscience 12(1) (2011) 68.
[49] C.-Y. Wang, K.-H. Zhang, C.-Y. Fan, X.-M. Mo, H.-J. Ruan, F.-F. Li, Aligned natural–synthetic polyblend nanofibers for peripheral nerve regeneration, Acta Biomater. 7(2) (2011) 634-643.
[50] T. Hadlock, C. Sundback, D. Hunter, M. Cheney, J.P. Vacanti, A polymer foam conduit seeded with Schwann cells promotes guided peripheral nerve regeneration, Tissue Eng. 6(2) (2000) 119-127.
[51] L. Yao, G.C. de Ruiter, H. Wang, A.M. Knight, R.J. Spinner, M.J. Yaszemski, A.J. Windebank, A. Pandit, Controlling dispersion of axonal regeneration using a multichannel collagen nerve conduit, Biomaterials 31(22) (2010) 5789-5797.
[52] G.C. De Ruiter, R.J. Spinner, M.J. Malessy, M.J. Moore, E.J. Sorenson, B.L. Currier, M.J. Yaszemski, A.J. Windebank, Accuracy of motor axon regeneration across autograft, single-lumen, and multichannel poly (lactic-co-glycolic acid) nerve tubes, Neurosurgery 63(1) (2008) 144-155.
[53] S. Madduri, B. Gander, Schwann cell delivery of neurotrophic factors for peripheral nerve regeneration, Journal of the Peripheral Nervous System 15(2) (2010) 93-103.
[54] C. Deister, C.E. Schmidt, Optimizing neurotrophic factor combinations for neurite outgrowth, Journal of neural engineering 3(2) (2006) 172.
[55] J. Peleshok, H. Saragovi, Functional mimetics of neurotrophins and their receptors, Portland Press Limited, 2006.
[56] J.A. Mohammad, P.H. Warnke, Y. Pan, S. Shenaq, Increased axonal regeneration through a biodegradable amnionic tube nerve conduit: effect of local delivery and incorporation of nerve growth factor/hyaluronic acid media, Annals of plastic surgery 44(1) (2000) 59-64.
[57] E.G. Fine, I. Decosterd, M. Papaloïzos, A.D. Zurn, P. Aebischer, GDNF and NGF released by synthetic guidance channels support sciatic nerve regeneration across a long gap, European Journal of Neuroscience 15(4) (2002) 589-601.
[58] E. Vögelin, J. Baker, J. Gates, V. Dixit, M.A. Constantinescu, N. Jones, Effects of local continuous release of brain derived neurotrophic

factor (BDNF) on peripheral nerve regeneration in a rat model, Experimental neurology 199(2) (2006) 348-353.
[59] K. Houschyar, A. Momeni, M. Pyles, J. Cha, Z. Maan, D. Duscher, O. Jew, F. Siemers, J.v. Schoonhoven, The role of current techniques and concepts in peripheral nerve repair, Plastic surgery international 2016 (2016).
[60] D.M. Shirley, S.A. Williams, P.M. Santos, Brain-derived neurotrophic factor and peripheral nerve regeneration: a functional evaluation, The Laryngoscope 106(5) (1996) 629-632.
[61] S. Madduri, K. Feldman, T. Tervoort, M. Papaloïzos, B. Gander, Collagen nerve conduits releasing the neurotrophic factors GDNF and NGF, Journal of Controlled Release 143(2) (2010) 168-174.
[62] G.R. Evans, K. Brandt, S. Katz, P. Chauvin, L. Otto, M. Bogle, B. Wang, R.K. Meszlenyi, L. Lu, A.G. Mikos, Bioactive poly (L-lactic acid) conduits seeded with Schwann cells for peripheral nerve regeneration, Biomaterials 23(3) (2002) 841-848.
[63] A.M. McGrath, L.N. Novikova, L.N. Novikov, M. Wiberg, BD™ PuraMatrix™ peptide hydrogel seeded with Schwann cells for peripheral nerve regeneration, Brain research bulletin 83(5) (2010) 207-213.
[64] D.F. Kalbermatten, P.J. Kingham, D. Mahay, C. Mantovani, J. Pettersson, W. Raffoul, H. Balcin, G. Pierer, G. Terenghi, Fibrin matrix for suspension of regenerative cells in an artificial nerve conduit, Journal of plastic, reconstructive & aesthetic surgery 61(6) (2008) 669-675.
[65] A. Ladak, J. Olson, E. Tredget, T. Gordon, Differentiation of mesenchymal stem cells to support peripheral nerve regeneration in a rat model, Experimental neurology 228(2) (2011) 242-252.
[66] P.G. di Summa, P.J. Kingham, W. Raffoul, M. Wiberg, G. Terenghi, D.F. Kalbermatten, Adipose-derived stem cells enhance peripheral nerve regeneration, Journal of Plastic, Reconstructive & Aesthetic Surgery 63(9) (2010) 1544-1552.
[67] A. Mosahebi, B. Woodward, M. Wiberg, R. Martin, G. Terenghi, Retroviral labeling of Schwann cells: in vitro characterization and in vivo transplantation to improve peripheral nerve regeneration, Glia 34(1) (2001) 8-17.
[68] L.Y. Santiago, J. Clavijo-Alvarez, C. Brayfield, J.P. Rubin, K.G. Marra, Delivery of adipose-derived precursor cells for peripheral nerve repair, Cell transplantation 18(2) (2009) 145-158.
[69] R. Dai, Z. Wang, R. Samanipour, K.-i. Koo, K. Kim, Adipose-Derived Stem Cells for Tissue Engineering and Regenerative Medicine Applications, Stem Cells Int. 2016 (2016) 19.

[70] B.A. Bunnell, M. Flaat, C. Gagliardi, B. Patel, C. Ripoll, Adipose-derived Stem Cells: Isolation, Expansion and Differentiation, Methods. 45(2) (2008) 115-120.
[71] J.M. Gimble, A.J. Katz, B.A. Bunnell, Adipose-derived stem cells for regenerative medicine, Circ.Res. 100(9) (2007) 1249-1260.
[72] J. Oliveira, F. Almeida, A. Biancalana, A.F. Baptista, M.A. Tomaz, P.A. Melo, A. Martinez, Mesenchymal stem cells in a polycaprolactone conduit enhance median-nerve regeneration, prevent decrease of creatine phosphokinase levels in muscle, and improve functional recovery in mice, Neuroscience 170(4) (2010) 1295-1303.
[73] C. Radtke, B. Schmitz, M. Spies, J. Kocsis, P. Vogt, Peripheral glial cell differentiation from neurospheres derived from adipose mesenchymal stem cells, International Journal of Developmental Neuroscience 27(8) (2009) 817-823.
[74] R. Kaewkhaw, A.M. Scutt, J.W. Haycock, Anatomical site influences the differentiation of adipose-derived stem cells for Schwann-cell phenotype and function, Glia 59(5) (2011) 734-749.
[75] P.G. di Summa, D.F. Kalbermatten, E. Pralong, W. Raffoul, P.J. Kingham, G. Terenghi, Long-term in vivo regeneration of peripheral nerves through bioengineered nerve grafts, Neuroscience 181 (2011) 278-291.
[76] Q. Li, P. Ping, H. Jiang, K. Liu, Nerve conduit filled with GDNF gene-modified schwann cells enhances regeneration of the peripheral nerve, Microsurgery: Official Journal of the International Microsurgical Society and the European Federation of Societies for Microsurgery 26(2) (2006) 116-121.
[77] M.R. Tannemaat, R. Eggers, W.T. Hendriks, G.C. De Ruiter, J.J. Van Heerikhuize, C.W. Pool, M.J. Malessy, G.J. Boer, J. Verhaagen, Differential effects of lentiviral vector-mediated overexpression of nerve growth factor and glial cell line-derived neurotrophic factor on regenerating sensory and motor axons in the transected peripheral nerve, European Journal of Neuroscience 28(8) (2008) 1467-1479.
[78] D. Gupta, J. Venugopal, M.P. Prabhakaran, V.G. Dev, S. Low, A.T. Choon, S. Ramakrishna, Aligned and random nanofibrous substrate for the in vitro culture of Schwann cells for neural tissue engineering, Acta. Biomater. 5(7) (2009) 2560-2569.
[79] L. He, S. Liao, D. Quan, K. Ma, C. Chan, S. Ramakrishna, J. Lu, Synergistic effects of electrospun PLLA fiber dimension and pattern on neonatal mouse cerebellum C17. 2 stem cells, Acta. Biomater. 6(8) (2010) 2960-2969.
[80] S.Y. Chew, R. Mi, A. Hoke, K.W. Leong, The effect of the alignment of electrospun fibrous scaffolds on Schwann cell maturation, Biomaterials 29(6) (2008) 653-661.

[81] S. Wang, L. Cai, Polymers for Fabricating Nerve Conduits, Int. J. Polym. Sci. 2010 (2010).
[82] S. Kehoe, X.F. Zhang, D. Boyd, FDA approved guidance conduits and wraps for peripheral nerve injury: A review of materials and efficacy, Injury 43(5) (2012) 553-572.
[83] M.A. Woodruff, D.W. Hutmacher, The return of a forgotten polymer—polycaprolactone in the 21st century, Prog. Polym. Sci. 35(10) (2010) 1217-1256.
[84] A.G. Kanani, S.H. Bahrami, Effect of changing solvents on poly (ε-caprolactone) nanofibrous webs morphology, J. Nanomater. 2011 (2011) 31.
[85] W.-J. Li, J.A. Cooper, R.L. Mauck, R.S. Tuan, Fabrication and characterization of six electrospun poly(α-hydroxy ester)-based fibrous scaffolds for tissue engineering applications, Acta. Biomater. 2(4) (2006) 377-385.
[86] F. Frattini, F.R. Pereira Lopes, F.M. Almeida, R.F. Rodrigues, L.C. Boldrini, M.A. Tomaz, A.F. Baptista, P.A. Melo, A.M.B. Martinez, Mesenchymal stem cells in a polycaprolactone conduit promote sciatic nerve regeneration and sensory neuron survival after nerve injury, Tissue Eng. Part A 18(19-20) (2012) 2030-2039.
[87] C.J. Chang, Effects of nerve growth factor from genipin-crosslinked gelatin in polycaprolactone conduit on peripheral nerve regeneration—In vitro and in vivo, Journal of Biomedical Materials Research Part A: An Official Journal of The Society for Biomaterials, The Japanese Society for Biomaterials, and The Australian Society for Biomaterials and the Korean Society for Biomaterials 91(2) (2009) 586-596.
[88] A. Martins, E.D. Pinho, S. Faria, I. Pashkuleva, A.P. Marques, R.L. Reis, N.M. Neves, Surface Modification of Electrospun Polycaprolactone Nanofiber Meshes by Plasma Treatment to Enhance Biological Performance, Small 5(10) (2009) 1195-1206.
[89] T. Führmann, P.N. Anandakumaran, M.S. Shoichet, Combinatorial therapies after spinal cord injury: how can biomaterials help?, Adv. Healthc. Mater. 6(10) (2017) 1601130.
[90] P. Cools, C. Mota, I. Lorenzo-Moldero, R. Ghobeira, N. De Geyter, L. Moroni, R. Morent, Acrylic Acid Plasma Coated 3D Scaffolds for Cartilage tissue engineering applications, Scientific Reports 8(1) (2018) 3830.
[91] R. Ghobeira, C. Philips, V. De Naeyer, H. Declercq, P. Cools, N. De Geyter, R. Cornelissen, R. Morent, Comparative Study of the Surface Properties and Cytocompatibility of Plasma-Treated Poly-ε-Caprolactone Nanofibers Subjected to Different Sterilization Methods, Journal of Biomedical Nanotechnology 13(6) (2017) 699-716.

[92] R. Bitar, P. Cools, N. De Geyter, R. Morent, Acrylic acid plasma polymerization for biomedical use, Appl. Surf. Sci. 148(2018) (2018) 168-185.
[93] H.K. Frost, T. Andersson, S. Johansson, U. Englund-Johansson, P. Ekström, L.B. Dahlin, F. Johansson, Electrospun nerve guide conduits have the potential to bridge peripheral nerve injuries in vivo, Scientific Reports 8(1) (2018) 16716.
[94] C.A. Hundepool, T.H. Nijhuis, B. Mohseny, R.W. Selles, S.E. Hovius, The effect of stem cells in bridging peripheral nerve defects: a meta-analysis: A review, Journal of neurosurgery 121(1) (2014) 195-209.
[95] K.P. Das, T.M. Freudenrich, W.R. Mundy, Assessment of PC12 cell differentiation and neurite growth: a comparison of morphological and neurochemical measures, Neurotoxicology and Teratology 26(3) (2004) 397-406.
[96] D.I. Braghirolli, D. Steffens, K. Quintiliano, G.A.X. Acasigua, D. Gamba, R.A. Fleck, C.L. Petzhold, P. Pranke, The effect of sterilization methods on electronspun poly(lactide-co-glycolide) and subsequent adhesion efficiency of mesenchymal stem cells, Journal of Biomedical Materials Research Part B: Applied Biomaterials 102(4) (2014) 700-708.
[97] K.D. Andrews, J.A. Hunt, R.A. Black, Effects of sterilisation method on surface topography and in-vitro cell behaviour of electrostatically spun scaffolds, Biomaterials 28(6) (2007) 1014-1026.
[98] S. De Vrieze, T. Van Camp, A. Nelvig, B. Hagström, P. Westbroek, K. De Clerck, The effect of temperature and humidity on electrospinning, Journal of materials science 44(5) (2009) 1357.
[99] L. Huang, N.N. Bui, S.S. Manickam, J.R. McCutcheon, Controlling electrospun nanofiber morphology and mechanical properties using humidity, Journal of polymer science part B: Polymer physics 49(24) (2011) 1734-1744.
[100] J. Pelipenko, J. Kristl, B. Janković, S. Baumgartner, P. Kocbek, The impact of relative humidity during electrospinning on the morphology and mechanical properties of nanofibers, International Journal of Pharmaceutics 456(1) (2013) 125-134.
[101] B. Wang, W. Zhou, M.W. Chang, Z. Ahmad, J.S. Li, Impact of substrate geometry on electrospun fiber deposition and alignment, Journal of Applied Polymer Science 134(19) (2017).
[102] M.M. Arras, C. Grasl, H. Bergmeister, H. Schima, Electrospinning of aligned fibers with adjustable orientation using auxiliary electrodes, Science and technology of advanced materials 13(3) (2012) 035008.
[103] F.J. O'Brien, Biomaterials & scaffolds for tissue engineering, Mater. Today 14(3) (2011) 88-95.

[104] F.G. Heineken, R. Skalak, Tissue Engineering - a Brief Overview, J. Biomech. Eng-T. Asme 113(2) (1991) 111-112.
[105] J. Black, Western Winter Workshop on Tissue Engineering-Granlibakken, Tohao-City, California, USA 26-27 February Biomaterials 9(4) (1988) 379-379.
[106] R. Langer, J. Vacanti, Tissue engineering, Science 260(5110) (1993) 920-926.
[107] L.S. Nair, S. Bhattacharyya, C.T. Laurencin, Nanotechnology and tissue engineering: the scaffold based approach, Nanotechnologies for the Life Sciences (2006) 1-65.
[108] Y. Kim, H. Ko, I.K. Kwon, K. Shin, Extracellular Matrix Revisited: Roles in Tissue Engineering, Int. Neurourol. J. 20 (2016) S23-S29.
[109] P. Supaphol, O. Suwantong, P. Sangsanoh, S. Srinivasan, R. Jayakumar, S.V. Nair, Electrospinning of Biocompatible Polymers and Their Potentials in Biomedical Applications, in: R. Jayakumar, S.V. Nair (Eds.), Biomedical Applications of Polymeric Nanofibers2012, pp. 213-239.
[110] B.D. Ulery, L.S. Nair, C.T. Laurencin, Biomedical Applications of Biodegradable Polymers, J. Polym. Sci. B Polym. Phys. 49(12) (2011) 832-864.
[111] M. Sokolsky-Papkov, K. Agashi, A. Olaye, K. Shakesheff, A.J. Domb, Polymer carriers for drug delivery in tissue engineering, Adv. Drug Deliv. Rev. 59(4-5) (2007) 187-206.
[112] H.K. Kleinman, D. Philp, M.P. Hoffman, Role of the extracellular matrix in morphogenesis, Curr. Opin. Biotechnol. 14(5) (2003) 526-532.
[113] A. Rainer, M. Centola, C. Spadaccio, G. Gherardi, J.A. Genovese, S. Licoccia, M. Trombetta, Comparative study of different techniques for the sterilization of poly-L-lactide electrospun microfibers: effectiveness vs. material degradation, Int. J. Artif. Organs 33(2) (2010) 76-85.
[114] D. Yan, J. Jones, X.Y. Yuan, X.H. Xu, J. Sheng, J.C.M. Lee, G.Q. Ma, Q.S. Yu, Plasma treatment of electrospun PCL random nanofiber meshes (NFMs) for biological property improvement, J. Biomed. Mater. Res. A 101(4) (2013) 963-972.
[115] M. Tallawi, E. Rosellini, N. Barbani, M.G. Cascone, R. Rai, G. Saint-Pierre, A.R. Boccaccini, Strategies for the chemical and biological functionalization of scaffolds for cardiac tissue engineering: a review, J. R. Soc. Interface 12(108) (2015) 1-24.
[116] Q. Cheng, K. Komvopoulos, S. Li, Plasma-assisted heparin conjugation on electrospun poly(l-lactide) fibrous scaffolds, J. Biomed. Mater. Res. A 102(5) (2014) 1408-1414.
[117] W. Zhu, N.J. Castro, X.Q. Cheng, M. Keidar, L.G. Zhang, Cold Atmospheric Plasma Modified Electrospun Scaffolds with Embedded

Microspheres for Improved Cartilage Regeneration, Plos One 10(7) (2015) 1-18.
[118] E.S. Place, J.H. George, C.K. Williams, M.M. Stevens, Synthetic polymer scaffolds for tissue engineering, Chem. Soc. Rev. 38(4) (2009) 1139-1151.
[119] C. Frantz, K.M. Stewart, V.M. Weaver, The extracellular matrix at a glance, J. Cell Sci. 123(24) (2010) 4195-4200.
[120] A.J. García, Get a grip: integrins in cell–biomaterial interactions, Biomaterials 26(36) (2005) 7525-7529.
[121] A.D. Bershadsky, C. Ballestrem, L. Carramusa, Y. Zilberman, B. Gilquin, S. Khochbin, A.Y. Alexandrova, A.B. Verkhovsky, T. Shemesh, M.M. Kozlov, Assembly and mechanosensory function of focal adhesions: experiments and models, Eur. J. Cell Biol. 85(3–4) (2006) 165-173.
[122] <https://www.khanacademy.org/science/biology/structure-of-a-cell/cytoskeleton-junctions-and-extracellular-structures/a/the-extracellular-matrix-and-cell-wall>).
[123] S. Badylak, T. Gilbert, J. Myers-Irvin, The extracellular matrix as a biologic scaffold for tissue engineering, Tissue Eng. 1 (2008) 121-143.
[124] H. Patel, M. Bonde, G. Srinivasan, Biodegradable polymer scaffold for tissue engineering, Trends Biomater. Artif. Organs 25(1) (2011) 20-29.
[125] S.M. Krane, The importance of proline residues in the structure, stability and susceptibility to proteolytic degradation of collagens, Amino Acids 35(4) (2008) 703-710.
[126] G. Rohman, J. Spadavecchia, Biodegradable polymeric nanomaterials, Nanomaterials and Regenerative Medicine (2016) 49-92.
[127] J.P. Chen, C.H. Su, Surface modification of electrospun PLLA nanofibers by plasma treatment and cationized gelatin immobilization for cartilage tissue engineering, Acta Biomater. 7(1) (2011) 234-243.
[128] L. Maleknia, Z.R. Majdi, Electrospinning of Gelatin nanofiber for biomedical application, Orient. J. Chem. 30(4) (2014) 2043-2048.
[129] M. Erencia, F. Cano, J.A. Tornero, M.M. Fernandes, T. Tzanov, J. Macanás, F. Carrillo, Electrospinning of gelatin fibers using solutions with low acetic acid concentration: Effect of solvent composition on both diameter of electrospun fibers and cytotoxicity, J. Appl. Polym. Sci. 132(25) (2015) 1-11.
[130] L. Ghasemi-Mobarakeh, M.P. Prabhakaran, M. Morshed, M.-H. Nasr-Esfahani, S. Ramakrishna, Electrospun poly (ε-caprolactone)/gelatin nanofibrous scaffolds for nerve tissue engineering, Biomaterials 29(34) (2008) 4532-4539.

[131] M.A. Alvarez-Perez, V. Guarino, V. Cirillo, L. Ambrosio, Influence of gelatin cues in PCL electrospun membranes on nerve outgrowth, Biomacromolecules 11(9) (2010) 2238-2246.
[132] L. Binan, C. Tendey, G. De Crescenzo, R. El Ayoubi, A. Ajji, M. Jolicoeur, Differentiation of neuronal stem cells into motor neurons using electrospun poly-l-lactic acid/gelatin scaffold, Biomaterials 35(2) (2014) 664-674.
[133] N.E. Zander, J.A. Orlicki, A.M. Rawlett, T.P. Beebe, Surface-modified nanofibrous biomaterial bridge for the enhancement and control of neurite outgrowth, Biointerphases 5(4) (2010) 149-158.
[134] H. Koh, T. Yong, C. Chan, S. Ramakrishna, Enhancement of neurite outgrowth using nano-structured scaffolds coupled with laminin, Biomaterials 29(26) (2008) 3574-3582.
[135] R.A. Neal, S.G. McClugage III, M.C. Link, L.S. Sefcik, R.C. Ogle, E.A. Botchwey, Laminin nanofiber meshes that mimic morphological properties and bioactivity of basement membranes, Tissue Eng. Part C Methods 15(1) (2008) 11-21.
[136] S.H. Lim, H.-Q. Mao, Electrospun scaffolds for stem cell engineering, Adv. Drug Deliv. Rev. 61(12) (2009) 1084-1096.
[137] P. Cools, R. Ghobeira, S. Van Vrekhem, N. De Geyterand, R. Morent, Non-thermal Plasma Technology for the Improvement of Scaffolds for Tissue Engineering and Regenerative Medicine-A Review, (2016) 201-240.
[138] M.P. Prabhakaran, J. Venugopal, C.K. Chan, S. Ramakrishna, Surface modified electrospun nanofibrous scaffolds for nerve tissue engineering, Nanotechnology 19(45) (2008) 1-8.
[139] S. Agarwal, J.H. Wendorff, A. Greiner, Use of electrospinning technique for biomedical applications, Polymer 49(26) (2008) 5603-5621.
[140] D. Kai, S.S. Liow, X.J. Loh, Biodegradable polymers for electrospinning: Towards biomedical applications, Mater. Sci. Eng. C 45 (2014) 659-670.
[141] L.S. Nair, C.T. Laurencin, Biodegradable polymers as biomaterials, Prog. Polym. Sci. 32(8) (2007) 762-798.
[142] J.A. Hubbell, Materials as morphogenetic guides in tissue engineering, Curr. Opin. Biotechnol. 14(5) (2003) 551-558.
[143] L.S. Nair, C.T. Laurencin, Biodegradable polymers as biomaterials, Prog. Polym. Sci. 32(8–9) (2007) 762-798.
[144] A. Göpferich, Polymer bulk erosion, Macromolecules 30(9) (1997) 2598-2604.
[145] N. De Geyter, R. Morent, Non-thermal plasma surface modification of biodegradable polymers, INTECH Open Access Publisher2012, pp. 225-246.

[146] P.B. Maurus, C.C. Kaeding, Bioabsorbable implant material review, Oper. Tech. Sports Med. 12(3) (2004) 158-160.
[147] R. Morent, N. De Geyter, T. Desmet, P. Dubruel, C. Leys, Plasma surface modification of biodegradable polymers: a review, Plasma Process. Polym. 8(3) (2011) 171-190.
[148] Y. Dong, T. Yong, S. Liao, C.K. Chan, M.M. Stevens, S. Ramakrishna, Distinctive degradation behaviors of electrospun polyglycolide, poly (dl-lactide-co-glycolide), and poly (l-lactide-co-ε-caprolactone) nanofibers cultured with/without porcine smooth muscle cells, Tissue Eng. Part A 16(1) (2009) 283-298.
[149] K. Ceonzo, A. Gaynor, L. Shaffer, K. Kojima, C.A. Vacanti, G.L. Stahl, Polyglycolic acid-induced inflammation: role of hydrolysis and resulting complement activation, Tissue Eng. 12(2) (2006) 301-308.
[150] J. Otto, M. Binnebösel, S. Pietsch, M. Anurov, S. Titkova, A. Öttinger, M. Jansen, R. Rosch, D. Kämmer, U. Klinge, Large-pore PDS mesh compared to small-pore PG mesh, J. Invest. Surg. 23(4) (2010) 190-196.
[151] R. Boni, A. Ali, A. Shavandi, A.N. Clarkson, Current and novel polymeric biomaterials for neural tissue engineering, Journal of biomedical science 25(1) (2018) 90.
[152] A.M. Moore, R. Kasukurthi, C.K. Magill, H.F. Farhadi, G.H. Borschel, S.E. Mackinnon, Limitations of conduits in peripheral nerve repairs, Hand 4(2) (2009) 180-186.
[153] R.M. Rasal, A.V. Janorkar, D.E. Hirt, Poly (lactic acid) modifications, Prog. Polym. Sci. 35(3) (2010) 338-356.
[154] J.C. Middleton, A.J. Tipton, Synthetic biodegradable polymers as orthopedic devices, Biomaterials 21(23) (2000) 2335-2346.
[155] E. Fukada, History and recent progress in piezoelectric polymers, IEEE Trans. Ultrason. Ferroelectr. Freq. Control 47(6) (2000) 1277-1290.
[156] C. Ribeiro, J. Pärssinen, V. Sencadas, V. Correia, S. Miettinen, V.P. Hytönen, S. Lanceros-Méndez, Dynamic piezoelectric stimulation enhances osteogenic differentiation of human adipose stem cells, J. Biomed. Mater. Res. A 103(6) (2015) 2172-2175.
[157] D. Garlotta, A literature review of poly (lactic acid), J. Polym. Environ. 9(2) (2001) 63-84.
[158] R. Casasola, N.L. Thomas, A. Trybala, S. Georgiadou, Electrospun poly lactic acid (PLA) fibres: Effect of different solvent systems on fibre morphology and diameter, Polymer 55(18) (2014) 4728-4737.
[159] J.M. Corey, C.C. Gertz, B.-S. Wang, L.K. Birrell, S.L. Johnson, D.C. Martin, E.L. Feldman, The design of electrospun PLLA nanofiber scaffolds compatible with serum-free growth of primary motor and sensory neurons, Acta Biomater. 4(4) (2008) 863-875.

[160] E. Zhang, C. Zhu, J. Yang, H. Sun, X. Zhang, S. Li, Y. Wang, L. Sun, F. Yao, Electrospun PDLLA/PLGA composite membranes for potential application in guided tissue regeneration, Mater. Sci. Eng. C 58 (2016) 278-285.
[161] H. Xu, W. Cui, J. Chang, Fabrication of patterned PDLLA/PCL composite scaffold by electrospinning, J. Appl. Polym. Sci. 127(3) (2013) 1550-1554.
[162] X. Qiao, S.J. Russell, X. Yang, G. Tronci, D.J. Wood, Compositional and in vitro evaluation of nonwoven type I collagen/poly-DL-lactic acid scaffolds for bone regeneration, J. Funct. Biomater. 6(3) (2015) 667-686.
[163] Z. Pan, J. Ding, Poly (lactide-co-glycolide) porous scaffolds for tissue engineering and regenerative medicine, Interface focus 2(3) (2012) 366-377.
[164] E.H. Gang, C.S. Ki, J.W. Kim, J. Lee, B.G. Cha, K.H. Lee, Y.H. Park, Highly porous three-dimensional poly (lactide-co-glycolide)(PLGA) microfibrous scaffold prepared by electrospinning method: A comparison study with other PLGA type scaffolds on its biological evaluation, Fiber. Polym. 13(6) (2012) 685-691.
[165] H.K. Makadia, S.J. Siegel, Poly lactic-co-glycolic acid (PLGA) as biodegradable controlled drug delivery carrier, Polymers 3(3) (2011) 1377-1397.
[166] H.J. Shin, C.H. Lee, I.H. Cho, Y.-J. Kim, Y.-J. Lee, I.A. Kim, K.-D. Park, N. Yui, J.-W. Shin, Electrospun PLGA nanofiber scaffolds for articular cartilage reconstruction: mechanical stability, degradation and cellular responses under mechanical stimulation in vitro, J. Biomater. Sci. Polym. Ed. 17(1-2) (2006) 103-119.
[167] M. Therin, P. Christel, S. Li, H. Garreau, M. Vert, In vivo degradation of massive poly(α-hydroxy acids): Validation of In vitro findings, Biomaterials 13(9) (1992) 594-600.
[168] K.A. Athanasiou, J. Schmitz, C. Agrawal, The effects of porosity on in vitro degradation of polylactic acid-polyglycolic acid implants used in repair of articular cartilage, Tissue Eng. 4(1) (1998) 53-63.
[169] T. Bini, S. Gao, S. Wang, A. Lim, L.B. Hai, S. Ramakrishna, Electrospun poly (L-lactide-co-glycolide) biodegradable polymer nanofibre tubes for peripheral nerve regeneration, Nanotechnology 15(11) (2004) 1459.
[170] J.Y. Lee, C.A. Bashur, A.S. Goldstein, C.E. Schmidt, Polypyrrole-coated electrospun PLGA nanofibers for neural tissue applications, Biomaterials 30(26) (2009) 4325-4335.
[171] A. Cipitria, A. Skelton, T. Dargaville, P. Dalton, D. Hutmacher, Design, fabrication and characterization of PCL electrospun scaffolds—a review, J. Mater. Chem. 21(26) (2011) 9419-9453.

[172] L. Van der Schueren, B. De Schoenmaker, Ö.I. Kalaoglu, K. De Clerck, An alternative solvent system for the steady state electrospinning of polycaprolactone, Eur. Polym. J. 47(6) (2011) 1256-1263.
[173] K. Lee, H. Kim, M. Khil, Y. Ra, D. Lee, Characterization of nano-structured poly (ε-caprolactone) nonwoven mats via electrospinning, Polymer 44(4) (2003) 1287-1294.
[174] W.-J. Li, J.A. Cooper, R.L. Mauck, R.S. Tuan, Fabrication and characterization of six electrospun poly (α-hydroxy ester)-based fibrous scaffolds for tissue engineering applications, Acta Biomater. 2(4) (2006) 377-385.
[175] M. Abedalwafa, F. Wang, L. Wang, C. Li, Biodegradable poly-epsilon-caprolactone (PCL) for tissue engineering applications: a review, Rev. adv. mater. sci. 34 (2013) 123-140.
[176] F. Mohamadi, S. Ebrahimi-Barough, M.R. Nourani, K. Mansoori, M. Salehi, A.A. Alizadeh, S.M. Tavangar, F. Sefat, S. Sharifi, J. Ai, Enhanced sciatic nerve regeneration by human endometrial stem cells in an electrospun poly (epsilon-caprolactone)/collagen/NBG nerve conduit in rat, Artificial Cells Nanomedicine and Biotechnology 46(8) (2018) 1731-1743.
[177] F. Mohamadi, S. Ebrahimi-Barough, M.R. Nourani, M.A. Derakhshan, V. Goodarzi, M.S. Nazockdast, M. Farokhi, R. Tajerian, R.F. Majidi, J. Ai, Electrospun nerve guide scaffold of poly(epsilon-caprolactone)/collagen/nanobioglass: an in vitro study in peripheral nerve tissue engineering, J. Biomed. Mater. Res. A 105(7) (2017) 1960-1972.
[178] M.H. Beigi, L. Ghasemi-Mobarakeh, M.P. Prabhakaran, K. Karbalaie, H. Azadeh, S. Ramakrishna, H. Baharvand, M.H. Nasr-Esfahani, In vivo integration of poly(epsilon-caprolactone)/gelatin nanofibrous nerve guide seeded with teeth derived stem cells for peripheral nerve regeneration, J. Biomed. Mater. Res. A 102(12) (2014) 4554-4567.
[179] X. Jiang, R.F. Mi, A. Hoke, S.Y. Chew, Nanofibrous nerve conduit-enhanced peripheral nerve regeneration, Journal of Tissue Engineering and Regenerative Medicine 8(5) (2014) 377-385.
[180] B.K. Lee, Y.M. Ju, J.G. Cho, J.D. Jackson, S.J. Lee, A. Atala, J.J. Yoo, End-to-side neurorrhaphy using an electrospun PCL/collagen nerve conduit for complex peripheral motor nerve regeneration, Biomaterials 33(35) (2012) 9027-9036.
[181] W.W. Yu, W. Zhao, C. Zhu, X.L. Zhang, D.X. Ye, W.J. Zhang, Y. Zhou, X.Q. Jiang, Z.Y. Zhang, Sciatic nerve regeneration in rats by a promising electrospun collagen/poly(epsilon-caprolactone) nerve conduit with tailored degradation rate, Bmc Neuroscience 12 (2011).

[182] S. Farzamfar, A. Ehterami, M. Salehi, A. Vaeez, A. Atashi, H. Sahrapeyma, Unrestricted Somatic Stem Cells Loaded in Nanofibrous Conduit as Potential Candidate for Sciatic Nerve Regeneration, Journal of Molecular Neuroscience 67(1) (2019) 48-61.
[183] X. Pan, B.B. Sun, X.M. Mo, Electrospun polypyrrole-coated polycaprolactone nanoyarn nerve guidance conduits for nerve tissue engineering, Frontiers of Materials Science 12(4) (2018) 438-446.
[184] S.L. Tao, T.A. Desai, Aligned arrays of biodegradable poly(epsilon-caprolactone) nanowires and nanofibers by template synthesis, Nano Lett. 7(6) (2007) 1463-1468.
[185] D.A.E. Rollings, S. Tsoi, J.C. Sit, J.G.C. Veinot, Formation and aqueous surface wettability of polysiloxane nanofibers prepared via surface initiated, vapor-phase polymerization of organotrichlorosilanes, Langmuir 23(10) (2007) 5275-5278.
[186] A. Yari, S. Teimourian, F. Amidi, M. Bakhtiyari, F. Heidari, N. Sajedi, S.J. Veijouye, M. Dodel, M. Nobakht, The role of biodegradable engineered random polycaprolactone nanofiber scaffolds seeded with nestin-positive hair follicle stem cells for tissue engineering, Adv. Biomed. Res. 5 (2016) 1-8.
[187] H. Chen, R. Truckenmuller, C. Van Blitterswijk, L. Moroni, Fabrication of nanofibrous scaffolds for tissue engineering applications, The Netherlands, nanomaterials in tissue engineering: fabrication and applications. Series in biomaterials 56 (2013) 158-182.
[188] D.H. Reneker, I. Chun, Nanometre diameter fibres of polymer, produced by electrospinning, Nanotechnology 7(3) (1996) 216-223.
[189] J. Doshi, D.H. Reneker, Electrospinning process and applications of electrospun fibers, Industry Applications Society Annual Meeting, 1993., Conference Record of the 1993 IEEE, IEEE, 1993, pp. 1698-1703.
[190] K. Park, H.J. Jung, J.J. Kim, K.D. Ahn, D.K. Han, Y.M. Ju, Acrylic acid-grafted hydrophilic electrospun nanofibrous poly(L-lactic acid) scaffold, Macromol. Res. 14(5) (2006) 552-558.
[191] A. Haider, S. Haider, I.-K. Kang, A comprehensive review summarizing the effect of electrospinning parameters and potential applications of nanofibers in biomedical and biotechnology, Arab. J. Chem. (2015) 1-24.
[192] N. Binulal, M. Deepthy, N. Selvamurugan, K. Shalumon, S. Suja, U. Mony, R. Jayakumar, S. Nair, Role of nanofibrous poly (caprolactone) scaffolds in human mesenchymal stem cell attachment and spreading for in vitro bone tissue engineering—response to osteogenic regulators, Tissue Eng. Part A 16(2) (2010) 393-404.
[193] J. Wang, R. Ye, Y. Wei, H. Wang, X. Xu, F. Zhang, J. Qu, B. Zuo, H. Zhang, The effects of electrospun TSF nanofiber diameter and alignment on neuronal differentiation of human embryonic stem cells, J. Biomed. Mater. Res. A 100(3) (2012) 632-645.

[194] F. Yang, R. Murugan, S. Wang, S. Ramakrishna, Electrospinning of nano/micro scale poly(l-lactic acid) aligned fibers and their potential in neural tissue engineering, Biomaterials 26(15) (2005) 2603-2610.
[195] D.I. Braghirolli, D. Steffens, K. Quintiliano, G.A.X. Acasigua, D. Gamba, R.A. Fleck, C.L. Petzhold, P. Pranke, The effect of sterilization methods on electronspun poly(lactide-co-glycolide) and subsequent adhesion efficiency of mesenchymal stem cells, J. Biomed. Mater. Res. Part B Appl. Biomater. 102(4) (2014) 700-708.
[196] M. Khayet, Polymeric Nano-Fibers and Modified Nano-Fibers Assembly in 3D Network for Different Potential Applications, J. mater. sci. nanotechnol. 1(1) (2013) 1-4.
[197] Z. Li, C. Wang, Effects of working parameters on electrospinning, One-Dimensional Nanostructures, Springer2013, pp. 15-28.
[198] C. Ru, F. Wang, M. Pang, L. Sun, R. Chen, Y. Sun, Suspended, Shrinkage-Free, Electrospun PLGA Nanofibrous Scaffold for Skin Tissue Engineering, ACS Appl. Mater. Interfaces 7(20) (2015) 10872-10877.
[199] H. Fong, I. Chun, D.H. Reneker, Beaded nanofibers formed during electrospinning, Polymer 40(16) (1999) 4585-4592.
[200] D.S. Katti, K.W. Robinson, F.K. Ko, C.T. Laurencin, Bioresorbable nanofiber-based systems for wound healing and drug delivery: Optimization of fabrication parameters, J. Biomed. Mater. Res. Part B Appl. Biomater. 70(2) (2004) 286-296.
[201] H.S. Kim, K. Kim, H.J. Jin, I.J. Chin, Morphological Characterization of Electrospun Nano-Fibrous Membranes of Biodegradable Poly (L-lactide) and Poly (lactide-co-glycolide), Macromol. Symp. 224(1) (2005) 145-154.
[202] W. Liu, S. Thomopoulos, Y. Xia, Electrospun nanofibers for regenerative medicine, Adv. Healthc. Mater. 1(1) (2012) 10-25.
[203] D.-H. Kim, P.P. Provenzano, C.L. Smith, A. Levchenko, Matrix nanotopography as a regulator of cell function, J. Cell. Biol. 197(3) (2012) 351-360.
[204] S. Gnavi, B. Fornasari, C. Tonda-Turo, G. Ciardelli, M. Zanetti, S. Geuna, I. Perroteau, The influence of electrospun fibre size on Schwann cell behaviour and axonal outgrowth, Mater. Sci. Eng. C. 48 (2015) 620-631.
[205] J. Pelipenko, P. Kocbek, J. Kristl, Nanofiber diameter as a critical parameter affecting skin cell response, Eur. J. Pharm. Sci. 66 (2015) 29-35.
[206] A.T. Nguyen, S.R. Sathe, E.K. Yim, From nano to micro: topographical scale and its impact on cell adhesion, morphology and contact guidance, J. Phys. Condens. Matter. 28(18) (2016) 183001.

[207] H. Jeon, C.G. Simon, G. Kim, A mini-review: cell response to microscale, nanoscale, and hierarchical patterning of surface structure, J. Biomed. Mater. Res. B Appl. Biomater. 102(7) (2014) 1580-1594.
[208] K.W. Leong, E.K. Yim, Significance of Synthetic Nanostructures in Dictating Cellular Response, Nanomedicine in Cancer, Pan Stanford2017, pp. 129-158.
[209] M. Chen, P.K. Patra, S.B. Warner, S. Bhowmick, Role of Fiber Diameter in Adhesion and Proliferation of NIH 3T3 Fibroblast on Electrospun Polycaprolactone Scaffolds, Tissue Eng. 13(3) (2007) 579-587.
[210] A.S. Badami, M.R. Kreke, M.S. Thompson, J.S. Riffle, A.S. Goldstein, Effect of fiber diameter on spreading, proliferation, and differentiation of osteoblastic cells on electrospun poly (lactic acid) substrates, Biomaterials. 27(4) (2006) 596-606.
[211] V. Chaurey, F. Block, Y.-H. Su, P.-C. Chiang, E. Botchwey, C.-F. Chou, N.S. Swami, Nanofiber size-dependent sensitivity of fibroblast directionality to the methodology for scaffold alignment, Acta. Biomater. 8(11) (2012) 3982-3990.
[212] Y.-P. Jiao, F.-Z. Cui, Surface modification of polyester biomaterials for tissue engineering, Biomed. Mater. 2(4) (2007) R24-R37.
[213] M.H. Ho, J.J. Lee, S.C. Fan, D.M. Wang, L.T. Hou, H.J. Hsieh, J.Y. Lai, Efficient modification on PLLA by ozone treatment for biomedical applications, Macromol. Biosci. 7(4) (2007) 467-474.
[214] G.-H. Koo, J. Jang, Surface modification of poly (lactic acid) by UV/Ozone irradiation, Fiber. Polym. 9(6) (2008) 674-678.
[215] S.C.J. Loo, C.P. Ooi, Y.C.F. Boey, Radiation effects on poly (lactide-co-glycolide)(PLGA) and poly (L-lactide)(PLLA), Polym. Degrad. Stab. 83(2) (2004) 259-265.
[216] Y. Zhu, C. Gao, X. Liu, J. Shen, Surface modification of polycaprolactone membrane via aminolysis and biomacromolecule immobilization for promoting cytocompatibility of human endothelial cells, Biomacromolecules 3(6) (2002) 1312-1319.
[217] T.I. Croll, A.J. O'Connor, G.W. Stevens, J.J. Cooper-White, Controllable surface modification of poly (lactic-co-glycolic acid)(PLGA) by hydrolysis or aminolysis I: physical, chemical, and theoretical aspects, Biomacromolecules 5(2) (2004) 463-473.
[218] Y. Zhu, M.F. Leong, W.F. Ong, M.B. Chan-Park, K.S. Chian, Esophageal epithelium regeneration on fibronectin grafted poly (L-lactide-co-caprolactone)(PLLC) nanofiber scaffold, Biomaterials 28(5) (2007) 861-868.
[219] M. Chong, C. Lee, S. Teoh, Characterization of smooth muscle cells on poly (ε-caprolactone) films, Mater. Sci. Eng. C 27(2) (2007) 309-312.

[220] J.M. Goddard, J. Hotchkiss, Polymer surface modification for the attachment of bioactive compounds, Prog. Polym. Sci. 32(7) (2007) 698-725.
[221] S.M. Desai, R. Singh, Surface modification of polyethylene, Long Term Properties of Polyolefins, Springer2004, pp. 231-294.
[222] W. He, T. Yong, W.E. Teo, Z. Ma, S. Ramakrishna, Fabrication and endothelialization of collagen-blended biodegradable polymer nanofibers: potential vascular graft for blood vessel tissue engineering, Tissue Eng. 11(9-10) (2005) 1574-1588.
[223] K.E. Swindle-Reilly, C.S. Paranjape, C.A. Miller, Electrospun poly (caprolactone)-elastin scaffolds for peripheral nerve regeneration, Prog. biomater. 3(1) (2014) 1-8.
[224] M.P. Prabhakaran, J.R. Venugopal, T.T. Chyan, L.B. Hai, C.K. Chan, A.Y. Lim, S. Ramakrishna, Electrospun biocomposite nanofibrous scaffolds for neural tissue engineering, Tissue Eng. Part A 14(11) (2008) 1787-1797.
[225] R.A. Neal, S.S. Tholpady, P.L. Foley, N. Swami, R.C. Ogle, E.A. Botchwey, Alignment and composition of laminin–polycaprolactone nanofiber blends enhance peripheral nerve regeneration, J. Biomed. Mater. Res. A. 100(2) (2012) 406-423.
[226] H.W. Kim, H.S. Yu, H.H. Lee, Nanofibrous matrices of poly (lactic acid) and gelatin polymeric blends for the improvement of cellular responses, J. Biomed. Mater. Res. A 87(1) (2008) 25-32.
[227] E. Seyedjafari, M. Soleimani, N. Ghaemi, I. Shabani, Nanohydroxyapatite-Coated Electrospun Poly(L-lactide) Nanofibers Enhance Osteogenic Differentiation of Stem Cells and Induce Ectopic Bone Formation, Biomacromolecules 11(11) (2010) 3118-3125.
[228] D. Gupta, J. Venugopal, S. Mitra, V.R. Giri Dev, S. Ramakrishna, Nanostructured biocomposite substrates by electrospinning and electrospraying for the mineralization of osteoblasts, Biomaterials 30(11) (2009) 2085-2094.
[229] G. Sui, X. Yang, F. Mei, X. Hu, G. Chen, X. Deng, S. Ryu, Poly-L-lactic acid/hydroxyapatite hybrid membrane for bone tissue regeneration, J. Biomed. Mater. Res. A 82(2) (2007) 445-454.
[230] J. Bockelmann, K. Klinkhammer, A. von Holst, N. Seiler, A. Faissner, G.A. Brook, D. Klee, J. Mey, Functionalization of electrospun poly (ε-caprolactone) fibers with the extracellular matrix-derived peptide GRGDS improves guidance of schwann cell migration and axonal growth, Tissue Eng. Part A 17(3-4) (2010) 475-486.
[231] C. Cohn, S. Leung, J. Crosby, B. Lafuente, Z. Zha, W. Teng, R. Downs, X. Wu, Lipid-mediated protein functionalization of electrospun polycaprolactone fibers, Express Polym. Lett. 10(5) (2016) 430-437.
[232] G. Jin, M.P. Prabhakaran, S. Ramakrishna, Stem cell differentiation to epidermal lineages on electrospun nanofibrous

substrates for skin tissue engineering, Acta Biomater. 7(8) (2011) 3113-3122.
[233] D.I. Zeugolis, S.T. Khew, E.S.Y. Yew, A.K. Ekaputra, Y.W. Tong, L.-Y.L. Yung, D.W. Hutmacher, C. Sheppard, M. Raghunath, Electro-spinning of pure collagen nano-fibres – Just an expensive way to make gelatin?, Biomaterials 29(15) (2008) 2293-2305.
[234] L. Yang, C.F.C. Fitié, K.O. van der Werf, M.L. Bennink, P.J. Dijkstra, J. Feijen, Mechanical properties of single electrospun collagen type I fibers, Biomaterials 29(8) (2008) 955-962.
[235] A.G. Guex, A. Frobert, J. Valentin, G. Fortunato, D. Hegemann, S. Cook, T.P. Carrel, H.T. Tevaearai, M.N. Giraud, Plasma-functionalized electrospun matrix for biograft development and cardiac function stabilization, Acta Biomater. 10(7) (2014) 2996-3006.
[236] K. Wulf, M. Teske, M. Löbler, F. Luderer, K.P. Schmitz, K. Sternberg, Surface functionalization of poly (ε-caprolactone) improves its biocompatibility as scaffold material for bioartificial vessel prostheses, J. Biomed. Mater. Res. Part B Appl. Biomater. 98(1) (2011) 89-100.
[237] M. Domingos, F. Intranuovo, A. Gloria, R. Gristina, L. Ambrosio, P. Bártolo, P. Favia, Improved osteoblast cell affinity on plasma-modified 3-D extruded PCL scaffolds, Acta Biomater. 9(4) (2013) 5997-6005.
[238] H. Shen, X. Hu, F. Yang, J. Bei, S. Wang, Combining oxygen plasma treatment with anchorage of cationized gelatin for enhancing cell affinity of poly(lactide-co-glycolide), Biomaterials 28(29) (2007) 4219-4230.
[239] H. Park, K.Y. Lee, S.J. Lee, K.E. Park, W.H. Park, Plasma-treated poly(lactic-co-glycolic acid) nanofibers for tissue engineering, Macromol. Res. 15(3) (2007) 238-243.
[240] M. Zelzer, D. Scurr, B. Abdullah, A.J. Urquhart, N. Gadegaard, J.W. Bradley, M.R. Alexander, Influence of the plasma sheath on plasma polymer deposition in advance of a mask and down pores, J. Phys. Chem. B 113(25) (2009) 8487-8494.
[241] N. Guerrouani, A. Baldo, A. Bouffin, C. Drakides, M.F. Guimon, A. Mas, Allylamine plasma-polymerization on PLLA surface evaluation of the biodegradation, J. Appl. Polym. Sci. 105(4) (2007) 1978-1986.
[242] A.G. Guex, D. Hegemann, M.N. Giraud, H.T. Tevaearai, A.M. Popa, R.M. Rossi, G. Fortunato, Covalent immobilisation of VEGF on plasma-coated electrospun scaffolds for tissue engineering applications, Colloids Surf. B Biointerfaces 123 (2014) 724-733.
[243] Z.W. Ma, W. He, T. Yong, S. Ramakrishna, Grafting of gelatin on electrospun poly(caprolactone) nanofibers to improve endothelial cell spreading and proliferation and to control cell orientation, Tissue Eng. 11(7-8) (2005) 1149-1158.

[244] Z. Cheng, S.-H. Teoh, Surface modification of ultra thin poly (ε-caprolactone) films using acrylic acid and collagen, Biomaterials 25(11) (2004) 1991-2001.
[245] J. Shi, L. Wang, F. Zhang, H. Li, L. Lei, L. Liu, Y. Chen, Incorporating protein gradient into electrospun nanofibers as scaffolds for tissue engineering, ACS Appl. Mater. Interfaces 2(4) (2010) 1025-1030.
[246] E. Schnell, K. Klinkhammer, S. Balzer, G. Brook, D. Klee, P. Dalton, J. Mey, Guidance of glial cell migration and axonal growth on electrospun nanofibers of poly-ε-caprolactone and a collagen/poly-ε-caprolactone blend, Biomaterials 28(19) (2007) 3012-3025.
[247] C. He, X. Xu, F. Zhang, L. Cao, W. Feng, H. Wang, X. Mo, Fabrication of fibrinogen/P (LLA-CL) hybrid nanofibrous scaffold for potential soft tissue engineering applications, J. Biomed. Mater. Res. A 97(3) (2011) 339-347.
[248] S. Heydarkhan-Hagvall, K. Schenke-Layland, A.P. Dhanasopon, F. Rofail, H. Smith, B.M. Wu, R. Shemin, R.E. Beygui, W.R. MacLellan, Three-dimensional electrospun ECM-based hybrid scaffolds for cardiovascular tissue engineering, Biomaterials 29(19) (2008) 2907-2914.
[249] G. Wang, X. Hu, W. Lin, C. Dong, H. Wu, Electrospun PLGA–silk fibroin–collagen nanofibrous scaffolds for nerve tissue engineering, In Vitro Cell. Dev. Biol.-Anim. 47(3) (2011) 234-240.
[250] C. Spadaccio, A. Rainer, M. Trombetta, M. Centola, M. Lusini, M. Chello, E. Covino, F. De Marco, R. Coccia, Y. Toyoda, AG-CSF functionalized scaffold for stem cells seeding: a differentiating device for cardiac purposes, J. Cell. Mol. Med. 15(5) (2011) 1096-1108.
[251] M.P. Prabhakaran, J. Venugopal, S. Ramakrishna, Electrospun nanostructured scaffolds for bone tissue engineering, Acta Biomater. 5(8) (2009) 2884-2893.
[252] H.S. Yoo, T.G. Kim, T.G. Park, Surface-functionalized electrospun nanofibers for tissue engineering and drug delivery, Adv. Drug Deliv. Rev. 61(12) (2009) 1033-1042.
[253] I. Langmuir, Oscillations in ionized gases, Proc. Natl. Acad. Sci. 14(8) (1928) 627-637.
[254] F.S. Denes, S. Manolache, Macromolecular plasma-chemistry: an emerging field of polymer science, Prog. Polym. Sci. 29(8) (2004) 815-885.
[255] P. Cools, N. De Geyter, R. Morent, Plasma modified textiles for biomedical applications, Advances in bioengineering (2015) 117-148.
[256] A. Bogaerts, E. Neyts, R. Gijbels, J. van der Mullen, Gas discharge plasmas and their applications, Spectrochim. Acta Part B At. Spectrosc. 57(4) (2002) 609-658.

[257] D.B. Graves, M.J. Kushner, Influence of modeling and simulation on the maturation of plasma technology: Feature evolution and reactor design, J. Vac. Sci. Technol., A 21(5) (2003) S152-S156.
[258] T. Desmet, R. Morent, N.D. Geyter, C. Leys, E. Schacht, P. Dubruel, Nonthermal plasma technology as a versatile strategy for polymeric biomaterials surface modification: a review, Biomacromolecules 10(9) (2009) 2351-2378.
[259] N. De Geyter, R. Morent, C. Leys, L. Gengembre, E. Payen, Treatment of polymer films with a dielectric barrier discharge in air, helium and argon at medium pressure, Surf. Coat. Technol. 201(16) (2007) 7066-7075.
[260] K. Webb, V. Hlady, P.A. Tresco, Relative importance of surface wettability and charged functional groups on NIH 3T3 fibroblast attachment, spreading, and cytoskeletal organization, J. Biomed. Mater. Res. 41(3) (1998) 422.
[261] J.H. Lee, G. Khang, J.W. Lee, H.B. Lee, Interaction of different types of cells on polymer surfaces with wettability gradient, J. Colloid Interface Sci. 205(2) (1998) 323-330.
[262] D. Yan, J. Jones, X.Y. Yuan, X.H. Xu, J. Sheng, J.C.M. Lee, G.Q. Ma, Q.S. Yu, Plasma Treatment of Random and Aligned Electrospun PCL Nanofibers, J. Med. Biol. Eng. 33(2) (2013) 171-178.
[263] Z. Gugala, S. Gogolewski, Attachment, growth, and activity of rat osteoblasts on polylactide membranes treated with various low-temperature radiofrequency plasmas, J. Biomed. Mater. Res. A 76(2) (2006) 288-299.
[264] R. Latkany, A. Tsuk, M.S. Sheu, I.H. Loh, V. Trinkaus–Randall, Plasma surface modification of artificial corneas for optimal epithelialization, J. Biomed. Mater. Res. 36(1) (1997) 29-37.
[265] W. Cui, X. Li, S. Zhou, J. Weng, Degradation patterns and surface wettability of electrospun fibrous mats, Polym. Degrad. Stab. 93(3) (2008) 731-738.
[266] L.S. Dolci, S.D. Quiroga, M. Gherardi, R. Laurita, A. Liguori, P. Sanibondi, A. Fiorani, L. Calza, V. Colombo, M.L. Focarete, Carboxyl Surface Functionalization of Poly(L-lactic acid) Electrospun Nanofibers through Atmospheric Non-Thermal Plasma Affects Fibroblast Morphology, Plasma Process. Polym. 11(3) (2014) 203-213.
[267] K. Fujihara, M. Kotaki, S. Ramakrishna, Guided bone regeneration membrane made of polycaprolactone/calcium carbonate composite nano-fibers, Biomaterials 26(19) (2005) 4139-4147.
[268] J. Venugopal, S. Low, A.T. Choon, A.B. Kumar, S. Ramakrishna, Electrospun-modified nanofibrous scaffolds for the mineralization of osteoblast cells, J. Biomed. Mater. Res. A 85A(2) (2008) 408-417.

[269] D. Hegemann, H. Brunner, C. Oehr, Plasma treatment of polymers for surface and adhesion improvement, Nucl. Instrum. Methods Phys. Res. B 208 (2003) 281-286.
[270] R. Morent, N. De Geyter, M. Trentesaux, L. Gengembre, P. Dubruel, C. Leys, E. Payen, Influence of Discharge Atmosphere on the Ageing Behaviour of Plasma-Treated Polylactic Acid, Plasma Chemistry and Plasma Processing 30(4) (2010) 525-536.
[271] J. Venugopal, S. Low, A.T. Choon, A.B. Kumar, S. Ramakrishna, Electrospun-modified nanofibrous scaffolds for the mineralization of osteoblast cells, J. Biomed. Mater. Res. A 85(2) (2008) 408-417.
[272] D. Sankar, K.T. Shalumon, K.P. Chennazhi, D. Menon, R. Jayakumar, Surface Plasma Treatment of Poly(caprolactone) Micro, Nano, and Multiscale Fibrous Scaffolds for Enhanced Osteoconductivity, Tissue Eng. Part A 20(11-12) (2014) 1689-1702.
[273] H.J. Jeon, H. Lee, G.H. Kim, Nano-Sized Surface Patterns on Electrospun Microfibers Fabricated Using a Modified Plasma Process for Enhancing Initial Cellular Activities, Plasma Process. Polym. 11(2) (2014) 142-148.
[274] H. Jahani, S. Kaviani, M. Hassanpour-Ezatti, M. Soleimani, Z. Kaviani, Z. Zonoubi, The Effect of Aligned and Random Electrospun Fibrous Scaffolds on Rat Mesenchymal Stem Cell Proliferation, Cell J. 14(1) (2012) 31-38.
[275] S. de Valence, J.C. Tille, C. Chaabane, R. Gurny, M.L. Bochaton-Piallat, B.H. Walpoth, M. Moller, Plasma treatment for improving cell biocompatibility of a biodegradable polymer scaffold for vascular graft applications, Eur. J. Pharm. Biopharm. 85(1) (2013) 78-86.
[276] N. Abbasi, S. Soudi, N. Hayati-Roodbari, M. Dodel, M. Soleimani, The Effects of Plasma Treated Electrospun Nanofibrous Poly (epsilon-caprolactone) Scaffolds with Different Orientations on Mouse Embryonic Stem Cell Proliferation, Cell J. 16(3) (2014) 245-254.
[277] S. Sharma, D. Gupta, S. Mohanty, M. Jassal, A.K. Agrawal, R. Tandon, Surface-Modified Electrospun Poly(epsilon-Caprolactone) Scaffold With Improved Optical Transparency and Bioactivity for Damaged Ocular Surface Reconstruction, Invest. Ophthalmol. Vis. Sci. 55(2) (2014) 899-907.
[278] A.M. Pappa, V. Karagkiozaki, S. Krol, S. Kassavetis, D. Konstantinou, C. Pitsalidis, L. Tzounis, N. Pliatsikas, S. Logothetidis, Oxygen-plasma-modified biomimetic nanofibrous scaffolds for enhanced compatibility of cardiovascular implants, Beilstein Journal of Nanotechnology 6 (2015) 254-262.
[279] N. Recek, M. Resnik, H. Motaln, T. Lah-Turnsek, R. Augustine, N. Kalarikkal, S. Thomas, M. Mozetic, Cell Adhesion on Polycaprolactone Modified by Plasma Treatment, Int. J. Polym. Sci. 2016 (2016) 1-9.

[280] S. Surucu, H. Turkoglu Sasmazel, DBD atmospheric plasma-modified, electrospun, layer-by-layer polymeric scaffolds for L929 fibroblast cell cultivation, J. Biomater. Sci. Polym. Ed. 27(2) (2016) 111-132.
[281] W. Liu, J.C. Zhan, Y. Su, T. Wu, C.C. Wu, S. Ramakrishna, X.M. Mo, S.S. Al-Deyab, M. El-Newehy, Effects of plasma treatment to nanofibers on initial cell adhesion and cell morphology, Colloids Surf. B Biointerfaces 113 (2014) 101-106.
[282] D.M. Correia, C. Ribeiro, G. Botelho, J. Borges, C. Lopes, F. Vaz, S.A.C. Carabineiro, A.V. Machado, S. Lanceros-Mendez, Superhydrophilic poly(L-lactic acid) electrospun membranes for biomedical applications obtained by argon and oxygen plasma treatment, Appl. Surf. Sci. 371 (2016) 74-82.
[283] Q. Cheng, B.L.P. Lee, K. Komvopoulos, Z.Q. Yan, S. Li, Plasma Surface Chemical Treatment of Electrospun Poly(L-Lactide) Microfibrous Scaffolds for Enhanced Cell Adhesion, Growth, and Infiltration, Tissue Eng. Part A 19(9-10) (2013) 1188-1198.
[284] W.T. Liu, Q. Cai, F. Zhang, Y. Wei, X.H. Zhang, Y. Wang, X.M. Deng, X.L. Deng, Dose-dependent enhancement of bone marrow stromal cells adhesion, spreading and osteogenic differentiation on atmospheric plasma-treated poly(l-lactic acid) nanofibers, J. Bioact. Compat. Polym. 28(5) (2013) 453-467.
[285] K.E. Park, K.Y. Lee, S.J. Lee, W.H. Park, Surface characteristics of plasma-treated PLGA nanofibers, Macromol. Symp. 249 (2007) 103-108.
[286] H. Park, J.W. Lee, K.E. Park, W.H. Park, K.Y. Lee, Stress response of fibroblasts adherent to the surface of plasma-treated poly (lactic-co-glycolic acid) nanofiber matrices, Colloids Surf. B Biointerfaces 77(1) (2010) 90-95.
[287] N. Inagaki, Plasma surface modification and plasma polymerization, CRC Press1996.
[288] Y.M. Ko, D.Y. Choi, S.C. Jung, B.H. Kim, Characteristics of Plasma Treated Electrospun Polycaprolactone (PCL) Nanofiber Scaffold for Bone Tissue Engineering, J. Nanosci. Nanotechnol. 15(1) (2015) 192-195.
[289] K. Park, Y.M. Ju, J.S. Son, K.-D. Ahn, D.K. Han, Surface modification of biodegradable electrospun nanofiber scaffolds and their interaction with fibroblasts, J. Biomater. Sci. Polym. Ed. 18(4) (2007) 369-382.
[290] B. Jarrell, S. Williams, G. Stokes, F. Hubbard, R. Carabasi, E. Koolpe, D. Greener, K. Pratt, M. Moritz, J. Radomski, Use of freshly isolated capillary endothelial cells for the immediate establishment of a monolayer on a vascular graft at surgery, Surgery 100(2) (1986) 392-399.

[291] M. Deutsch, J. Meinhart, T. Fischlein, P. Preiss, P. Zilla, Clinical autologous in vitro endothelialization of infrainguinal ePTFE grafts in 100 patients: a 9-year experience, Surgery 126(5) (1999) 847-855.
[292] W. He, Z.W. Ma, T. Yong, W.E. Teo, S. Ramakrishna, Fabrication of collagen-coated biodegradable polymer nanofiber mesh and its potential for endothelial cells growth, Biomaterials 26(36) (2005) 7606-7615.
[293] F. Yang, J.G.C. Wolke, J.A. Jansen, Biomimetic calcium phosphate coating on electrospun poly (epsilon-caprolactone) scaffolds for bone tissue engineering, Chem. Eng. J. 137(1) (2008) 154-161.
[294] N.E. Zander, J.A. Orlicki, A.M. Rawlett, T.P. Beebe, Quantification of Protein Incorporated into Electrospun Polycaprolactone Tissue Engineering Scaffolds, ACS Appl. Mater. Interfaces 4(4) (2012) 2074-2081.
[295] J. Jia, Y.Y. Duan, J. Yu, J.W. Lu, Preparation and immobilization of soluble eggshell membrane protein on the electrospun nanofibers to enhance cell adhesion and growth, J. Biomed. Mater. Res. A 86A(2) (2008) 364-373.
[296] R. Safaeijavan, M. Soleimani, A. Divsalar, A. Eidi, A. Ardeshirylajimi, Biological behavior study of gelatin coated PCL nanofiberous electrospun scaffolds using fibroblasts, J. paramed. sci. 5(1) (2013) 67-73.
[297] N.J. Schaub, C. Le Beux, J.J. Miao, R.J. Linhardt, J.G. Alauzun, D. Laurencin, R.J. Gilbert, The Effect of Surface Modification of Aligned Poly-L-Lactic Acid Electrospun Fibers on Fiber Degradation and Neurite Extension, Plos One 10(9) (2015) 1-19.
[298] J.R.J. Paletta, S. Bockelmann, A. Walz, C. Theisen, J.H. Wendorff, A. Greiner, S. Fuchs-Winkelmann, M.D. Schofer, RGD-functionalisation of PLLA nanofibers by surface coupling using plasma treatment: influence on stem cell differentiation, J. Mater. Sci. Mater. Med. 21(4) (2010) 1363-1369.
[299] M. Ghaedi, M. Soleimani, I. Shabani, Y. Duan, A.S. Lotfi, Hepatic differentiation from human mesenchymal stem cells on a novel nanofiber scaffold, Cell. Mol. Biol. Lett. 17(1) (2012) 89-106.
[300] H.J. Seo, M.H. Lee, B.J. Kwon, H.L. Kim, S.J. Lee, B.J. Kim, K.K. Wang, Y.R. Kim, J.C. Park, Plasma treatment induces internal surface modifications of electrospun poly(L-lactic) acid scaffold to enhance protein coating, J. Appl. Phys. 114(7) (2013) 1-6.
[301] B.J. Park, H.J. Seo, J. Kim, H.L. Kim, J.K. Kim, J.B. Choi, I. Han, S.O. Hyun, K.H. Chung, J.C. Park, Cellular responses of vascular endothelial cells on surface modified polyurethane films grafted electrospun PLGA fiber with microwave-induced plasma at atmospheric pressure, Surf. Coat. Technol. 205 (2010) S222-S226.

[302] K.A. Meade, K.J. White, C.E. Pickford, R.J. Holley, A. Marson, D. Tillotson, T.H. van Kuppevelt, J.D. Whittle, A.J. Day, C.L.R. Merry, Immobilization of Heparan Sulfate on Electrospun Meshes to Support Embryonic Stem Cell Culture and Differentiation, J. Biol. Chem. 288(8) (2013) 5530-5538.
[303] R.V. Goreham, R.D. Short, K. Vasilev, Method for the generation of surface-bound nanoparticle density gradients, The Journal of Physical Chemistry C 115(8) (2011) 3429-3433.
[304] D.J. Menzies, B. Cowie, C. Fong, J.S. Forsythe, T.R. Gengenbach, K.M. McLean, L. Puskar, M. Textor, L. Thomsen, M. Tobin, One-step method for generating PEG-like plasma polymer gradients: chemical characterization and analysis of protein interactions, Langmuir 26(17) (2010) 13987-13994.
[305] R.V. Goreham, A. Mierczynska, M. Pierce, R.D. Short, S. Taheri, A. Bachhuka, A. Cavallaro, L.E. Smith, K. Vasilev, A substrate independent approach for generation of surface gradients, Thin Solid Films 528 (2013) 106-110.
[306] F. Harding, R. Goreham, R. Short, K. Vasilev, N.H. Voelcker, Surface bound amine functional group density influences embryonic stem cell maintenance, Advanced healthcare materials 2(4) (2013) 585-590.
[307] M. Zelzer, M.R. Alexander, N.A. Russell, Hippocampal cell response to substrates with surface chemistry gradients, Acta biomaterialia 7(12) (2011) 4120-4130.
[308] B.J. Dickson, Molecular mechanisms of axon guidance, Science 298(5600) (2002) 1959-1964.
[309] D. Mortimer, T. Fothergill, Z. Pujic, L.J. Richards, G.J. Goodhill, Growth cone chemotaxis, Trends in neurosciences 31(2) (2008) 90-98.
[310] J. Li, L. Zhu, M. Zhang, F. Lin, Microfluidic device for studying cell migration in single or co-existing chemical gradients and electric fields, Biomicrofluidics 6(2) (2012) 024121.
[311] K. Moore, M. Macsween, M. Shoichet, Immobilized concentration gradients of neurotrophic factors guide neurite outgrowth of primary neurons in macroporous scaffolds, Tissue Eng. 12(2) (2006) 267-278.
[312] D. Guarnieri, A. De Capua, M. Ventre, A. Borzacchiello, C. Pedone, D. Marasco, M. Ruvo, P. Netti, Covalently immobilized RGD gradient on PEG hydrogel scaffold influences cell migration parameters, Acta Biomater. 6(7) (2010) 2532-2539.
[313] J. Mai, L. Fok, H. Gao, X. Zhang, M.-m. Poo, Axon initiation and growth cone turning on bound protein gradients, Journal of Neuroscience 29(23) (2009) 7450-7458.
[314] M.C. Dodla, R.V. Bellamkonda, Differences between the effect of anisotropic and isotropic laminin and nerve growth factor presenting

scaffolds on nerve regeneration across long peripheral nerve gaps, Biomaterials 29(1) (2008) 33-46.
[315] S. Tang, J. Zhu, Y. Xu, A.P. Xiang, M.H. Jiang, D. Quan, The effects of gradients of nerve growth factor immobilized PCLA scaffolds on neurite outgrowth in vitro and peripheral nerve regeneration in rats, Biomaterials 34(29) (2013) 7086-7096.
[316] C.-W. Yeh, L.-W. Wang, H.-C. Wu, Y.-K. Hsieh, J. Wang, M.-H. Chen, T.-W. Wang, Development of biomimetic micro-patterned device incorporated with neurotrophic gradient and supportive Schwann cells for the applications in neural tissue engineering, Biofabrication 9(1) (2017) 015024.
[317] D.E. Robinson, A. Marson, R.D. Short, D.J. Buttle, A.J. Day, K.L. Parry, M. Wiles, P. Highfield, A. Mistry, J.D. Whittle, Surface gradient of functional heparin, Advanced Materials 20(6) (2008) 1166-1169.
[318] D. Mangindaan, W.-H. Kuo, M.-J. Wang, Two-dimensional amine-functionality gradient by plasma polymerization, Biochemical engineering journal 78 (2013) 198-204.
[319] K.L. Parry, A. Shard, R. Short, R. White, J. Whittle, A. Wright, ARXPS characterisation of plasma polymerised surface chemical gradients, Surface and interface analysis 38(11) (2006) 1497-1504.
[320] W.G. Pitt, Fabrication of a continuous wettability gradient by radio frequency plasma discharge, Journal of colloid and interface science 133(1) (1989) 223-227.
[321] C.G. Gölander, W.G. Pitt, Characterization of hydrophobicity gradients prepared by means of radio frequency plasma discharge, Biomaterials 11(1) (1990) 32-35.
[322] J.H. Lee, H.G. Kim, G.S. Khang, H.B. Lee, M.S. Jhon, Characterization of wettability gradient surfaces prepared by corona discharge treatment, J. Colloid Interface Sci. 151(2) (1992) 563-570.
[323] Y.N. Shin, B.S. Kim, H.H. Ahn, J.H. Lee, K.S. Kim, J.Y. Lee, M.S. Kim, G. Khang, H.B. Lee, Adhesion comparison of human bone marrow stem cells on a gradient wettable surface prepared by corona treatment, Appl. Surf. Sci. 255(2) (2008) 293-296.
[324] S.J. Lee, G. Khang, Y.M. Lee, H.B. Lee, The effect of surface wettability on induction and growth of neurites from the PC-12 cell on a polymer surface, J. Colloid Interface Sci. 259(2) (2003) 228-235.
[325] M.S. Kim, K.S. Seo, G. Khang, H.B. Lee, First preparation of biotinylated gradient polyethylene surface to bind photoactive caged streptavidin, Langmuir 21(9) (2005) 4066-4070.
[326] S.Y. Lee, J.Y. Youn, B.S. Kim, Y.H. Cho, M.S. Kim, G. Khang, H.B. Lee, Quantum dots-modified gradient polymer surface, Colloids and Surfaces A: Physicochemical and Engineering Aspects 313 (2008) 136-139.

[327] H.T. Spijker, R. Bos, W. van Oeveren, J. de Vries, H.J. Busscher, Protein adsorption on gradient surfaces on polyethylene prepared in a shielded gas plasma, Colloids Surf. B Biointerfaces 15(1) (1999) 89-97.
[328] H.T. Spijker, R. Bos, H.J. Busscher, T.G. van Kooten, W. van Oeveren, Platelet adhesion and activation on a shielded plasma gradient prepared on polyethylene, Biomaterials 23(3) (2002) 757-766.
[329] J.D. Whittle, D. Barton, M.R. Alexander, R.D. Short, A method for the deposition of controllable chemical gradients, Chemical Communications (14) (2003) 1766-1767.
[330] K. Vasilev, A. Mierczynska, A.L. Hook, J. Chan, N.H. Voelcker, R.D. Short, Creating gradients of two proteins by differential passive adsorption onto a PEG-density gradient, Biomaterials 31(3) (2010) 392-397.
[331] R.A. Walker, V.T. Cunliffe, J.D. Whittle, D.A. Steele, R.D. Short, Submillimeter-scale surface gradients of immobilized protein ligands, Langmuir 25(8) (2009) 4243-4246.
[332] N. Wells, M.A. Baxter, J.E. Turnbull, P. Murray, D. Edgar, K.L. Parry, D.A. Steele, R.D. Short, The geometric control of E14 and R1 mouse embryonic stem cell pluripotency by plasma polymer surface chemical gradients, Biomaterials 30(6) (2009) 1066-1070.
[333] F.J. Harding, L.R. Clements, R.D. Short, H. Thissen, N.H. Voelcker, Assessing embryonic stem cell response to surface chemistry using plasma polymer gradients, Acta biomaterialia 8(5) (2012) 1739-1748.
[334] P.-Y. Wang, L.R. Clements, H. Thissen, W.-B. Tsai, N.H. Voelcker, Screening rat mesenchymal stem cell attachment and differentiation on surface chemistries using plasma polymer gradients, Acta biomaterialia 11 (2015) 58-67.
[335] D. Mangindaan, W.H. Kuo, H. Kurniawan, M.J. Wang, Creation of biofunctionalized plasma polymerized allylamine gradients, Journal of Polymer Science Part B: Polymer Physics 51(18) (2013) 1361-1367.
[336] J. Lai, B. Sunderland, J. Xue, S. Yan, W. Zhao, M. Folkard, B.D. Michael, Y. Wang, Study on hydrophilicity of polymer surfaces improved by plasma treatment, Applied Surface Science 252(10) (2006) 3375-3379.
[337] J.J. Barry, D. Howard, K.M. Shakesheff, S.M. Howdle, M.R. Alexander, Using a core–sheath distribution of surface chemistry through 3D tissue engineering scaffolds to control cell ingress, Advanced Materials 18(11) (2006) 1406-1410.
[338] M. Zelzer, R. Majani, J.W. Bradley, F.R. Rose, M.C. Davies, M.R. Alexander, Investigation of cell–surface interactions using chemical gradients formed from plasma polymers, Biomaterials 29(2) (2008) 172-184.

[339] D.E. Robinson, D.J. Buttle, J.D. Whittle, K.L. Parry, R.D. Short, D.A. Steele, The substrate and composition dependence of plasma polymer stability, Plasma Processes and Polymers 7(2) (2010) 102-106.
[340] B. Delalat, R.V. Goreham, K. Vasilev, F.J. Harding, N.H. Voelcker, Subtle changes in surface chemistry affect embryoid body cell differentiation: lessons learnt from surface-bound amine density gradients, Tissue Engineering Part A 20(11-12) (2014) 1715-1725.
[341] X. Liu, S. Shi, Q. Feng, A. Bachhuka, W. He, Q. Huang, R. Zhang, X. Yang, K. Vasilev, Surface chemical gradient affects the differentiation of human adipose-derived stem cells via ERK1/2 signaling pathway, ACS applied materials & interfaces 7(33) (2015) 18473-18482.
[342] G.C.C. Mendes, T.R.S. Brandao, C.L.M. Silva, Ethylene oxide sterilization of medical devices: A review, American Journal of Infection Control 35(9) (2007) 574-581.
[343] Z. Dai, J. Ronholm, Y. Tian, B. Sethi, X. Cao, Sterilization techniques for biodegradable scaffolds in tissue engineering applications, Journal of tissue engineering 7 (2016) 2041731416648810.
[344] T.A.M. Valente, D.M. Silva, P.S. Gomes, M.H. Fernandes, J.D. Santos, V. Sencadas, Effect of Sterilization Methods on Electrospun Poly(lactic acid) (PLA) Fiber Alignment for Biomedical Applications, Acs Applied Materials & Interfaces 8(5) (2016) 3241-3249.
[345] C. Fischbach, J. Tessmar, A. Lucke, E. Schnell, G. Schmeer, T. Blunk, A. Gopferich, Does UV irradiation affect polymer properties relevant to tissue engineering?, Surf. Sci. 491(3) (2001) 333-345.
[346] B.D. Ratner, A.S. Hoffman, F.J. Schoen, J.E. Lemons, Biomaterials science: an introduction to materials in medicine, Elsevier2004.
[347] M. Silindir, A.Y. Özer, Sterilization methods and the comparison of e-beam sterilization with gamma radiation sterilization, Fabad Journal of Pharmaceutical Sciences 34(1) (2009) 43.
[348] G. McDonnell, D. Sheard, A practical guide to decontamination in healthcare, John Wiley & Sons2012.
[349] S. Gogolewski, P. Mainil-Varlet, The effect of thermal treatment on sterility, molecular and mechanical properties of various polylactides: I. Poly (L-lactide), Biomaterials 17(5) (1996) 523-528.
[350] F. Rozema, R. Bos, G. Boering, J. Van Asten, A. Nijenhuis, A. Pennings, The effects of different steam-sterilization programs on material properties of poly (l-lactide), Journal of applied biomaterials 2(1) (1991) 23-28.
[351] S. Gogolewski, P. Mainil-Varlet, Effect of thermal treatment on sterility, molecular and mechanical properties of various polylactides:

2. Poly (l/d-lactide) and poly (l/dl-lactide), Biomaterials 18(3) (1997) 251-255.
[352] D. Leonard, F. Buchanan, D. Farrar, Investigation into depth dependence of effect of E-beam radiation on mechanical and degradation properties of polylactide, Plastics, rubber and composites 35(8) (2006) 303-309.
[353] A.P. Fraise, P.A. Lambert, J.-Y. Maillard, Russell, Hugo & Ayliffe's Principles and Practice of Disinfection, Preservation & Sterilization, John Wiley & Sons2008.
[354] M.H.F. Spoto, C.R. Gallo, A.R. Alcarde, M.S.d.A. Gurgel, L. Blumer, J.M.M. Walder, R.E. Domarco, Gamma irradiation in the control of pathogenic bacteria in refrigerated ground chicken meat, Scientia Agricola 57(3) (2000) 389-394.
[355] P. Plikk, K. Odelius, M. Hakkarainen, A.-C. Albertsson, Finalizing the properties of porous scaffolds of aliphatic polyesters through radiation sterilization, Biomaterials 27(31) (2006) 5335-5347.
[356] C.E. Holy, C. Cheng, J.E. Davies, M.S. Shoichet, Optimizing the sterilization of PLGA scaffolds for use in tissue engineering, Biomaterials 22(1) (2000) 25-31.
[357] E. Cottam, D.W. Hukins, K. Lee, C. Hewitt, M.J. Jenkins, Effect of sterilisation by gamma irradiation on the ability of polycaprolactone (PCL) to act as a scaffold material, Medical engineering & physics 31(2) (2009) 221-226.
[358] K.A. Hooper, J.D. Cox, J. Kohn, Comparison of the effect of ethylene oxide and gamma-irradiation on selected tyrosine-derived polycarbonates and poly(L-lactic acid), Journal of Applied Polymer Science 63(11) (1997) 1499-1510.
[359] Y.X. Dong, T. Yong, S. Liao, C.K. Chan, S. Ramakrishna, Degradation of electrospun nanofiber scaffold by short wave length ultraviolet radiation treatment and its potential applications in tissue engineering, Tissue Engineering Part A 14(8) (2008) 1321-1329.
[360] Y. Dai, Y. Xia, H.B. Chen, N. Li, G. Chen, F.M. Zhang, N. Gu, Optimization of sterilization methods for electrospun poly(epsilon-caprolactone) to enhance pre-osteoblast cell behaviors for guided bone regeneration, Journal of Bioactive and Compatible Polymers 31(2) (2016) 152-166.
[361] C.-Y. Hsiao, S.-J. Liu, S.W.-N. Ueng, E.-C. Chan, The influence of γ irradiation and ethylene oxide treatment on the release characteristics of biodegradable poly (lactide-co-glycolide) composites, Polymer degradation and stability 97(5) (2012) 715-720.
[362] T.M. Moore, E. Gendler, E. Gendler, Viruses adsorbed on musculoskeletal allografts are inactivated by terminal ethylene oxide disinfection, Journal of orthopaedic research 22(6) (2004) 1358-1361.

[363] S.J. Peniston, S.J. Choi, Effect of sterilization on the physicochemical properties of molded poly(L-lactic acid), Journal of Biomedical Materials Research Part B-Applied Biomaterials 80B(1) (2007) 67-77.
[364] E. Phillip, N.S. Murthy, D. Bolikal, P. Narayanan, J. Kohn, L. Lavelle, S. Bodnar, K. Pricer, Ethylene oxide's role as a reactive agent during sterilization: Effects of polymer composition and device architecture, J. Biomed. Mater. Res. B Appl. Biomater. 101B(4) (2013) 532-540.
[365] P. Vink, K. Pleijsier, Aeration of ethylene oxide-sterilized polymers, Biomaterials 7(3) (1986) 225-230.
[366] T. Ramos, M. Ahmed, P. Wieringa, L. Moroni, Schwann cells promote endothelial cell migration, Cell adhesion & migration 9(6) (2015) 441-451.
[367] P.R. Marreco, P.d.L. Moreira, S.C. Genari, Â.M. Moraes, Effects of different sterilization methods on the morphology, mechanical properties, and cytotoxicity of chitosan membranes used as wound dressings, Journal of Biomedical Materials Research Part B: Applied Biomaterials: An Official Journal of The Society for Biomaterials, The Japanese Society for Biomaterials, and The Australian Society for Biomaterials and the Korean Society for Biomaterials 71(2) (2004) 268-277.
[368] H. Shearer, M.J. Ellis, S.P. Perera, J.B. Chaudhuri, Effects of common sterilization methods on the structure and properties of poly (D, L lactic-co-glycolic acid) scaffolds, Tissue engineering 12(10) (2006) 2717-2727.
[369] C.E. Holy, C. Cheng, J.E. Davies, M.S. Shoichet, Optimizing the sterilization of PLGA scaffolds for use in tissue engineering, Biomaterials 22(1) (2001) 25-31.
[370] H. Shintani, A. Sakudo, P. Burke, G. McDonnell, Gas plasma sterilization of microorganisms and mechanisms of action (Review), Experimental and Therapeutic Medicine 1(5) (2010) 731-738.
[371] N. De Geyter, R. Morent, Nonthermal plasma sterilization of living and nonliving surfaces, Annual review of biomedical engineering 14 (2012) 255-274.
[372] F. Rossi, O. Kylián, H. Rauscher, D. Gilliland, L. Sirghi, Use of a low-pressure plasma discharge for the decontamination and sterilization of medical devices, Pure and Applied Chemistry 80(9) (2008) 1939-1951.
[373] M. Laroussi, F. Leipold, Evaluation of the roles of reactive species, heat, and UV radiation in the inactivation of bacterial cells by air plasmas at atmospheric pressure, International Journal of Mass Spectrometry 233(1) (2004) 81-86.

[374] S.G. Joshi, M. Paff, G. Friedman, G. Fridman, A. Fridman, A.D. Brooks, Control of methicillin-resistant Staphylococcus aureus in planktonic form and biofilms: A biocidal efficacy study of nonthermal dielectric-barrier discharge plasma, American Journal of Infection Control 38(4) (2010) 293-301.
[375] S. Lerouge, M.R. Wertheimer, L.H. Yahia, Plasma Sterilization: A Review of Parameters, Mechanisms, and Limitations, Plasmas and Polymers 6(3) 175-188.
[376] N. Philip, B. Saoudi, M.-C. Crevier, M. Moisan, J. Barbeau, J. Pelletier, The respective roles of UV photons and oxygen atoms in plasma sterilization at reduced gas pressure: the case of N/sub 2/-O/sub 2/mixtures, IEEE Transactions on Plasma Science 30(4) (2002) 1429-1436.
[377] N. Munakata, M. Saito, K. Hieda, Inactivation action spectra of Bacillus subtilis spores in extended ultraviolet wavelengths (50–300nm) obtained with synchrotron radiation, Photochemistry and photobiology 54(5) (1991) 761-768.
[378] O. Kylián, M. Hasiwa, D. Gilliland, F. Rossi, Experimental Study of the Influence of Ar/H2 microwave discharges on lipid A, Plasma Processes and Polymers 5(1) (2008) 26-32.
[379] M. Moisan, J. Barbeau, M.-C. Crevier, J. Pelletier, N. Philip, B. Saoudi, Plasma sterilization. Methods and mechanisms, Pure and applied chemistry 74(3) (2002) 349-358.
[380] K. Kelly-Wintenberg, T. Montie, C. Brickman, J.R. Roth, A. Carr, K. Sorge, L. Wadsworth, P. Tsai, Room temperature sterilization of surfaces and fabrics with a one atmosphere uniform glow discharge plasma, Journal of Industrial Microbiology and Biotechnology 20(1) (1998) 69-74.
[381] B.J. Park, D. Lee, J.-C. Park, I.-S. Lee, K.-Y. Lee, S. Hyun, M.-S. Chun, K.-H. Chung, Sterilization using a microwave-induced argon plasma system at atmospheric pressure, Physics of Plasmas 10(11) (2003) 4539-4544.
[382] K.-Y. Lee, B.J. Park, D.H. Lee, I.-S. Lee, S.O. Hyun, K.-H. Chung, J.-C. Park, Sterilization of Escherichia coli and MRSA using microwave-induced argon plasma at atmospheric pressure, Surface and Coatings Technology 193(1-3) (2005) 35-38.
[383] S. Lerouge, M. Tabrizian, M.R. Wertheimer, R. Marchand, L. Yahia, Safety of plasma-based sterilization: Surface modifications of polymeric medical devices induced by Sterrad((R)) and Plazlyte (TM) processes, Bio-Medical Materials and Engineering 12(1) (2002) 3-13.
[384] M.C. Krebs, P. Becasse, D. Verjat, J.C. Darbord, Gas-plasma sterilization: relative efficacy of the hydrogen peroxide phase compared with that of the plasma phase, International Journal of Pharmaceutics 160(1) (1998) 75-81.

[385] S. Lerouge, C. Guignot, M. Tabrizian, D. Ferrier, N. Yagoubi, L.H. Yahia, Plasma-based sterilization: Effect on surface and bulk properties and hydrolytic stability of reprocessed polyurethane electrophysiology catheters, Journal of Biomedical Materials Research 52(4) (2000) 774-782.
[386] H.E. Wagner, R. Brandenburg, K.V. Kozlov, A. Sonnenfeld, P. Michel, J.F. Behnke, The barrier discharge: basic properties and applications to surface treatment, Vacuum 71(3) (2003) 417-436.
[387] R. Kaewkhaw, A.M. Scutt, J.W. Haycock, Integrated culture and purification of rat Schwann cells from freshly isolated adult tissue, Nature protocols 7(11) (2012) 1996.
[388] N. De Geyter, R. Morent, C. Leys, L. Gengembre, E. Payen, S. Van Vlierberghe, E. Schacht, DBD treatment of polyethylene terephthalate: Atmospheric versus medium pressure treatment, Surface & Coatings Technology 202(13) (2008) 3000-3010.
[389] F. Massines, N. Gherardi, A. Fornelli, S. Martin, Atmospheric pressure plasma deposition of thin films by Townsend dielectric barrier discharge, Surface & Coatings Technology 200(5-6) (2005) 1855-1861.
[390] E.D. Yildirim, H. Ayan, V.N. Vasilets, A. Fridman, S. Guceri, G. Friedman, W. Sun, Effect of dielectric barrier discharge plasma on the attachment and proliferation of osteoblasts cultured over poly(epsilon-caprolactone) scaffolds (vol 4, pg 58, 2007), Plasma Processes and Polymers 5(4) (2008) 397-397.
[391] F. Massines, G. Gouda, N. Gherardi, M. Duran, E. Croquesel, The Role of Dielectric Barrier Discharge Atmosphere and Physics on Polypropylene Surface Treatment, Plasmas and Polymers 6(1) 35-49.
[392] D.M.S. El-Zeer, A. A.; Rashed, U. M.; Abd-Elbaset, T. A.; Ghalab, S. , A Comparative Study between the Filamentary and Glow Modes of DBD Plasma in the Treatment of Wool Fibers, Journal of Engineering Research and Applications 4(3) (2014) 401-410.
[393] A. Marmur, Soft contact: measurement and interpretation of contact angles, Soft Matter. 2(1) (2006) 12-17.
[394] D. Hegemann, H. Brunner, C. Oehr, Plasma treatment of polymers for surface and adhesion improvement, Nuclear Instruments & Methods in Physics Research Section B-Beam Interactions with Materials and Atoms 208 (2003) 281-286.
[395] R. Morent, N. De Geyter, C. Leys, L. Gengembre, E. Payen, Study of the ageing behaviour of polymer films treated with a dielectric barrier discharge in air, helium and argon at medium pressure, Surface & Coatings Technology 201(18) (2007) 7847-7854.
[396] P. Slepicka, N.S. Kasalkova, E. Stranska, L. Bacakova, V. Svorcik, Surface characterization of plasma treated polymers for applications as biocompatible carriers, Express Polymer Letters 7(6) (2013) 535-545.

[397] A. Manakhov, D. Necas, J. Cechal, D. Pavlinak, M. Elias, L. Zajickova, Deposition of stable amine coating onto polycaprolactone nanofibers by low pressure cyclopropylamine plasma polymerization, Thin Solid Films 581 (2015) 7-13.
[398] N. De Geyter, R. Morent, T. Desmet, M. Trentesaux, L. Gengembre, P. Dubruel, C. Leys, E. Payen, Plasma modification of polylactic acid in a medium pressure DBD, Surface & Coatings Technology 204(20) (2010) 3272-3279.
[399] M. Domingos, F. Chiellini, S. Cometa, E.D. Giglio, E. Grillo-Fernandes, P. Bartolo, E. Chiellini, Evaluation of in vitro degradation of PCL scaffolds fabricated via BioExtrusion – Part 2: Influence of pore size and geometry, Virtual and Physical Prototyping 6(3) (2011) 157-165.
[400] M. Moisan, J. Barbeau, M.C. Crevier, J. Pelletier, N. Philip, B. Saoudi, Plasma sterilization. Methods mechanisms, Pure and Applied Chemistry 74(3) (2002) 349-358.
[401] H.H. Ahn, I.W. Lee, H.B. Lee, M.S. Kim, Cellular Behavior of Human Adipose- Derived Stem Cells on Wettable Gradient Polyethylene Surfaces, International Journal of Molecular Sciences 15(2) (2014) 2075-2086.
[402] L. Bacakova, E. Filova, M. Parizek, T. Ruml, V. Svorcik, Modulation of cell adhesion, proliferation and differentiation on materials designed for body implants, Biotechnology Advances 29(6) (2011) 739-767.
[403] P. Slepicka, S. Trostova, N.S. Kasalkova, Z. Kolska, P. Sajdl, V. Svorcik, Surface Modification of Biopolymers by Argon Plasma and Thermal Treatment, Plasma Processes and Polymers 9(2) (2012) 197-206.
[404] R. Ghobeira, C. Philips, H. Declercq, P. Cools, N. De Geyter, R. Cornelissen, R. Morent, Effects of different sterilization methods on the physico-chemical and bioresponsive properties of plasma-treated PCL films, Biomedical Materials (Submitted) (2016).
[405] N. Recek, M. Resnik, H. Motaln, T. Lah-Turnsek, R. Augustine, N. Kalarikkal, S. Thomas, M. Mozetic, Cell Adhesion on Polycaprolactone Modified by Plasma Treatment, Int. J. Polym. Sci. (2016).
[406] T. Jacobs, N. De Geyter, R. Morent, T. Desmet, P. Dubruel, C. Leys, Plasma treatment of polycaprolactone at medium pressure, Surface & Coatings Technology 205 (2011) S543-S547.
[407] D.M. El-Zeer, A.A. Salem, U.M. Rashed, T.A. Abd Elbaset, S. Ghalab, A Comparative Study between the Filamentary and Glow Modes of DBD Plasma in the Treatment of Wool Fibers, Int. j. eng. res. appl. 4 (2014) 401-410.

[408] S. Lerouge, M.R. Wertheimer, L.H. Yahia, Plasma Sterilization: A Review of Parameters, Mechanisms, and Limitations, Plasmas Polym. 6(3) (2001) 175-188.
[409] S. Duzyer, S. Koral Koc, A. Hockenberger, E. Evke, Z. Kahveci, A. Uguz, EFFECTS OF DIFFERENT STERILIZATION METHODS ON POLYESTER SURFACES, Tekstil Ve Konfeksiyon 23(4) (2013) 319-324.
[410] C.L. Beyler, M.M. Hirschler, Thermal decomposition of polymers, SFPE handbook of fire protection engineering 2 (2002) 110-131.
[411] J.R. White, Polymer ageing: physics, chemistry or engineering? Time to reflect, Comptes Rendus Chimie 9(11) (2006) 1396-1408.
[412] J. Pospisil, Z. Horak, J. Pilar, N.C. Billingham, H. Zweifel, S. Nespurek, Influence of testing conditions on the performance and durability of polymer stabilisers in thermal oxidation, Polym. Degradation Stab. 82(2) (2003) 145-162.
[413] W.G. Cui, X.H. Li, S.B. Zhou, J. Weng, Degradation patterns and surface wettability of electrospun fibrous mats, Polym. Degradation Stab. 93(3) (2008) 731-738.
[414] M.P. Prabhakaran, J. Venugopal, C.K. Chan, S. Ramakrishna, Surface modified electrospun nanofibrous scaffolds for nerve tissue engineering, Nanotechnology 19(45) (2008).
[415] D.P. Dowling, I.S. Miller, M. Ardhaoui, W.M. Gallagher, Effect of Surface Wettability and Topography on the Adhesion of Osteosarcoma Cells on Plasma-modified Polystyrene, J. Biomater. Appl. 26(3) (2011) 327-347.
[416] R. Ghobeira, N. De Geyter, R. Morent, Plasma surface functionalization of biodegradable electrospun scaffolds for tissue engineering applications, in: G. Rohman (Ed.), Biodegradable polymers: recent developments and new perspectives, IAPC Publishing, Zagreb Croatia, 2017, pp. 191-236.
[417] C. Luo, E. Stride, M. Edirisinghe, Mapping the influence of solubility and dielectric constant on electrospinning polycaprolactone solutions, Macromolecules 45(11) (2012) 4669-4680.
[418] E.-J. Lee, S.-H. Teng, T.-S. Jang, P. Wang, S.-W. Yook, H.-E. Kim, Y.-H. Koh, Nanostructured poly(ε-caprolactone)–silica xerogel fibrous membrane for guided bone regeneration, Acta Biomaterialia 6(9) (2010) 3557-3565.
[419] B.S. Jha, R.J. Colello, J.R. Bowman, S.A. Sell, K.D. Lee, J.W. Bigbee, G.L. Bowlin, W.N. Chow, B.E. Mathern, D.G. Simpson, Two pole air gap electrospinning: Fabrication of highly aligned, three-dimensional scaffolds for nerve reconstruction, Acta Biomaterialia 7(1) (2011) 203-215.
[420] W.-J. Li, R. Tuli, C. Okafor, A. Derfoul, K.G. Danielson, D.J. Hall, R.S. Tuan, A three-dimensional nanofibrous scaffold for cartilage tissue

engineering using human mesenchymal stem cells, Biomaterials 26(6) (2005) 599-609.
[421] V. Beachley, X. Wen, Effect of electrospinning parameters on the nanofiber diameter and length, Materials science & engineering. C, Materials for biological applications 29(3) (2009) 663-668.
[422] F. Khodkar, N. Golshan Ebrahimi, Preparation and properties of antibacterial, biocompatible core–shell fibers produced by coaxial electrospinning, Journal of Applied Polymer Science 134(25) (2017) 44979.
[423] N.H. Marei, I.M. El-Sherbiny, A. Lotfy, A. El-Badawy, N. El-Badri, Mesenchymal stem cells growth and proliferation enhancement using PLA vs PCL based nanofibrous scaffolds, International journal of biological macromolecules 93 (2016) 9-19.
[424] M.A. Alfaro De Prá, R.M. Ribeiro-do-Valle, M. Maraschin, B. Veleirinho, Effect of collector design on the morphological properties of polycaprolactone electrospun fibers, Materials Letters 193 (2017) 154-157.
[425] K. Mubyana, R.A. Koppes, K.L. Lee, J.A. Cooper, D.T. Corr, The influence of specimen thickness and alignment on the material and failure properties of electrospun polycaprolactone nanofiber mats, Journal of Biomedical Materials Research Part A 104(11) (2016) 2794-2800.
[426] O. Suwantong, Biomedical applications of electrospun polycaprolactone fiber mats, Polymers for Advanced Technologies 27(10) (2016) 1264-1273.
[427] P. Kiselev, J. Rosell-Llompart, Highly aligned electrospun nanofibers by elimination of the whipping motion, Journal of Applied Polymer Science 125(3) (2012) 2433-2441.
[428] N. Lavielle, A.-M. Popa, M. de Geus, A. Hébraud, G. Schlatter, L. Thöny-Meyer, R.M. Rossi, Controlled formation of poly (ε-caprolactone) ultrathin electrospun nanofibers in a hydrolytic degradation-assisted process, European Polymer Journal 49(6) (2013) 1331-1336.
[429] S.-L. Liu, Y.-Z. Long, Z.-H. Zhang, H.-D. Zhang, B. Sun, J.-C. Zhang, W.-P. Han, Assembly of oriented ultrafine polymer fibers by centrifugal electrospinning, J. Nanomaterials 2013(2514103) (2013) 8-8.
[430] M.L.A. Matthias, G. Christian, B. Helga, S. Heinrich, Electrospinning of aligned fibers with adjustable orientation using auxiliary electrodes, Science and Technology of Advanced Materials 13(3) (2012) 035008.
[431] W.E. Teo, M. Kotaki, X.M. Mo, S. Ramakrishna, Porous tubular structures with controlled fibre orientation using a modified electrospinning method, Nanotechnology. 16(6) (2005) 918.

[432] D. Yang, B. Lu, Y. Zhao, X. Jiang, Fabrication of Aligned Fibrous Arrays by Magnetic Electrospinning, Advanced Materials 19(21) (2007) 3702-3706.
[433] P. Supaphol, O. Suwantong, P. Sangsanoh, S. Srinivasan, R. Jayakumar, S.V. Nair, Electrospinning of Biocompatible Polymers and Their Potentials in Biomedical Applications, in: R. Jayakumar, S. Nair (Eds.), Biomedical Applications of Polymeric Nanofibers, Springer Berlin Heidelberg, Berlin, Heidelberg, 2012, pp. 213-239.
[434] Z. Li, C. Wang, Effects of Working Parameters on Electrospinning, in: Z. Li, C. Wang (Eds.), One-Dimensional nanostructures: Electrospinning Technique and Unique Nanofibers, Springer Berlin Heidelberg, 2013, pp. 15-28.
[435] B. Veleirinho, M.F. Rei, J.A. Lopes-Da-Silva, Solvent and concentration effects on the properties of electrospun poly(ethylene terephthalate) nanofiber mats, Journal of Polymer Science Part B: Polymer Physics 46(5) (2008) 460-471.
[436] B. Tarus, N. Fadel, A. Al-Oufy, M. El-Messiry, Effect of polymer concentration on the morphology and mechanical characteristics of electrospun cellulose acetate and poly (vinyl chloride) nanofiber mats, Alexandria Engineering Journal 55(3) (2016) 2975-2984.
[437] A. Haider, S. Haider, I.-K. Kang, A comprehensive review summarizing the effect of electrospinning parameters and potential applications of nanofibers in biomedical and biotechnology, Arab. J. Chem. (2015).
[438] K.P. Matabola, R.M. Moutloali, The influence of electrospinning parameters on the morphology and diameter of poly(vinyledene fluoride) nanofibers- effect of sodium chloride, Journal of Materials Science 48(16) (2013) 5475-5482.
[439] T. Wang, S. Kumar, Electrospinning of polyacrylonitrile nanofibers, Journal of Applied Polymer Science 102(2) (2006) 1023-1029.
[440] A. Bertea, L.R. Manea, A. Popa, A. Bertea, The Influence of Process Parameters on the Characteristics of Electrospun 3D Nanostructures, IOP Conference Series: Materials Science and Engineering 209(1) (2017) 012074.
[441] W. Ding, S. Wei, J. Zhu, X. Chen, D. Rutman, Z. Guo, Manipulated Electrospun PVA Nanofibers with Inexpensive Salts, Macromolecular Materials and Engineering 295(10) (2010) 958-965.
[442] X. Lai, D. Wu, D. Sun, Electro spinning under sub critical voltage, 2010 IEEE 5th International Conference on Nano/Micro Engineered and Molecular Systems (2010) 1170-1173.
[443] H.X. Li, C.L. Zhu, J.J. Xue, Q.F. Ke, Y.N. Xia, Enhancing the Mechanical Properties of Electrospun Nanofiber Mats through

Controllable Welding at the Cross Points, Macromolecular Rapid Communications 38(9) (2017).
[444] J.M. Deitzel, W. Kosik, S.H. McKnight, N.C. Beck Tan, J.M. DeSimone, S. Crette, Electrospinning of polymer nanofibers with specific surface chemistry, Polymer. 43(3) (2002) 1025-1029.
[445] R. Ghobeira, C. Philips, H. Declercq, P. Cools, N. De Geyter, R. Cornelissen, R. Morent, Effects of different sterilization methods on the physico-chemical and bioresponsive properties of plasma-treated polycaprolactone films, Biomed. Mater. 12(1) (2017) 015017.
[446] D. Cho, S. Chen, Y. Jeong, Y.L. Joo, Surface hydro-properties of electrospun fiber mats, Fiber. Polym. 16(7) (2015) 1578-1586.
[447] L.S. Dolci, S.D. Quiroga, M. Gherardi, R. Laurita, A. Liguori, P. Sanibondi, A. Fiorani, L. Calzà, V. Colombo, M.L. Focarete, Carboxyl Surface Functionalization of Poly(L-lactic acid) Electrospun Nanofibers through Atmospheric Non-Thermal Plasma Affects Fibroblast Morphology, Plasma Process. Polym. 11(3) (2014) 203-213.
[448] V. Milleret, T. Hefti, H. Hall, V. Vogel, D. Eberli, Influence of the fiber diameter and surface roughness of electrospun vascular grafts on blood activation, Acta. Biomater. 8(12) (2012) 4349-4356.
[449] C. Xu, F. Yang, S. Wang, S. Ramakrishna, In vitro study of human vascular endothelial cell function on materials with various surface roughness, J. Biomed. Mater. Res. A. 71A(1) (2004) 154-161.
[450] H.H. Kim, M.J. Kim, S.J. Ryu, C.S. Ki, Y.H. Park, Effect of fiber diameter on surface morphology, mechanical property, and cell behavior of electrospun poly(ε-caprolactone) mat, Fiber. Polym. 17(7) (2016) 1033-1042.
[451] J.L. Ifkovits, K. Wu, R.L. Mauck, J.A. Burdick, The Influence of Fibrous Elastomer Structure and Porosity on Matrix Organization, PLoS ONE 5(12) (2010) e15717.
[452] G.H. Kim, Electrospun PCL nanofibers with anisotropic mechanical properties as a biomedical scaffold, Biomed. Mater. 3(2) (2008) 025010.
[453] S.-C. Wong, A. Baji, S. Leng, Effect of fiber diameter on tensile properties of electrospun poly (ε-caprolactone), Polymer. 49(21) (2008) 4713-4722.
[454] C. Lim, E. Tan, S. Ng, Effects of crystalline morphology on the tensile properties of electrospun polymer nanofibers, Appl. Phys. Lett. 92(14) (2008) 141908.
[455] J. Yao, C.W. Bastiaansen, T. Peijs, High strength and high modulus electrospun nanofibers, Fibers. 2(2) (2014) 158-186.
[456] Z. Yin, X. Chen, J.L. Chen, W.L. Shen, T.M. Hieu Nguyen, L. Gao, H.W. Ouyang, The regulation of tendon stem cell differentiation by the alignment of nanofibers, Biomaterials. 31(8) (2010) 2163-2175.

[457] A. Doustgani, E. Vasheghani-Farahani, M. Soleimani, S. Hashemi-Najafabadi, Physical and chemical investigation of polycaprolactone, nanohydroxyapatite and poly (vinyl alcohol) nanocomposite scaffolds, Int J Cheml Biol Eng 6 (2012) 158-161.
[458] Y.-M. Ko, D.-Y. Choi, S.-C. Jung, B.-H. Kim, Characteristics of plasma treated electrospun polycaprolactone (PCL) nanofiber scaffold for bone tissue engineering, J. Nanosci. Nanotechnol. 15(1) (2015) 192-195.
[459] D. Yan, J. Jones, X.Y. Yuan, X.H. Xu, J. Sheng, J.C.M. Lee, G.Q. Ma, Q.S. Yu, Plasma treatment of electrospun PCL random nanofiber meshes (NFMs) for biological property improvement, J. Biomed. Mater. Res. A. 101A(4) (2013) 963-972.
[460] J.C. Lee, G. Ma, Q. Yu, Plasma treatment of random and aligned electrospun PCL nanofibers, J. Med. Biol. Eng. 33(3) (2013) 171-178.
[461] T. Jacobs, N. De Geyter, R. Morent, T. Desmet, P. Dubruel, C. Leys, Plasma treatment of polycaprolactone at medium pressure, Surf. Coat. Technol. 205 (2011) S543-S547.
[462] N. De Geyter, R. Morent, T. Desmet, M. Trentesaux, L. Gengembre, P. Dubruel, C. Leys, E. Payen, Plasma modification of polylactic acid in a medium pressure DBD, Surf. Coat. Technol. 204(20) (2010) 3272-3279.
[463] R. Ghobeira, C. Philips, V. De Naeyer, H. Declercq, P. Cools, N. De Geyter, R. Cornelissen, R. Morent, Comparative Study of the Surface Properties and Cytocompatibility of Plasma-Treated Poly-ε-Caprolactone Nanofibers Subjected to Different Sterilization Methods, J. Biomed. Nanotechnol. 13(6) (2017) 699-716.
[464] D. Sankar, K. Shalumon, K. Chennazhi, D. Menon, R. Jayakumar, Surface plasma treatment of poly (caprolactone) micro, nano, and multiscale fibrous scaffolds for enhanced osteoconductivity, Tissue Eng. Part A. 20(11-12) (2014) 1689-1702.
[465] M. Gazzano, C. Gualandi, A. Zucchelli, T. Sui, A.M. Korsunsky, C. Reinhard, M.L. Focarete, Structure-morphology correlation in electrospun fibers of semicrystalline polymers by simultaneous synchrotron SAXS-WAXD, Polymer. 63 (2015) 154-163.
[466] M. Richard-Lacroix, C. Pellerin, Molecular orientation in electrospun fibers: from mats to single fibers, Macromolecules. 46(24) (2013) 9473-9493.
[467] H.H. Ahn, I.W. Lee, H.B. Lee, M.S. Kim, Cellular behavior of human adipose-derived stem cells on wettable gradient polyethylene surfaces, Int. J. Mol. Sci. 15(2) (2014) 2075-2086.
[468] W. Liu, J. Zhan, Y. Su, T. Wu, C. Wu, S. Ramakrishna, X. Mo, S.S. Al-Deyab, M. El-Newehy, Effects of plasma treatment to nanofibers on initial cell adhesion and cell morphology, Colloids Surf. B Biointerfaces. 113 (2014) 101-106.

[469] H. Jahani, S. Kaviani, M. Hassanpour-Ezatti, M. Soleimani, Z. Kaviani, Z. Zonoubi, The effect of aligned and random electrospun fibrous scaffolds on rat mesenchymal stem cell proliferation, Yakhteh. 14(1) (2012) 31.
[470] N. Abbasi, S. Soudi, N. Hayati-Roodbari, M. Dodel, M. Soleimani, The effects of plasma treated electrospun nanofibrous poly (ε-caprolactone) scaffolds with different orientations on mouse embryonic stem cell proliferation, Yakhteh. 16(3) (2014) 245.
[471] M.P. Prabhakaran, J. Venugopal, C.K. Chan, S. Ramakrishna, Surface modified electrospun nanofibrous scaffolds for nerve tissue engineering, Nanotechnology. 19(45) (2008) 455102.
[472] N. Recek, M. Resnik, H. Motaln, T. Lah-Turnšek, R. Augustine, N. Kalarikkal, S. Thomas, M. Mozetič, Cell adhesion on polycaprolactone modified by plasma treatment, International Journal of Polymer Science 2016 (2016).
[473] G.T. Christopherson, H. Song, H.-Q. Mao, The influence of fiber diameter of electrospun substrates on neural stem cell differentiation and proliferation, Biomaterials. 30(4) (2009) 556-564.
[474] D.M. Thompson, H.M. Buettner, Neurite outgrowth is directed by schwann cell alignment in the absence of other guidance cues, Annals of biomedical engineering 34(4) (2006) 669.
[475] H.B. Wang, M.E. Mullins, J.M. Cregg, C.W. McCarthy, R.J. Gilbert, Varying the diameter of aligned electrospun fibers alters neurite outgrowth and Schwann cell migration, Acta Biomater. 6(8) (2010) 2970-2978.
[476] A. Subramanian, U.M. Krishnan, S. Sethuraman, Fabrication of uniaxially aligned 3D electrospun scaffolds for neural regeneration, Biomed. Mater. 6(2) (2011) 025004.
[477] F.J. Rodríguez, N. Gómez, G. Perego, X. Navarro, Highly permeable polylactide-caprolactone nerve guides enhance peripheral nerve regeneration through long gaps, Biomaterials 20(16) (1999) 1489-1500.
[478] N. De Geyter, R. Morent, C. Leys, Penetration of a dielectric barrier discharge plasma into textile structures at medium pressure, Plasma Sources Science and Technology 15(1) (2006) 78.
[479] H. Poll, U. Schladitz, S. Schreiter, Penetration of plasma effects into textile structures, Surf. Coat. Technol. 142 (2001) 489-493.
[480] P. Cools, M. Asadian, W. Nicolaus, H. Declercq, R. Morent, N. De Geyter, Surface treatment of PEOT/PBT (55/45) with a dielectric barrier discharge in air, helium, argon and nitrogen at medium pressure, Materials 11(3) (2018) 391.
[481] F. Massines, G. Gouda, A comparison of polypropylene-surface treatment by filamentary, homogeneous and glow discharges in helium

at atmospheric pressure, Journal of Physics D: Applied Physics 31(24) (1998) 3411.
[482] Z. Fang, X. Xie, J. Li, H. Yang, Y. Qiu, E. Kuffel, Comparison of surface modification of polypropylene film by filamentary DBD at atmospheric pressure and homogeneous DBD at medium pressure in air, Journal of Physics D: Applied Physics 42(8) (2009) 085204.
[483] I. Onyshchenko, N. De Geyter, A.Y. Nikiforov, R. Morent, Atmospheric pressure plasma penetration inside flexible polymeric tubes, Plasma Process. Polym. 12(3) (2015) 271-284.
[484] J. Jarrige, M. Laroussi, E. Karakas, Formation and dynamics of plasma bullets in a non-thermal plasma jet: influence of the high-voltage parameters on the plume characteristics, Plasma Sources Science and Technology 19(6) (2010) 065005.
[485] J. Jansky, P. Le Delliou, F. Tholin, Z. Bonaventura, P. Tardiveau, A. Bourdon, S. Pasquiers, Propagation of an air discharge at atmospheric pressure in a capillary glass tube: influence of the tube radius on the discharge structure, IEEE Transactions on Plasma Science 39(11) (2011) 2106-2107.
[486] J. Jánský, A. Bourdon, Simulation of helium discharge ignition and dynamics in thin tubes at atmospheric pressure, Applied Physics Letters 99(16) (2011) 161504.
[487] E. Robert, E. Barbosa, S. Dozias, M. Vandamme, C. Cachoncinlle, R. Viladrosa, J.M. Pouvesle, Experimental study of a compact nanosecond plasma gun, Plasma Process. Polym. 6(12) (2009) 795-802.
[488] Y. Akishev, M. Grushin, V. Karalnik, A. Monich, A. Petryakov, N. Trushkin, Self-pulsing regime of dc electric discharge in dielectric tube filled with water containing gas bubble, IEEE Transactions on Plasma Science 36(4) (2008) 1142-1143.
[489] S. Schröter, R. Pothiraja, P. Awakowicz, N. Bibinov, M. Böke, B. Niermann, J. Winter, Time-resolved characterization of a filamentary argon discharge at atmospheric pressure in a capillary using emission and absorption spectroscopy, Journal of Physics D: Applied Physics 46(46) (2013) 464009.
[490] M. Olde Riekerink, M. Claase, G. Engbers, D. Grijpma, J. Feijen, Gas plasma etching of PEO/PBT segmented block copolymer films, Journal of Biomedical Materials Research Part A: An Official Journal of The Society for Biomaterials, The Japanese Society for Biomaterials, and The Australian Society for Biomaterials and the Korean Society for Biomaterials 65(4) (2003) 417-428.
[491] A. Nandakumar, Z.T. Birgani, D. Santos, A. Mentink, N. Auffermann, K. van der Werf, M. Bennink, L. Moroni, C. van Blitterswijk, P. Habibovic, Surface modification of electrospun fibre meshes by oxygen plasma for bone regeneration, Biofabrication 5(1) (2012) 015006.

[492] J. Wu, Z. Mao, H. Tan, L. Han, T. Ren, C. Gao, Gradient biomaterials and their influences on cell migration, Interface focus 2(3) (2012) 337-355.
[493] S. Singer, A. Kupfer, The directed migration of eukaryotic cells, Annual review of cell biology 2(1) (1986) 337-365.
[494] E.W. Chan, M.N. Yousaf, A photo-electroactive surface strategy for immobilizing ligands in patterns and gradients for studies of cell polarization, Molecular BioSystems 4(7) (2008) 746-753.
[495] V.C. Hirschfeld-Warneken, M. Arnold, A. Cavalcanti-Adam, M. López-García, H. Kessler, J.P. Spatz, Cell adhesion and polarisation on molecularly defined spacing gradient surfaces of cyclic RGDfK peptide patches, Eur. J. Cell Biol. 87(8-9) (2008) 743-750.
[496] M. Arnold, V.C. Hirschfeld-Warneken, T. Lohmüller, P. Heil, J. Blümmel, E.A. Cavalcanti-Adam, M. López-García, P. Walther, H. Kessler, B. Geiger, Induction of cell polarization and migration by a gradient of nanoscale variations in adhesive ligand spacing, Nano Lett. 8(7) (2008) 2063-2069.
[497] T.J. Stefonek-Puccinelli, K.S. Masters, Co-immobilization of gradient-patterned growth factors for directed cell migration, Annals of biomedical engineering 36(12) (2008) 2121.
[498] A. Cooper, N. Bhattarai, M. Zhang, Fabrication and cellular compatibility of aligned chitosan–PCL fibers for nerve tissue regeneration, Carbohydrate Polymers 85(1) (2011) 149-156.
[499] E. Masaeli, M. Morshed, M.H. Nasr-Esfahani, S. Sadri, J. Hilderink, A. van Apeldoorn, C.A. van Blitterswijk, L. Moroni, Fabrication, characterization and cellular compatibility of poly (hydroxy alkanoate) composite nanofibrous scaffolds for nerve tissue engineering, PloS one 8(2) (2013) e57157.
[500] W. Wang, S. Itoh, K. Konno, T. Kikkawa, S. Ichinose, K. Sakai, T. Ohkuma, K. Watabe, Effects of Schwann cell alignment along the oriented electrospun chitosan nanofibers on nerve regeneration, Journal of Biomedical Materials Research Part A: An Official Journal of The Society for Biomaterials, The Japanese Society for Biomaterials, and The Australian Society for Biomaterials and the Korean Society for Biomaterials 91(4) (2009) 994-1005.
[501] R. Martini, Y. Xin, M. Schachner, Restricted localization of L1 and N-CAM at sites of contact between Schwann cells and neurites in culture, Glia 10(1) (1994) 70-74.
[502] I. Whitworth, R. Brown, C. Dore, C. Green, G. Terenghi, Orientated mats of fibronectin as a conduit material for use in peripheral nerve repair, Journal of Hand Surgery 20(4) (1995) 429-436.
[503] N. Dubey, P. Letourneau, R. Tranquillo, Guided neurite elongation and Schwann cell invasion into magnetically aligned

collagen in simulated peripheral nerve regeneration, Experimental neurology 158(2) (1999) 338-350.
[504] D.N. Adams, E.Y.C. Kao, C.L. Hypolite, M.D. Distefano, W.S. Hu, P.C. Letourneau, Growth cones turn and migrate up an immobilized gradient of the laminin IKVAV peptide, Journal of neurobiology 62(1) (2005) 134-147.